Polyester micro- and nanoparticles for the delivery of therapeutic peptides or proteins

Lucía Amine
Martínez Jothar

Polyester micro- and nanoparticles for the delivery of therapeutic peptides or proteins

Lucía Amine Martínez Jothar

Polyester micro- and nanoparticles for the delivery of
therapeutic peptides or proteins.
PhD thesis, Utrecht University, the Netherlands

ISBN: 978-90-393-7140-4
Cover by: Alejandro Lee
Printed by: Ridderprint
Typeset in LaTeX

The printing of this thesis was (partly) supported by Utrecht Institute of Pharmaceutical Sciences (UIPS), Utrecht, the Netherlands.

Polyester micro- and nanoparticles for the delivery of therapeutic peptides or proteins

Polyester micro- en nanodeeltjes voor de afgifte van therapeutische peptiden of eiwitten

(met een samenvatting in het Nederlands)

Proefschrift

ter verkrijging van de graad van doctor aan de
Universiteit Utrecht
op gezag van de
rector magnificus, prof.dr. H.R.B.M. Kummeling,
ingevolge het besluit van het college voor promoties
in het openbaar te verdedigen op

vrijdag 14 juni 2019 des middags te 12.45 uur

door

Lucía Amine Martínez Jothar

geboren op 30 juni 1987
te San Luis Potosí, México

Promotor:
Prof. dr. ir. W.E. Hennink

Copromotoren:
Dr. C.F. van Nostrum
Dr. S. Oliveira

This thesis was (partly) accomplished with financial support of the Mexican National Council for Science and Technology (Consejo Nacional de Ciencia y Tecnología - CONACYT, México)

"You cannot hope to build a better world without improving the individuals. To that end, each of us must work for his own improvement and, at the same time, share a general responsibility for all humanity..."

— Marie Curie

Contents

Chapter 1

General introduction

1 Therapeutic proteins and peptides

1.1 General considerations

The therapeutic potential of proteins has been explored for more than a century, for instance with the development of serum therapy in the late 1800s[1], and the use of insulin in the early 1900s[2]. Since then, the scientific and technological advances have facilitated the study, production, purification and modification of peptides and proteins, resulting in the approval of > 160 therapeutic proteins[3,4] and > 60 therapeutic peptides[5], with many more being currently under development. These therapeutic proteins and peptides are commonly classified based on their pharmacological activity in: (1) molecules with enzymatic or regulatory activity, (2) therapeutics with targeting activities (i.e. monoclonal antibodies that block a specific molecule or that deliver other molecules to a specific site), (3) vaccines and (4) agents that assist in diagnosis[6].

1.2 Examples of therapeutic proteins and peptides

Proteins and peptides can have intracellular or extracellular targets. Since targets on the surface of cells, most commonly receptors, are easier to reach than intracellular molecules, the majority of the therapeutic proteins and peptides currently available on the market have exogenous action sites. Nevertheless, advances in protein engineering and formulation technologies have also been directed towards the exploitation of those therapeutic agents with intracellular targets. For instance, proteins can be fused or covalently attached to cell penetrating peptides or to supercharged proteins which facilitate their endocytosis and, when used in combination with an endosomal escape strategy, result in cytosolic delivery[7,8]. Additionally, therapeutic proteins and peptides can be encapsulated in or attached to lipidic, polymeric or inorganic nanocarriers, which enter the cell through endocytosis[9,10]. Endosomal escape of these carriers can be favored by an external stimulus or by components present in the carrier, such as highly charged or pH sensitive moieties, as further discussed in section 4.2 of this Introduction.

To exemplify the wide range of pharmacological applications, target sites and mechanisms of action of therapeutic proteins and peptides, two different molecules will be discussed in this text: saporin (a ribosome-inactivating protein) and (Nle^4, D-Phe^7)-α-melanocyte-stimulating hormone (NDP-MSH, a derivative of the α-melanocyte-stimulating hormone). For both saporin and

NDP-MSH the development of suitable formulations with added therapeutic value was the subject of investigation described in this thesis.

1.2.1 Ribosome-inactivating proteins

Ribosome-inactivating proteins (RIPs) are toxins from plant, bacterial or fungal origin, that damage the ribosomal RNA, block protein synthesis and as a result cause cell death. RIPs are classified in three types: type I which consists of an A chain with catalytic activity, type II which is composed of an A chain and a B chain that mediates its binding to and entrance in cells, and type III which requires proteolytic processing to yield an active RIP [11,12].

Their potent cytotoxic activity has positioned RIPs as promising agents for cancer therapy, with saporin being one of the most widely studied proteins for this purpose. Saporin, a type I RIP of M_w ~28,000 Da produced by the plant *Saponaria officinalis*, causes cell death by inhibition of protein synthesis, DNA-fragmentation and induction of apoptosis, and has shown promising cytotoxicity in different cancer cells [13–16]. The lack of a B chain limits the ability of saporin to enter cells, which has prompted its use in combination with antibodies (thus forming immunotoxins) [17] or with nanocarriers that favor its intracellular localization [18].

1.2.2 α-melanocyte-stimulating hormone

The α-melanocyte-stimulating hormone (α-MSH) is a peptide composed by 13 amino acids (M_w 1,665 Da) that originates from the proteolytic processing of the pro-hormone proopiomelanocortin. α-MSH binds to melanocortin receptors (Mcr) that are expressed in the central and peripheral nervous system, in the adrenal cortex, on the skin and in cells participating in the immune system [19]. The binding of α-MSH to Mc1r, Mc2r and Mc5r plays a role in skin pigmentation, the production of steroid hormones and thermoregulation, while its binding to Mc3r and Mc4r regulates food intake and the energy balance [20]. While clinical applications of α-MSH have been limited by its high susceptibility to proteolytic inactivation, analogues of this peptide such as (Nle^4, D-Phe^7)-α-MSH (NDP-MSH) are less sensitive towards proteolysis and therefore have increased pharmacological activity [21]. NDP-MSH is currently approved for the treatment of erythropoietic porphyria [22], but it was recently reported that it could also be an interesting drug candidate for the treatment of some neurological disorders due to its neuroprotective effect resulting from its anti-inflammatory and immunomodulatory properties [23].

1.3 Challenges for the delivery of therapeutic proteins and peptides

In spite of the therapeutic advantages of protein and peptide based drugs, unfavorable physicochemical and pharmacokinetic properties often hinder their clinical application.

The physical and chemical instability of these molecules is probably the main concern, since structural changes and degradation can occur both before and after administration to the patient. For instance, denaturation and aggregation are important risks during handling and storage, particularly for protein pharmaceuticals. On the other hand, proteolysis, pH dependent degradation and accelerated clearance are significant concerns after administration.

Even if proteins and peptides are generally well tolerated by patients, immunogenic responses can still occur and must be carefully considered. The activation of the immune system can have different consequences, from the neutralization of the protein/peptide, to severe reactions. As a result of the advances in molecular biology and protein engineering, the immunogenicity associated to some proteins from non-human origin has been reduced to some extent through humanization of their amino acid sequence.

Another set of concerns arise from the poor permeability of proteins and peptides through biological membranes, resulting from their large size and their mixed structure consisting of hydrophilic and hydrophobic domains[6]. Poor membrane permeability requires innovative delivery solutions for molecules with intracellular targets, for instance the use of nanocarriers that are internalized by living cells, as discussed in more detail in the following paragraphs.

2 Polymeric particles for the delivery of therapeutic proteins and peptides

2.1 General information

The physicochemical stability, pharmacokinetics and pharmacodynamics of therapeutic proteins and peptides can be improved by their encapsulation and using carriers such as liposomes, dendrimers, micelles and polymeric particles[24,25].

In this section we will focus on polymeric particles, solid drug carriers of micro- or nano- metric size made of natural or synthetic polymers. Particles have tunable properties in terms of size, surface charge, degradation, drug loading and drug release, and they are more stable in biological fluids than

liposomes[26]. Proteins and peptides can be attached to the surface of the particles by covalent or non-covalent linkages or they can be entrapped on their inside, either in the polymer matrix or in an inner aqueous core of vesicle-like particles. Polymeric particles have been studied for protein and peptide delivery through oral, subcutaneous, intramuscular, nasal, pulmonary, ocular and intravenous routes[27]. For the latter, the surface of the particles is normally coated with a non-charged hydrophilic polymer (mostly PEG) to avoid their opsonization and recognition by the mononuclear phagocyte system (MPS), resulting in prolonged circulation times[28,29].

2.2 Polymeric particles made of poly(lactic-co-glycolic) acid

Poly(lactic-co-glycolic acid) (PLGA) is commonly used for the preparation of drug delivery systems because of its biodegradability, biocompatibility, and tunable properties[24,25,30,31]. The degradation of PLGA, which occurs by ester bond hydrolysis, ranges between 2 and 6 months and depends on the copolymer composition, polymer molecular weight and the end group capping[32–35].

PLGA can be used for the preparation of drug loaded particles of different sizes, namely microparticles (μPs) and nanoparticles (NPs). Due to their smaller size, NPs are preferred for intravenous administration and in applications where extravasation and/or cellular uptake are required. In contrast, μPs can be used as depot formulations for the controlled and sustained long-term release of therapeutic agents and are mostly administered locally (SC or IM).

Several PLGA μP formulations have been approved for peptide delivery, including Lupron Depot® (leuprolide), Zoladex Depot® (goserelin), Trelstar® (triptorelin), Sandostatin® LAR Depot (octreotide) and Somatuline® Depot (lanreotide)[36]. In contrast, PLGA μP formulations have proven to be much more challenging and one of the few products approved for this purpose (Nutropin Depot®, goserelin) was discontinued 5 years after its market introduction as a result of the significant resources needed for its manufacturing and commercialization[37].

In spite of the clinical success of some PLGA-based formulations, concerns remain about the stability of the proteins and peptides encapsulated in micro- and nano-particles. These concerns arise from the degradation process of PLGA, which results in the formation of short oligomers of lactic and glycolic acid, and finally in these acids. These acid degradation products remain entrapped in the particles which results in acidification of the polymer matrix. As a consequence, proteins and peptides can undergo unwanted structural modifications such as degradation, unfolding, aggregation, deamidation, oxi-

dation and acylation[38–40]. Our research group has therefore developed other biodegradable aliphatic polyesters with better protein and peptide compatibility, which will be discussed in the next section.

2.3 Polymeric particles made of aliphatic polyesters with pendant hydroxyl groups

The risk of unwanted protein and peptide modification resulting from the degradation/acidification of PLGA particles has encouraged the search of new polymers with better protein compatibility. In this regard, polymers with higher hydrophilicity could pose a solution to this issue by favoring the hydration of the polymer matrix and the diffusion of the acidic degradation products out of the particles.

Two structurally related polyesters with pendant hydroxyl groups were developed in our research group as a more hydrophilic alternative to PLGA: poly(D,L-lactic-co-hydroxymethyl glycolic acid) (PLHMGA) and poly(D,L-lactic-co-glycolic-co-hydroxymethyl glycolic acid) (PLGHMGA) (Figure 1)[41]. These polymers have been evaluated for applications in the delivery of proteins[42–45], peptides[46,47] and antibiotics[48]. Studies comparing the structure of a peptide (octreotide) released from PLGA or PLHMGA μPs, showed that the latter displayed enhanced peptide compatibility (i.e. less acylation)[46]. Similar results were obtained for PLGHMGA μPs[49], which positions these polymers as promising candidates for protein and peptide delivery.

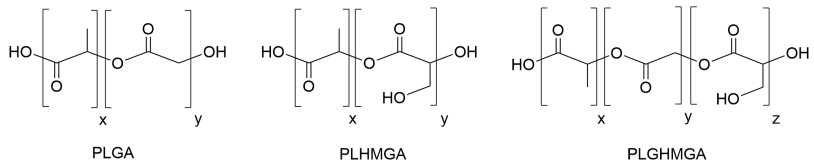

Figure 1: Structure of aliphatic polyesters with applications in protein and peptide delivery.

Besides increasing the peptide/protein compatibility of the polymers, the pendant hydroxyl groups of PLHMGA and PLGHMGA can also serve other functions. For instance, these groups can be used for the functionalization of the polymer with targeting ligands, fluorescent dyes and PEG chains, amongst others. Additionally, the increased hydrophilicity conferred by the hydroxyl groups results in relatively fast polymer degradation and protein release from

NPs[45], which is convenient for applications where drug action is needed over a period of days to a few weeks.

3 Targeted and non-targeted particles for the delivery of proteins and peptides

When discussing drug delivery by intravenous administration of polymeric NPs (and other nanocarriers), two approaches are most often documented: non-targeted (also sometimes referred to as passive targeting) and targeted (or active targeting). Even though the accuracy of this terminology is under debate[50–52], the word targeting is still extensively used in pharmaceutical nanomedicine literature. These terms will therefore also be used in the present thesis, but following the considerations mentioned in sections 3.1 and 3.2.

3.1 Non-targeted particles

After i.v. injection, the distribution and accumulation of NPs in pathological areas is driven by A) the physicochemical characteristics of the particles and B) the anatomy and physiology of the site.

3.1.1 Physicochemical properties of the particles

The physicochemical characteristics of polymeric particles govern their interactions with biomolecules and cells, which in turn determines their (bio)distribution, accumulation and retention in the target site and clearance. Size and surface charge are the main physicochemical parameters that mediate the biological interactions of particles, though others such as shape, hydrophobicity, surface roughness and rigidity, also play a role[24,53].

3.1.1.1 Size

Size is a key determinant in the ability of particles to reach their target site, and is also an important factor in their circulation kinetics. For treatments that require direct contact or even internalization of the particles in the diseased cells (i.e. the delivery of biotherapeutics, including protein and nucleic acid based drugs), NPs with diameters of 10 to ∼200 nm are preferred. The lower limit is based on the glomerular filtration size threshold and particles of this size (in contrast to smaller ones) are not cleared by the kidneys, thus prolonging their circulation time[54]. The upper limit (which is less strictly defined), is correlated with the anatomical characteristics of the delivery site: for

instance, intravenously administered NPs often have to extravasate through (large) fenestrations in the vascular endothelium in order to reach their targets. Smaller sizes would therefore make it easier for the NPs to pass through these gaps[50,55,56].

Sufficiently long circulation times are necessary for the accumulation of NPs in their target sites. The pharmacokinetics of nanocarriers are affected by their size, for instance, small particles $\leq$ 5.5 nm are filtered by the kidney, particles $<$ 50 nm are subject to accumulation in the liver, and particles of 300 - 400 nm tend to accumulate in the spleen[57,58]. These cutoffs suggest that a size of $\sim$100 nm is favorable to avoid rapid clearance of nanocarriers. Size is a far less important issue in particles intended for use as a depot for the prolonged and sustained release of drugs, in which case subcutaneous or intramuscular administration of drug-loaded μPs is often used. In this case, the size of the μPs will determine their degradation rate and the release profile of their contents, and it will also influence their interaction with immune cells. For instance, μPs of a size $\leq$ 10 μm can be taken up by macrophages and dendritic cells, an event that is undesired for particles loaded with therapeutic proteins/peptides, but that can be exploited for vaccination purposes.[59–61]

3.1.1.2 Surface charge

The surface charge of NPs governs their interaction with proteins and cells, which in turn has important effects on their circulation kinetics, distribution in the body and their retention at the target site. Interactions between positively charged NPs and negatively charged proteins (which are abundant in the blood) results in the opsonization of the NPs and their rapid clearance by the MPS. Positively charged particles can also interact with negatively charged molecules present on the surface of the cells, such as phospholipids, glycans and proteins, which favors their binding and uptake by cells, or even the direct penetration of the cell membrane[24]. Even though the effects of the interactions between negatively charged NPs and proteins and cells are less well documented than for positive NPs, the presence of negative charges also accelerates the clearance of NPs[54] and reduces their accumulation in target sites.

So far, the most popular approach to shield the surface properties of NPs is PEGylation[28,29,62]. Grafting of PEG chains on the surface results in stealth particles with close to neutral surface charges, decreased non-specific binding to biomolecules and reduced clearance by the MPS. Recently, PEG alternatives have also been studied, including polymers of natural origin (i.e. heparin, dextran and chitosan), poly(amino acid)s (i.e. poly(glutamic acid) and

poly(hydroxyethyl-L-glutamine), poly(2-oxazoline)s, and vinyl polymers (i.e. poly(acrylamide)s and poly(vinylpyrrolidone))[63,64]. A few drug delivery systems stabilized with alternatives for PEG, such as poly(N-2-hydroxypropyl) methacrylamide) and poly(glutamic acid), have entered clinical trials[64,65].

3.1.2 Anatomy and physiology of the target tissues

The structure and physiology of both the target tissue and its vasculature determine the accessibility for NPs. For NPs that are administered intravenously, the vascular endothelium constitutes the first barrier between them and their target tissues, unless the target is the endothelium itself. Pathological conditions such as cancer and inflammatory processes are accompanied by an increase in the permeability of blood vessels due to the presence of fenestrae or gaps between endothelial cells, which can facilitate the extravasation of NPs[66]. These abnormalities in the structure of the blood vessels are at the basis of one of the events most commonly associated to non-targeted drug delivery: the enhanced permeability and retention effect (EPR). Even though EPR has favored the accumulation of nanocarriers in sites with leaky vasculature in some disease models, EPR-mediated drug targeting has been hindered by the high heterogeneity of EPR both between and within patients[67–70]. In this regard, other strategies that modify the structure and functioning of the blood vessels have been proposed to increase the accumulation of nanocarriers in disease sites. Some examples are vascular permeabilization, normalization, disruption or promotion, as well as hyperthermia and sonoporation[71].

Even though the increased vascular permeability allows for the extravasation of NPs and should favor their accumulation in the disease site, this is not always the case. Increased leakiness of blood vessels often increases the pressure in the interstitium, which limits the diffusion of NPs into the target site and instead favors their accumulation in the perivascular region. Additionally, even if NPs do reach the interstitium, their mobility is limited by the extracellular matrix present in this region. In this regard, the diffusion of NPs through the interstitium and to the target site can be improved by tuning the size and charge of the NPs[66].

3.2 Targeted nanoparticles

Targeted delivery requires surface modification of the NPs with a ligand that specifically binds to a protein that is (over)expressed on the membrane of the cells of interest. This binding event mediates the interaction between the cells and the NPs, favors the retention of the NPs in the target site and will

often trigger NPs internalization via endocytosis. It has to be emphasized that targeted delivery is only possible after the NPs have efficiently reached the site of the disease, an event that is not mediated by the targeting ligand itself but by the parameters governing non-targeted delivery [51,72] (discussed in section 3.1).

3.2.1 Functionalization of NPs with targeting ligands

The decoration of targeting ligands on the surface of the NPs can be achieved through non-covalent interactions and covalent bonds.

Non-covalent methods include ligand adsorption on the surface of the NPs via hydrophobic interactions, hydrogen bonding or electrostatic interactions, as well as the interaction between biotin and avidin (one of them incorporated on the NPs and the other on the ligand) [73].

Covalent attachment can be achieved by several strategies, including maleimide-thiol chemistry (formation of a thioether linkage between maleimide groups on the NPs and free thiols on the ligands), reactions with N-hydroxysuccinimide (formation of an amide bond between NHS groups on the NPs and primary amines on the ligands), carbodiimide chemistry (formation of an amide bond between activated carboxylic acids on the NPs and primary amines on the ligands), and click chemistry (for example, thiol-ene reaction between alkenes and free thiols on the ligands) [73].

3.2.2 Types of targeting ligands

Numerous ligands have been described for the preparation of targeted NPs and most of them can be grouped within the following categories according to their nature [74]:

- Proteins. Most of the ligands fall in this category which comprises (monoclonal) antibodies and their fragments, as well as affibodies and nanobodies, which generally target receptors on the cell surface (i.e. those from the epidermal growth factor receptor family). This category also includes iron-binding proteins lactoferrin and transferrin.
- Peptides. The most prominent example in this group is the RGD peptide. Cell penetrating peptides such as Lyp1 are also frequently used.
- Aptamers. Single stranded DNA or RNA fragments that selectively bind different proteins on the cell surface.

- Saccharides, such as galactose which binds to asialoglycoprotein receptors present on hepatocellular carcinoma cells.
- Small molecules, including folic acid and biotin.

In this thesis, two different targeting ligands with promising applications in cancer treatment have been exploited for the preparation of targeted NPs, namely the 11A4 nanobody and the RGD peptide which are both described in more detail below.

3.2.2.1 11A4 nanobodies

Nanobodies are the variable domains of the heavy chain only antibodies present in animals from the Camalidae family (i.e. camels, llamas and alpacas)[75]. With a M_w of around 15,000 Da, these proteins are the smallest antigen binding fragments of natural origin. Nanobodies have several advantages over antibodies due to their smaller size, including easier production, higher solubility and stability, less propensity to aggregation, and the ability to bind to targets that are inaccessible to antibodies[76,77]. Sequence homology between the variable domains of human and camelid antibodies, as well as the low propensity of nanobodies to aggregation, and the existence of a universal humanized nanobody scaffold, are expected to result in low immunogenicity[78,79]. These advantages, have prompted the exploration of nanobodies as targeting ligands for liposomes[80,81], micelles[82], albumin NPs[83] and polymersomes[84].

The nanobody 11A4 (M_w ~14,800 Da) targets the Human Epidermal Growth Factor Receptor 2 (HER2), which is overexpressed in breast, gastric, lung and ovarian cancers, among others[85]. HER2, a receptor with tyrosine kinase activity, promotes cell growth and survival and is often associated with more aggressive tumor phenotypes and poor prognosis[86]. Because of the specificity and high binding affinity of the nanobody 11A4 for the HER2 receptor ($k_D < 1$ nM), this nanobody has been used as a tool for *in vivo* optical imaging of breast cancer[87,88] and for immunolabeling of HER2 for electron microscopy[89]. In our research group, the nanobody 11A4 has also been used as a suitable ligand for the targeted delivery of protein loaded polymeric NPs to HER2 positive cancer cells[90].

3.2.2.2 RGD peptide

The Arg-Gly-Asp tripeptide sequence, commonly referred to as RGD, is present in several extracellular matrix proteins including fibronectin, vitro-

nectin, fibrinogen, laminin and thrombospondin. In these proteins, RGD serves as a recognition site for the $\alpha_v\beta_3$ integrin present in endothelial cells[91]. This integrin mediates important cell processes such as adhesion, migration and growth, and it also plays a central role in angiogenesis[92]. The high expression levels of the integrin $\alpha_v\beta_3$ in proliferative endothelial cells, but also in several types of tumors (melanoma, glioblastoma, breast, prostate, pancreatic, ovarian and cervical cancers) make the RGD peptide an ideal candidate for the design and preparation of targeted NPs[93,94].

While RGD as such can function as a targeting moiety, derivatives of this peptide with improved properties have also been synthesized. In this regard, cyclic RGD peptides (cRGD) have emerged as leading molecules because of their higher stability[95] and increased binding affinities compared to their linear analogues[96]. RGD and its derivatives have so far been studied for the delivery of imaging agents, drugs and therapeutic biomolecules to tumors and to the tumor vasculature[97–102]. While RGD has been broadly investigated for targeted drug delivery, a recent study reported lethal immune responses in mice treated with cRGD-decorated liposomes, advocating for more comprehensive evaluations of the immunogenicity of ligand-decorated nanocarriers[103].

4 Intracellular delivery of therapeutic molecules using NPs

One of the most promising features of NPs is their potential use for the intracellular delivery of therapeutic molecules with cytosolic targets, such as the proteins mentioned in section 1.2.1. The internalization pathways of NPs and their intracellular trafficking will be discussed in the following sections.

4.1 Internalization of NPs

The cell-nanoparticle interactions that drive the internalization of these nanocarriers are dependent on both the type of cells involved (i.e. phagocytic or non-phagocytic) and the physicochemical characteristics of the NPs. Some examples of the influence of NPs properties on their cellular uptake are:

A) NPs size. It is generally accepted that NPs with sizes > 500 nm are taken up by phagocytosis. While the exact mechanism of uptake for smaller NPs is difficult to predict, an indication can be given based on the size of the vesicles that are formed during different uptake pathways: caveolae-mediated endocytosis comprises vesicles of 50 - 80 nm, while clathrin-mediated endocy-

tosis results in the formation of larger vesicles and could therefore mediate the uptake of larger NPs (∼300 nm)[104].

B) NPs surface properties. The influence of surface charge on cell-particle interactions is discussed in section 3.1.1.2. Apart from charge, the hydrophobic/hydrophilic balance of the NPs surface will also affect their interaction with and uptake by cells. This parameter depends on the properties of the polymer used to prepare the NPs, on the excipients used in the preparation process (i.e. surfactants), as well as on the presence of PEG and targeting ligands (addressed in more detail in the next section). While hydrophobic nanoparticles show higher cellular association and internalization than more hydrophilic and uncharged NPs[105], it should be mentioned that the surface characteristics will influence opsonization, which will in turn modify the particle-cell interactions as compared to non-opsonized particles.

C) Presence of targeting ligands. The interaction between ligands on the NPs and receptors on target cells can trigger receptor-mediated endocytosis of the NPs. Normally, several ligands as well as several receptors (of the same type) are present on each particle and on each cell, which can result in multiple simultaneous binding events. This process, also known as multi- or poly-valency, normally results in stronger interactions (compared to single events) and in enhanced binding and endocytosis of NPs[106]. The occurrence of multivalent interactions is determined by the shape, size, flexibility, valency and surface ligand density[107], as well as by the distribution, accessibility, valency and abundance of the receptor.

4.2 Intracellular trafficking of NPs

Upon internalization by endocytosis, NPs generally follow the degradative pathway. During this process, endocytic vesicles containing the NPs fuse with early endosomes (pH 6.8 - 6.5), are then trafficked through the late endosome (pH 6.2 - 5.2) and eventually reach the lysosomes (pH 5.2 - 4.5)[107]. Unless the lysosomes are the final target of the NPs (i.e. for the treatment of lysosomal storage diseases[108]), lysosomal localization is undesired because it will lead to degradation of the NPs and their therapeutic cargo, thus resulting in treatment failure. To prevent this, several strategies have been proposed and investigated to promote the translocation of the NPs from the endosomes to the cytosol before they reach the lysosome.

Endosomal escape of NPs can be achieved by altering the endosomal membrane through several mechanisms. For instance, pore formation can be induced by cationic amphiphilic agents that interact with the lipid bilayer. Membrane destabilization can be established with fusogenic peptides like hemag-

glutinin, whereas membrane disruption can be caused by cell-penetrating peptides or other endosomolytic agents such as chloroquine. Alternatively, the endosomal membrane can be disrupted through the proton sponge effect by using polymers with high buffering capacity that, upon protonation at the endosomal pH, will cause the osmotic influx of ions and water leading to endosomal swelling and finally disruption [109,110].

In the 1990s, photochemical internalization (PCI) emerged as a new strategy for the induction of endosomal escape of drugs and nanocarriers. PCI requires the use of a photosensitizer (PS) with amphiphilic properties that can solubilize in cell membranes. Upon endocytosis of drugs or nanocarriers, the PS will become part of the endosomal membrane. Subsequently, the cells will be exposed to light of the appropriate wavelength in order to excite the PS, which will produce reactive oxygen species that will damage the endosomal membrane which in turn will result in the release of the endosomal contents into the cytosol [111] (Figure 2). *In vitro* and *in vivo* studies have proven the suitability of PCI for the intracellular delivery of proteins, genetic material, immunotoxins, chemotherapeutic drugs and nanocarriers, including dendrimers, liposomes and nanogels [112]. Importantly, PCI has also shown potential applications in clinical settings, with promising results being obtained in trials combining PCI with bleomycin for the treatment of cutaneous and subcutaneous malignancies [113] and PCI and gemcitabine for the treatment of cholangiocarcinomas [114].

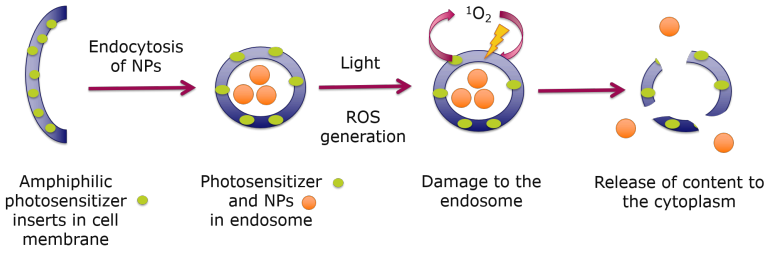

Figure 2: Schematic representation of photochemical internalization of NPs.

5 Aim and outline of the thesis

In this thesis, the suitability of polymeric particles for targeted and non-targeted delivery of therapeutic proteins and peptides was evaluated.

In **Chapter 2** PLGA NPs decorated with the cRGD peptide (M_w ~700 Da) or the nanobody 11A4 (M_w ~14,800 Da) were prepared exploiting the maleimide-thiol conjugation reaction. Even though maleimide-thiol chemistry is widely used for the functionalization of nanocarriers, the influence of different conditions on the efficiency of the reaction has not been systematically studied. In this regard, parameters such as reaction time, reactant ratios, and maleimide stability upon NPs preparation and storage, were evaluated in this chapter. The insights obtained in this study allowed for the optimization of the maleimide-thiol reaction conditions, and were used in **Chapter 3** for the preparation of PLGA-NPs with controlled cRGD densities. The impact of surface density on the interactions between cRGD-NPs and human umbilical vein endothelial cells was studied under static conditions, which is the most common *in vitro* approach to evaluate the targeting potential of NPs decorated with ligands. Additionally, the association of NPs to the cells was studied under flow with and without red blood cells, which allowed for the evaluation of vascular cell targeting in more realistic and physiologically relevant conditions.

While PLGA has been extensively used for the preparation of nanocarriers, our research group has also shown the potential of a structurally related polymer, PLGHMGA, for this purpose. Slight changes in the protocol for the synthesis of PLGHMGA resulted in the accumulation of an impurity that was identified and removed as discussed in **Chapter 4** of this thesis. The cytocompatibility of the purified and non-purified polymer were also compared in this chapter. Subsequently, the purified polymer was used in **Chapter 5** for the preparation of 11A4 nanobody-targeted NPs loaded with a cytotoxic protein (saporin). These NPs were used in combination with photochemical internalization for the controlled and targeted intracellular delivery of this protein to HER2 positive breast cancer cells.

In **Chapter 6** PLGA microparticles were investigated as a sustained release formulation of NDP-MSH, a neuroprotective peptide tested in a mouse model of neuroinflammatory disease.

Finally, in **Chapter 7** the findings of this thesis are summarized and future research directions are discussed.

References

[1] Graham, B. S. and Ambrosino, D. M. History of passive antibody administration for prevention and treatment of infectious diseases. *Current Opinion in HIV and AIDS*, 10, 2015.

[2] Vecchio, I., Tornali, C., Bragazzi, N. L., and Martini, M. The discovery of insulin: an important milestone in the history of medicine. *Frontiers in Endocrinology*, 9, 2018.

[3] Dimitrov, D. S. Therapeutic Proteins. In Voynov, V. and Caravella, J., editors, *Therapeutic Proteins. Methods in Molecular Biology (Methods and Protocols)*, volume 899. Humana Press, Totowa, NJ, 2012.

[4] Lagassé, H. A. D., Alexaki, A., Simhadri, V. L., Katagiri, N. H., Jankowski, W., Sauna, Z. E., and Kimchi-Sarfaty, C. Recent advances in (therapeutic protein) drug development. *F1000Research*, 6, 2017.

[5] Lau, J. L. and Dunn, M. K. Therapeutic peptides: Historical perspectives, current development trends, and future directions. *Bioorganic and Medicinal Chemistry*, 26, 2018.

[6] Leader, B., Baca, Q., and Golan, D. Protein therapeutics: A summary and pharmacological classification. *Nature Reviews Drug Discovery*, 7, 2008.

[7] Fu, A., Tang, R., Hardie, J., Farkas, M. E., and Rotello, V. M. Promises and pitfalls of intracellular delivery of proteins. *Bioconjugate Chemistry*, 25, 2014.

[8] Ray, M., Lee, Y.-W., Scaletti, F., Yu, R., and Rotello, V. M. Intracellular delivery of proteins by nanocarriers. *Nanomedicine*, 12, 2017.

[9] Du, J., Jin, J., Yan, M., and Lu, Y. Synthetic Nanocarriers for Intracellular Protein Delivery. *Current Drug Metabolism*, 13, 2012.

[10] Gu, Z., Biswas, A., Zhao, M., and Tang, Y. Tailoring nanocarriers for intracellular protein delivery. *Chemical Society Reviews*, 40, 2011.

[11] de Virgilio, M., Lombardi, A., Caliandro, R., and Fabbrini, M. S. Ribosome-inactivating proteins: From plant defense to tumor attack. *Toxins*, 2, 2010.

[12] Stirpe, F. and Batelli, M. G. Ribosome-inactivating proteins: progress and problems. *Cellular and Molecular Life Sciences*, 63, 2006.

[13] Bagga, S., Seth, D., and Batra, J. K. The cytotoxic activity of ribosome-inactivating protein saporin-6 is attributed to its rRNA N-glycosidase and internucleosomal DNA fragmentation activities. *Journal of Biological Chemistry*, 278, 2003.

[14] Cimini, A., Mei, S., Benedetti, E., Laurenti, G., Koutris, I., Cinque, B., Cifone, M. G., Galzio, R., Pitari, G., Di Leandro, L., Giansanti, F., Lombardi, A., Fabbrini, M. S., and Ippoliti, R. Distinct cellular responses induced by saporin and a transferrin-saporin conjugate in two different human glioblastoma cell lines. *Journal of Cellular Physiology*, 227, 2012.

[15] Polito, L., Bortolotti, M., Farini, V., Battelli, M. G., Barbieri, L., and Bolognesi, A. Saporin induces multiple death pathways in lymphoma cells with different intensity and timing as compared to ricin. *International Journal of Biochemistry and Cell Biology*, 41, 2008.

[16] Sikriwal, D., Ghosh, P., and Batra, J. K. Ribosome inactivating protein saporin induces apoptosis through mitochondrial cascade, independent of translation inhibition. *International Journal of Biochemistry and Cell Biology*, 40, 2008.

[17] Polito, L., Bortolotti, M., Pedrazzi, M., and Bolognesi, A. Immunotoxins and other conjugates containing saporin-s6 for cancer therapy. *Toxins*, 3, 2011.

[18] Polito, L., Bortolotti, M., Mercatelli, D., Battelli, M. G., and Bolognesi, A. Saporin-S6: A useful tool in cancer therapy. *Toxins*, 5, 2013.

[19] Ramachandrappa, S., Gorrigan, R. J., Clark, A. J. L., and Chan, L. F. Melanocortin receptors and their accessory proteins. *Frontiers in endocrinology*, 4, 2013.

[20] D'Agostino, G. and Diano, S. alpha-Melanocyte stimulating hormone: production and degradation. *Journal of Molecular Medicine*, 88, 2010.

[21] Hadley, M. E., Hruby, V. J., Blanchard, J., Dorr, R. T., Levine, N., Dawson, B. V., Al-Obeidi, F., and Sawyer, T. K. Chapter 25 Discovery and development of novel melanogenic drugs. In *Integration of Pharmaceutical Discovery and Development*, pages 575–595. Springer, 2002.

[22] Scenesse® Assessment Report. Report, European Medicines Agency, 2014.

[23] Mykicki, N., Herrmann, A. M., Schwab, N., Deenen, R., Sparwasser, T., Limmer, A., Wachsmuth, L., Klotz, L., Köhrer, K., Faber, C., Wiendl, H., Luger, T. A., Meuth, S. G., and Loser, K. Melanocortin-1 receptor activation is neuroprotective in mouse models of neuroinflammatory disease. *Science Translational Medicine*, 8, 2016.

[24] Kamaly, N., Xiao, Z., Valencia, M. P., Radovic-Moreno, A. F., and C, F. O. Targeted polymeric therapeutic nanoparticles: design, development and clinical translation. *Chemical Society Reviews*, 41, 2012.

[25] Yu, M., Wu, J., Shi, J., and Farokhzad, O. C. Nanotechnology for Protein Delivery: Overview and Perspectives. *Journal of Controlled Release*, 240, 2016.

[26] Patel, A., Patel, M., Yang, X., and Mitra, A. Recent Advances in Protein and Peptide Drug Delivery: A Special Emphasis on Polymeric Nanoparticles. *Protein & Peptide Letters*, 21, 2014.

[27] Pinto Reis, C., Neufeld, R. J., Ribeiro, A. J., and Veiga, F. Nanoencapsulation II. Biomedical applications and current status of peptide and protein nanoparticulate delivery systems. *Nanomedicine: Nanotechnology, Biology, and Medicine*, 2, 2006.

[28] Couvreur, P. and Vauthier, C. Nanotechnology : Intelligent Design to Treat Complex Disease. *Pharmaceutical Research*, 23, 2006.

[29] Owens, D. E. and Peppas, N. A. Opsonization, biodistribution, and pharmacokinetics of polymeric nanoparticles. *International Journal of Pharmaceutics*, 307, 2006.

[30] Mundargi, R. C., Babu, V. R., Rangaswamy, V., Patel, P., and Aminabhavi, T. M. Nano/micro technologies for delivering macromolecular therapeutics using poly(d,l-lactide-co-glycolide) and its derivatives. *Journal of Controlled Release*, 125, 2008.

[31] Rezvantalab, S., Drude, N. I., Moraveji, M. K., and Gagliardi, P. A. PLGA-Based Nanoparticles in Cancer Treatment. *Frontiers in Pharmacology*, 9, 2018.

[32] Fredenberg, S., Wahlgren, M., Reslow, M., and Axelsson, A. The mechanisms of drug release in poly (lactic-co-glycolic acid) -based drug delivery systems A review. *International Journal of Pharmaceutics*, 415, 2011.

[33] Kamaly, N., Yameen, B., Wu, J., and Farokzhad, O. C. Degradable Controlled-Release Polymers and Polymeric Nanoparticles: Mechanisms of Controlling Drug Release. *Chemical Reviews*, 116, 2016.

[34] Makadia, K. H. and Siegel, S. J. Poly Lactic-co-Glycolic Acid (PLGA) as Biodegradable Controlled Drug Delivery Carrier. *Polymers*, 3, 2011.

[35] Samadi, N., Abbadessa, A., Di Stefano, A., Van Nostrum, C. F., Vermonden, T., Rahimian, S., Teunissen, E. A., Van Steenbergen, M. J., Amidi, M., and Hennink, W. E. The effect of lauryl capping group on protein release and degradation of poly(d,l-lactic-co-glycolic acid) particles. *Journal of Controlled Release*, 172, 2013.

[36] Lu, Y., Sturek, M., and Park, K. Microparticles Produced by the Hydrogel Template Method for Sustained Drug Delivery. *International Journal of Pharmaceutics*, 461, 2014.

[37] Brown, L. R. Commercial challenges of protein drug delivery. *Expert Opinion on Drug Delivery*, 2, 2005.

[38] Houchin, M. L. and Topp, E. M. Chemical degradation of peptides and proteins in PLGA: A review of reactions and mechanisms. *Journal of Pharmaceutical Sciences*, 97, 2008.

[39] Schwendeman, S. P. Recent Advances in the Stabilization of Proteins Encapsulated in Injectable PLGA Delivery Systems. *Critical Reviews in Therapeutic Drug Carrier Systems*, 19, 2002.

[40] van de Weert, M., Hennink, W. E., and Jiskoot, W. Protein Instability in Poly (Lactic-co-Glycolic Acid) Microparticles. *Pharmaceutical research*, 17, 2000.

[41] Leemhuis, M., Kruijtzer, J. A. W., Nostrum, C. F. V., and Hennink, W. E. In Vitro Hydrolytic Degradation of Hydroxyl-Functionalized Poly (alpha-hydroxy acid)s. *Biomacromolecules*, 8, 2007.

[42] Ghassemi, A. H., Steenbergen, M. J. V., Talsma, H., van Nostrum, C. F., Jiskoot, W., Crommelin, D. J. A., and Hennink, W. E. Preparation and characterization of protein loaded microspheres based on a hydroxylated aliphatic polyester , poly (lactic-co-hydroxymethyl glycolic acid). *Journal of Controlled Release*, 138, 2009.

[43] Kazazi-Hyseni, F., van Vuuren, S., van der Giezen, D., Pieters, E., Ramazani, F., Rodriguez, S., Veldhuis, G., Goldschmeding, R., van Nostrum, C., Hennink, W., and Kok, R. Release and pharmacokinetics of near-infrared labeled albumin from monodisperse poly(d,l-lactic-co-hydroxymethyl glycolic acid) microspheres after subcapsular renal injection. *Acta Biomaterialia*, 22, 2015.

[44] Rahimian, S., Kleinovink, J. W., Fransen, M. F., Mezzanotte, L., Gold, H., Wisse, P., Overkleeft, H., Amidi, M., Jiskoot, W., Lowik, C. W., Ossendorp, F., and Hennink, W. E. Near-infrared labeled, ovalbumin loaded polymeric nanoparticles based on a hydrophilic polyester as model vaccine : In vivo tracking and evaluation of antigen-specific CD8+ T cell immune response. *Biomaterials*, 37, 2015.

[45] Samadi, N., van Steenbergen, M. J., van den Dikkenberg, J. B., Vermonden, T., van Nostrum, C. F., Amidi, M., and Hennink, W. E. Nanoparticles based on a hydrophilic polyester with a sheddable PEG coating for protein delivery. *Pharmaceutical Research*, 31, 2014.

[46] Ghassemi, A. H., Steenbergen, M. J. V., Barendregt, A., Talsma, H., Kok, R. J., van Nostrum, C. F., Crommelin, D. J. A., and Hennink, W. E. Controlled Release of Octreotide and Assessment of Peptide Acylation from Poly (D,L-lactide-co-hydroxymethyl glycolide) Compared to PLGA Microspheres. *Pharmaceutical Research*, 29, 2012.

[47] Rahimian, S., Fransen, M., F., Kleinovink, J. W., Riis Christensen, J., Amidi, M., Hennink, W. E., and Ossendorp, F. Polymeric nanoparticles for co-delivery of synthetic long peptide antigen and poly IC as therapeutic cancer vaccine formulation. *Journal of Controlled Release*, 10, 2015.

[48] Ritsema, J. A. S., Herschberg, E. M. A., Borgos, S. E., Løvmo, C., Schmid, R., te Welscher, Y. M., Storm, G., and van Nostrum, C. F. Relationship Between Polarities of Antibiotic and Polymer Matrix on Nanoparticle Formulations Based on Aliphatic Polyesters. *International Journal of Pharmaceutics*, 548, 2018.

[49] Shirangi, M., Hennink, W. E., Somsen, G. W., and Van Nostrum, C. F. Identification and Assessment of Octreotide Acylation in Polyester Microspheres by LC-MS/MS. *Pharmaceutical Research*, 32, 2015.

[50] Bae, Y. H. and Park, K. Targeted drug delivery to tumors: Myths, reality and possibility. *Journal of Controlled Release*, 153, 2011.

[51] Reineke, J. Terminology matters: There is no targeting, but retention. *Journal of Controlled Release*, 273, 2018.

[52] Ruenraroengsak, P., Cook, J. M., and Florence, A. T. Nanosystem drug targeting : Facing up to complex realities. *Journal of Controlled Release*, 141, 2010.

[53] Zhao, Z., Ukidve, A., Krishnan, V., and Mitragotri, S. Effect of physicochemical and surface properties on in vivo fate of drug nanocarriers. *Advanced Drug Delivery Reviews*, In press, 2019.

[54] Davis, M. E., Chen, Z., and Shin, D. M. Nanoparticle therapeutics: an emerging treatment modality for cancer. *Nature Reviews Drug Discovery*, 7, 2008.

[55] Kirtane, A. R., Siegel, R. A., and Panyam, J. A Pharmacokinetic Model for Quantifying the Effect of Vascular Permeability on the Choice of Drug Carrier : A Framework for Personalized Nanomedicine. *Pharmaceutical Nanotehcnology*, 104, 2015.

[56] Maeda, H., Bharate, G. Y., and Daruwalla, J. Polymeric drugs for efficient tumor-targeted drug delivery based on EPR-effect. *European Journal of Pharmaceutics and Biopharmaceutics*, 71, 2009.

[57] Ernsting, M. J., Murakami, M., Roy, A., and Li, S. D. Factors controlling the pharmacokinetics, biodistribution and intratumoral penetration of nanoparticles. *Journal of Controlled Release*, 172, 2013.

[58] Li, S.-D. and Huang, L. Pharmacokinetics and Biodistribution of Nanoparticles. *Molecular Pharmaceutics*, 5, 2008.

[59] Doshi, N. and Mitragotri, S. Macrophages Recognize Size and Shape of Their Targets. *PLoS ONE*, 5, 2010.

[60] Rahimian, S., Franse, M. F., Kleinovink, J. W., Amidi, M., Ossendorp, F., and Hennink, W. E. Particulate systems based on poly(lactic-co-glycolic)acid (PLGA) for immunotherapy of cancer. *Current Pharmaceutical Design*, 21, 2015.

[61] Singh, M., Chakrapani, A., and O'Hagan, D. Nanoparticles and microparticles as vaccine-delivery systems. *Expert Review of Vaccines*, 6, 2007.

[62] Vonarbourg, A., Passirani, C., Saulnier, P., and Benoit, J.-P. Parameters influencing the stealthiness of colloidal drug delivery systems. *Biomaterials*, 27, 2006.

[63] Barz, M., Luxenhofer, R., Zentel, R., and Vicent, M. J. Overcoming the PEG-addiction: well defined alternatives to PEG, from structure property relationships to better defined therapeutics. *Polymer Chemistry*, 2, 2011.

[64] Knop, K., Hoogenboom, R., Fischer, D., and Schubert, U. S. Poly (ethylene glycol) in Drug Delivery : Pros and Cons as Well as Potential Alternatives. *Angewandte Chemie - International Edition*, 49, 2010.

[65] Duncan, R. Development of HPMA copolymer anticancer conjugates: Clinical experience and lessons learnt. *Advanced Drug Delivery Reviews*, 61, 2009.

[66] Rabanel, M. J., Aoun, V., Elkin, I., Mokhtar, M., and Hildgen, P. Drug-Loaded Nanocarriers: Passive Targeting and Crossing of Biological Barriers. *Current Medicinal Chemistry*, 19, 2012.

[67] Danhier, F. To exploit the tumor microenvironment: Since the EPR effect fails in the clinic, what is the future of nanomedicine? *Journal of Controlled Release*, 244, 2016.

[68] Fang, J., Nakamura, H., and Maeda, H. The EPR effect: Unique features of tumor blood vessels for drug delivery, factors involved, and limitations and augmentation of the effect. *Advanced Drug Delivery Reviews*, 63, 2011.

[69] Lammers, T., Kiessling, F., Hennink, W. E., and Storm, G. Drug targeting to tumors: Principles, pitfalls and (pre-) clinical progress. *Journal of Controlled Release*, 161, 2012.

[70] Prabhakar, U., Maeda, H., Jain, R. K., Sevick-muraca, E. M., and Zamboni, W. Challenges and Key Considerations of the Enhanced Permeability and Retention Effect for Nanomedicine Drug Delivery in Oncology. *Cancer Research*, 73, 2013.

[71] Ojha, T., Pathak, V., Shi, Y., Hennink, W., Moonen, C., Storm, G., Kiessling, F., and Lammers, T. Pharmacological and Physical Vessel Modulation Strategies to Improve EPR-mediated Drug Targeting to Tumors. *Advanced Drug Delivery Reviews*, 119, 2017.

[72] Kunjachan, S., Pola, R., Gremse, F., Theek, B., Ehling, J., Moeckel, D., Hermanns-Sachweh, B., Pechar, M., Ulbrich, K., Hennink, W. E., Storm, G., Lederle, W., Kiessling, F., and Lammers, T. Passive versus active tumor targeting using RGD- and NGR-modified polymeric nanomedicines. *Nano Letters*, 14, 2014.

[73] Abd Ellah, N. H. and Abouelmagd, S. A. Surface functionalization of polymeric nanoparticles for tumor drug delivery: approaches and challenges. *Expert Opinion on Drug Delivery*, 14, 2017.

[74] Zhong, Y., Meng, F., Deng, C., and Zhong, Z. Ligand-directed active tumor-targeting polymeric nanoparticles for cancer chemotherapy. *Biomacromolecules*, 15, 2014.

[75] Muyldermans, S. and Lauwereys, M. Unique single-domain antigen binding fragments derived from naturally occurring camel heavy-chain antibodies. *Journal of Molecular Recognition*, 12, 1999.

[76] Kolkman, J. A. and Law, D. A. Nanobodies - From llamas to therapeutic proteins. *Drug Discovery Today: Technologies*, 7, 2010.

[77] Oliveira, S., Heukers, R., Sornkom, J., Kok, R. J., and Van Bergen En Henegouwen, P. M. P. Targeting tumors with nanobodies for cancer imaging and therapy. *Journal of Controlled Release*, 172, 2013.

[78] Arbabi-Ghahroudi, M. Camelid single-domain antibodies: Historical perspective and future outlook. *Frontiers in Immunology*, 8, 2017.

[79] Vincke, C., Loris, R., Saerens, D., Martinez-Rodriguez, S., Muyldermans, S., and Conrath, K. General strategy to humanize a camelid single - domain antibody and identification of a universal humanized nanobody scaffold. *Journal of Biological Chemistry*, 284, 2009.

[80] Oliveira, S., Schiffelers, R. M., van der Veeken, J., van der Meel, R., Vongpromek, R., van Bergen en Henegouwen, P. M. P., Storm, G., and Roovers, R. C. Downregulation of EGFR by a novel multivalent nanobody-liposome platform. *Journal of Controlled Release*, 145, 2010.

[81] Van Der Meel, R., Oliveira, S., Altintas, I., Haselberg, R., Van Der Veeken, J., Roovers, R. C., Van Bergen En Henegouwen, P. M. P., Storm, G., Hennink, W. E., Schiffelers, R. M., and Kok, R. J. Tumor-targeted Nanobullets: Anti-EGFR nanobody-liposomes loaded with anti-IGF-1R kinase inhibitor for cancer treatment. *Journal of Controlled Release*, 159, 2012.

[82] Talelli, M., Oliveira, S., Rijcken, C. J. F., Pieters, E. H. E., Etrych, T., Ulbrich, K., van Nostrum, R. C. F., Storm, G., Hennink, W. E., and Lammers, T. Intrinsically active nanobody-modified polymeric micelles for tumor-targeted combination therapy. *Biomaterials*, 34, 2013.

[83] Heukers, R., Altintas, I., Raghoenath, S., De Zan, E., Pepermans, R., Roovers, R. C., Haselberg, R., Hennink, W. E., Schiffelers, R. M., Kok, R. J., and Van Bergen en Henegouwen, P. M. P. Targeting hepatocyte growth factor receptor (Met) positive tumor cells using internalizing nanobody-decorated albumin nanoparticles. *Biomaterials*, 35, 2014.

[84] Zou, T., Dembele, F., Beugnet, A., Sengmanivong, L., Trepout, S., Marco, S., Marco, A. d., and Li, M. H. Nanobody-functionalized PEG-b-PCL polymersomes and their targeting study. *Journal of Biotechnology*, 214, 2015.

[85] Omar, N., Yan, B., and Salto-Tellez, M. HER2: An emerging biomarker in non-breast and non-gastric cancers. *Pathogenesis*, 2, 2015.

[86] Tai, W., Mahato, R., and Cheng, K. The role of HER2 in cancer therapy and targeted drug delivery. *Journal of Controlled Release*, 146, 2010.

[87] Kijanka, M. M., van Brussel, A. S. A., van der Wall, E., Mali, W. P. T. M., van Diest, P. J., van Bergen En Henegouwen, P. M. P., and Oliveira, S. Optical imaging of pre-invasive breast cancer with a combination of VHHs targeting CAIX and HER2 increases contrast and facilitates tumour characterization. *European Journal of Nuclear Medicine and Molecular Imaging*, 6, 2016.

[88] Kijanka, M., Warnders, F. J., El Khattabi, M., Lub-De Hooge, M., Van Dam, G. M., Ntziachristos, V., De Vries, L., Oliveira, S., and Van Bergen En Henegouwen, P. M. P. Rapid optical imaging of human breast tumour xenografts using anti-HER2 VHHs site-directly conjugated to IRDye 800CW for image-guided surgery. *European Journal of Nuclear Medicine and Molecular Imaging*, 40, 2013.

[89] Kijanka, M., van Donselaar, E. G., Müller, W. H., Dorresteijn, B., Popov-eleketi, D., el Khattabi, M., Verrips, C. T., van Bergen en Henegouwen, P. M. P., and Post, J. A. A novel immuno-gold labeling protocol for nanobody-based detection of HER2 in breast cancer cells using immuno-electron microscopy. *Journal of Structural Biology*, 199, 2017.

[90] Samadi, N. *Biodegradable nanoparticles based on aliphatic polyesters; towards intracellular delivery of protein therapeutics*. Thesis, Utrecht University, 2014.

[91] Ruoslahti, E. Rgd and Other Recognition Sequences for Integrins. *Annual Review of Cell and Developmental Biology*, 12, 1996.

[92] Brooks, P., Clark, R., and Cheresh, D. Requirement of vascular integrin $\alpha v\beta 3$ for angiogenesis. *Science*, 264, 1994.

[93] Desgrosellier, J. S. and Cherech, D. A. Integrins in cancer: biological implications in therapeutic opportunities. *Nature Reviews Cancer*, 10, 2010.

[94] Eble, J. A. and Haier, J. Integrins in Cancer Treatment. *Current Cancer Drug Targets*, 2006.

[95] Bogdanowich-Knipp, S. J., Chakrabarti, S., Williams, T. D., Dillman, R. K., and Siahaan, T. J. Solution stability of linear vs. cyclic RGD peptides. *Journal of Peptide Research*, 53, 1999.

[96] Haubner, R., Gratias, R., Diefenbach, B., Goodman, S. L., Jonczyk, A., and Kessler, H. Structural and functional aspects of RGD-containing cyclic pentapeptides as highly potent and selective integrin $\alpha v\beta 3$ antagonists. *Journal of the American Chemical Society*, 118, 1996.

[97] Gajbhiye, K. R., Gajbhiye, V., Siddiqui, I. A., and Gajbhiye, J. M. cRGD functionalised nanocarriers for targeted delivery of bioactives. *Journal of Drug Targeting*, 0, 2018.

[98] Liu, S. Radiolabeled Cyclic RGD Peptide Bioconjugates as Radiotracers Targeting Multiple Integrins. *Bioconjugate Chemistry*, 26, 2015.

[99] Park, J., Singha, K., Son, S., Kim, J., Namgung, R., Yun, C. O., and Kim, W. J. A review of RGD-functionalized nonviral gene delivery vectors for cancer therapy. *Cancer Gene Therapy*, 19, 2012.

[100] Schiffelers, R. M., Ansari, A., Xu, J., Zhou, Q., Tang, Q., Storm, G., Molema, G., Lu, P. Y., Scaria, P. V., and Woodle, M. C. Cancer siRNA therapy by tumor selective delivery with ligand-targeted sterically stabilized nanoparticle. *Nucleic Acids Research*, 32, 2004.

[101] Temming, K., Schiffelers, R. M., Molema, G., and Kok, R. J. RGD-based strategies for selective delivery of therapeutics and imaging agents to the tumour vasculature. *Drug Resistance Updates*, 8, 2005.

[102] Wang, F., Li, Y., Shen, Y., Wang, A., Wang, S., and Xie, T. The Functions and Applications of RGD in Tumor Therapy and Tissue Engineering. *International Journal of Molecular Sciences*, 14, 2013.

[103] Wang, X., Wang, H., Jiang, K., Zhang, Y., Zhan, C., Ying, M., Zhang, M., Lu, L., Wang, R., Wang, S., Burgess, D. J., and Wang, H. Liposomes with cyclic RGD peptide motif triggers acute immune response in mice. *Journal of Controlled Release*, 293, 2019.

[104] Canton, I. and Battaglia, G. Endocytosis at the nanoscale. *Chemical Society Reviews*, 41, 2012.

[105] Mailaender, V. and Landfester, K. Interaction of nanoparticles with cells. *Biomacromolecules*, 10, 2009.

[106] Mammen, M., Choi, S.-K., and Whitesides, G. M. Polyvalent Interactions in Biological Systems: Implications for Design and Use of Multivalent Ligands and Inhibitors. *Angewandte Chemie International Edition*, 37, 1998.

[107] Xu, S., Olenyuk, B. Z., Okamoto, C. T., and Hamm-Alvarez, S. F. Targeting receptor-mediated endocytotic pathways with nanoparticles: Rationale and advances. *Advanced Drug Delivery Reviews*, 65, 2013.

[108] Muro, S. New biotechnological and nanomedicine strategies for treatment of lysosomal storage disorders. *Wiley Interdisciplinary Reviews: Nanomedicine and Nanobiotechnology*, 2, 2010.

[109] Selby, L. I., Cortez-Jugo, C. M., Such, G. K., and Johnston, A. P. R. Nanoescapology: progress toward understanding the endosomal escape of polymeric nanoparticles. *Wiley Interdisciplinary Reviews: Nanomedicine and Nanobiotechnology*, 9, 2017.

[110] Varkouhi, A. K., Scholte, M., Storm, G., and Haisma, H. J. Endosomal escape pathways for delivery of biologicals. *Journal of Controlled Release*, 151, 2011.

[111] Selbo, P. K., Høgset, A., Prasmickaite, L., and Berg, K. Photochemical Internalisation: A Novel Drug Delivery System. *Tumor Biology*, 23, 2002.

[112] Selbo, P. K., Weyergang, A., Høgset, A., Norum, O. J., Berstad, M. B., Vikdal, M., and Berg, K. Photochemical internalization provides time- and space-controlled endolysosomal escape of therapeutic molecules. *Journal of Controlled Release*, 148, 2010.

[113] Sultan, A. A., Jerjes, W., Berg, K., Høgset, A., Mosse, C. A., Hamoudi, R., Hamdoon, Z., Simeon, C., Carnell, D., Forster, M., and Hopper, C. Disulfonated tetraphenyl chlorin ($TPCS_{2a}$)-induced photochemical internalisation of bleomycin in patients with solid malignancies: a phase 1, dose-escalation, first-in-man trial. *The Lancet Oncology*, 17, 2016.

[114] Selbo, P. K., Finnesand, L., Ekholt, K., Berg, K., Høgset, A., and Sturgess, R. Photochemical internalization (PCI) of gemcitabine and chemotherapy for the treatment of cholangiocarcinomas From lab bench to bedside. *Photodiagnosis and Photodynamic Therapy*, 17, 2017.

Chapter **2**

Insights into maleimide - thiol conjugation chemistry: conditions for efficient surface functionalization of nanoparticles for receptor targeting

Lucía Martínez-Jothar[†], Sofia Doulkeridou[‡], Raymond M. Schiffelers[§], Javier Sastre Torano[¶], Sabrina Oliveira[†,‡], Cornelus F. van Nostrum[†] and Wim E. Hennink[†]

† Department of Pharmaceutics, Utrecht Institute for Pharmaceutical Sciences, Utrecht University, Utrecht, The Netherlands

‡ Division of Cell Biology, Department of Biology, Utrecht University, Utrecht, the Netherlands

§ Department of Clinical Chemistry and Haematology, University Medical Center Utrecht, Utrecht, the Netherlands

¶ Department of Chemical Biology & Drug Discovery, Utrecht Institute for Pharmaceutical Sciences, Utrecht University, Utrecht, the Netherlands

Journal of Controlled Release 2018, 282, 101 - 109

Abstract

Maleimide-thiol chemistry is widely used for the design and preparation of ligand-decorated drug delivery systems such as poly(lactide-co-glycolide) (PLGA) based nanoparticles (NPs). While many publications on nanocarriers functionalized exploiting this strategy are available in the literature, the conditions at which this reaction takes place vary amongst publications. This paper presents a comprehensive study on the conjugation of the peptide cRGDfK and the nanobody 11A4 (both containing a free thiol group) to maleimide functionalized PLGA NPs by means of the maleimide-thiol click reaction. The influence of different parameters, such as the nanoparticles preparation method and storage conditions as well as the molar ratio of maleimide to ligand used for conjugation, on the reaction efficiency has been evaluated. The NPs were prepared by a single or double emulsion method using different types and concentrations of surfactants and stored at 4 or 20 °C before reaction with the targeting moieties. Several maleimide to ligand molar ratios and different reaction times were studied and the conjugation efficiency was determined by quantification of the not-bound ligand by liquid chromatography. The kind of emulsion used to prepare the NPs as well as the type and concentration of surfactant used had no effect on the conjugation efficiency. Reaction between the maleimide groups present in the NPs and cRGDfK was optimal at a maleimide to thiol molar ratio of 2:1, reaching a conjugation efficiency of 84 ± 4% after 30 minutes at room temperature in 10 mM HEPES pH 7.0. For 11A4 nanobody the optimal reaction efficiency, 58 ± 12%, was achieved after 2 hours of incubation at room temperature in PBS pH 7.4 using a 5:1 maleimide to protein molar ratio. Storage of the NPs at 4 °C for 7 days prior to their exposure to the ligands resulted in approximately 10% decrease in the reactivity of maleimide in contrast to storage at 20 °C which led to almost 40% of the maleimide being unreactive after the same storage time. Our findings demonstrate that optimization of this reaction, particularly in terms of reactant ratios, can represent a significant increase in the conjugation efficiency and prevent considerable waste of resources.

1 Introduction

The capacity of nanoparticulate drug delivery systems to improve the therapeutic index (ratio of efficacy/toxicity) of pharmacologically active compounds, such as drugs and drug candidates as well as protein and nucleic acid based drugs, makes these particles promising systems for the treatment of different diseases. Targeting can be achieved by relying on the physicochemical properties of the drug-loaded nanoparticle and on the anatomy and physiology of the target, leading to accumulation of the drug delivery system mostly on sites with increased permeability of the vascular endothelium, for instance tumors and inflamed tissues [1–4]. Cells of the reticuloendothelial system (e.g. macrophages present in liver and spleen) can also be targeted since they are in charge of the clearance of foreign bodies from the circulation and can easily take up nanocarriers [5–7]. Ligand decorated systems are more suitable for the treatment of pathologies unrelated to the reticuloendothelial system or in which the structure of the endothelium is not compromised. To achieve this, the nanocarrier is functionalized with a ligand that specifically recognizes and interacts with receptors preferably overexpressed on the pathological cells. This in turn can result in an increase in the accumulation and retention of the active principle in the diseased tissue/organ. Since ligand decorated systems are normally internalized by the target cells, they can also be used for the delivery of drugs that do not have the ability to penetrate the cellular membrane by Fickian diffusion, for instance pDNA, siRNA or mRNA [8] as well as therapeutic proteins that have their target intracellularly [9,10]. Although most of the ligand targeted systems currently under clinical evaluation are developed for cancer treatment [11], other applications such as vaccination [12,13] and drug delivery through the blood brain barrier [14,15] are also possible.

As mentioned, receptor-mediated targeting requires the covalent attachment of targeting ligands at the surface of nano-sized delivery vehicles that can be performed by several methods including carbodiimide chemistry [16], reactions with N-hydrosuccinimide (NHS) active esters, click chemistry reactions such as azide-alkyne cycloaddition and thiol-ene reaction [17,18], and the use of thiol reactive maleimide groups. The reaction of maleimide derivatives and thiol containing biological molecules was reported more than 55 years ago [19,20], but it was not until the early 1980s that its potential as a tool for the functionalization of nanocarriers was shown and exploited [21]. Importantly, the commercial availability of lipids and polymers that contain maleimide groups has enabled the fabrication of liposomes, polymeric nanoparticles, polymeric micelles, polymeric nanogels and polymersomes that can be conjugated to thiol containing ligands to target specific cells or tissues [22–24]. In comparison

to more recently developed functionalization strategies, the maleimide-thiol reaction is still frequently applied in functionalization protocols because of the high reactivity of maleimide under mild conditions (i.e. room temperature and aqueous buffers), its selectivity towards thiol groups at physiological pH and the formation of a thioether bond that is relatively stable under most conditions[25]. Additionally, this reaction makes use of the thiol group of cysteine residues naturally present in peptides and proteins or that can be easily introduced in these molecules. However, under certain conditions such as alkaline pH values (pH $\geq$ 8)[26,27] maleimide is susceptible to hydrolysis resulting in ring opening and formation of a maleic acid amide derivative that is not reactive towards thiol groups[28–30]. Additionally, when maleimide-functionalized building blocks are used in the fabrication of nanocarriers, the preparation method can also have a detrimental effect on the stability of the maleimide groups. For instance, liposome purification by dialysis in PBS (pH 7.0 - 7.5) for 5 hours, resulted in a 50% decrease in maleimide reactivity[31], which highlights the importance of assessing the compatibility of the preparation procedure with the preservation of the structure of maleimide.

Even though maleimide-thiol chemistry has been widely used, the conditions for preparation and functionalization of maleimide containing liposomes and polymer-based drug delivery vehicles, such as poly(lactic acid), poly(ε -caprolactone), or poly(lactic-co-glycolic acid) (PLGA) nanoparticles (NPs), often differ widely between publications (Table S1). While this speaks to the robustness of the aforementioned conjugation reaction, it also brings into question the efforts being done to evaluate and optimize the reaction conditions. In this regard, the current work provides an in-depth study of the influence of preparation, handling and functionalization conditions on the reactivity of maleimide groups incorporated in PLGA based nanocarriers. NPs based on blends of PLGA and maleimide-poly(ethylene glycol) $(PEG)_{5,000}$-PLGA were chosen as a model formulation due to the well documented and appealing properties of PLGA systems for targeted drug delivery including their biocompatibility, biodegradability, relatively easy production and overall tailorability[32–36]. The last point allows for control of properties such as degradation/release profile, stealth behavior (through the incorporation of PEG chains in the formulation) and, as previously mentioned, decoration of the surface of the particles with targeting moieties. In the present study, two ligands of different molecular weight were chosen, both with potential applications in cancer treatment: cRGDfK and 11A4. cRGDfK is a cyclic peptide (approx. 700 Da) able to target the integrin $\alpha_v\beta_3$ which is overexpressed in some types of tumors including breast cancer and has been correlated with metastasis[37]. The ability of the RGD motif to bind to the aforementioned integrin has been

explored as a tool for drug targeting to tumors by preparing drug-RGD conjugates or RGD-targeted carriers[38–41]. Additionally, several radiolabeled RGD peptides for imaging of tumor angiogenesis are currently undergoing clinical trials[42]. The nanobody 11A4 is a C-terminal cysteine modified molecule capable of selectively binding to the HER-2 receptor[43] overexpressed in 15 - 20% breast cancers[44]. Nanobodies (approx. 15 kDa) are the variable fragments of heavy chain antibodies from camelids[45]. Nanobodies can be easily produced by recombinant technologies and have favorable physicochemical properties, such as high solubility and stability, as well as a relatively small size as compared to full sized antibodies which allows them to efficiently bind to epitopes that are inaccessible to antibodies[46–48].

This paper presents an in-depth study on the functionalization of maleimide-PEG-PLGA NPs with cRGDfK and 11A4 by means of maleimide-thiol conjugation chemistry and explores the influence of the NPs preparation and storage conditions on the efficiency of conjugation. Additionally, reactant ratios and reaction kinetics are studied for both ligands with the objective of identifying the critical parameters and finding the optimal conditions for the maleimide-thiol conjugation reaction.

2 Experimental section

2.1 Chemicals

PLGA (50:50 ratio DL-lactide / glycolide, IV 0.39 dl/g, M_w ~44,000 Da) was obtained from Purac (Gorinchem, The Netherlands). Methoxy poly(ethylene glycol)-b-poly(lactide-co-glycolide) ($mPEG_{5,000}$-$PLGA_{20,000}$) and poly(lactide-co-glycolide)-b-poly(ethylene glycol)-maleimide (maleimide-$PEG_{5,000}$-$PLGA_{20,000}$) were purchased from Polyscitech, Akina Inc (West Lafayette, IN, USA). Poly(vinyl alcohol) (PVA) of M_w 30,000 - 70,000 Da, 87 - 90% hydrolyzed, sodium cholate hydrate, dimethyl sulfone ($DMSO_2$) and methoxy poly(ethylene glycol)-maleimide (M_n 2,000 Da) were acquired from Sigma-Aldrich. c[RGDfK(Ac-SCH_2CO)] (M_w: 719.8 g/mol) (Figure S1) was purchased from Peptides International (Louisville, KY, USA).

2.2 Nanoparticle preparation and characterization

Polymeric NPs were prepared using blends of PLGA and maleimide-PEG-PLGA. For particles prepared using the double emulsion solvent evaporation method[49,50], the polymers were dissolved in dichloromethane at 5% w/v of

polymer and 4:1 or 9:1 w/w ratio of PLGA and maleimide-PEG-PLGA, respectively. NPs prepared using a 4:1 w/w ratio were used for conjugation with cRGDfK, while those prepared with a 9:1 w/w ratio were used for conjugation with 11A4.

A W/O emulsion consisting of 100 μL of water and 1 mL of the polymer solution was prepared by probe sonication for 1 minute at 10% power (SONOPULS HD 2200 Bandelin, Berlin, Germany). This emulsion (1.1 mL) was subsequently added to 10 mL of an external aqueous phase containing either sodium cholate 1% w/v (pH 7.1) or PVA 1, 2.5 or 5% w/v in water. The samples were then sonicated for 2 minutes at 10% power to form a W/O/W emulsion. The double emulsion method was used for NPs preparation because they are intended for future application as a carrier of hydrophilic molecules. After evaporation of the organic solvent under stirring at room temperature for 2 hours, the NPs were collected by centrifugation for 20 minutes, 20,000 g at 4 °C, washed 2 times with 10 mM HEPES (pH 7.0) and one time with MilliQ water. The NPs were stored in PBS (8.0 g NaCl, 1.15 g Na_2HPO_4, 0.2 g KCl and 0.2 g KH_2PO_4 in 1 L of water, pH 7.4) or HEPES at 4 °C until further use. Control NPs were prepared similarly from a blend of PLGA and mPEG-PLGA in a 4:1 or 9:1 w/w ratio.

Maleimide-PEG-PLGA NPs were also prepared by single emulsion method following a procedure similar as described for the double emulsion. Briefly, PLGA (40 mg) and maleimide-PEG-PLGA (10 mg) were dissolved in 1 mL of dichloromethane (final concentration of polymer 5% w/v), added to 10 mL of an external aqueous phase containing PVA 5% w/v in water and subject to sonication for 2 minutes at 10%. After evaporation of the solvent the NPs were collected, washed and stored as described for the double emulsion preparation.

The weight fraction of PEG present in the NPs was determined by ^{1}H-NMR. PLGA and maleimide-PEG-PLGA in 4:1 or 9:1 w/w ratio respectively, were dissolved in deuterated chloroform ($CDCl_3$). Maleimide-PEG-PLGA NPs prepared by double emulsion method using the procedure described above were freeze dried and dissolved in $CDCl_3$. The blends of PLGA and maleimide-PEG-PLGA of known composition and the NPs were analyzed by ^{1}H-NMR and the PEG weight fraction (%) in the samples was determined based on the integrals of the signals of PEG, lactic acid and glycolic acid, as follows[49]:

$$I_{\text{PEG}} = (I_{3.6})/4 \times \text{M}_w \text{ PEG unit}$$
$$I_{\text{glycolic acid}} = (I_{4.6-4.9})/2 \times \text{M}_w \text{ glycolic acid unit}$$
$$I_{\text{lactic acid}} = (I_{5.1-5.3})/1 \times \text{M}_w \text{ lactic acid unit}$$
$$\text{PEG weight fraction (\%)} = [I_{\text{PEG}}/(I_{\text{PEG}} + I_{\text{glycolic acid}} + I_{\text{lactic acid}})] \times 100$$

The size of the NPs was determined by Dynamic Light Scattering (ALV CGS-3, Malvern) at 25 °C in deionized water and the zeta potential was measured in HEPES 10 mM pH 7.0 at 25 °C (Zetasizer Nano Z, Malvern). An aliquot of NPs suspended in deionized water was freeze dried at -40 °C, <1 mbar (Christ Alpha 1-2 freeze dryer, Osterode am Harz, Germany).

2.3 Hydrolytic stability of maleimide under NPs preparation conditions

A solution of 0.5 mg/mL of methoxy poly(ethylene glycol)-maleimide in HEPES 10 mM pH 7.0 was treated similarly to the polymer solutions used for NPs preparation. Briefly, 10 mL of the PEGylated maleimide in HEPES was sonicated for 3 minutes at 10% power (SONOPULS HD 2200 Bandelin, Berlin, Germany) and stirred for 2 hours at room temperature. The NPs washing procedure was mimicked by centrifuging the solution for 20 minutes at 20,000 g and at 4 °C. Four centrifugation cycles were conducted with a waiting time of 20 minutes between the cycles, which is the approximate time for washing/resuspension of the actual polymeric NPs. Samples of the PEGylated maleimide solution were taken before treatment, directly after sonication and at the end of the procedure (sonication + washings). The maleimide content in the samples was determined by UV absorbance at 302 nm [29,51,52] (Shimadzu UV-Vis Spectrophotometer UV 2450) using a calibration curve obtained by preparing solutions of methoxy poly(ethylene glycol)-maleimide in PBS (pH 7.4) in a concentration range of 0.1 - 0.8 mg/mL. After UV analysis, the samples were freeze dried, resuspended in deuterium oxide (D_2O) and their PEG content was determined by ^{1}H-NMR analysis using $DMSO_2$ as internal standard.

2.4 Preparation of ligands for conjugation to maleimide-PEG-PLGA NPs

Prior to the conjugation reaction, the peptide c[RGDfK(Ac-SCH_2CO)] bearing one protected thiol group on the lysine residue (structure of the peptide

is shown in Scheme S1) was dissolved in HEPES 10 mM / ethylenediaminetetraacetic acid (EDTA) 0.4 mM (pH 7.0). Deprotection was conducted by addition of 1:10 v/v of deacetylation buffer (HEPES 10 mM / hydroxylamine 0.5 M / EDTA 0.4 mM pH 5.5) (Scheme S1), followed by incubation for 30 minutes at room temperature[53] (the molecular weight of the deprotected peptide, as determined by LC-MS analysis was 678.5 Da) (Figure S2).

The 11A4 nanobody bearing a C-terminal cysteine followed by a FLAG tag (theoretical molecular weight 14,813 Da) was produced in BL21 bacteria and purified by protein A affinity chromatography, as described elsewhere[43]. To guarantee the presence of the free thiol on the nanobody, the protein was exposed to reducing conditions for 15 minutes at room temperature in PBS (8.0 g NaCl, 1.15 g Na_2HPO_4, 0.2 g KCl and 0.2 g KH_2PO_4 in 1 L of water, pH 7.4) / 20 mM Tris(2-carboxyethyl)phosphine hydrochloride / 0.4 mM EDTA[54]. The reducing agent was removed using Zeba Spin Desalting columns, with buffer exchange to PBS / EDTA 0.4 mM (pH 7.4), before the nanobody was incubated with the NPs.

2.5 Conjugation of cRGDfK and 11A4 to maleimide-PEG-PLGA NPs

The general procedure for the reaction between maleimide-PEG-PLGA NPs and the targeting ligands was the following: a NPs suspension (prepared by either single emulsion using 5% w/v PVA or by double emulsion using sodium cholate 1% w/v or PVA 1, 2.5 or 5% w/v) was prepared in deionized water and its concentration was determined by taking an aliquot and freeze drying it overnight at -40 °C, <1 mbar (Christ Alpha 1-2 freeze dryer, Osterode am Harz, Germany). The NPs suspensions of known concentration were used to prepare NPs samples for reaction with the targeting ligands. For example, aliquots containing 1 or 3 mg of NPs were taken from the NPs suspension and their volume was adjusted to 300 μL with PBS (8.0 g NaCl, 1.15 g Na_2HPO_4, 0.2 g KCl and 0.2 g KH_2PO_4 in 1 L of water, pH 7.4) / 0.4 mM EDTA, or to 600 μL using HEPES (pH 7.0) / 0.4 mM EDTA, respectively. The samples prepared in HEPES were used for reaction with cRGDfK and those prepared with PBS for reaction with 11A4.

The NPs suspensions were incubated with cRGDfK at molar ratios 3:1, 2:1 and 1:1 of maleimide-PEG-PLGA to peptide, or with 11A4 at molar ratios of 20:1, 10:1, 5:1, 2:1 and 1:1 of maleimide-PEG-PLGA to protein. As an example, for the 1:1 ratio maleimide-PEG-PLGA to 11A4, 59 μg of protein was used for conjugation with 1 mg of NPs; while for 1:1 ratio maleimide-PEG-PLGA to cRGDfK, 5 μg of peptide was used for conjugation with 1 mg

of NPs. The samples were placed on a nutating mixer and after incubation at room temperature, pH 7.0 - 7.4 (for cRGDfK and 11A4 respectively), for 2 hours (unless stated otherwise), the NPs were recovered by centrifugation for 10 minutes, 3,000 g, 4 °C, and washed once with PBS. The unbound ligands present in the supernatants were quantified by HPLC (for cRGDfK) or UPLC (for 11A4) as described in the section Quantification of cRGDfK and 11A4 by HPLC or UPLC to determine the conjugation efficiencies. Based on the obtained results, the maleimide-PEG-PLGA to ligand molar ratios resulting in highest conjugation efficiencies, namely 2:1 for cRGDfK and 5:1 for 11A4, were chosen for other tests.

The influence of the NPs preparation conditions on the efficiency of the maleimide - thiol reaction was evaluated by conjugating cRGDfK to NPs prepared by a single or double emulsion method. The influence of the surfactant used for NPs preparation on the conjugation efficiency was also studied by conjugating cRGDfK and 11A4 to NPs prepared by a double emulsion method using either sodium cholate 1% w/v or PVA 1, 2.5 or 5% w/v. Conjugation was done at maleimide to ligand molar ratios of 2:1 for cRGDfK and 5:1 for 11A4.

To obtain insight into the reaction kinetics, the targeting ligands cRGDfK and 11A4 were incubated with maleimide-PEG-PLGA NPs at 2:1 and 5:1 maleimide to ligand molar ratios respectively, for different times (5 minutes to 16 hours), after which the samples were placed in an ice bath and subsequently centrifuged (3,000 g, 10 minutes, 4 °C) in order to recover and quantify the unbound ligand by HPLC as detailed in the section Quantification of cRGDfK and 11A4 by HPLC or UPLC to determine the conjugation efficiencies.

For determining the stability of the maleimide groups, PLGA NPs containing 20% maleimide-PEG-PLGA were stored either at 4 °C or room temperature (∼20 °C) in buffer HEPES 10 mM / EDTA 0.4 mM (pH 7.0) for 1 to 7 days, after which they were subjected to conjugation with cRGDfK at a 2:1 maleimide to ligand molar ratio as described above. The stability of maleimide was calculated by comparing the conjugation efficiency obtained immediately after NPs preparation (T_0) to the ones found at the subsequent incubation times.

2.6 Quantification of cRGDfK and 11A4 by HPLC or UPLC to determine the conjugation efficiencies

Deprotected cRGDfK was quantified by HPLC (Waters Alliance System) using a XBridge BEH C18 column (3.5 μm, 100 mm x 2.1 mm, Waters) and a gradient from 100% eluent A (5.0% ACN, 94.9% water, 0.1% acetic acid) to

75% eluent B (94.9% ACN, 5.0% water, 0.1% acetic acid) over 12 minutes, and subsequently 100% eluent B for 1 minute. The injection volume was 50 μL and the peptide was detected by absorbance at 214 nm (detection limit was 2 μg/mL). Standard solutions of deprotected cRGDfK (2 - 30 μg/mL in HEPES 10 mM / EDTA 0.4 mM) were used for calibration (Figure S3).

Quantification of 11A4 was performed by UPLC (Acquity UPLC) using a BEH C4 300Å column (1.7 μm, 50 mm x 2.1 mm, Waters) using a gradient from 100% eluent A (5.0% ACN, 94.9% water, 0.1% trifluoroacetic acid) to 100% eluent B (99.9% ACN, 0.1% trifluoroacetic acid) over 5 minutes (Figure S4). The injection volume was 7.5 μL, the protein was detected by fluorescence (excitation at 280 nm, emission at 340 nm) and the detection limit was 5 μg/mL. Standard solutions of 11A4 (5 - 100 μg/mL in PBS / EDTA 0.4 mM) were used for calibration (Figure S5).

The conjugation efficiency was calculated as follows:

$$\text{Conjugation efficiency (\%)} = \left(1 - \frac{\text{Ligand in the supernatant } \left(\frac{\mu g}{mL}\right)}{\text{Ligand added in the conjugation reaction } \left(\frac{\mu g}{mL}\right)}\right) \times 100\%$$

Ligand in the supernatant is the sum of the amount of cRGDfK or 11A4 found in the supernatant after recovery of the NPs at the end of the conjugation reaction and the amount of ligand found in the solution used to wash the NPs pellet. As controls, NPs prepared from a blend of PEG-PLGA and PLGA (thus lacking maleimide groups) were exposed to cRGDfK or 11A4 under the same conditions as NPs containing maleimide groups.

3 Results and Discussion

3.1 Nanoparticle preparation

Maleimide functionalized PEG-PLGA NPs were prepared by emulsification of dichloromethane solutions of PLGA and maleimide-PEG-PLGA in an aqueous phase containing PVA or sodium cholate as surfactant and subsequent evaporation of the solvent. The NPs were washed and collected by centrifugation, and the chemical composition of the isolated nanoparticles was analyzed by ^{1}H-NMR (Figure S6A). Additionally, the PEG signal can be detected by ^{1}H-NMR after NPs suspension in D_2O (Figure S6B). The PEG peak for NPs suspended in D_2O is broader as compared to those dissolved in $CDCl_3$, which can be explained by a reduced mobility of the PEG chains anchored to the surface of the NPs[55–57]. The weight fraction of PEG in the NPs was determined

by ^{1}H-NMR analysis of blends of PLGA and maleimide-PEG-PLGA (4:1 or 9:1 w/w ratio, respectively) and of NPs dissolved in $CDCl_3$ (Figure S7). This analysis confirmed the quantitative incorporation of maleimide-PEG-PLGA in the NPs (Table S2). The NPs prepared had diameters in the range of 300 - 360 nm, with larger sizes being observed for NPs with higher maleimide-PEG-PLGA content. The size distributions were narrow as reflected by the low PDI values (∼0.1). Slightly negative zeta potentials (∼ -7.0 mV) were obtained for both types of NPs (Table S3), which can be explained by the shielding of the negatively charged carboxyl end groups of PLGA (uncapped polymer).

3.2 Hydrolytic stability of maleimide under NPs preparation conditions

Possible hydrolysis of maleimide (Figure S8) can be followed by UV-Vis spectroscopy [29,52] since as a cyclic imide it absorbs at ∼300 nm while its hydrolysis product, maleamic acid, lacks absorbance at this wavelength [51]. To investigate whether the NPs preparation method results in the hydrolysis of maleimide groups, PEG-maleimide in an aqueous buffer was subjected to similar conditions as those used for NPs preparation (i.e. sonication and incubation at pH 7.0 and 20 °C for 2 - 5 hours) and the maleimide content was monitored at 302 nm. Compared to the PEGylated maleimide control (sample not subjected to sonication or mimicking of the washings), the concentration of maleimide in the treated samples decreased only by 15 ± 1% (n=2) under the experimental conditions. ^{1}H-NMR analysis of the samples in D_2O, using $DMSO_2$ as internal standard, confirmed that the PEG content remained constant in the samples during the procedure, which indicates that the decrease in the UV signal of maleimide can be attributed to its hydrolysis and not to a decrease in the concentration of PEG-maleimide e.g. precipitation of the product. Since the decrease in the signal of maleimide became apparent after sonication, and because the rate of hydrolysis is known to increase at higher temperatures [52], the hydrolysis of maleimide is likely caused by an increase in temperature during sonication of the sample.

3.3 Characterization of maleimide-PEG-PLGA NPs functionalized with cRGDfK or 11A4

The size and charge of PEG-PLGA NPs and maleimide-PEG-PLGA NPs was monitored before and after incubation with cRGDfK and 11A4 (Table 1). The negative control consisting of NPs containing mPEG-PLGA without maleimide functionalities did not show conjugation nor binding of either

cRGDfK or 11A4, while both ligands could effectively be coupled to the NPs containing maleimide-PEG-PLGA. This finding shows that the functionalization of NPs is indeed established via the chemical conjugation reaction between maleimide and the thiol group present in the ligands and not by physical interactions.

Table 1: Size, zeta potential and conjugation efficiency of polymeric NPs of different compositions[a] incubated with cRGDfK and 11A4[b]

PEGylated polymer content (%w/w)	Ligand used for conjugation	Diameter (nm)	PDI	Zeta potential (mV)	Conjugation efficiency (%)
10% PEG-PLGA	None	296 ± 9	0.09 ± 0.02	-7.0 ± 0.3	NA
10% PEG-PLGA	11A4	309 ± 5	0.09 ± 0.07	-6.7 ± 0.4	0
10% maleimide-PEG-PLGA	None	294 ± 5	0.10 ± 0.01	-7.5 ± 0.3	NA
10% maleimide-PEG-PLGA	11A4	311 ± 1	0.08 ± 0.01	-13.6 ± 0.8	45
20% PEG-PLGA	None	322 ± 4	0.03 ± 0.00	-5.7 ± 0.2	NA
20% PEG-PLGA	cRGDfK	329 ± 5	0.03 ± 0.01	-5.8 ± 0.3	0
20% maleimide-PEG-PLGA	None	356 ± 4	0.15 ± 0.02	-8.4 ± 0.3	NA
20% maleimide-PEG-PLGA	cRGDfK	353 ± 6	0.10 ± 0.01	-9.1 ± 0.0	86

[a]: NPs prepared by double emulsion method, n=1.
[b]: Conjugation reaction performed in molar ratios of 2:1 maleimide-polymer to cRGDfK and 5:1 maleimide-polymer to 11A4.

Conjugation of the cyclic peptide cRGDfK to the maleimide-PEG-PLGA NPs did not significantly alter their size and zeta potential. Similar zeta potentials for nanoparticles before and after conjugation to RGD derivatives have also been reported by other authors [58,59]. The diameter of NPs decorated with 11A4 was almost 20 nm larger than the particles before conjugation and a slight increase in PDI for the former was also observed. The dimensions of the nanobody are 3 x 3 x 4 nm [60] and therefore its attachment to the surface of the NPs can be expected to result in an increase in their hydrodynamic diameter of up to 10 nm, which is close to the increase observed for the NPs. Most notably, the zeta potential of the NPs became more negative after conjugation to 11A4. The pI of 11A4 (determined by the ExPASy ProtParam Tool) is 7.94, which would confer a slightly positive charge under the conditions tested (pH 7.4). Nonetheless, this value refers to the charge of the nanobody based on its amino acid sequence, while in reality the folded form of the protein is present on the

NPs surface, meaning that the amino acid residues exposed to the medium may actually result in an overall negative charge.

3.4 Conjugation of cRGDfK and 11A4 to maleimide-PEG-PLGA NPs: effect of maleimide-PEG-PLGA to ligand molar ratio

One of the main parameters to consider for functionalization of maleimide-PEG-PLGA NPs is the molar ratio between the ligand and the reactive surface group. However, authors seldom report optimization studies for their formulation and, in some cases, the molar ratios of maleimide to ligand used for the reaction are not even reported (see Table S1). In this work, the relationship between the ratios of reactants and the coupling efficiency was evaluated by conjugating cRGDfK and 11A4 to maleimide-PEG-PLGA NPs at different maleimide polymer to ligand molar ratios. For this set of experiments, as well as all others described from here on, NPs with 10 and 20% w/w maleimide-PEG-PLGA were prepared which were subsequently incubated with 11A4 and cRGDfK, respectively. For conjugation of cRGDfK we chose a higher maleimide content since this peptide is much smaller than the nanobody and occupies less space on the surface of the NPs. The efficiencies of the conjugation reaction are shown in Figure 1.

At a molar excess of maleimide units, and equal reaction time (2 h), higher maximum conjugation efficiencies were observed for cRGDfK (almost 100% at a molar ratio of 3 maleimide-PEG-PLGA to 1 cRGDfK as compared to 11A4 (around 70% at a 20:1 ratio), which can be explained by the larger size of the protein compared to that of the peptide. The thiol group of cRGDfK is present on the lateral chain of a lysine residue (Scheme S1) and is therefore present on the outside of the cyclic structure, which makes it excellently accessible for reaction with the maleimide groups present on the surface of the NPs. In line with our observations, high conjugation efficiencies ($> 95\%$) have been previously reported for cRGDfK to liposomes and to maleimide-PEG-poly(lactic acid) NPs when using an excess of maleimide[53,61].

Figure 1 also shows that with an increasing amount of peptide or protein with respect to maleimide units, a decrease in conjugation efficiency was observed. For the nanobody, the use of a 5:1 maleimide to protein molar ratio during the reaction resulted in a conjugation efficiency of $58 \pm 12\%$. In contrast, at equimolar or even a two-fold excess of maleimide the coupling efficiency was $13 \pm 4\%$ and $31 \pm 9\%$ respectively. The bulkier nature of the 11A4 molecules already bound to the NPs surface very likely hinder accessi-

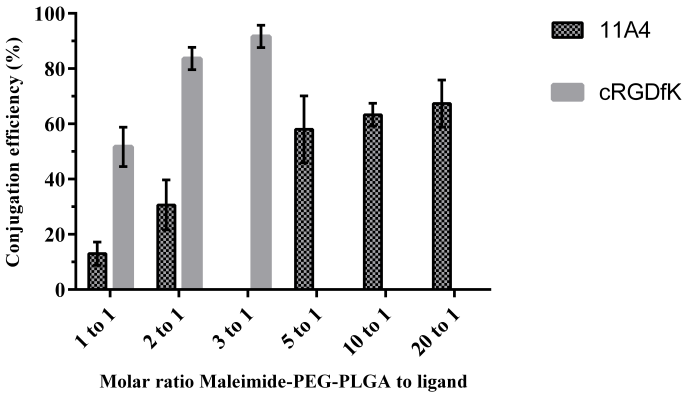

Figure 1: Conjugation efficiencies (%) at different maleimide-PEG-PLGA to ligand molar ratios. Conjugation efficiency to cRGDfK and 11A4 (n=3, except for 11A4 1:1 ratio). NPs containing 10% maleimide-PEG-PLGA were used for conjugation to 11A4 and NPs with 20% maleimide-PEG-PLGA were used for reaction with cRGDfK. NPs were prepared using the double emulsion solvent evaporation method.

bility of unbound protein present in the bulk to neighboring coupling sites. In other words, a more cost-effective preparation of protein-targeted drug delivery systems can be achieved when the stoichiometry is optimized and in this case a larger excess (5:1) of maleimide in respect to 11A4 is used. For a smaller ligand like cRGDfK steric hindrance is less likely to have a large impact on the efficiency of the reaction and at a 1:1 ratio of cRGDfK peptide to maleimide, 52 ± 7% of the peptide was conjugated. Taking into account that ∼90% of the PEG-maleimide used for NPs preparation was incorporated (Table S2) and that the NPs preparation method does not result in significant hydrolysis of maleimide groups (see section Hydrolytic stability of maleimide under NPs preparation conditions), it can be concluded that either not all maleimide groups were available for conjugation or that the surface of the NPs is fully covered with peptides at a conjugation ratio 2:1. The preparation of (nano)particles by adding amphiphilic PEGylated block copolymers to the feed relies on the principle that PEG migrates to the particle/water interface and will form a structure consisting of a hydrophobic PLGA core and a shell of PEG chains. However, due to the miscibility of PEG and PLGA[62–64], the core likely also contains PEG. Additionally, the presence of aqueous domains inside the particles resulting from the W/O/W emulsion method could also

lead to solubilization of PEG chains in their core[65], which means that not all PEG chains present in the NPs are exposed on the surface. Indeed, considering that almost full conjugation is achieved at a 2:1 molar ratio (84 ± 4%) while lower efficiencies are observed at a 1:1 molar ratio (52 ± 7%), we can speculate that about 50 - 60% of the maleimide-PEG-PLGA used for NPs preparation is actually available for conjugation on the NPs surface.

An estimation of the number of ligands on the surface of a NP can be obtained by calculating the surface area of a NP, the number of NPs and the surface concentration of ligand (based on the conjugation efficiency) (Calculations S1 and Calculations S2). It is calculated that for a conjugation reaction between NPs and cRGDfK at a maleimide to peptide molar ratio of 3:1 almost 40,000 ± 5,100 peptides were present per NP. The number of cRGDfK molecules per NP further increased to ∼50,600 ± 2,600 and ∼62,500 ± 8,600 for the 2:1 and 1:1 ratios respectively (Figure 2A). Despite the presence of two times more peptide in the reaction at a 1:1 ratio compared to that at 2:1, the number of cRGDfK molecules per NP increased only by a factor ∼1.2, which could be an indication of either the saturation of binding sites (maleimide) present per NP or a complete coverage of the NP surface. For NPs conjugated with 11A4 at a molar ratio of 20:1 an average of ∼1,600 ± 200 molecules of 11A4 per NP was calculated (Figure 2B). This amount nearly doubled at the ratio 10:1 (∼3,000 ± 200) and was almost 3.5 fold higher at the ratio 5:1 (∼5,500 ± 1,200). At ratios of 2:1 and 1:1 no further increase in number of 11A4 molecules was observed, indicating that the at a ratio of 5:1 the surface of the NPs is fully covered with nanobody molecules.

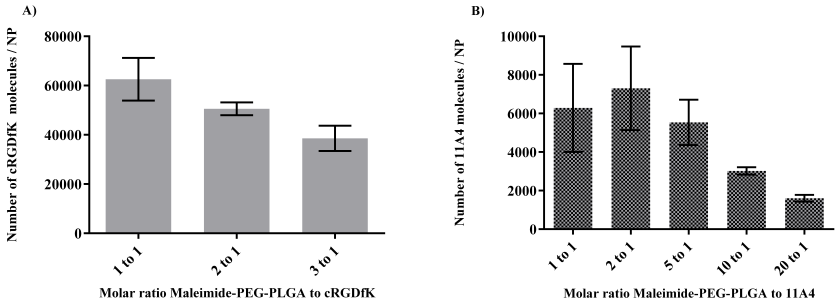

Figure 2: Number of A) cRGDfK or B) 11A4 molecules conjugated to the surface of one NP at different conjugation ratios.

Based on the information from Figure 2, it is possible to estimate the surface area occupied by one molecule of ligand (Calculations S1 and Calculations S2). For cRGDfK, after reaction at a molar ratio of 3:1 one molecule occupies 10 nm^2 and 6 nm^2 when the ratio is increased to 1:1. In the case of 11A4, a molecule of nanobody is calculated to be present per 197 nm^2 at a reaction ratio of 20:1 and 49 nm^2 at 1:1, which is quite similar to the data obtained for the ratios 2:1 and 5:1 (46 and 59 nm^2, respectively). Based on the dimensions of the nanobody (3 x 3 x 4 nm)[60], the surface area that one nanobody in an adsorbed monolayer would occupy on the surface of a NP can be calculated as $\sim$12 nm^2. The area occupied by the nanobody according to the calculations is 4 - 5 fold larger, which can be explained by the fact the protein is coupled to a very flexible $PEG_{5,000}$ chain. Therefore, for entropic reasons full surface coverage will not be obtained. Furthermore, depending on the PEG density on the NPs surface, PEG chains can adopt different configurations (i.e. brush or mushroom) which will occupy different surface areas on the NPs[65–67]. The optimal maleimide to ligand molar ratios for reaction, 2 to 1 for cRGDfK and 5 to 1 for 11A4, were used in the experiments described in the following sections of this manuscript. The experiments in which the parameters tested are not expected to be influenced by the size of the ligand were conducted only with cRGDfK because of the higher conjugation efficiencies obtained for this peptide (84 $\pm$ 4%) as compared to the nanobody (58 $\pm$ 12%) at the optimal ratios for reaction.

3.5 Kinetics of the conjugation reaction between maleimide-PEG-PLGA NPs and cRGDfK or 11A4

The kinetics of the conjugation reaction of the targeting ligands and the polymeric NPs was determined with particular interest in finding the point at which the reaction is complete. Figure 3A shows that reaction kinetics were particularly fast for cRGDfK, i.e. more than 65% of the ligand had already reacted with the maleimide groups on the NPs within the first 5 minutes of incubation and conjugation reached a plateau value upon 30 minutes of incubation (around 80% conjugation efficiency for 2:1 maleimide to cRGDfK molar ratio). A longer incubation time of $\sim$16 hours did not result in a further increase in conjugation efficiency. Similar fast reaction kinetics, consistent with those found for cRGDfK, have been previously reported between maleimide derivatives and other small thiol containing molecules. For instance, completion of the reaction between maleimide or N-ethylmaleimide and L-cysteine in solution is reached in less than 2 minutes[68], with similar results being obtained for the reaction between a carboxy-PEG maleimide derivative and

2-mercaptoethanol, L-cysteine and the peptide CGIRGERA[69]. In the aforementioned cases the reaction reaches completion at faster rates than those observed in the present study, which is expected since faster reaction rates, attributable to diffusional effects, have been observed for systems in which the reactants are soluble in the reaction media as opposed to at least one of them being anchored to a solid particle, for instance liposomes[69] and resin beads[70,71].

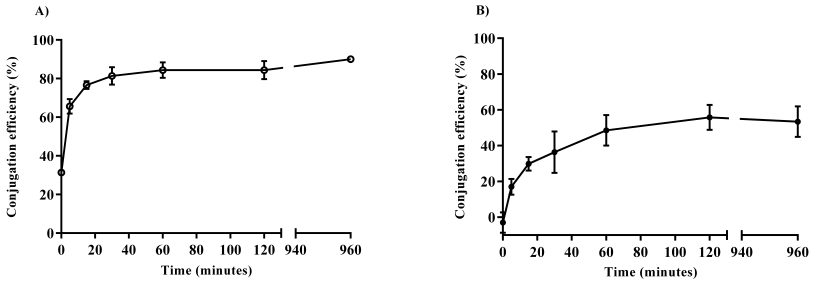

Figure 3: Kinetics of the conjugation reaction between maleimide-PEG-PLGA NPs and A) cRGDfK (n=3) or B) 11A4 (n=2). t=0 corresponds to the addition of the ligand to the NPs suspension immediately followed by a 10 minute centrifugation cycle at 4 °C.

The kinetics of the reaction between 11A4 and maleimide-PEG-PLGA NPs are presented in Figure 3B. A relatively slow and steady increase in the amount of protein conjugated to the NPs was observed during the first 2 hours of incubation, after which the maximum coupling efficiency was reached (55% at a 5:1 maleimide to 11A4 molar ratio). Similar to cRGDfK, incubation times longer than 2 hours did not result in increased conjugation efficiency of the protein. In comparison to cRGDfK, 11A4 exhibited slower reaction kinetics, which is not surprising since the reaction rate is dependent on the diffusion coefficient of the reactants in the medium which, in its turn, is dependent on their size and shape. cRGDfK, being a cyclic structure that is more than 20 times smaller than 11A4, consequently has a larger diffusion coefficient than the latter. When using maleimide-thiol chemistry for functionalization of drug delivery systems authors often favor long reaction times, for instance $\geq$ 9 hours (Table S1). Such long incubations may not be necessary since, according to our findings, the kinetics for coupling of a ligand to a polymeric NPs system are relatively fast, with reaction completion in a time frame of 30 minutes (peptide) to 2 hours (nanobody).

3.6 Influence of the NPs preparation method on maleimide accessibility and conjugation efficiency

The efficiency of the functionalization of maleimide-PEG-PLGA NPs with cRGDfK and 11A4 does not only rely on the reactivity of the maleimide group, but also on its accessibility for reaction with the thiol containing molecule, which in turn is most likely dependent on the NPs preparation procedure. Emulsification methods are commonly used for the preparation of PLGA NPs and the choice of single or double emulsion depends mostly on the nature of the cargo, i.e. whether it is hydrophobic or hydrophilic, respectively, though for amphiphilic drugs both options could be explored[33,72,73]. In an O/W emulsion the drug is dissolved or dispersed in a solution of PLGA in a suitable solvent like dichloromethane or chloroform. This solution is subsequently emulsified in water resulting in the formation of drug-loaded particles upon evaporation of the volatile solvent. In a W/O/W emulsion procedure water droplets containing the drug are emulsified in the organic phase that in turn is dispersed in an external aqueous phase. When PEGylated PLGA is present, one could hypothesize that, due to the presence of aqueous cavities inside the particles prepared by double emulsion, PEG chains could remain entrapped in said cavities due to their hydrophilic nature and thereby not be exposed to the outer surface. This phenomenon is not expected for particles prepared by O/W emulsion since a hydrophobic/hydrophilic interface is only present at the outer surface (Figure 4).

To investigate the hypothesis that the NPs prepared by the single emulsion method have more maleimide groups exposed at the surface than NPs prepared by the double emulsion method, both procedures were used to prepare NPs which were subsequently reacted with cRGDfK in a 2:1 maleimide-polymer to thiol molar ratio. The results however showed that cRGDfK was conjugated to the NPs to the same extent regardless of the preparation method: 81 ± 4% and 79 ± 4% for the NPs prepared by W/O/W and O/W respectively (n=2). This suggests that the number of PEG and consequently of maleimide molecules located on the surface of the NPs is not influenced by the type of emulsion used for their preparation. Our data are consistent with a previous report in which analysis of the surface PEG content by ^{1}H-NMR in D_2O showed comparable PEG coating efficiencies for NPs prepared by single and double emulsion methods[74]. Since PEG and PLGA are miscible[62–64], it is possible that PEG chains that are not located on the surface of the NPs are dissolved in the polymeric matrix to a similar extent for the NPs prepared by both single (O/W) and double (W/O/W) emulsion methods. Since the NPs preparation method does not influence the conjugation efficiency, and

because the nanoparticulate system described in this manuscript is intended for future use as a vehicle for molecules of hydrophilic nature, the double emulsion solvent evaporation method used in previous sections was also chosen for preparation of the NPs used in the experiments described in the next sections.

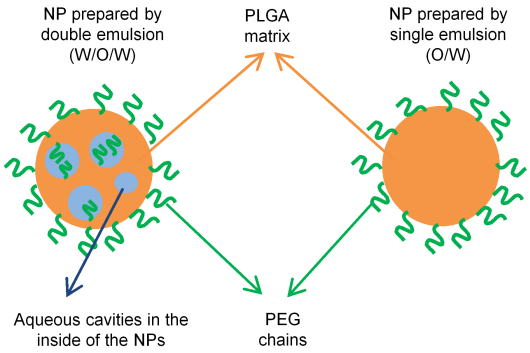

Figure 4: Schematic illustration of PEG-PLGA NPs prepared by double (W/O/W) and single (O/W) emulsion methods.

3.7 Influence of the surfactant used for NPs preparation on conjugation efficiency

A surfactant that adequately stabilizes the emulsion is a key component in the preparation of NPs by emulsification methods. While PVA is one of the preferred surfactants because it allows for the preparation of relatively small NPs with a narrow size distribution, its complete removal from the formulation after preparation is often difficult [75,76]. Residual PVA associated to the surface of polymeric NPs can range from 5 to 20% depending, among others, on the concentration of the surfactant used [50,77]. PVA can modify the properties of the NPs by altering their charge, their degradation profile and even their interaction with and uptake by living cells [78]. It is therefore imaginable that PVA associated to the NPs could also affect their functionalization by partly masking the maleimide groups present on their surface, limiting accessibility and hindering its reaction with thiol containing ligands. In order to investigate whether the type and concentration of surfactant used in the formulation have an influence on its functionalization, NPs were prepared using either sodium cholate, an anionic surfactant which can be almost completely washed

off from NPs surface[79], or different concentrations of PVA. The results shown in Table 2 indicate that the conjugation of cRGDfK to maleimide-PEG-PLGA NPs was not affected by either the nature (ionic or nonionic) or the concentration of the surfactants used for NPs preparation. Because cRGDfK is a small molecule, it can be argued that it could find the space to reach and react with maleimide even in the presence of PVA. Therefore, the conjugation reaction was repeated with 11A4, which has a molecular weight ∼20 times larger than that of cRGDfK. In line with the findings for cRGDfK, the conjugation efficiency for 11A4 was, albeit lower, also not significantly dependent on the type and concentration of surfactant used to prepare the formulation (Table 2). It can therefore be concluded that in the conditions used for NPs preparation (which include 3 washing steps), the possible residual PVA present on the surface of the NPs did not affect the extent of ligand conjugation when compared to sodium cholate.

Table 2: Conjugation of cRGDfK and 11A4 to maleimide-PEG-PLGA NPs prepared using different types and concentrations of surfactant (n=1).

Surfactant used for NPs preparation (% w/v in the external phase)	Conjugation efficiency(%) cRGDfK	11A4
sodium cholate 1.0	87	44
PVA 1.0	86	49
PVA 2.5	83	50
PVA 5.0	86	52

3.8 Preservation of the reactivity of maleimide upon NPs storage as aqueous dispersion at different temperatures

Hydrolysis of maleimide (Figure S8) may not only occur during preparation, but also upon storage of the NPs before the conjugation reaction. A direct, practical approach to study possible hydrolysis of this functional group during storage of the NPs is through its reaction with thiol containing ligands. For this purpose, maleimide-PEG-PLGA NPs were stored in buffer of pH 7.0 at either room temperature (∼20 °C) or 4 °C for different periods of time after which they were subject to conjugation with the peptide cRGDfK in a 2:1 maleimide to peptide molar ratio. Conjugation of the peptide to the NPs immediately after their preparation (t_0, no storage) resulted in 85% conjugation efficiency and was used as reference for the other time points. As shown in Figure 5, NPs stored at room temperature showed a more rapid decrease in

conjugation efficiency towards cRGDfK than those stored at 4 °C. Relative to t_0 around 90% of the maleimide groups remained reactive after storage at 4 °C for up to 7 days. In contrast, for the samples kept at room temperature reactivity decreased by 15% already after 1 day of storage and continued to drop over time, with approximately 40% of maleimide being unreactive after 7 days. Based on the information obtained from this study, half-life of maleimide on the NPs is estimated at 32 days when stored at 4 °C and 11 days at 20 °C (Figure S9 and Table S4) showing that the effect of storage conditions on maleimide hydrolysis cannot be neglected. Likewise, other authors have studied the stability of a maleimide derivative (8armPEG$_{10,000}$-maleimide) under different conditions and found that the percentage of hydrolyzed maleimide groups increased with increasing incubation temperatures[52].

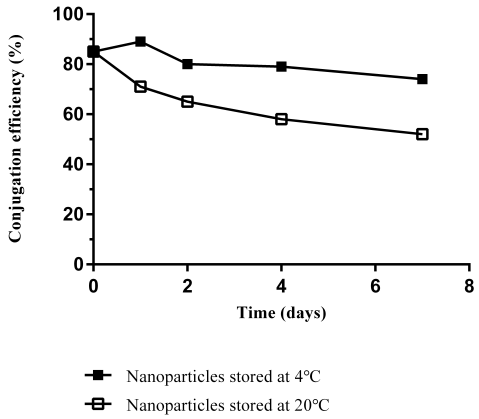

Figure 5: Reactivity of maleimide groups in NPs upon storage. Maleimide-PEG-PLGA NPs were stored in aqueous medium (HEPES 10 mM pH 7.0) at 4 or 20 °C for different periods of time after which the reactivity of maleimide was assessed by conjugation to cRGDfK.

4 Conclusions

The findings presented in this work demonstrate the relevance of exploring and optimizing the reaction conditions (i.e. time and stoichiometric ratio) used for functionalization of nanoparticles by maleimide-thiol click reaction, a matter of interest considering that the availability of ligands can often be

limited for technical or economic reasons. In this study, the efficiency of the conjugation reaction between maleimide-PEG-PLGA NPs and biomolecules of two different sizes (a 678 Da peptide and a 14.8 kDa protein) was particularly susceptible to the molar ratios used, one of the parameters that was optimized in the present study. As the molar ratios tested in the reaction shift to larger amounts of ligand in comparison to maleimide, it is likely that the saturation of the surface area of the NPs becomes the limiting factor for achieving a high coupling efficiency, which is particularly evident for the larger ligand under study (11A4 nanobody). Identifying the molar ratio at which surface saturation occurs is important in order to avoid the use of excessive amounts of ligand that will no longer fit on the surface of the NPs and will ultimately be discarded in the unbound fraction. In addition to a better use of resources, optimization of the conjugation process results in a better knowledge of the composition of ligand-targeted systems, for instance the surface density of targeting ligand. The structure of the surface of these systems deeply influences their interaction with cells and therefore their performance *in vitro* and *in vivo* (i.e. circulation kinetics of NPs and their uptake by cells).

Acknowledgements

Lucía Martínez-Jothar would like to thank the Consejo Nacional de Ciencia y Tecnología (CONACYT), Mexico (grant no. 384743) for the financial support during her PhD.

References

[1] Fang, J., Nakamura, H., and Maeda, H. The EPR effect: unique features of tumor blood vessels for drug delivery, factors involved, and limitations and augmentation of the effect. *Adv. Drug Delivery Rev.*, 63(3):136–151, 2011.

[2] Kunjachan, S., Pola, R., Gremse, F., Theek, B., Ehling, J., Moeckel, D., Hermanns-Sachweh, B., Pechar, M., Ulbrich, K., Hennink, W. E., Storm, G., Lederle, W., Kiessling, F., and Lammers, T. Passive versus active tumor targeting using RGD- and NGR-modified polymeric nanomedicines. *Nano Lett.*, 14(2):972–981, 2014.

[3] Nehoff, H., Parayath, N. N., Domanovitch, L., Taurin, S., and Greish, K. Nanomedicine for drug targeting: strategies beyond the enhanced permeability and retention effect. *Int. J. Nanomed.*, 9:2539–2555, 2014.

[4] Torchilin, V. P. Drug targeting. *Eur. J. Pharm. Sci.*, 11:S81–S91, 2000.

[5] Brigger, I., Dubernet, C., and Couvreur, P. Nanoparticles in cancer therapy and diagnosis. *Adv. Drug Delivery Rev.*, 54:631–651, 2002.

[6] Ernsting, M. J., Murakami, M., Roy, A., and Li, S. D. Factors controlling the pharmacokinetics, biodistribution and intratumoral penetration of nanoparticles. *J. Controlled Release*, 172(3):782–794, 2013.

[7] Owens, D. E. and Peppas, N. A. Opsonization, biodistribution, and pharmacokinetics of polymeric nanoparticles. *Int. J. Pharm.*, 307(1):93–102, 2006.

[8] Lachelt, U. and Wagner, E. Nucleic acid therapeutics using polyplexes: a journey of 50 years (and beyond). *Chem. Rev.*, 115(19):11043–11078, 2015.

[9] Chen, J., Ouyang, J., Chen, Q., Deng, C., Meng, F., Zhang, J., Cheng, R., Lan, Q., and Zhong, Z. EGFR and CD44 dual-targeted multifunctional hyaluronic acid nanogels boost protein delivery to ovarian and breast cancers in vitro and in vivo. *ACS Appl. Mater. Interfaces*, 9(28):24140–24147, 2017.

[10] Li, D., van Nostrum, C. F., Mastrobattista, E., Vermonden, T., and Hennink, W. E. Nanogels for intracellular delivery of biotherapeutics. *J. Controlled Release*, 259:16–28, 2017.

[11] van der Meel, R., Vehmeijer, L. J., Kok, R. J., Storm, G., and van Gaal, E. V. Ligand-targeted particulate nanomedicines undergoing clinical evaluation: current status. *Adv. Drug Delivery Rev.*, 65(10):1284–1298, 2013.

[12] Irvine, D. J., Hanson, M. C., Rakhra, K., and Tokatlian, T. Synthetic nanoparticles for vaccines and immunotherapy. *Chem. Rev.*, 115(19):11109–11146, 2015.

[13] Joshi, M. D., Unger, W. J., Storm, G., van Kooyk, Y., and Mastrobattista, E. Targeting tumor antigens to dendritic cells using particulate carriers. *J. Controlled Release*, 161 (1):25–37, 2012.

[14] Pinzon-Daza, M., Campia, I., Kopecka, J., Garzon, R., Ghigo, D., and Rigant, C. Nanoparticle- and liposome-carried drugs: new strategies for active targeting and drug delivery across blood-brain barrier. *Curr. Drug Metab.*, 14(6):625–640, 2013.

[15] van Rooy, I., Mastrobattista, E., Storm, G., Hennink, W. E., and Schiffelers, R. M. Comparison of five different targeting ligands to enhance accumulation of liposomes into the brain. *J. Controlled Release*, 150(1):30–36, 2011.

[16] Nakajima, N. and Ikada, Y. Mechanism of amide formation by carbodiimide for bioconjugation in aqueous media. *Bioconjugate Chem.*, 6(1):123–130, 1995.

[17] King, M. and Wagner, A. Developments in the field of bioorthogonal bond forming reactions-past and present trends. *Bioconjugate Chem.*, 25(5):825–839, 2014.

[18] van Dijk, M., Rijkers, D., Liskamp, R., van Nostrum, C., and Hennink, W. Synthesis and applications of biomedical and pharmaceutical polymers via click chemistry methodologies. *Bioconjugate Chem.*, 20(11):2001–2016, 2009.

[19] Friedmann, E., Marrian, D., and Simon-Reuss, I. Antimitotic action of maleimide and related substances. *Br. J. Pharmacol.*, 4:105–108, 1949.

[20] Lee, C. and Samuels, E. Adducts from the reaction of N-ethylmaleimide with L-cysteine and with gluthatione. *Can. J. Chem.*, 39:1152–1154, 1961.

[21] Martin, F. J. and Papahadjopoulos, D. Irreversible coupling of immunoglobulin fragments to preformed vesicles. An improved method for liposome targeting. *J. Biol. Chem.*, 257(1):286–288, 1982.

[22] Jiang, Y., Chen, J., Deng, C., Suuronen, E. J., and Zhong, Z. Click hydrogels, microgels and nanogels: Emerging platforms for drug delivery and tissue engineering. *Biomaterials*, 35(18):4969–4985, 2014.

[23] Nobs, L., Buchegger, F., Gurny, R., and Allemann, E. Current methods for attaching targeting ligands to liposomes and nanoparticles. *J. Pharm. Sci.*, 93(8):1980–1992, 2004.

[24] Yu, M. K., Park, J., and Jon, S. Targeting strategies for multifunctional nanoparticles in cancer imaging and therapy. *Theranostics*, 2(1):3–44, 2012.

[25] Fontaine, S. D., Reid, R., Robinson, L., Ashley, G. W., and Santi, D. V. Long-term stabilization of maleimide-thiol conjugates. *Bioconjugate Chem.*, 26(1):145–152, 2015.

[26] Gregory, J. D. The stability of N-ethylmaleimide and its reaction with sulfhydryl groups. *J. Am. Chem. Soc.*, 77(14):3922–3923, 1955.

[27] Webb, J. L. N-ethylmaleimide. In *Enzyme and Metabolic Inhibitors*, pages 337–365. Academic Press, New York, 1966.

[28] Koniev, O. and Wagner, A. Developments and recent advancements in the field of endogenous amino acid selective bond forming reactions for bioconjugation. *Chem. Soc. Rev.*, 44(15):5495–5551, 2015.

[29] Matsui, S. and Aida, H. Hydrolysis of some N-alkylmaleimides. *J. Chem. Soc., Perkin Trans. 2*, (12):1277–1280, 1978.

[30] Ryan, C. P., Smith, M. E., Schumacher, F. F., Grohmann, D., Papaioannou, D., Waksman, G., Werner, F., Baker, J. R., and Caddick, S. Tunable reagents for multifunctional bioconjugation: reversible or permanent chemical modification of proteins and peptides by control of maleimide hydrolysis. *Chem. Commun.*, 47(19):5452–5454, 2011.

[31] Oswald, M., Geissler, S., and Goepferich, A. Determination of the activity of maleimide-functionalized phospholipids during preparation of liposomes. *Int. J. Pharm.*, 514(1): 93–102, 2016.

[32] Acharya, S. and Sahoo, S. K. PLGA nanoparticles containing various anticancer agents and tumour delivery by EPR effect. *Adv. Drug Delivery Rev.*, 63(3):170–183, 2011.

[33] Danhier, F., Ansorena, E., Silva, J. M., Coco, R., Le Breton, A., and Preat, V. PLGA-based nanoparticles: an overview of biomedical applications. *J. Controlled Release*, 161(2):505–522, 2012.

[34] Jain, R. The manufacturing techniques of various drug loaded biodegradable poly(lactide-co-glycolide) (PLGA) devices. *Biomaterials*, 21:2475–2490, 2000.

[35] Makadia, H. K. and Siegel, S. J. Poly lactic-co-glycolic acid (PLGA) as biodegradable controlled drug delivery carrier. *Polymers*, 3(3):1377–1397, 2011.

[36] Mundargi, R. C., Babu, V. R., Rangaswamy, V., Patel, P., and Aminabhavi, T. M. Nano/micro technologies for delivering macromolecular therapeutics using poly(D,L-lactide-co-glycolide) and its derivatives. *J. Controlled Release*, 125(3):193–209, 2008.

[37] Desgrosellier, J. S. and Cheresh, D. A. Integrins in cancer: biological implications and therapeutic opportunities. *Nat. Rev. Cancer*, 10(1):9–22, 2010.

[38] Schiffelers, R. M., Ansari, A., Xu, J., Zhou, Q., Tang, Q., Storm, G., Molema, G., Lu, P. Y., Scaria, P. V., and Woodle, M. C. Cancer siRNA therapy by tumor selective delivery with ligand-targeted sterically stabilized nanoparticle. *Nucleic Acids Res.*, 32 (19):e149, 2004.

[39] Sun, Y., Kang, C., Liu, F., Zhou, Y., Luo, L., and Qiao, H. RGD peptide-based target drug delivery of doxorubicin nanomedicine. *Drug Dev. Res.*, 78(6):283–291, 2017.

[40] Temming, K., Schiffelers, R. M., Molema, G., and Kok, R. J. RGD-based strategies for selective delivery of therapeutics and imaging agents to the tumour vasculature. *Drug Resist. Updates*, 8(6):381–402, 2005.

[41] Zhu, Y., Zhang, J., Meng, F., Deng, C., Cheng, R., Feijen, J., and Zhong, Z. cRGD-functionalized reduction-sensitive shell-sheddable biodegradable micelles mediate enhanced doxorubicin delivery to human glioma xenografts in vivo. *J. Controlled Release*, 233:29–38, 2016.

[42] Chen, H., Niu, G., Wu, H., and Chen, X. Clinical application of radiolabeled RGD peptides for PET imaging of integrin $\alpha v\beta 3$. *Theranostics*, 6(1):78–92, 2016.

[43] Kijanka, M., Warnders, F. J., El Khattabi, M., Lub-de Hooge, M., van Dam, G. M., Ntziachristos, V., de Vries, L., Oliveira, S., and van Bergen en Henegouwen, P. M. Rapid optical imaging of human breast tumour xenografts using anti-HER2 VHHs site-directly conjugated to IRDye 800CW for image-guided surgery. *Eur. J. Nucl. Med. Mol. Imaging*, 40(11):1718–1729, 2013.

[44] Wolff, A. C., Hammond, M. E., Hicks, D. G., Dowsett, M., McShane, L. M., Allison, K. H., Allred, D. C., Bartlett, J. M., Bilous, M., Fitzgibbons, P., Hanna, W., Jenkins, R., Mangu, P. B., Paik, S., Perez, E. A., Press, M. F., Spears, P. A., Vance, G. H., Viale, G., and Hayes, D. F. Recommendations for human epidermal growth factor receptor 2 testing in breast cancer: American Society of Clinical Oncology/College of American Pathologists clinical practice guideline update. *J. Clin. Oncol.*, 31(31): 3997–4013, 2013.

[45] Hassanzadeh-Ghassabeh, G., Devoogdt, N., De Pauw, P., Vincke, C., and Muyldermans, S. Nanobodies and their potential applications. *Nanomedicine*, 8(6):1013–1026, 2013.

[46] Chakravarty, R., Goel, S., and Cai, W. Nanobody: the "magic bullet" for molecular imaging? *Theranostics*, 4(4):386–98, 2014.

[47] Harmsen, M. M. and De Haard, H. J. Properties, production, and applications of camelid single-domain antibody fragments. *Appl. Microbiol. Biotechnol.*, 77(1):13–22, 2007.

[48] Oliveira, S., Heukers, R., Sornkom, J., Kok, R. J., and van Bergen En Henegouwen, P. M. Targeting tumors with nanobodies for cancer imaging and therapy. *J. Controlled Release*, 172(3):607–617, 2013.

[49] Samadi, N., van Steenbergen, M. J., van den Dikkenberg, J. B., Vermonden, T., van Nostrum, C. F., Amidi, M., and Hennink, W. E. Nanoparticles based on a hydrophilic polyester with a sheddable PEG coating for protein delivery. *Pharm. Res.*, 31(10): 2593–2604, 2014.

[50] Zambaux, M. F., Bonneaux, F., Gref, R., Maincent, P., Dellacherie, E., Alonso, M. J., Labrude, P., and Vigneron, C. Influence of experimental parameters on the characteristics of poly(lactic acid) nanoparticles prepared by a double emulsion method. *J. Controlled Release*, 50(1-3):31–40, 1998.

[51] Khan, M. N. Kinetics and mechanism of the alkaline hydrolysis of maleimide. *J. Pharm. Sci.*, 73(12):1767–1771, 1984.

[52] Kirchhof, S., Strasser, A., Wittmann, H. J., Messmann, V., Hammer, N., Goepferich, A. M., and Brandl, F. P. New insights into the cross-linking and degradation mechanism of DielsAlder hydrogels. *J. Mater. Chem. B*, 3(3):449–457, 2015.

[53] Schiffelers, R. M., Koning, G. A., ten Hagen, T. L., Fens, M. H., Schraa, A. J., Janssen, A. P., Kok, R. J., Molema, G., and Storm, G. Anti-tumor efficacy of tumor vasculature-targeted liposomal doxorubicin. *J. Controlled Release*, 91(1-2):115–122, 2003.

[54] Kijanka, M. M., van Brussel, A. S., van der Wall, E., Mali, W. P., van Diest, P. J., van Bergen en Henegouwen, P. M., and Oliveira, S. Optical imaging of pre-invasive breast cancer with a combination of VHHs targeting CAIX and HER2 increases contrast and facilitates tumour characterization. *EJNMMI Res.*, 6(1):14, 2016.

[55] de Graaf, A. J., Boere, K. W., Kemmink, J., Fokkink, R. G., van Nostrum, C. F., Rijkers, D. T., van der Gucht, J., Wienk, H., Baldus, M., Mastrobattista, E., Vermonden, T., and Hennink, W. E. Looped structure of flowerlike micelles revealed by 1H NMR relaxometry and light scattering. *Langmuir*, 27(16):9843–9848, 2011.

[56] Hrkach, J., Peracchia, M., Domb, A., Lotan, N., and Langer, R. Nanotechnology for biomaterials engineering: structural characterization of amphiphilic polymeric nanoparticles by 1H NMR spectroscopy. *Biomaterials*, 18(1):27–30, 1997.

[57] Poe, G., Jarret, W., Scales, C., and McCormick, C. Enhanced coil expansion and intrapolymer complex formation of linear poly(methacrylic acid) containing poly(ethylene glycol) grafts. *Macromolecules*, 37(7):2603–2612, 2004.

[58] Danhier, F., Vroman, B., Lecouturier, N., Crokart, N., Pourcelle, V., Freichels, H., Jerome, C., Marchand-Brynaert, J., Feron, O., and Preat, V. Targeting of tumor endothelium by RGD-grafted PLGA-nanoparticles loaded with paclitaxel. *J. Controlled Release*, 140(2):166–173, 2009.

[59] Xu, Q., Liu, Y., Su, S., Li, W., Chen, C., and Wu, Y. Anti-tumor activity of paclitaxel through dual-targeting carrier of cyclic RGD and transferrin conjugated hyperbranched copolymer nanoparticles. *Biomaterials*, 33(5):1627–1639, 2012.

[60] Kijanka, M., van Donselaar, E. G., Muller, W. H., Dorresteijn, B., Popov-Celeketic, D., El Khattabi, M., Verrips, C. T., van Bergen en Henegouwen, P. M. P., and Post, J. A. A novel immuno-gold labeling protocol for nanobody-based detection of HER2 in breast cancer cells using immuno-electron microscopy. *J. Struct. Biol.*, 199(1):1–11, 2017.

[61] Yao, W., Xu, P., Zhao, J., Ling, L., Li, X., Zhang, B., Cheng, N., and Pang, Z. RGD functionalized polymeric nanoparticles targeting periodontitis epithelial cells for the enhanced treatment of periodontitis in dogs. *J. Colloid Interface Sci.*, 458:14–21, 2015.

[62] Javiya, C. and Jonnalagadda, S. Physicochemical characterization of spray-dried PLGA/PEG microspheres, and preliminary assessment of biological response. *Drug Dev. Ind. Pharm.*, 42(9):1504–1514, 2016.

[63] Malzert, A., Boury, F., Saulnier, P., Benoit, J., and Proust, J. Interfacial properties of mixed polyethylene glycol / poly(D,L-lactide-co-glycolide) films spread at the air / water interface. *Langmuir*, 16:1861–1867, 2000.

[64] Vega, E., Egea, M. A., Calpena, A. C., Espina, M., and Garcia, M. L. Role of hydroxypropyl-beta-cyclodextrin on freeze-dried and gamma-irradiated PLGA and PLGA-PEG diblock copolymer nanospheres for ophthalmic flurbiprofen delivery. *Int. J. Nanomed.*, 7:1357–1371, 2012.

[65] Rabanel, J. M., Hildgen, P., and Banquy, X. Assessment of PEG on polymeric particles surface, a key step in drug carrier translation. *J. Controlled Release*, 185:71–87, 2014.

[66] Perry, J. L., Reuter, K. G., Kai, M. P., Herlihy, K. P., Jones, S. W., Luft, J. C., Napier, M., Bear, J. E., and DeSimone, J. M. PEGylated PRINT nanoparticles: the impact of PEG density on protein binding, macrophage association, biodistribution, and pharmacokinetics. *Nano Lett.*, 12(10):5304–5310, 2012.

[67] Stolnik, S., Daudali, B., Arien, A., Whetstone, J., Heald, C., Garnett, M., Davis, S., and Illum, L. The effect of surface coverage and conformation of poly(ethylene oxide) (PEO) chains of poloxamer 407 on the biological fate of model colloidal drug carriers. *Biochim. Biophys. Acta*, 1514:261–279, 2001.

[68] Lee, C. and Samuels, E. The kinetics of reaction between L-cysteine hydrochloride and some maleimides. *Can. J. Chem.*, 42:168–170, 1964.

[69] Schelte, P., Boeckler, C., Frisch, B., and Schuber, F. Differential reactivity of maleimide and bromoacetyl functions with thiols: application to the preparation of liposomal diepitope constructs. *Bioconjugate Chem.*, 11(1):118–123, 2000.

[70] Gokmen, M. T., Brassinne, J., Prasath, R. A., and Du Prez, F. E. Revealing the nature of thio-click reactions on the solid phase. *Chem. Commun.*, 47(16):4652–4654, 2011.

[71] Nguyen, L.-T. T., Gokmen, M. T., and Du Prez, F. E. Kinetic comparison of 13 homogeneous thiol-X reactions. *Polym. Chem.*, 4(22):5527–5536, 2013.

[72] Ramazani, F., Chen, W., van Nostrum, C. F., Storm, G., Kiessling, F., Lammers, T., Hennink, W. E., and Kok, R. J. Strategies for encapsulation of small hydrophilic and amphiphilic drugs in PLGA microspheres: State-of-the-art and challenges. *Int. J. Pharm.*, 499(1-2):358–367, 2016.

[73] Wischke, C. and Schwendeman, S. P. Principles of encapsulating hydrophobic drugs in PLA/PLGA microparticles. *Int. J. Pharm.*, 364(2):298–327, 2008.

[74] Vila, A., Gill, H., McCallion, O., and Alonso, M. J. Transport of PLA-PEG particles across the nasal mucosa: effect of particle size and PEG coating density. *J. Controlled Release*, 98(2):231–244, 2004.

[75] Boury, F., Ivanova, T., Panaiotov, I., Proust, J. E., Bois, A., and Richou, J. Dynamic properties of poly(DL-lactide) and polyvinyl alcohol monolayers at the air/water and dichloromethane/water interfaces. *J. Colloid Interface Sci.*, 169(2):380–392, 1995.

[76] Lee, S. C., Oh, J. T., Jang, M. H., and Chung, S. I. Quantitative analysis of polyvinyl alcohol on the surface of poly(D, L-lactide-co-glycolide) microparticles prepared by solvent evaporation method: effect of particle size and PVA concentration. *J. Controlled Release*, 59(2):123–132, 1999.

[77] Sengel-Turk, C. T., Hascicek, C., Dogan, A. L., Esendagli, G., Guc, D., and Gonul, N. Preparation and in vitro evaluation of meloxicam-loaded PLGA nanoparticles on HT-29 human colon adenocarcinoma cells. *Drug Dev. Ind. Pharm.*, 38(9):1107–1116, 2012.

[78] Sahoo, S. K., Panyam, J., Prabha, S., and Labhasetwar, V. Residual polyvinyl alcohol associated with poly (D,L-lactide-co-glycolide) nanoparticles affects their physical properties and cellular uptake. *J. Controlled Release*, 82(1):105–114, 2002.

[79] Gref, R., Domb, A., Quellec, P., Blunk, T., Muller, R. H., Verbavatz, J. M., and Langer, R. The controlled intravenous delivery of drugs using PEG-coated sterically stabilized nanospheres. *Adv. Drug Delivery Rev.*, 16(2-3):215–233, 1995.

Supporting Information

Table S1: Conditions used in the literature for conjugating thiolated ligands to maleimide groups on polymeric nanoparticles. [1–9]

Group	Name	Parameters
NPs preparation method	Double emulsion solvent evaporation	3 [3,5,6]
	Single emulsion solvent evaporation	3 [4,8,9]
	Nanoprecipitation	1 [1]
	Others	2 [2,7]
Surfactant used for NPs preparation	sodium cholate	5 [3,5,6,8,9]
	PVA	1 [7]
	Not reported / not applicable	3 [1,2,4]
Mass fraction of maleimide (polymer) in blend	$< 10\%$	3 [2,5,6]
	$10 - 20\%$	6 [2–4,7–9]
	100%	1 [1]
M_w of the ligand used for functionalization (kDa)	< 1.5	5 [4,5,7–9]
	~ 15	1 [1]
	> 60	3 [2,3,6]
Number of thiol groups per molecule of ligand	1	6 [1,4,5,7–9]
	Not reported	3 [2,3,6]
Maleimide (polymer):ligand molar ratio in the feed	1:1	1 [4]
	3:1	2 [4,6]
	4:1	1 [1]
	20:1	1 [1]
	> 20:1	1 [1]
	Not reported	6 [2,3,5,7–9]
Reaction conditions	Incubation time 2 hours, pH 7.2[a]	1 [2]
	Incubation time 2 hours[a,b]	1 [9]
	Incubation time 8 - 9 hours, room temperature[b]	2 [3,4,8]
	Incubation overnight, pH 7.0[a]	1 [5]
	Incubation overnight[a,b]	1 [6]
	Incubation time 12 h, room temperature[b]	1 [7]
	Incubation time not reported[a,b]	1 [1]

[a] temperature not reported [b] pH not reported

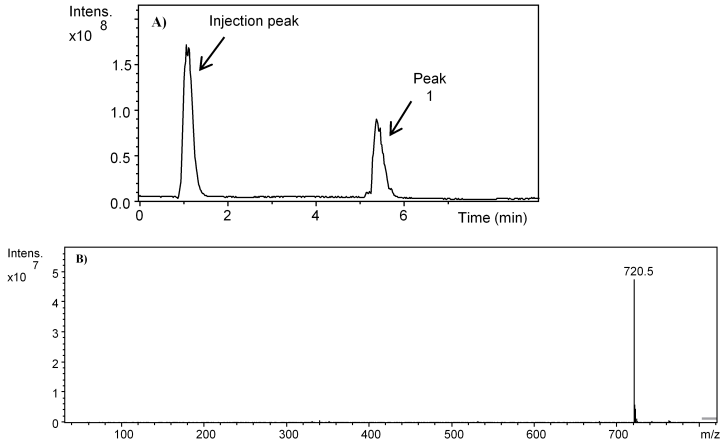

Figure S1: c[RGDfK(Ac-SCH_2CO)] A) HPLC chromatogram, B) Mass spectrum.

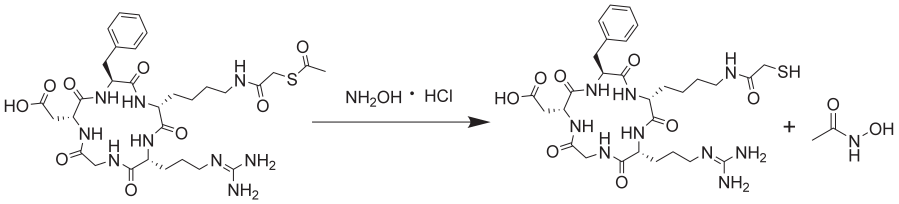

Scheme S1: Deprotection of c[RGDfK(Ac-SH)]

Table S2: PEG weight fraction (%) incorporated in the polymer blends or in the NPs.

Sample	Theoretical PEG weight fraction (%)[a]	Practical PEG weight fraction (%)[b]
Blend 10% maleimide-PEG-PLGA + 90% PLGA	2.0	1.9
NPs 10% maleimide-PEG-PLGA + 90% PLGA	2.0	1.7 ± 0.0 (n=2)
Blend 20% maleimide-PEG-PLGA + 80% PLGA	4.0	3.5
NPs 20% maleimide-PEG-PLGA + 80% PLGA	4.0	3.1 ± 0.0 (n=2)

[a] Based on the molecular weights of PEG (∼5,000 Da) and PLGA (∼20,000 Da), the weight fraction of PEG in the maleimide-PEG-PLGA block copolymer is 20%. The theoretical PEG weight fraction (%) was calculated assuming incorporation of all the maleimide-PEG-PLGA used in the feed of the blend or the NPs.
[b] Determined by ^{1}H-NMR analysis.

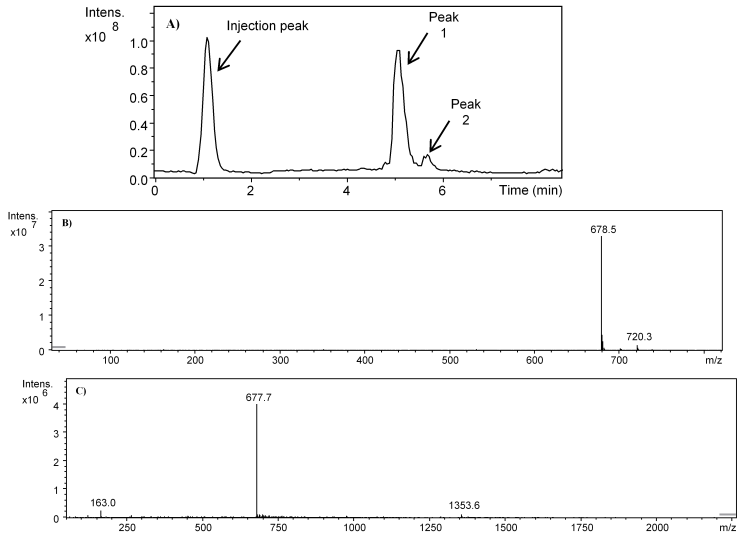

Figure S2: c[RGDfK(Ac-SH)] A) HPLC chromatogram, B) Mass spectrum of peak 1 with retention time 4.9 - 5.4 min. C) Mass spectrum of peak 2 with retention time 5.6 - 5.9 min.

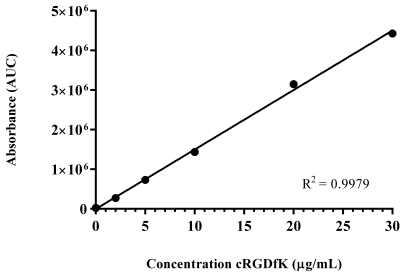

Figure S3: Calibration curve of the peptide cRGDfK obtained by HPLC.

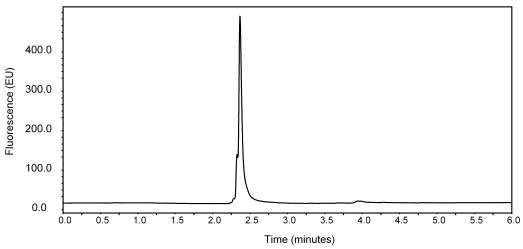

Figure S4: UPLC chromatogram of the nanobody 11A4.

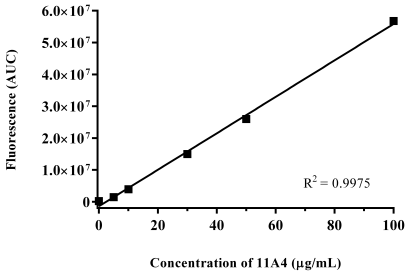

Figure S5: Calibration curve of the nanobody 11A4 obtained by UPLC.

Table S3: Characteristics of maleimide-PEG-PLGA NPs of different compositions[a].

Feed composition of the NPs	Diameter (nm)	PDI	Zeta potential (mV)	PEG weight fraction (%)	Yield (%)
10% maleimide-PEG-PLGA + 90% PLGA	315 ± 20	0.09 ± 0.02	-6.5 ± 1.0	1.7 ± 0.0	57 ± 3
20% maleimide-PEG-PLGA + 80% PLGA	349 ± 11	0.13 ± 0.02	-7.6 ± 1.2	3.1 ± 0.0	59 ± 1

[a] NPs prepared by double emulsion method, n=3 for 10% maleimide-PEG-PLGA + 90% PLGA and n=2 for 20% maleimide-PEG-PLGA + 80% PLGA.

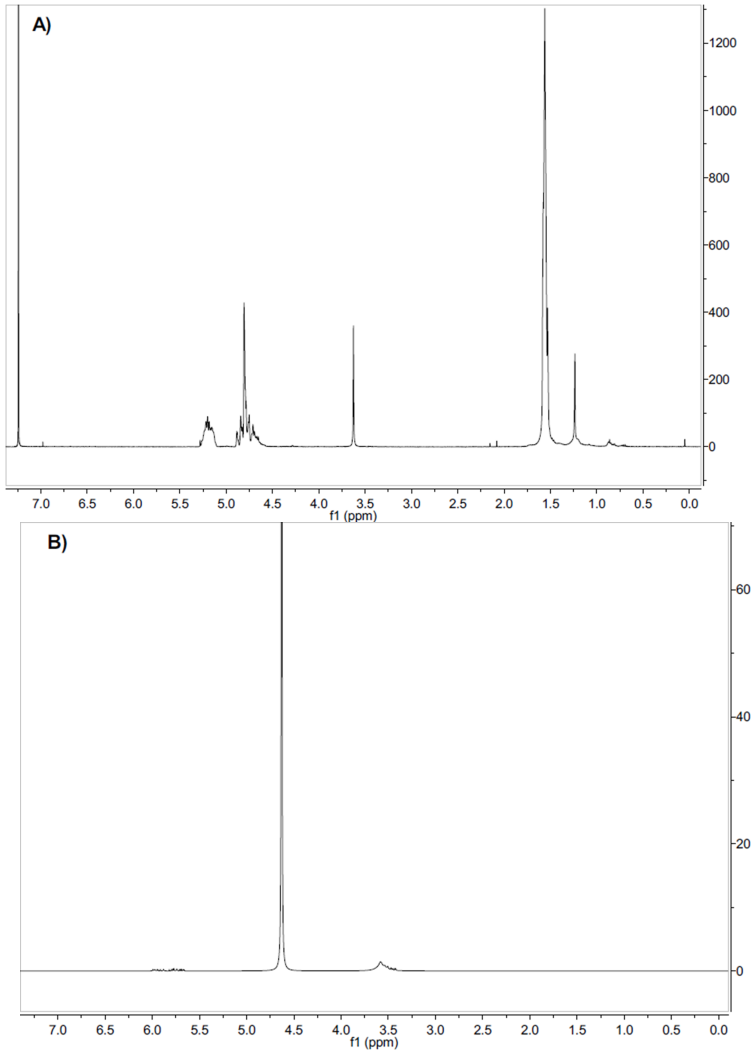

Figure S6: ^{1}H-NMR spectra of maleimide-PEG-PLGA in A) $CDCl_3$ and B) D_2O. A) The NPs are composed of PEG and PLGA. δ = 1.5 (m, 3 H, CH_3); 3.6 (4 H, -$\underline{CH_2}$-$\underline{CH_2}$ of PEG); 4.6 - 4.9 (2 H, O-$\underline{CH_2}$-C(O)O); 5.1 - 5.3 (1 H, -$\underline{CH}$-CH_3); 7.2 (1 H, CH, chloroform). B) Signal of PEG present at the surface of the NPs visible after NPs suspension in D_2O. δ = 3.6 (4 H, -$\underline{CH_2}$-$\underline{CH_2}$ of PEG); 4.6 (2H, H-O-H).

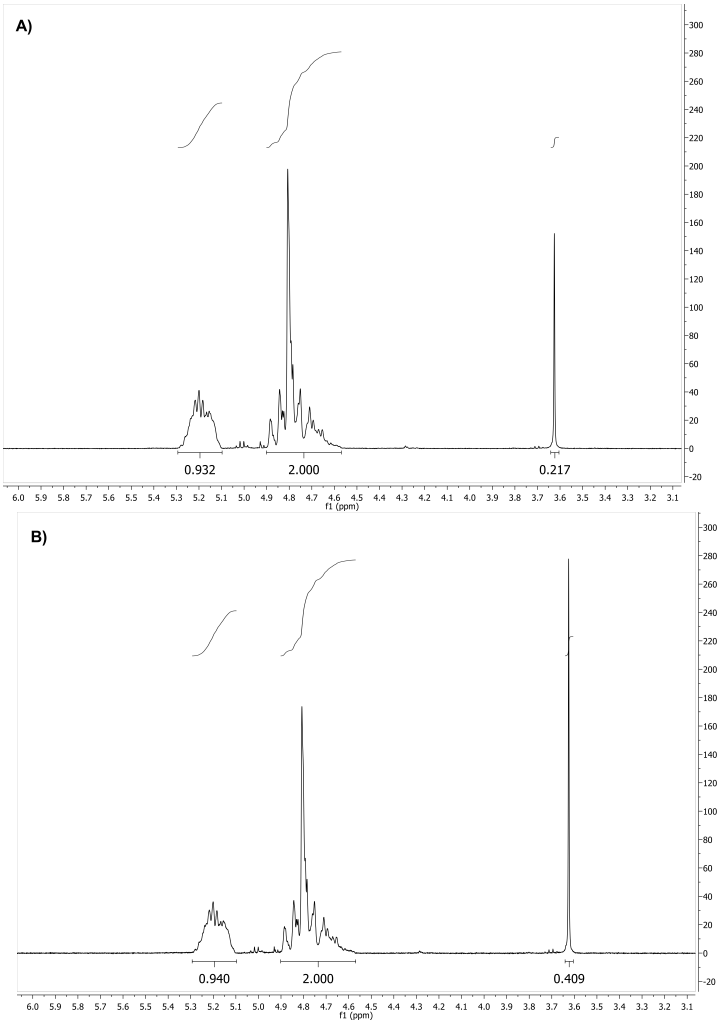

Figure S7: ^{1}H-NMR spectra of blends of A) 90% PLGA and 10% maleimide-PEG-PLGA and B) 80% PLGA and 20% maleimide-PEG-PLGA in $CDCl_3$. δ = 1.5 (m, 3 H, CH_3); 3.6 (4 H, -$\underline{CH_2}$-$\underline{CH_2}$ of PEG); 4.6 - 4.9 (2 H, O-$\underline{CH_2}$-C(O)O); 5.1 - 5.3 (1 H, -$\underline{CH}$-CH_3).

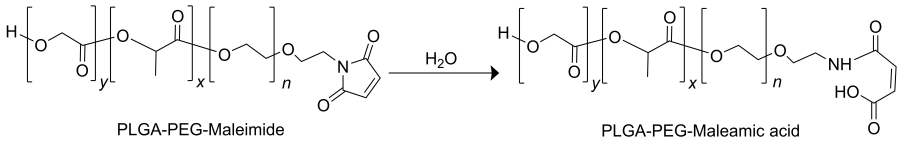

Figure S8: Hydrolysis of the maleimide group in PLGA-PEG-maleimide.

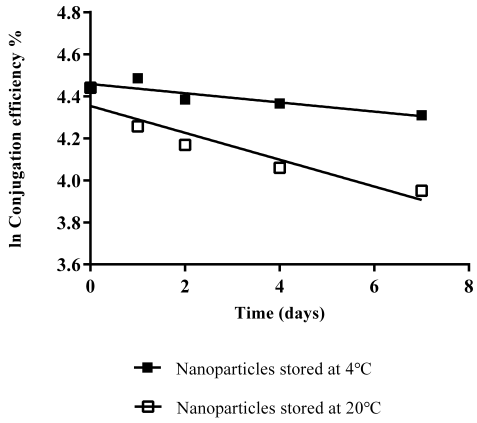

Figure S9: Reactivity of maleimide in NPs upon storage. Maleimide-PEG-PLGA NPs were stored in aqueous medium (HEPES 10 mM pH 7.0) at 4 or 20 °C for different periods of time after which the reactivity of maleimide was assessed by conjugation to cRGDfK.

Table S4: Half-life of maleimide in maleimide-PEG-PLGA NPs stored as aqueous dispersion at different temperatures.

Storage temperature	Slope (day^{-1})[a]	$t_{1/2}$ (days)	R^2
4°C	0.022	32	0.799
20°C	0.064	11	0.892

[a] Slope calculated from Figure S9.

Calculations S1. Calculation of the number of 11A4 molecules present on the surface of a single NP.

The number of molecules of 11A4 bound to the surface of a single NP containing 10% maleimide-PEG-PLGA and 90% PLGA (NP10%) can be calculated as follows:

First, the mass and surface area of a single NP (m_{NP}) are calculated based on the following information:

The diameters of the maleimide-PEG-PLGA NPs used in this study were, in average, 3.15 x 10^{-5} cm. Since the NPs are made from 90% w/w of PLGA their density will be considered as that of this polymer, namely $\rho = 1.25$ g/cm^3 [10,11]. Therefore,

$$m_{NP10\%} = \left(\frac{4}{3} \times \pi \times (1.58 \times 10^{-5} cm)^3\right) \times 1.25 \, \frac{g}{cm^3} = 2.06 \times 10^{-14} \, \frac{g}{NP}$$

$$Area_{NP10\%} = 4 \times \pi \times (1.58 \times 10^{-5} cm)^2 = 3.14 \times 10^{-9} \, \frac{cm^2}{NP}$$

For a conjugation reaction in a molar ratio of 1:1 maleimide-PEG-PLGA to 11A4, 1 mg of NPs and 59 μg of protein were used. The number of NPs taking part in the reaction is then:

$$Number\ of\ NPs_{NP10\%} = \frac{1.00 \times 10^{-3}\, g}{2.06 \times 10^{-14}\, g/NP} = 4.85 \times 10^{10}\ NPs$$

The total surface area available for conjugation of 11A4 to the NPs in the reaction is:

$$Total\ Surface\ Area_{NP10\%} = 3.14 \times 10^{-9}\, \frac{cm^2}{NP} \times 4.85 \times 10^{10}\, NPs = 152.3\, cm^2$$

An average conjugation efficiency of 13% (Figure 3) was achieved for the reaction at 1:1 ratio, meaning that 7.67 μg of the 59 μg of 11A4 used in process is actually conjugated to the surface of the NPs. The surface concentration of 11A4 can be calculated as:

$$Surface\ conc_{11A4} = \frac{7.67 \times 10^{-3}\, mg}{152.3\, cm^2} = 5.04 \times 10^{-5}\, \frac{mg}{cm^2}$$

Since the molecular weight of 11A4 as 14,812 g/mol, the number of 11A4 molecules on the surface is:

$$Molecules_{11A4} =$$

$$\left(\frac{5.04 \times 10^{-8}\, g/cm^2}{14,812\, g/mol}\right) \times 6.02 \times 10^{23}\, \frac{molecules}{mol} = 2.05 \times 10^{12}\, \frac{molecules}{cm^2}$$

If calculated for a single NP, the number of molecules of 11A4 on the surface is:

$$Molecules_{11A4/NP} =$$

$$3.14 \times 10^{-9}\, \frac{cm^2}{NP} \times 2.05 \times 10^{12}\, \frac{molecules_{11A4}}{cm^2} = 6,437\, \frac{molecules_{11A4}}{NP}$$

The surface area that a molecule of 11A4 occupies on a single NP is therefore equivalent to:

$$Total\ Surface\ Area_{11A4} =$$

$$\frac{3.14 \times 10^{-9}\, cm^2/NP}{6,437\, molecules/NP} = 4.88 \times 10^{-13}\, \frac{cm^2}{molecule} = 48.8\, \frac{nm^2}{molecule}$$

Calculations S2. Calculation of the number of cRGDfK molecules present on the surface of a single NP.

The number of molecules of cRGDfK bound to the surface of a single NP containing 20% maleimide-PEG-PLGA and 80% PLGA (NP20%) can be calculated as follows:

First, the mass and surface area of a single NP (m_{NP}) are calculated based on the diameter of the maleimide-PEG-PLGA NPs used in this study, in average, 3.49 x 10^{-5} cm. Since these NPs are made from 80% w/w of PLGA their density will be considered as that of this polymer, namely ρ = 1.25 g/cm^3 [10,11]. Therefore,

$$m_{NP20\%} = \left(\frac{4}{3} \times \pi \times (1.75 \times 10^{-5} cm)^3\right) \times 1.25\, \frac{g}{cm^3} = 2.81 \times 10^{-14}\, \frac{g}{NP}$$

$$Area_{NP20\%} = 4 \times \pi \times (1.75 \times 10^{-5} cm)^2 = 3.85 \times 10^{-9}\, \frac{cm^2}{NP}$$

For a conjugation reaction in a molar ratio of 1:1 maleimide-PEG-PLGA to cRGDfK, 1 mg of NPs and 5 μg of peptide were used. The amount of NPs taking part in the reaction is then:

$$Number\ of\ NPs_{NP20\%} = \frac{1.00 \times 10^{-3}\ g}{2.81 \times 10^{-14}\ g/NP} = 3.56 \times 10^{10}\ NPs$$

The total surface area available for conjugation of cRGDfK to the NPs in the reaction is:

$$Total\ Surface\ Area_{NP20\%} = 3.85 \times 10^{-9} \frac{cm^2}{NP} \times 3.56 \times 10^{10}\ NPs = 137.1\ cm^2$$

An average conjugation efficiency of 52% (Figure 3) was achieved for the reaction at 1:1 ratio, meaning that 2.60 μg of the 5 μg of cRGDfK used in the process is actually conjugated to the surface of the NPs. The surface concentration of cRGDfK can be calculated as:

$$Surface\ conc_{cRGDfK} = \frac{2.60 \times 10^{-3} mg}{137.1\ cm^2} = 1.90 \times 10^{-5}\ \frac{mg}{cm^2}$$

Since the molecular weight of cRGDfK is 678.5 g/mol, the number of cRGDfK molecules on the surface of all the NPs participating in the reaction is:

$$Molecules_{cRGDfK/NP} =$$

$$\left(\frac{1.90 \times 10^{-8}\ g/cm^2}{678.5\ g/mol}\right) \times 6.02 \times 10^{23}\ \frac{molecules}{mol} = 1.68 \times 10^{13} \frac{molecules}{cm^2}$$

If calculated for a single NP, the number of molecules of cRGDfK on the surface is:

$$Molecules_{cRGDfK/NP} =$$

$$3.85 \times 10^{-9}\ \frac{cm^2}{NP} \times 1.68 \times 10^{13}\ \frac{molecules}{cm^2} = 64,680\ \frac{molecules_{cRGDfK}}{NP}$$

The surface area that a molecule of cRGDfK occupies on a single NP is therefore equivalent to:

$$Total\ Surface\ Area_{cRGDfK} =$$

$$\frac{3.85 \times 10^{-9}\ cm^2/NP}{64,680\ molecules/NP} = 5.95 \times 10^{-14}\ \frac{cm^2}{molecule} = 5.95\ \frac{nm^2}{molecule}$$

References

[1] Alexis, F., Basto, P., Levy-Nissenbaum, E., Radovic-Moreno, A. F., Zhang, L., Pridgen, E., Wang, A. Z., Marein, S. L., Westerhof, K., Molnar, L. K., and Farokhzad, O. C. HER-2-targeted nanoparticle-affibody bioconjugates for cancer therapy. *ChemMedChem.*, 3(12):1839–1843, 2008.

[2] Bai, M. Y. and Liu, S. Z. A simple and general method for preparing antibody-PEG-PLGA sub-micron particles using electrospray technique: an in vitro study of targeted delivery of cisplatin to ovarian cancer cells. *Colloids Surf., B*, 117:346–353, 2014.

[3] Hu, K., Shi, Y., Jiang, W., Han, J., Huang, S., and Jiang, X. Lactoferrin conjugated PEG-PLGA nanoparticles for brain delivery: preparation, characterization and efficacy in Parkinson's disease. *Int. J. Pharm.*, 415(1-2):273–283, 2011.

[4] Li, J., Feng, L., Fan, L., Zha, Y., Guo, L., Zhang, Q., Chen, J., Pang, Z., Wang, Y., Jiang, X., Yang, V. C., and Wen, L. Targeting the brain with PEG-PLGA nanoparticles modified with phage-displayed peptides. *Biomaterials*, 32(21):4943–4950, 2011.

[5] Luo, G., Yu, X., Jin, C., Yang, F., Fu, D., Long, J., Xu, J., Zhan, C., and Lu, W. LyP-1-conjugated nanoparticles for targeting drug delivery to lymphatic metastatic tumors. *Int. J. Pharm.*, 385(1-2):150–156, 2010.

[6] Olivier, J. C., Huertas, R., Lee, H. J., Calon, F., and Pardridge, W. M. Synthesis of pegylated immunonanoparticles. *Pharm. Res.*, 19(8):1137–1143, 2002.

[7] Toti, U. S., Guru, B. R., Grill, A. E., and Panyam, J. Interfacial activity assisted surface functionalization: a novel approach to incorporate maleimide functional groups and cRGD peptide on polymeric nanoparticles for targeted drug delivery. *Mol. Pharm.*, 7(4):1108–1117, 2010.

[8] Wang, Y., Liu, P., Duan, Y., Yin, X., Wang, Q., Liu, X., Wang, X., Zhou, J., Wang, W., Qiu, L., and Di, W. Specific cell targeting with APRPG conjugated PEG-PLGA nanoparticles for treating ovarian cancer. *Biomaterials*, 35(3):983–992, 2014.

[9] Yao, W., Xu, P., Zhao, J., Ling, L., Li, X., Zhang, B., Cheng, N., and Pang, Z. RGD functionalized polymeric nanoparticles targeting periodontitis epithelial cells for the enhanced treatment of periodontitis in dogs. *J. Colloid Interface Sci.*, 458:14–21, 2015.

[10] Cu, Y. and Saltzman, W. M. Controlled surface modification with poly(ethylene)glycol enhances diffusion of PLGA nanoparticles in human cervical mucus. *Mol. Pharmaceutics*, 6(1):173–181, 2009.

[11] Qi, R., Guo, R., Shen, M., Cao, X., Zhang, L., Xu, J., Yu, J., and Shi, X. Electrospun poly(lactic-co-glycolic acid)/halloysite nanotube composite nanofibers for drug encapsulation and sustained release. *J. Mater. Chem.*, 20(47):10622–10629, 2010.

Chapter 3

Endothelial cell targeting by cRGD-functionalized polymeric nanoparticles under static and flow conditions

Lucía Martínez-Jothar[†], Arjan D. Barendrecht[‡], Sabrina Oliveira[†,§], Cornelus F. van Nostrum[†], Raymond M.Schiffelers [‡], Wim E. Hennink[†] and Marcel H.A.M Fens[†]

† Department of Pharmaceutics, Utrecht Institute for Pharmaceutical Sciences, Utrecht University, Utrecht, the Netherlands

‡ Department of Clinical Chemistry and Haematology, University Medical Center Utrecht, Utrecht, the Netherlands

§ Division of Cell Biology, Department of Biology, Utrecht University, Utrecht, the Netherlands

Manuscript in preparation

Abstract

The interaction between the Arg-Gly-Asp (RGD) tripeptide motif, present in many extracellular matrix proteins, and $\alpha_v\beta_3$ integrin expressed by activated endothelial cells mediates cell adhesion, migration and growth. Since $\alpha_v\beta_3$ integrin is a key component of angiogenesis in health and disease, RGD-functionalized nanocarriers have been proposed as vehicles for targeted delivery of drugs to the neovasculature of tumors. In this work, PEGylated nanoparticles (NPs) based on poly(lactic-co-glycolic acid) (PLGA) with a size of ∼300 nm and functionalized with cyclic-RGD (cRGD) were evaluated as nanocarriers for the targeting of angiogenic endothelium. For this purpose, NPs functionalized with cRGD with different surface densities were prepared by maleimide-thiol chemistry and their interactions with human umbilical vein endothelial cells (HUVECs) were evaluated under different conditions using flow cytometry and microscopy. The cell association of cRGD-NPs under static conditions was time-, concentration- and cRGD- density dependent. The interactions between HUVECs and cRGD-NPs dispersed in cell culture medium under flow conditions (shear rate 300 sec^{-1}, similar to the mean shear rate reported for the human carotid artery) were also time- and cRGD- density dependent. When washed red blood cells (RBCs) were added to the medium (hematocrit 32%), a remarkable increase in NPs association to HUVECs was observed, i.e. 3 times higher association for high cRGD-NPs and 6 times higher association for low cRGD-NPs (16 h perfusion). Flowing RBCs are likely to push the NPs towards the endothelial cells, decreasing the distance between these two and thus facilitating their interaction. The findings of this work indicate that the interactions between polymeric NPs and endothelial cells are favored by increasing cRGD surface densities. Furthermore, experiments conducted under flow using medium that contains a physiologic RBC volume fraction and shear rate that matches the one occurring in human blood vessels, are a step forward in the prediction of *in vivo* cell-particle association. This approach has the potential to assist the development and high-throughput screening of new endothelium-targeted nanocarriers, and could facilitate the reduction of the number of tests conducted in laboratory animals.

1 Introduction

Angiogenesis, an essential process for tissue formation and repair, relies on complex cell-cell and cell-matrix interactions mediated by adhesion molecules[1–3]. One of the most extensive families of cell adhesion molecules is that of integrins, which are transmembrane receptors consisting of an α and a β subunit capable of bidirectional signaling. The extracellular domain of integrins binds to ligands present on proteins of the extracellular matrix (ECM) or to receptors on neighboring cells, while the cytoplasmic domain transfers external stimuli to the cytoskeleton and plays a role in the activation of intracellular signaling pathways[4]. Integrin $\alpha_v\beta_3$, one of the 24 integrin subtypes, is highly expressed in activated (angiogenic) endothelial cells but not on quiescent cells, and is therefore an important mediator of angiogenesis under normal and pathological conditions[5,6]. The most important ligand of integrin $\alpha_v\beta_3$ is the RGD peptide, which is present in proteins such as lactadherin, fibronectin, vitronectin, laminin and vonWillebrand factor, and is involved in the regulation of cell adhesion, migration and growth[7,8]. Besides participating in tumor angiogenesis, integrin $\alpha_v\beta_3$ is also associated with increased proliferation, survival and/or metastasis of some tumors, including gliomas, melanomas, gastric, breast, ovarian and pancreatic tumors[9–11], which positions it as an important pharmacological target in cancer treatment[12]. While the inhibition of integrin $\alpha_v\beta_3$ suppresses angiogenesis, tumor growth and metastasis in pre-clinical studies[13,14], these findings have not yet been successfully translated to the clinic[15]. Alternatively, some researchers have explored the possibility of using integrin $\alpha_v\beta_3$ as a target for the delivery of anti-cancer agents via RGD-functionalized nanocarriers[16–21]. In this regard, RGD-functionalized polymeric nanoparticles (NPs) loaded with cytotoxic drugs have shown increased anti-cancer activity *in vitro* and *in vivo* compared to non-functionalized polymeric NPs and/or free drugs[22–25]. The higher efficacy of RGD-NPs *in vivo* can be attributed to several factors, including improved pharmacokinetics of the drugs by encapsulation in PEGylated NPs (i.e. prolonged circulation time), as well as the interactions between RGD grafted on the NPs and integrin $\alpha_v\beta_3$ present on cellular membranes of angiogenic endothelial cells of the tumor vasculature. In respect to this, the number and density of RGD moieties on the surface of NPs is very likely to play a role on the extent of the binding with the target cells in terms of kinetics and number of particles bound per cell. In fact, the relevance of multivalent interactions has been highlighted by the superior binding affinity and internalization of multimeric-RGD structures (i.e. radiolabeled or fluorescent peptides) in comparison to their monomeric analogues[26–29]. These findings

prompted us to study the influence of ligand density on the interaction between NPs functionalized with cRGD and human umbilical vein endothelial cells (HUVECs), an extensively used *in vitro* model for angiogenic endothelial cells[30,31]. For this purpose, HUVECs were incubated with poly(lactic-co-glycolic acid) (PLGA) NPs surface functionalized with cRGD at different densities, and the nanoparticle-cell interactions were evaluated under static incubation conditions. Since the integrin $\alpha_v\beta_3$ is preferentially expressed by endothelial cells of nascent blood vessels, we also studied these interactions under physiological flow conditions. For this purpose, we used a perfusion system and conducted experiments using either cell culture medium or a suspension of washed red blood cells (RBCs) as the flow medium. It has been suggested that cell culture and tests under flow provide a better representation of the (patho)physiological conditions under which nanocarrier-endothelial cell contact occurs *in vivo*[32,33]. In this regard, the generation of flow-induced shear stress can influence cellular responses such as cell-cell adhesion[34], the uptake of NPs[35,36] and the cytocompatibility with lipid, polymeric and metallic NPs[37,38]. Taking into consideration this information, we conducted studies with the purpose to gain a better understanding of the influence of a) the surface properties of the NPs, in terms of ligand density and b) the test conditions (i.e. static vs flow, and tests in cell culture medium vs washed RBCs), on the cell association and uptake of $\alpha_v\beta_3$ targeted and non-targeted PLGA-NPs by HUVECs.

2 Experimental section

2.1 Chemicals

PLGA (50:50 ratio DL-lactide/glycolide, IV 0.39 dl/g, M_w ~44,000 Da) was obtained from Corbion (Gorinchem, the Netherlands). Poly(lactide-co-glycolide)-b-poly(ethylene glycol)-maleimide (maleimide-$PEG_{5,000}$-$PLGA_{20,000}$) was purchased from Polyscitech, Akina Inc (West Lafayette, IN, USA). Poly(vinyl alcohol) (PVA) of M_w 30,000 - 70,000 Da, 87 - 90% hydrolyzed, L-cysteine hydrochloride monohydrate and hydroxylamine hydrochloride were acquired from Sigma-Aldrich (Steinheim, Germany). Dicyclohexylcarbodiimide (DCC) was purchased from Aldrich (Steinheim, Germany). 4-(Dimethylamino)pyridine (DMAP) was obtained from Fluka (Steinheim, Germany). Dichloromethane (DCM), diethyl ether, acetonitrile and dimethyl sulfoxide (DMSO) were obtained from Biosolve (Valkenswaard, the Netherlands). Cyanine5 free carboxylic acid (Cy5-COOH) was purchased

from Lumiprobe (Hannover, Germany). The cyclic peptide c[RGDfK(Ac-SCH_2CO)] (M_w: 719.8 g/mol) was purchased from Peptides International (Louisville, KY, USA). HEPES, EDTA disodium salt dihydrate, gelatin from bovine skin and Dulbecco's phosphate buffered saline (8.0 g NaCl, 1.15 g Na_2HPO_4, 0.2 g KCl and 0.2 g KH_2PO_4 in 1 L of water, pH 7.4) were products of Sigma (Steinheim, Germany). Micro BCA™ Protein Assay Kit was purchased from Thermo Scientific (Illinois, USA).

2.2 Synthesis of Cy5 labelled poly(D,L-lactic-co-glycolic-co-hydroxymethyl glycolic acid) (Cy5-PLGHMGA)

Poly(D,L-lactic-co-glycolic-co-hydroxymethyl glycolic acid) (PLGHMGA) was synthesized as reported in chapters 4 and 5 of this thesis. The fluorescent label Cy5-COOH was covalently attached to the pendant hydroxyl groups in PLGHMGA by DCC-DMAP chemistry. Briefly, 50 mg of PLGHMGA was dissolved in 5 mL of dry DCM and placed under stirring in a round bottom flask with a rubber stopper. Subsequently, 18 μL of DCC (1.6 mg/mL dissolved in DCM), 60 μL of Cy5-COOH (1 mg/mL dissolved in DCM) and 4 μL of DMAP (0.5 mg/mL DCM) were added to the polymer solution and the mixture was stirred and flushed with N_2 for 10 minutes at room temperature (RT). The reaction was allowed to proceed overnight under stirring and protected from light. Next, the reaction mixture was concentrated under reduced pressure (removal of ∼80% of the DCM volume) and the polymer was precipitated in cold diethylether (25 mL). The fluorescent polymer was recovered by filtration, dried under reduced pressure, dissolved in 2 mL of DCM and dialyzed against DMSO for 48 h to remove the free dye (dialysis membrane MWCO 6 - 8 kDa, Spectra/Por™, Spectrumlabs). The purified polymer was freeze dried at -40 °C, <1 mbar (Christ Alpha 1-2 freeze dryer). The Cy5 labelled polymer (yield 92%) was characterized by gel permeation chromatography (GPC) using two PL-gel 5 μm Mixed-D columns and tetrahydrofuran/lithium chloride 10 mM as the mobile phase (1 mL/min) at 60 °C. Dual RI and UV detection (λ 650 nm) was used for analysis, and polystyrene standards (EasiCal Agilent, California, USA) were used for calibration. The M_w of the polymer was 62 kDa (M_n 42 kDa, PDI 1.46) and no signal for the free dye was detected after purification.

2.3 Preparation and characterization of the polymeric nanoparticles (NPs)

Fluorescent NPs were prepared by double emulsion solvent evaporation method[39,40]. A mixture of PLGA, maleimide-PEG-PLGA and Cy5-PLGHMGA (ratio 65/20/15 wt%) was dissolved in DCM at 5% w/v. To prepare the first emulsion W/O (water-in-oil), 100 μL of water was added to 1 mL of polymer solution and the mixture was emulsified using a probe sonicator (SONOPULS HD 2200 Bandelin, Berlin, Germany) for 1 minute at 20 W power in an ice bath. The W/O emulsion was subsequently added dropwise to 10 mL of an aqueous solution of PVA 5% w/w. The addition was done under sonication for 2 minutes at 20 W in an ice bath and resulted in the formation of a W/O/W/ emulsion (water-in-oil-in-water). This emulsion was stirred (600 rpm) for 2 h at RT to evaporate DCM. The NPs formed after solvent evaporation were collected by centrifugation for 20 min, 20,000 x g at 4 °C, washed twice with HEPES 10 mM (pH 7.0) and once with distilled water. After the last washing, the NPs were resuspended in 1 mL of distilled water and divided into aliquots of 250 μL. One of the aliquots was freeze dried in order to determine the yield of the preparation process, while the other aliquots were supplemented with sucrose at a final concentration of 5% w/v prior to freeze drying (-40 °C, <1 mbar, Christ Alpha 1-2 freeze dryer).

The size of the NPs was determined by Dynamic Light Scattering (Zetasizer Nano S, Malvern, Worcestershire, UK) at 25 °C in MilliQ water and their zeta potential (Zetasizer Nano Z, Malvern, Worcestershire, UK) was determined at 25 °C in HEPES 10 mM, pH 7.0.

2.4 Conjugation of cRGD to the NPs

The cRGD peptide was conjugated to the fluorescent NPs by maleimide-thiol chemistry as described in previous work of our group[41] (also chapter 2 of this thesis). Briefly, c[RGDfK(Ac-SCH_2-CO)] was deprotected by incubation for 30 minutes at RT in a buffer containing 10 mM HEPES/0.4 mM of EDTA/45 mM hydroxylamine (pH 7.0), in order to remove the acetyl group to generate a free thiol per peptide molecule. Next, deprotected cRGD was conjugated to the fluorescent NPs at different molar ratios cRGD to maleimide-polymer, namely 1:10 ("low" cRGD-NPs), 1:5 ("medium" cRGD-NPs) and 1:2 ("high" cRGD-NPs), as follows. Freeze dried NPs were resuspended in distilled water and recovered by centrifugation at 3,000 x g, 10 min, 4 °C. The pelleted NPs were resuspended in a buffer 10 mM HEPES/0.4 mM EDTA (pH 7.0) to a concentration of ∼7 mg/mL and aliquots containing 2 mg of NPs were

incubated with deprotected cRGD (13, 5.0 and 2.5 μL of cRGD 0.45 mg/mL to 300 μL of NPs suspension), for 30 minutes at RT in the dark. The NPs were recovered by centrifugation (3,000 x g, 10 min, 4 °C), the supernatant was removed and stored for analysis of the cRGD concentration (described in section 2.5) and the pellet was resuspended in 10 mM HEPES/0.4 mM EDTA to a concentration of ∼7 mg/mL. Cysteine dissolved in 10 mM HEPES/0.4 mM (pH 7.0) was added to the NPs suspension in a molar ratio of 2:1 cysteine to maleimide-polymer (6.0 μL of cysteine 0.5 mg/mL to 300 μL of NPs suspension) to block the remaining unreacted maleimide groups. Subsequently, the suspension was incubated for 30 minutes at RT in the dark, the NPs were recovered by centrifugation (3,000 x g, 10 min, 4 °C), the supernatant was stored for quantification of cysteine (section 2.5) and the pellet was washed with 10 mM HEPES/0.4 mM EDTA. Finally, the NPs pellet was resuspended in PBS at a concentration of 10 mg/mL and stored at 4 °C in the dark until further use. Control (non-targeted) NPs functionalized with cysteine at a molar ratio of 2:1 cysteine to maleimide-polymer (Cys-NPs) were prepared as described for the NPs functionalized with cRGD, but skipping the addition of this peptide. The size and zeta potential of the cRGD-NPs and the Cys-NPs were determined as mentioned in section 2.3.

2.5 Quantification of cRGD by HPLC to determine the conjugation efficiency to the NPs

The concentration of cRGD present in the supernatants of the pelleted functionalized NPs was quantified by HPLC (Waters Alliance System) equipped with a UV detector (analysis at 214 nm) as previously reported[41]. Briefly, the samples (50 μL injection volume) were run through a XBridge BEH C18 column (3.5 μm, 2.1 mm x 100 mm) using a gradient from 100% eluent A (94.9% H_2O, 5.0% ACN, 0.1% acetic acid) to eluent B (94.9% ACN, 5.0% H_2O, 0.1% acetic acid) in 12 minutes followed by 100% eluent B in 1 min. The detection limit was 2 μg/mL.

The cysteine concentration in the supernatants of the pelleted NP dispersions was quantified by MicroBCA assay according to the protocol of the manufacturer. Detection limit was 2 μg/mL.

The conjugation efficiency was calculated as:

$$\text{Conjugation efficiency (\%)} = \left(1 - \frac{[\text{Ligand in the supernatant}]}{[\text{Ligand added in the conjugation reaction}]}\right) \times 100\%$$

Since cysteine was added in excess compared to the maleimide groups in the NPs (2:1 molar ratio), the maximum achievable conjugation efficiency was 50%. Therefore, the conjugation efficiency of cysteine was normalized to this value.

2.6 Cell culture conditions

Pooled human umbilical vein endothelial cells (HUVECs) were obtained from Lonza (Verviers, Belgium) and cultured in Endothelial Basal Medium (EBM-2) supplemented with growth factors (Growth Medium 2 SupplementMix®, PromoCell, Heidelberg Germany) and antibiotics (gentamicin/amphotericin B, Gibco, New York, USA) up to passage number 6. The cells were incubated at 37 °C, 5% CO_2, in a humidified atmosphere during culture as well as during the experiments (sections 2.7 - 2.9). For the flow experiments, HUVECs were seeded on a perfusion slide (μ-Slide I Luer®, Ibidi, Martinsried, Germany) at a density of 2.4 x 10^5 cells/slide and allowed to attach for 2 h. Next, the slide was connected to the a pump-controlled perfusion set (Ibidi, Martinsried, Germany) and the cells were cultured in EGM-2 (EBM-2 medium supplemented with growth factors and antibiotics), under continuous flow (shear rate 300 sec^{-1}, shear stress 0.3 N/m^2 (3.0 dyn/cm^2), viscosity 1 mPa.s (0.01 dyn.s $/cm^2$) at 37 °C and 5% CO_2.

2.7 Association of Cys-NPs and cRGD-NPs with HUVECs under static conditions

HUVECs were seeded in a 12 well plate at a density of 50,000 cells/well. After 24 hours of incubation, the cell medium was replaced and fluorescent Cys-NPs or fluorescent cRGD-NPs were added to the cells at final concentrations of 0.016, 0.08 and 0.4 mg/mL. HUVECs were incubated with the NPs for 1 or 3 h, after which they were washed twice with PBS and detached from the wells using trypsin/EDTA (0.05%). Trypsin was neutralized with Dulbecco's PBS containing 0.5% bovine serum albumin, the cells were recovered by centrifugation at 300 x g for 5 minutes at RT and the supernatant was removed. The cell pellet was resuspended in PBS also containing 0.5% bovine serum albumin. The fluorescence associated to the cells was determined by fluorescence-activated cell sorting (FACS, Canto II, BD Biosciences) using an APC laser (λ 660 nm, used to detect the Cy5 signal from the NPs). Initially, HUVECs were gated by plotting FSC/SSC and 10,000 events were recorded (P1). The mean fluorescence intensity (MFI) was determined for the P1 population and subsequent gating of P1 was done to calculate the percentage of

cells in P1 that showed above background fluorescence (P2), using untreated HUVECs as a control.

2.8 Uptake of Cys-NPs and cRGD-NPs by HUVECs under static incubation conditions

Glass bottom 16 well chamber slides (Nunc™) were coated with 0.5% gelatin from bovine skin (30 min, 37 °C) followed by 0.5% glutaraldehyde in PBS (10 min, RT) and wells were finally washed three times with PBS. HUVECs were seeded in the coated wells at a density of 10,000 cells/well and incubated overnight at 37 °C. Next, the cell medium was replaced and fluorescent Cys-NPs or fluorescent cRGD-NPs dispersed in PBS were added to the cells at a final concentration of 0.4 mg/mL. The cells were incubated with the NPs for 1 or 3 h, after which they were washed twice with PBS and fixed with 2% paraformaldehyde/0.2% glutaraldehyde in PBS for 1 h at RT and then stored overnight at 4 °C. The nuclei were stained using Hoechst 33342 (Fluka), 1 μg/mL in PBS for 20 mins, washed once with PBS and the F-actin cytoskeleton was stained with phalloidin Alexa Fluor 488 (Life Technologies), 1:50 in PBS for 30 mins. After washing, the cells were mounted with FluorSave™ reagent (Calbiochem). HUVECs were visualized by confocal microscopy using a Leica TCS SP8 X confocal microscope with a white light laser (continuous spectral output between λ 470 - 670 nm) and a 63X objective. Two fields were imaged per condition and images were captured in three channels: Hoechst 33342 for nuclei (λex 419 nm, λem 500 nm), phalloidin 488 (λex 510 nm, λem 562 nm) for F-actin cytoskeleton and Cy5 for visualization of the NPs (λex 660 nm, λem 700 nm).

2.9 Association of Cys-NPs and RGD-NPs with HUVECs under flow

The experiments under flow were performed using an Ibidi pump system®. The cells were cultured under flow as mentioned in section 2.6 for 3 days prior to the addition of NPs.

2.9.1 Experiments under flow, 1 hour incubation in EBM-2 medium

The medium in the perfusion system was replaced with EBM-2 medium and the system was allowed to equilibrate for 2 minutes under flow. Next, Cys-NPs or cRGD-NPs dispersed in PBS were added to the system (flow was stopped

during addition) at a final concentration of 0.08 mg/mL and the HUVECs were incubated with the NPs for 1 h at 37 °C under flow (shear rate 300 sec^{-1}, viscosity 1 mPa.s, shear stress 0.3 N/m^2). The incubation was followed by medium refreshment and washing of the cells for 5 minutes (with EBM-2). Finally, the slide was disconnected from the system and an additional washing of the cells was done manually by carefully flushing 3 mL of EBM-2 through the slide. The cells were then fixed with 2% paraformaldehyde/0.2% glutaraldehyde in PBS for 1 h at RT, and then stored overnight at 4 °C. After fixation, HUVECs were stained with Hoechst 33342 and phalloidin 488 as described in section 2.8. Cell images (epifluorescence) were captured using a Zeiss Z1 microscope equipped with Colibri LEDs (365 nm used for visualization of nuclei, 470 nm used for visualization of the cytoskeleton and 625 nm for the NPs labelled with Cy5), using a 40X objective and an AxioCam MRm. Ten images, captured along the slide, were processed using the Fiji image analysis software (NIH, USA) as follows: background noise was eliminated for all images. A threshold was set for the images from the experiments under flow in EBM-2 (1 h and 16 h) and in EBM-2 with washed RBCs (16 h) in order to reduce remaining background signal. The Integrated Density was determined in the channel containing the signal of the Cy5 labeled NPs.

2.9.2 Experiments under flow, 18 hours incubation in EBM-2 medium

The medium in the system was replaced by EBM-2 medium and the system was allowed to equilibrate for 2 minutes. Cys-NPs or cRGD-NPs dispersed in PBS were added at a final concentration of 0.08 mg/mL and the cells were incubated under flow (shear rate 300 sec^{-1}, viscosity 1 mPa.s, shear stress 0.3 N/m^2) for 18 h at 37 °C and 5% CO_2. Subsequently, the medium was refreshed and the cells were washed for 5 minutes. Finally, the slide was disconnected from the system, an additional washing of the cells was done manually by flushing 3 mL of EBM-2 through the slide, and the cells were fixed and stained as described in section 2.9.1.

2.9.3 Experiments under flow, 18 hours incubation in washed red blood cells (RBCs)

Whole blood anticoagulated using sodium citrate 3.2% (from a single donor) was obtained from the mini donor service at University Medical Center Utrecht (the Netherlands) and centrifuged at 1,000 x g for 15 minutes. Next, RBCs were separated from the plasma and the buffy coat, and washed once with

PBS. A suspension of washed RBCs was prepared in EBM-2 (20 mL washed RBC and 26 mL medium). The medium in the Ibidi system was replaced with the RBCs suspension (hematocrit 32% as measured by Cell-Dyn Hematology Analyzer, Abbot) and the system was allowed to equilibrate for 5 minutes. Cys-NPs or cRGD-NPs dispersed in PBS were added at a final concentration of 0.08 mg/mL and the cells were incubated under flow (shear rate 300 sec^{-1}, viscosity 1.8 mPa.s, shear stress 0.54 N/m^2) for 18 h at 37 °C and 5% CO_2. The washed RBCs suspension was replaced with EBM-2 medium and the HUVECs were washed for 5 minutes. The slide was disconnected from the system and an additional washing was done manually by flushing 3 mL of EBM-2 through the slide. The cells were then fixed and stained as described in section 2.9.1.

3 Results and Discussion

3.1 Preparation and characterization of the polymeric nanoparticles (NPs)

Cy5 labelled maleimide-PEG-PLGA NPs were prepared by double emulsion solvent evaporation method using a blend of PLGA, maleimide-PEG-PLGA and Cy5-PLGHMGA at 65/20/15 wt%, respectively. The yield of NPs preparation was 50%. cRGD peptides (bearing one thiol group per cRGD molecule) were conjugated to the surface of the NPs by maleimide-thiol chemistry to prepare particles specifically targeting $\alpha_v\beta_3$ integrins, while NPs conjugated to cysteine were prepared as a non-targeted control. For the preparation of the targeted NPs, different molar ratios of cRGD to maleimide-PEG-PLGA were used in order to obtain formulations with different surface ligand densities, designated as low (1:10 molar ratio), medium (1:5 ratio) and high (1:2 ratio).

Cys-NPs and cRGD-NPs with different ligand densities were similar in size, surface area (0.31 - 0.35 μm^2) and surface charge (Table 1). The conjugation efficiency of cysteine to the NPs was ∼40%. Theoretically, 100% conjugation efficiency could have been reached because a molar excess of cysteine to maleimide was used in the reaction. Nevertheless, previous work conducted in our group has indicated that the surface availability of maleimide groups might actually be lower than expected[41] (chapters 2 and 5 of this thesis), probably due to the miscibility of PEG and PLGA[42,43] that leads to the solubilization of the maleimide groups in the polymer matrix of the NPs. The conjugation efficiencies of cRGD to the NPs ranged between 40 - 70%. These efficiencies resulted in the successful preparation of NPs with different cRGD

surface densities (Table 1 and Calculations S1). The ligand density on the high cRGD-NPs is ∼3.5 times higher than on the medium cRGD-NPs and ∼10 times higher than on the low cRGD-NPs.

Table 1: Size, zeta potential and conjugation efficiency of Cy5-PLGA NPs.

Formulation	Diameter (nm)	PDI	Zeta potential (mV)	Conjugation efficiency (%)[a]	RGD peptides coupled per NP[b]	Density (cRGD/ μm^2)[b]
NPs	303 ± 34	0.25 ± 0.10	-10.1 ± 0.7	NA[c]	NA[c]	NA[c]
Cys-NPs	316 ± 19	0.22 ± 0.02	-12.2 ± 0.6	39 ± 12	NA[c]	NA[c]
Low cRGD-NPs	313 ± 11	0.21 ± 0.00	-12.0 ± 0.4	38 ± 5	∼3,400	∼11,000
Medium cRGD-NPs	312 ± 14	0.19 ± 0.03	-11.4 ± 0.2	50 ± 8	∼9,700	∼31,700
High cRGD-NPs	332 ± 22	0.23 ± 0.04	-10.1 ± 0.6	71 ± 8	∼40,700	∼117,600

n=4 independently prepared batches. [a] Conjugation efficiency = (1 - ([Ligand in the supernatant] / [Ligand added in the conjugation reaction])) x 100%, [b] calculated as reported in Calculations S1, [c] not applicable

3.2 Association of Cys-NPs and RGD-NPs with HUVECs under static incubation conditions

Dispersions of different concentrations of fluorescently labelled NPs with and without cRGD decoration, were incubated with HUVECs for 1 or 3 h and the association of NPs to the cells was assessed by FACS. Cell association was virtually absent for Cys-NPs (non-targeted control). On the contrary, cell association was observed for cRGD-NPs with all three ligand densities, and the fluorescent signal of the NPs was distributed homogeneously over the cell population. The association of cRGD-NPs to HUVECs showed a positive correlation with the NPs concentration, the incubation time and the cRGD surface density (Table 2 and Figure 1). For high cRGD-NPs at 0.4 mg/mL (highest concentration tested), ∼100% of the HUVECs were associated to NPs already after 1 h of incubation. Based on the average fluorescent signals obtained by FACS, cell association of cRGD-NPs was 2.9 to 4.0 fold higher for high cRGD-NPs compared to low cRGD-NPs after 1 h of incubation, and 2.2 to 3.7 fold higher after 3 h of incubation (at different concentrations of NPs). Medium cRGD-NPs displayed values that were in between the low and high density NPs. An increase in the incubation time of all cRGD-NPs with

HUVECs from 1 to 3 h resulted in 1.3 to 2.3 times more cell association. The increase in fluorescence intensity observed upon incubation of the cells with these NPs for 3 h, shows that more particles were associated per cell.

Table 2: Fluorescence distribution (% of positive cells) in HUVECs upon static incubation at 37 °C with Cys-NPs and cRGD-NPs of different ligand densities.

Concentration of fluorescent NPs (mg/mL)	Percentage of fluorescence positive HUVECs							
	Cys-NPs		Low cRGD-NPs		Med cRGD-NPs		High cRGD-NPs	
	1 h	3 h	1 h	3 h	1 h	3 h	1 h	3 h
0.016	0.3±0.2	0.2±0.1	8±1	15±5	15±4	36±3	43±8	60±9
0.08	0.5±0.2	0.9±0.4	30±4	58±8	51±11	83±2	83±5	93±3
0.4	3±1	12±7	71±1	91±4	85±5	98±1	97±1	99±0

% of fluorescence positive HUVECs (P2) obtained from a gated HUVECs population (P1), n=4

Confocal microscopy analysis was used to gain insight into the cellular localization of the fluorescent signal detected by flow cytometry and thus on the intracellular distribution of the NPs. Confocal imaging of Cys-NPs (Figure 2) showed negligible intracellular accumulation, which is in agreement with its poor cell association demonstrated by FACS. In contrast, cytoplasmic accumulation (confirmed by phalloidin staining of F-actin cytoskeleton) was observed upon incubation with the different cRGD-NPs (Figure 2). Similar to the FACS data (Figure 1), confocal microscopy observations indicate that the cRGD density on the surface of the NPs is positively correlated with their accumulation (uptake) in HUVECs. Moreover, the signal of the cRGD-NPs in the cytoplasm showed a dotted pattern rather than diffused fluorescence, suggesting that the NPs localize to endosomes after their uptake.

The much higher cell association and uptake of cRGD-NPs in comparison to Cys-NPs suggests that cRGD mediates the binding of the NPs to HUVECs. Other studies comparing non-targeted and targeted PEGylated PLGA NPs (∼100 - 200 nm) also found increased binding to and uptake by HUVECs for targeted NPs. Nevertheless, non-specific cell interactions of non-targeted NPs were also observed, particularly at incubation times $\geq$ 1 hour[22,44]. These findings are in contrast with the low cell association observed for the Cys-NPs in our study even after 3 h of incubation. Endocytosis of non-targeted NPs is highly influenced, amongst others, by their size, charge and surface chemistry. The Cys-NPs used in this study have a relatively large size (∼300 nm) which would limit their caveolae-mediated uptake and their uptake by other non-clathrin mediated mechanisms generally associated with the formation of small

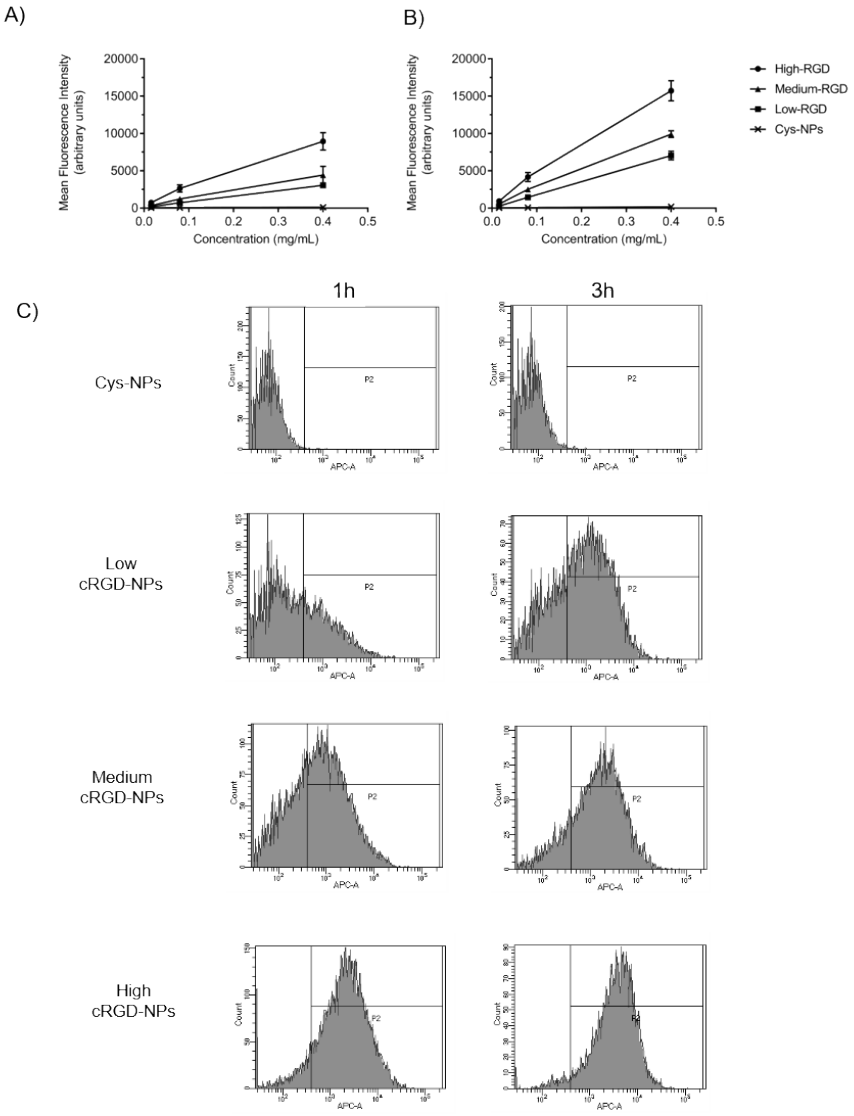

Figure 1: Association of Cys-NPs or cRGD-NPs of different ligand densities to HUVECs under static conditions at 37 °C. A) Association measured with FACS after 1 h, and B) 3 h of incubation (n=4). C) Representative FACS histograms of the fluorescence distribution in HUVECs incubated with 0.08 mg/mL of Cys-NPs or cRGD-NPs for 1 or 3 hours.

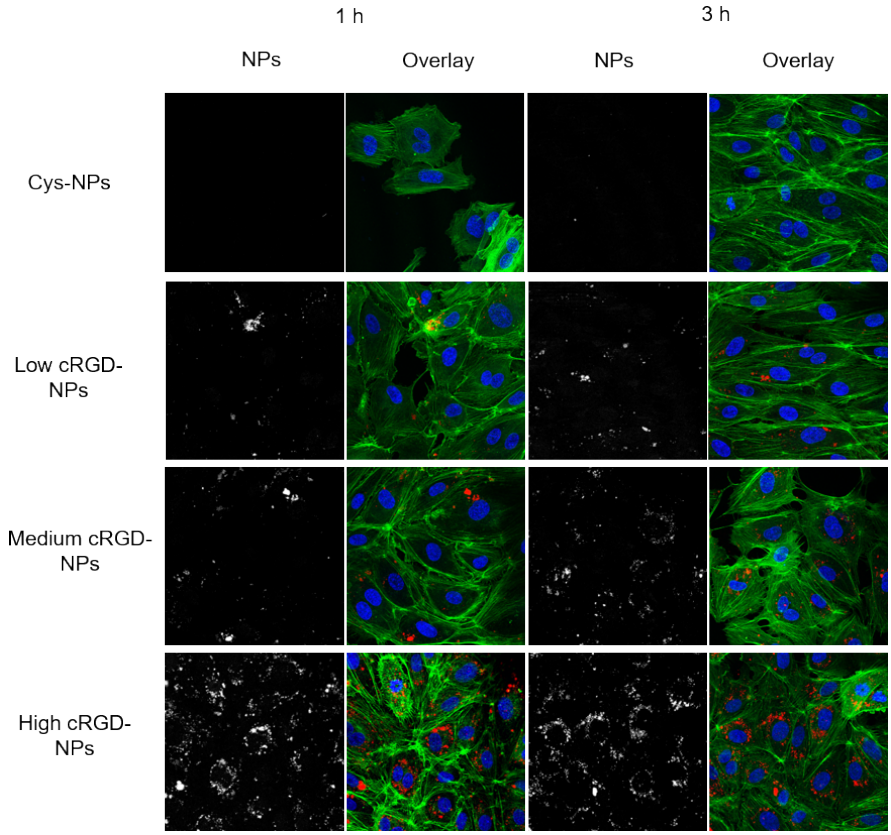

Figure 2: Uptake of Cys-NPs and cRGD-NPs of different ligand densities by HUVECs under static incubation conditions. Confocal images of HUVECs incubated with NPs for 1 and 3 h at 37 °C. Nuclei are stained in blue, cytoskeleton (F-actin) is stained in green, and NPs are observed in red.

vesicles (∼50 - 100 nm)[45,46]. Additionally, Cys-NPs have a slightly negative surface charge (zeta potential ∼ -12 mV), which limits the charge-driven NPs-cell interaction and uptake that is often reported for positively charged NPs[47].

Particles decorated with RGD can be internalized by receptor-mediated endocytosis[48] or by phagocytosis[49] driven by the interaction between RGD and $\alpha_v\beta_3$. In the present study, the association of cRGD-NPs to HUVECs was time- and concentration-dependent, which is in line with reports on the interactions between other RGD-functionalized nanocarriers and $\alpha_v\beta_3$ overexpressing cells[50,51]. Cell association of NPs was also highly influenced by the surface density of cRGD (Figures 1 and 2). Similarly, other research groups have found that increasing RGD-densities on the surface of nanocarriers generally result in increasing binding to the integrin $\alpha_v\beta_3$, coated on plate surfaces or present on the surface of cells[52,53]. In the present work, the NPs association to HUVECs increased with increasing RGD-densities and reached a maximum at ∼118,000 RGD/μm^2 (density on the high cRGD-NPs). In a similar study with PLGA-NPs prepared with cRGD densities ∼26,000 - 137,000 RGD/μm^2, the association to HUVECs was also dependent on the cRGD density and also reached a maximum for the NPs with the highest surface density[54]. The increased cell association observed for increasing cRGD densities on the NPs can be attributed to the multivalent interactions between this peptide and the integrin $\alpha_v\beta_3$. In line with our findings, several authors have reported that multivalency in RGD systems enhances $\alpha_v\beta_3$ integrin binding and internalization[55–59].

3.3 Association of Cys-NPs and RGD-NPs with HUVECs under flow

In (patho)physiological conditions, the contact between cRGD-NPs and endothelial cells in (angiogenic) blood vessels will be subjected to the effects of constant blood flow (i.e. shear stress and presence of blood cells). These effects probably modify the way the NPs interact with the cells compared to static conditions frequently used in *in vitro* assays that aim to study cellular interactions. For this reason, it was decided to evaluate nanoparticle-cell interactions under flow in media of different complexities (EBM-2 cell culture medium and washed RBCs) and at different incubation times (1 and 16 h). These experiments were conducted at a shear rate of 300 sec^{-1}, which is comparable to the mean shear rate reported for the human carotid artery[60,61].

Incubation of HUVECs with Cys-NPs (0.08 mg/mL) dispersed in EBM-2 for 1 h under flow resulted in negligible association of these nanoparticles with HUVECs, as shown by epifluorescence microscopy images (Figure 3A).

In contrast, a dotted pattern inside the cytoplasm of the cells was observed for HUVECs incubated with cRGD-NPs under the same conditions (Figure 3A). Based on the image analysis of the fluorescent signal from the NPs (expressed as integrated density), cell association of cRGD-NPs with HUVECs was dependent on ligand density, with the association of high cRGD-NPs being 9 fold higher than the association of low cRGD-NPs (Figure 3B). A comparison between cell association in static and flow conditions is not possible, since this was determined using different methods for each condition, i.e. FACS for static and image analysis for flow.

Cell association of cRGD-NPs incubated with HUVECs in EBM-2 under flow for 16 h at 37 °C was also dependent on cRGD-density, as shown by epifluorescence microscopy visualization and image analysis (Figure 4). In this case, the association of high cRGD-NPs was 6.5 fold higher than that of low cRGD-NPs (Figure 4B). For all cRGD-NPs tested, higher associations were observed after 16 h incubation compared to the 1 h incubation (6 - 8 fold difference, Figure 6A).

HUVECs were also incubated for 16 h under flow with Cys-NPs and cRGD-NPs (0.08 mg/mL) dispersed in EBM-2 containing washed RBCs (∼30% hematocrit). The microscopy observations at the end of this experiment (Figure 5A) showed alterations in cell morphology (i.e. shrinking and in some cases rounding-up) compared to the cells from the flow experiments without RBCs. In some instances the actin cytoskeleton seemed somewhat disrupted (based on the observations made with phalloidin staining). These morphological changes can likely be a result of the collisions between RBCs and HUVECs. In line with the previous experiments under static and flow conditions (EBM-2), cell association was observed for cRGD-NPs, but not for Cys-NPs. Association of cRGD-NPs was dependent on ligand density and it was 2.3 fold higher for high cRGD-NPs than for low cRGD-NPs (Figure 5B).

Notably, the association of cRGD-NPs under flow was higher for all cRGD densities when the experiment was conducted in EBM-2 containing washed RBCs compared to EBM-2 without RBCs (Figure 6B). The presence of RBCs had a large influence on the cell association of low and medium cRGD-NPs, which increased by a factor 6 and 8, respectively. In comparison, the association of high cRGD-NPs increased by a factor 3.

The striking increment in cell association observed for all cRGD-NPs in medium containing RBCs can be partly attributed to the increased shear stress in this medium (at equal shear rates). In fact, shear stress-related differences in cellular binding/uptake of NPs have been previously reported. While some have shown an inverse correlation between uptake and shear rates[36,62], others showed a direct correlation between these parameters[63]. Differences in

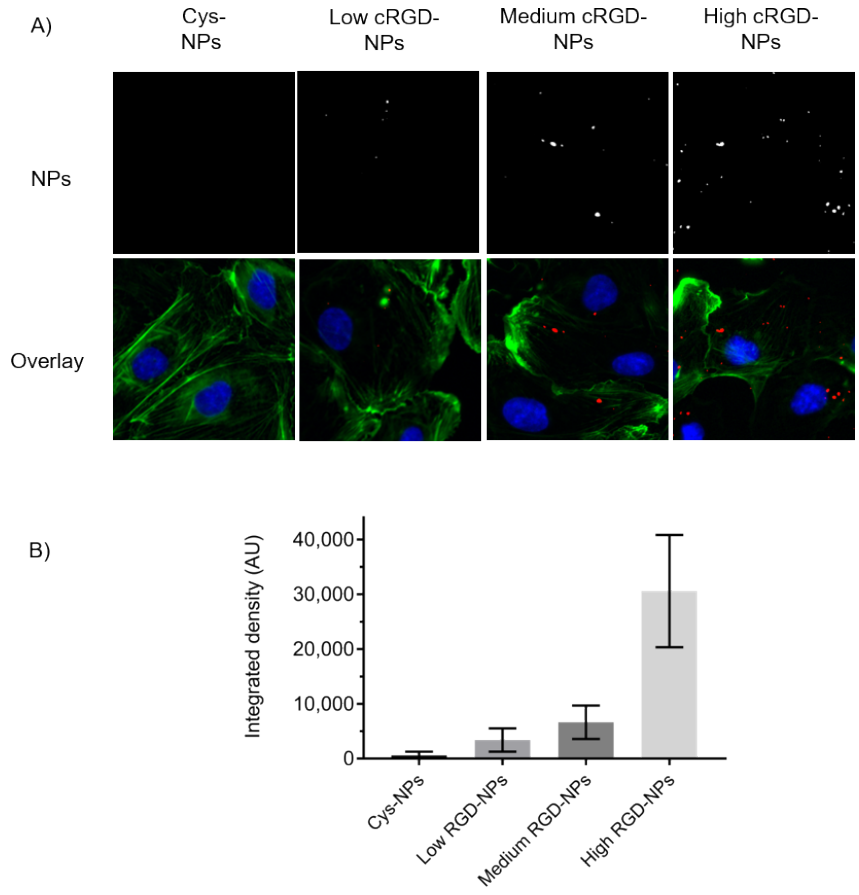

Figure 3: Association of Cys-NPs and cRGD-NPs of different ligand densities to HUVECs after 1 h incubation under flow (shear rate 300 sec^{-1}) in EBM-2 medium at 37 °C. A) Representative images obtained with an epifluorescence microscope (cropped images). Nuclei are stained in blue, cytoskeleton (F-actin) is stained in green, and NPs are observed in red. The same brightness and contrast settings were used for the red channel in all images. B) Image analysis: fluorescent signal for the NPs is reported as integrated density (n=10). All images obtained from the different formulations were processed in the same manner (background subtraction and equal thresholding).

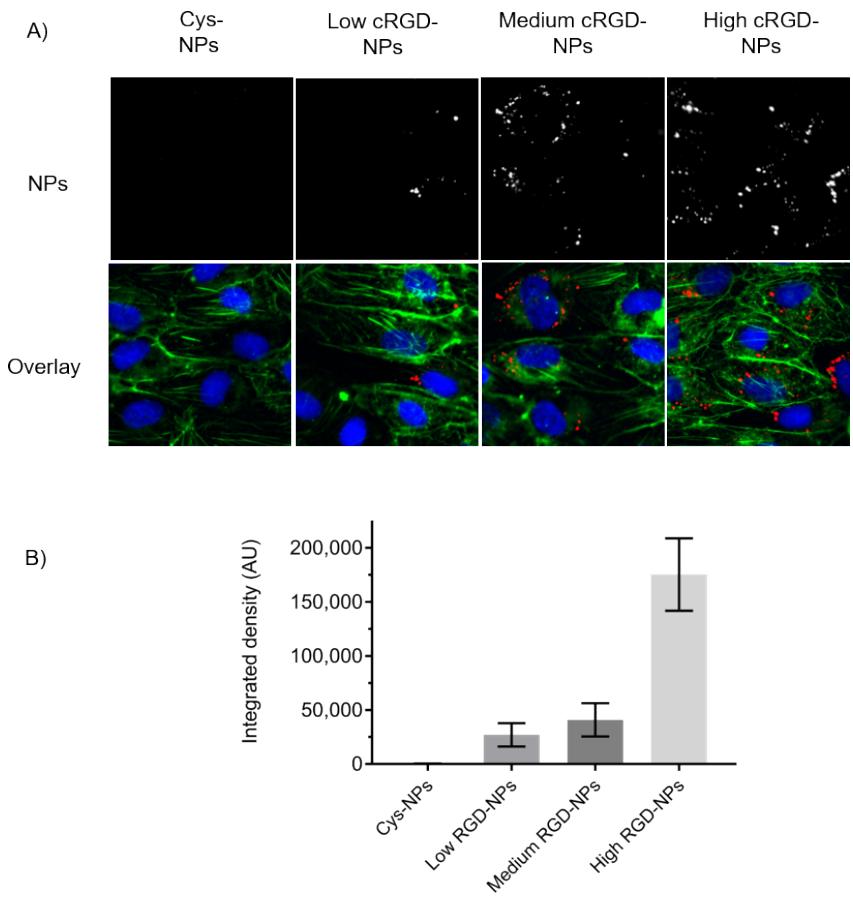

Figure 4: Association of Cys-NPs and cRGD-NPs of different ligand densities to HUVECs after 16 h incubation under flow (shear rate 300 sec^{-1}) in EBM-2 medium at 37 °C. A) Representative images obtained with an epifluorescence microscope (cropped images). Nuclei are stained in blue, cytoskeleton (F-actin) is stained in green, and NPs are observed in red. The same brightness and contrast settings were used for the red channel in all images. B) Image analysis: fluorescent signal for the NPs is reported as integrated density (n=10). All images obtained from the different formulations were processed in the same manner (background subtraction and equal thresholding).

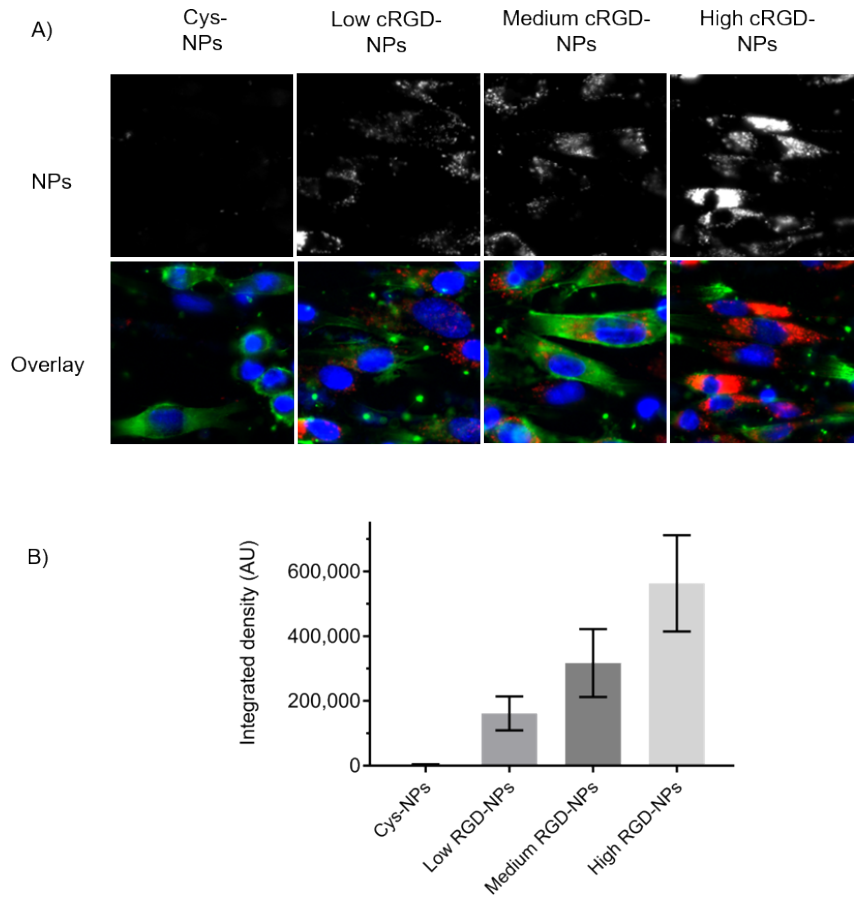

Figure 5: Association of Cys-NPs and cRGD-NPs of different ligand densities to HUVECs after 16 h incubation under flow (shear rate 300 sec^{-1}) in EBM-2 medium containing washed RBCs (hematocrit 32%) at 37 °C. A) Representative images obtained with an epifluorescence microscope (cropped images). Nuclei are stained in blue, cytoskeleton (F-actin) is stained in green, and NPs are observed in red. The same brightness and contrast settings were used for the red channel in all images. B) Image analysis: fluorescent signal for the NPs is reported as integrated density (n=10). All images obtained from the different formulations were processed in the same manner (background subtraction and equal thresholding).

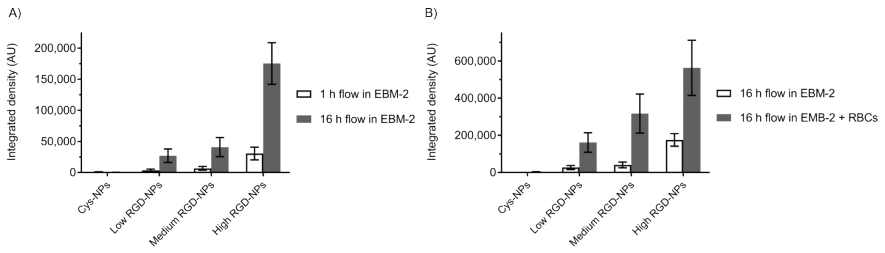

Figure 6: Comparison of the cell association of Cys-NPs and cRGD-NPs of different ligand densities to HUVECs at 37 °C under flow (shear rate 300 sec^{-1}) at different conditions. A) Cell association after 1 or 16 h of incubation in EBM-2 medium. B) Cell association after 16 h of incubation in EBM-2 medium with and without washed RBCs. The fluorescent signal for the NPs is reported as integrated density (n=10).

the composition and physicochemical characteristics of the nanocarriers evaluated, as well as in the cell types and experimental set-ups, could contribute to the discrepancies between these studies. The differences in association of cRGD-NPs to HUVECs observed under flow with and without washed RBCs, indicate that these blood components influence the association of the NPs with the endothelial cells. It has been proposed that the presence of RBCs facilitates the contact of nanocarriers with vascular endothelium by two main mechanisms: (1) RBCs localize mainly to the center of blood vessels, pushing smaller particles close to the vessel wall[64,65], and (2) RBCs rotate and tumble, colliding with small particles and pushing them towards the vessel wall[64,66,67]. The presence of RBCs in the medium has indeed been shown to enhance the binding of adhesion molecule-targeted particles to HUVECs under flow conditions[68,69]. Though these studies were carried out using particles with relatively large sizes (0.5 - 10 μm), our findings, as well as previously published data[66], indicate that RBCs also have an effect on the cell association of smaller size NPs (∼300 nm). In future studies, more insights into the behavior of different types of NPs (i.e. size, charge, composition etc.) in conditions approximating physiological settings could be gained by conducting flow experiments in the presence of whole blood.

4 Conclusions

The results presented in this work show that polymeric NPs functionalized with cRGD can target endothelial cells, and that cell association of these

nanocarriers is positively correlated with the surface density of cRGD. Targeting of endothelial cells was evaluated using two approaches, under static and flow conditions. Experiments conducted using washed RBCs in the medium, which represent more realistic and physiologically relevant conditions, showed that the presence of these blood components facilitates the association of NPs to endothelial cells under flow. The setup used for the experiments under flow is, as such, particularly appropriate for the study of endothelial cell targeting, rather than tumor cell targeting. This approach is likely a step forward in predicting the *in vivo* association of endothelial-cell targeted nanocarriers administered intravenously. Such an *in vitro* assay would therefore allow for high-throughput screening of different targeted formulations and is a potential asset for the reduction of laboratory animal testing.

Acknowledgements

The authors would like to thank Anko M. de Graaff for his help with confocal cell imaging. Lucía Martínez-Jothar would like to thank the Consejo Nacional de Ciencia y Tecnología (CONACYT), México (grant no. 384743) for the funding provided in the framework of her PhD.

References

[1] Carmeliet, P. and Jain, R. Molecular mechanisms and clinical applications of angiogenesis. *Nature*, 473, 2011.

[2] Otrock, Z., Mahfouz, R., Makarem, J., and Shamseddine, A. Understanding the biology of angiogenesis: Review of the most important molecular mechanisms. *Blood Cells, Molecules and Diseases*, 39, 2007.

[3] Stromblad, S. and Cheresh, D. Cell adhesion and angiogenesis. *Trends in Cell Biology*, 6, 1996.

[4] Hynes, R. O. Integrins: Bidirectional, allosteric signaling machines. *Cell*, 110, 2002.

[5] Avraamides, C., Garmy-Susini, B., and Varner, J. Integrins in angiogenesis and lymphangiogenesis. *Nature Reviews Cancer*, 8, 2008.

[6] Brooks, P., Clark, R., and Cheresh, D. Requirement of vascular integrin alpha v beta 3 for angiogenesis. *Science*, 264, 1994.

[7] Kapp, T., Rechenmacher, F., Neubauer, S., Maltsev, O., Cavalcanti-Adam, E., Zarka, R., Reuning, U., Notni, J., Wester, H.-J., Mas-Moruno, C., Spatz, J., Geiger, B., and Kessler, H. A comprehensive evaluation of the activity and selectivity profile of ligands for RGD-binding integrins. *Nature Publishing Group*, 2017.

[8] Ruoslahti, E. RGD and other recognition sequences for integrins. *Annual Review of Cell and Developmental Biology*, 12, 1996.

[9] Desgrosellier, J. and Cherech, D. Integrins in cancer: biological implications in therapeutic opportunities. *Nature Reviews Cancer*, 10, 2010.

[10] Mizejewski, G. Role of integrins in cancer: Survey of expression patterns. *Proceedings of the Society for Experimental Biology and Medicine*, 222, 1999.

[11] Nieberler, M., Reuning, U., Reichart, F., Notni, J., Wester, H.-J., Schwaiger, M., Weinmüller, M., and Räder, A. Exploring the role of RGD-recognizing integrins in cancer. *Cancers*, 9, 2017.

[12] Eble, J. A. and Haier, J. Integrins in cancer treatment. *Current Cancer Drug Targets*, 2006.

[13] Kumar, C. C. Integrin $\alpha v\beta 3$ as a therapeutic target for blocking tumor-induced angiogenesis. *Current Drug Targets*, 4, 2003.

[14] Liu, Z., Wang, F., and Chen, X. Integrin $\alpha v\beta 3$ -targeted cancer therapy. *Drug Development Research*, 69, 2008.

[15] Raab-Westphal, S., Marshall, J., and Goodman, S. Integrins as therapeutic targets: Successes and cancers. *Cancers*, 9, 2017.

[16] Gajbhiye, K., Gajbhiye, V., Siddiqui, I., and Gajbhiye, J. cRGD functionalised nanocarriers for targeted delivery of bioactives. *Journal of Drug Targeting*, 27, 2019.

[17] Kunjachan, S., Pola, R., Gremse, F., Theek, B., Ehling, J., Hermanns-Sachweh, B., Pechar, M., Ulbrich, K., Hennink, W. E., Storm, G., Lederle, W., Kiessling, F., and Lammers, T. Passive vs. active tumor targeting using RGD- and NGR- modified polymeric nanomedicines. *Nano Letters*, 14, 2014.

[18] Park, J., Singha, K., Son, S., Kim, J., Namgung, R., Yun, C., and Kim, W. A review of RGD-functionalized nonviral gene delivery vectors for cancer therapy. *Cancer Gene Therapy*, 19, 2012.

[19] Schiffelers, R., Ansari, A., Xu, J., Zhou, Q., Tang, Q., Storm, G., Molema, G., Lu, P. Y., Scaria, P., and Woodle, M. Cancer siRNA therapy by tumor selective delivery with ligand-targeted sterically stabilized nanoparticle. *Nucleic Acids Research*, 32, 2004.

[20] Wang, F., Li, Y., Shen, Y., Wang, A., Wang, S., and Xie, T. The functions and applications of RGD in tumor therapy and tissue engineering. *International Journal of Molecular Sciences*, 14, 2013.

[21] Zhu, Y., Zhang, J., Meng, F., Deng, C., Cheng, R., Feijen, J., and Zhong, Z. cRGD-functionalized reduction-sensitive shell-sheddable biodegradable micelles mediate enhanced doxorubicin delivery to human glioma xenografts in vivo. *Journal of Controlled Release*, 233, 2016.

[22] Danhier, F., Pourcelle, V., Marchand-Brynaert, J., Jérôme, C., Feron, O., and Préat, V. Targeting of tumor endothelium by RGD-grafted PLGA-nanoparticles. *Journal of Controlled Release*, 140, 2009.

[23] Graf, N., Bielenberg, D., Kolishetti, N., Muus, C., Banyard, J., Farokhzad, O., and Lippard, S. alpha V beta 3 integrin-targeted PLGA-PEG nanoparticles for enhanced anti-tumor efficacy of a Pt (IV) prodrug. *ACS Nano*, 6, 2012.

[24] Liu, P., Qin, L., Wang, Q., Sun, Y., Zhu, M., Shen, M., and Duan, Y. cRGD-functionalized mPEG-PLGA-PLL nanoparticles for imaging and therapy of breast cancer. *Biomaterials*, 33, 2012.

[25] Yin, P., Wang, Y., Qiu, Y. Y., Hou, L. L., Liu, X., Qin, J., Duan, Y., Liu, P., Qiu, M., and Li, Q. Bufalin-loaded mPEG-PLGA-PLL-cRGD nanoparticles: Preparation, cellular uptake, tissue distribution, and anticancer activity. *International Journal of Nanomedicine*, 7, 2012.

[26] Garanger, E., Boturyn, D., Coll, J. L., Favrot, M. C., and Dumy, P. Multivalent RGD synthetic peptides as potent $\alpha v\beta 3$ integrin ligands. *Organic and Biomolecular Chemistry*, 4, 2006.

[27] Li, Z.-B., Cai, W., Cao, Q., Chen, K., Wu, Z., He, L., and Chen, X. 64Cu-Labeled tetrameric and octameric RGD peptides for small-animal pet of tumor $\alpha v\beta 3$ integrin expression. *Journal of Nuclear Medicine*, 48, 2007.

[28] Liu, S. Radiolabeled cyclic RGD peptide bioconjugates as radiotracers targeting multiple integrins. *Bioconjugate Chemistry*, 26, 2015.

[29] Ye, Y., Bloch, S., Xu, B., and Achilefu, S. Design, synthesis, and evaluation of near infrared fluorescent multimeric RGD peptides for targeting tumors. *Journal of Medicinal Chemistry*, 49, 2006.

[30] Goodwin, A. M. In vitro assays of angiogenesis for assessment of angiogenic and anti-angiogenic agents. *Microvascular Research*, 74, 2007.

[31] Zimrin, A. B., Villeponteau, B., and Maciag, T. Models of in vitro angiogenesis: Endothelial cell differentiation on fibrin but not matrigel is transcriptionally dependent. *Biochemical and Biophysical Research Communications*, 213, 1995.

[32] Valencia, P., Farokhzad, O., Karnik, R., and Langer, R. Microfluidic technologies for accelerating the clinical translation of nanoparticles. *Nature Nanotechnology*, 7, 2012.

[33] van der Meer, A. D., Poot, A. A., Duits, M. H. G., Feijen, J., and Vermes, I. Microfluidic technology in vascular research. *Journal of Biomedicine and Biotechnology*, 2009.

[34] Cicha, I., Beronov, K., Ramirez, E., Osterode, K., Goppelt-Struebe, M., Raaz, D., Yilmaz, A., Daniel, W., and Garlichs, C. Shear stress preconditioning modulates endothelial susceptibility to circulating TNF-α and monocytic cell recruitment in a simplified model of arterial bifurcations. *Atherosclerosis*, 207, 2009.

[35] Klingberg, H., Loft, S., Oddershede, L., and Møller, P. The influence of flow, shear stress and adhesion molecule targeting on gold nanoparticle uptake in human endothelial cells. *Nanoscale*, 7, 2015.

[36] Samuel, S., Jain, N., O'Dowd, F., Paul, T., Kashanin, D., Gerard, V., Gun'ko, Y., Prina-Mello, A., and Volkov, Y. Multifactorial determinants that govern nanoparticle uptake by human endothelial cells under flow. *International Journal of Nanomedicine*, 7, 2012.

[37] Fede, C., Fortunati, I., Weber, V., Rossetto, N., Bertasi, F., Petrelli, L., Guidolin, D., Signorini, R., De Caro, R., Albertin, G., and Ferrante, C. Evaluation of gold nanoparticles toxicity towards human endothelial cells under static and flow conditions. *Microvascular Research*, 97, 2015.

[38] Matuszak, J., Baumgartner, J., Zaloga, J., Juenet, M., Da Silva, A. E., Franke, D., Almer, G., Texier, I., Faivre, D., Metselaar, J. M., Navarro, F. P., Chauvierre, C., Prassl, R., Dézsi, L., Urbanics, R., Alexiou, C., Mangge, H., Szebeni, J., Letourneur, D., and Cicha, I. Nanoparticles for intravascular applications: Characterization and cytotoxicity testing. *Nanomedicine*, 11, 2016.

[39] Samadi, N., van Steenbergen, M., van den Dikkenberg, J., Vermonden, T., van Nostrum, C., Amidi, M., and Hennink, W. Nanoparticles based on a hydrophilic polyester with a sheddable PEG coating for protein delivery. *Pharmaceutical Research*, 31, 2014.

[40] Zambaux, M. F., Bonneaux, F., Gref, R., Maincent, P., Dellacherie, E., Alonso, M. J., Labrude, P., and Vigneron, C. Influence of experimental parameters on the characteristics of poly (lactic acid) nanoparticles prepared by a double emulsion method. *Journal of Controlled Release*, 50, 1998.

[41] Martínez-Jothar, L., Doulkeridou, S., Schiffelers, R., Sastre Torano, J., Oliveira, S., van Nostrum, C., and Hennink, W. Insights into maleimide-thiol conjugation chemistry: Conditions for efficient surface functionalization of nanoparticles for receptor targeting. *Journal of Controlled Release*, 282, 2018.

[42] Javiya, C. and Jonnalagadda, S. Physicochemical characterization of spray-dried PLGA/PEG microspheres, and preliminary assessment of biological response. *Drug Development and Industrial Pharmacy*, 42, 2016.

[43] Malzert, A., Boury, F., Saulnier, P., Benoit, J. P., and Proust, J. E. Interfacial properties of mixed polyethylene glycol/poly (d,l-lactide-co-glycolide) films spread at the air/water interface. *Langmuir*, 16, 2000.

[44] Zhang, N., Chittapuso, C., Ampassavate, C., Siahaan, T., and Berkland, C. PLGA nanoparticle-peptide conjugate effectively targets intercellular cell-adhesion molecule-1. *Bioconjugate Chemistry*, 19, 2008.

[45] Canton, I. and Battaglia, G. Endocytosis at the nanoscale. *Chemical Society Reviews*, 41, 2012.

[46] Petros, R. and Desimone, J. Strategies in the design of nanoparticles for therapeutic applications. *Nature Reviews Drug Discovery*, 9, 2010.

[47] Verma, A. and Stellacci, F. Effect of surface properties on nanoparticle cell interactions. *Small*, 6, 2010.

[48] Danhier, F., Le Breton, A., and Préat, V. RGD-based strategies to target alpha (v) beta (3) integrin in cancer therapy and diagnosis. *Molecular Pharmaceutics*, 9, 2012.

[49] Fens, M., Mastrobattista, E., de Graaff, A., Flesch, F., Ultee, A., Rasmussen, J., Molema, G., Storm, G., and Schiffelers, R. Angiogenic endothelium shows lactadherin-dependent phagocytosis of aged erythrocytes and apoptotic cells. *Blood*, 111, 2008.

[50] Amin, M., Mansourian, M., Koning, G., Badiee, A., Jaafari, M., and Ten Hagen, T. Development of a novel cyclic RGD peptide for multiple targeting approaches of liposomes to tumor region. *Journal of Controlled Release*, 220, 2015.

[51] Wang, Z., Chui, W. K., and Ho, P. Design of a multifunctional PLGA nanoparticulate drug delivery system: Evaluation of its physicochemical properties and anticancer activity to malignant cancer cells. *Pharmaceutical Research*, 26, 2009.

[52] Hoekman, J., Srivastava, P., and Ho, R. Aerosol stable peptide-coated liposome nanoparticles: A proof-of-concept study with opioid fentanyl in enhancing analgesic effects and reducing plasma drug exposure. *Journal of Pharmaceutical Sciences*, 103, 2014.

[53] Shan, D., Li, J., Cai, P., Prasad, P., Liu, F., Rauth, A. M., and Wu, X. RGD-conjugated solid lipid nanoparticles inhibit adhesion and invasion of $\alpha v\beta 3$ integrin-overexpressing breast cancer cells. *Drug Delivery and Translational Research*, 5, 2015.

[54] Valencia, P., Hanewich-Hollatz, M., Gao, W., Karim, F., Langer, R., Karnik, R., and Farokhzad, O. C. Effects of ligands with different water solubilities on self- assembly and properties of targeted nanoparticles. *Biomaterials*, 32, 2011.

[55] Kok, R., Schraa, A. J., Bos, E., Moorlag, H., Ásgeirsdóttir, S., Everts, M., Meijer, D., and Molema, G. Preparation and functional evaluation of RGD-modified proteins as $\alpha v\beta 3$ integrin directed therapeutics. *Bioconjugate Chemistry*, 13, 2002.

[56] Sancey, L., Garanger, E., Foillard, S., Schoehn, G., Hurbin, A., Albiges Rizo, C., Boturyn, D., Souchier, C., Grichine, A., Dumy, P., and Coll, J.-L. Clustering and internalization of integrin $\alpha v\beta 3$ with a tetrameric RGD-synthetic peptide. *Molecular Therapy*, 17, 2009.

[57] Shukla, R., Thomas, T., Peters, J., Kotlyar, A., Myc, A., and Baker, J. Tumor angiogenic vasculature targeting with PAMAM dendrimer-RGD conjugates. *Chemical Communications*, 2005.

[58] Temming, K., Schiffelers, R., Molema, G., and Kok, R. RGD-based strategies for selective delivery of therapeutics and imaging agents to the tumour vasculature. *Drug Resistance Updates*, 8, 2005.

[59] Wu, Y., Zhang, X., Xiong, Z., Cheng, Z., Fisher, D. R., Liu, S., Gambhir, S. S., and Chen, X. MicroPET imaging of glioma integrin $\alpha v\beta 3$ expression using 64Cu-labeled tetrameric RGD peptide. *The Journal of Nuclear Medicine*, 46, 2005.

[60] Reneman, R., Arts, T., and Hoeks, A. Wall shear stress an important determinant of endothelial cell function and structure in the arterial system in vivo. *Journal of Vascular Research*, 43, 2006.

[61] Stroev, P., Hoskins, P., and Easson, W. Distribution of wall shear rate throughout the arterial tree: A case study. *Atherosclerosis*, 191, 2007.

[62] Lin, A., Sabnis, A., Kona, S., Nattama, S., Patel, H., Dong, J. F., and Nguyen, K. T. Shear-regulated uptake of nanoparticles by endothelial cells and development of endothelial-targeting nanoparticles. *Journal of Biomedical Materials Research Part A*, 93, 2010.

[63] Rinkenauer, A., Press, A., Raasch, M., Pietsch, C., Schweizer, S., Schwörer, S., Rudolph, K., Mosig, A., Bauer, M., Traeger, A., and Schubert, U. Comparison of the uptake of methacrylate-based nanoparticles in static and dynamic in vitro systems as well as in vivo. *Journal of Controlled Release*, 216, 2015.

[64] Howard, M., Zern, B., Anselmo, A., Shuvaev, V. V., Mitragotri, S., Muzykantov, V., and Al, H. E. T. Vascular targeting of nanocarriers: Perplexing aspects of the seemingly straightforward paradigm. *ACS Nano*, 8, 2014.

[65] Zhang, J., Johnson, P., and Popel, A. Effects of erythrocyte deformability and aggregation on the cell free layer and apparent viscosity of microscopic blood flows. *Microvascular Research*, 77, 2009.

[66] Tan, J., Thomas, A., and Liu, Y. Influence of red blood cells on nanoparticle targeted delivery in microcirculation. *Soft Matter*, 8, 2011.

[67] Tan, J., Keller, W., Sohrabi, S., Yang, J., and Liu, Y. Characterization of nanoparticle dispersion in red blood cell suspension by the lattice boltzmann-immersed boundary method. *Nanomaterials*, 6, 2016.

[68] Charoenphol, P., Huang, R. B., and Eniola-adefeso, O. Potential role of size and hemodynamics in the efficacy of vascular-targeted spherical drug carriers. *Biomaterials*, 31, 2010.

[69] Kiani, M. F., Yuan, H., Chen, X., Smith, L., Gaber, M., and Goetz, D. Targeting microparticles to select tissue via radiation-induced upregulation of endothelial cell adhesion molecules. *Pharmaceutical Research*, 19, 2002.

Supporting Information

Calculations S1. Calculation of cRGD density on the surface of a single NP.

The density of cRGD on the surface of a single NP prepared using 20% maleimide-PEG-PLGA can be calculated as follows:

The diameter of the NPs is used to calculate the mass (m_{NP}) and surface area of a single NP. Because the NPs are composed mostly of PLGA, their density will be considered as that of this polymer = 1.25 g/cm^3 [1]. Taking as an example the Low cRGD-NPs:

$$Area_{Low\,cRGD-NPs} = 4 \times \pi \times (1.57 \times 10^{-5} cm)^2 = 3.10 \times 10^{-9}\,\frac{cm^2}{NP}$$

$$m_{Low\,cRGD-NPs} = \left(\frac{4}{3} \times \pi \times (1.57 \times 10^{-5} cm)^3\right) \times 1.25 \frac{g}{cm^3} = 2.03 \times 10^{-14}\,\frac{g}{NP}$$

For the preparation of Low cRGD-NPs, a molar ratio of 1:10 cRGD to maleimide-PEG-PLGA was used, which is equal to 1 mg of NPs and 0.5 μg of peptide. Therefore, the amount of NPs in the reaction is:

$$Number\ of\ NPs = \frac{1.00 \times 10^{-3} g}{2.03 \times 10^{-14} g/NP} = 4.93 \times 10^{10} NPs$$

An average conjugation efficiency of 38% (Table 1) was achieved during the preparation of the Low cRGD-NPs, which is equivalent to 0.19 μg of the 0.5 μg of cRGD used in the reaction. Therefore, the amount of cRGDfK molecules (M_w 678.5 g/mol) conjugated to the surface of the NPs is:

$$Molecules_{cRGD} = \left(\frac{1.9 \times 10^{-7} g}{678.5\ g/mol}\right) \times 6.02 \times 10^{23}\ \frac{molecules}{mol} = 1.69 \times 10^{14}\ cRGD\ molecules$$

The number of cRGD molecules on a single NP and the cRGD density can therefore be calculated as:

$$Number\ of\ cRGD\ per\ NP_{Low\,cRGD-NPs} = \frac{1.69 \times 10^{14}\ cRGD}{4.93 \times 10^{10}\ NPs} = 3,428\ \frac{cRGD}{NP}$$

$$cRGDfK\ density_{Low\ cRGD-NPs} =$$
$$\frac{3,428\ cRGD/NP}{3.10 \times 10^{-9}\ cm^2/NP} = 1.10 \times 10^{12}\ cRGD/cm^2 = 11,000\ cRGD/\mu m^2$$

References

[1] Qi, R., Guo, R., Shen, M., Cao, X., Zhang, L., Xu, J., Yu, J., and Shi, X. Electrospun poly(lactic-co-glycolic acid)/halloysite nanotube composite nanofibers for drug encapsulation and sustained release. *Journal of Materials Chemistry*, 20(47):10622–10629, 2010.

Chapter 4

Effect of the solvent stabilizer 2,6-di-tert-butyl-4-methylphenol on the cytocompatibility of poly(D,L-lactic-co-glycolic-co-hydroxymethyl glycolic acid) nanoparticles

Lucía Martínez-Jothar[†], Sofia Doulkeridou[‡], Sabrina Oliveira[†,‡], Cornelus F. van Nostrum[†] and Wim E. Hennink[†]

† Department of Pharmaceutics, Utrecht Institute for Pharmaceutical Sciences, Utrecht University, Utrecht, the Netherlands

‡ Division of Cell Biology, Department of Biology, Utrecht University, Utrecht, the Netherlands

Abstract

Drug delivery systems based on poly(D,L-lactic-co-glycolic-co-hydroxymethyl glycolic acid) (PLGHMGA) are attractive systems for the controlled release of biotherapeutics. PLGHMGA is synthesized by copolymerization of lactide with a dilactone containing a benzyl-protected hydroxyl group, followed by benzyl removal through hydrogenation using a palladium on carbon (Pd/C) catalyst. Hydrogenation is carried out in tetrahydrofuran (THF), a solvent commonly stabilized with 2,6-di-tert-butyl-4-methylphenol, also known as butylated hydroxytoluene (BHT). In this work, we studied the effects of BHT accumulation on the cytocompatibility of PLGHMGA and PEGylated PLGHMGA (MePEG-PLGHMGA). For this purpose, polymer batches obtained directly after hydrogenation (i.e. non-purified) and batches obtained after purification by polymer dissolution in dichloromethane and precipitation in diethyl ether (i.e. purified) were used for the preparation of nanoparticles (NPs) that were evaluated in cytocompatibility assays. According to ^{1}H NMR analysis, 4 and 12% w/w BHT were present in non-purified PLGHMGA and MePEG-PLGHMGA respectively. After purification, these amounts decreased to 0.2 and 0.4% w/w, confirming the almost quantitative removal of BHT from these polymers. Differential scanning calorimetry revealed that the T_g of the non-purified polymers was ∼20 °C lower than the T_g of purified polymers, indicating that BHT dissolved in the polymer matrix and acted as a plasticizer. NPs prepared from purified polymers were more cytocompatible than those prepared from non-purified polymers tested using SkBr3 and MDA-MB-231 cells. These findings show that BHT, which is present in small amounts in THF (0.02 - 0.03% w/w), can accumulate in PLGHMGA and MePEG-PLGHMGA up to cytotoxic levels, highlighting the importance of adequate polymer purification and characterization.

1 Introduction

Aliphatic polyesters, such as polylactic acid, poly(lactic-co-glycolic acid) and poly(ε-caprolactone), are commonly used to design controlled drug delivery systems[1–4]. However, since release of therapeutic biomacromolecules is mostly driven by matrix degradation, the long degradation times of these polymers (spanning from a couple of months to a couple of years) is inconvenient for systems that are intended to release the entrapped drug in a few days/weeks. Polymers with faster degradation rates can be obtained from monomers that possess protected pendant carboxyl[5,6] or hydroxyl groups[7,8]. Besides increasing the hydrophilicity of the polymers, by which the water absorbing capacity and thus the degradation rate increase, these groups can also be exploited for conjugation to hydrophilic polymers (such as PEG) and/or targeting ligands[9,10].

Two polymers with pendant hydroxyl groups, poly(D,L-lactic-co-hydroxymethyl glycolic acid) (PLHMGA) and poly(D,L-lactic-co-glycolic-co-hydroxymethyl glycolic acid) (PLGHMGA), as well as their PEGylated derivatives, have been synthesized in our research group and used to prepare drug-loaded microspheres and nanoparticles. These polymers are obtained by copolymerization of lactide with dilactones containing benzyl-protected hydroxyl groups, i.e. benzyloxymethyl methyl glycolide or benzyloxymethyl glycolide. After polymerization, the benzyl groups are removed by hydrogenation catalyzed by palladium on carbon (Pd/C)[11,12] yielding aliphatic polyesters with pendant hydroxyl groups.

PLHMGA and PLGHMGA have been evaluated for applications in drug delivery[13–16] and they have shown enhanced compatibility with peptides in comparison to PLGA (i.e. less formation of acylated adducts)[17,18]. Importantly, the degradation time of these polymers was shorter than that of PLGA and the degradation kinetics (and release of entrapped proteins) could be tailored by the copolymer composition[17,19]. These findings highlight the potential of PLHMGA and PLGHMGA for the delivery of biotherapeutics and have prompted us to explore the application of these polymers for the preparation of nanoparticles (NPs) for the intracellular delivery of cytotoxic proteins for cancer treatment[20]. Since fast protein release from the NPs is desirable, PLGHMGA was chosen for the preparation of these nanocarriers because this polymer degrades faster than PLHMGA due to the presence of the more hydrophilic glycolic acid groups in its structure[11].

As a starting point of the formulation process, the purity of the starting materials (in this case PLGHMGA and MePEG-PLGHMGA) should be guaranteed. When dealing with polymers, toxic effects have been at-

tributed to impurities such as unreacted monomers[21], catalysts[22,23], reaction by-products[24] and residual solvents[25–27]. In the case of PLGHMGA and MePEG-PLGHMGA, unexpected toxicity of NPs prepared from the non-purified polymers was observed, and it was shown to be caused by 2,6-di-tert-butyl-4-methylphenol, (also known as butylated hydroxytoluene, BHT). This compound is an antioxidant with applications in the food, pharmaceutical, cosmetic and polymer industries[28], and is used as a stabilizer to avoid peroxide formation in tetrahydrofuran (THF). Since relatively large amounts of THF are used during the synthesis of PLGHMGA and MePEG-PLGHMGA (i.e. in the final hydrogenation step), this could explain the accumulation of BHT in the non-purified polymers. In this work, the toxic effect associated to the accumulation of BHT in PLGHMGA and MePEG-PLGHMGA was evaluated by comparing the cytocompatibility of NPs prepared from purified and non-purified polymer batches.

2 Experimental section

2.1 Chemicals

Tin(II) 2-ethylhexanoate, benzyl alcohol and poly(vinyl alcohol) (PVA) M_w 30,000 - 70,000 Da (87 - 90% hydrolyzed), HyFlo® Super Cell and butylated hydroxytoluene were acquired from Sigma-Aldrich (Steinheim, Germany). D,L-lactide was purchased from Corbion (Gorinchem, the Netherlands). Benzyloxymethyl glycolide (BMG), a dilactone with a protected hydroxyl group, was synthesized as previously reported[7]. Poly(ethylene glycol) monomethyl ether (M_n ∼2,000 Da) and palladium on carbon (Pd/C, 10 wt% loading) were purchased from Aldrich (Steinheim, Germany). Chloroform, methanol, tetrahydrofuran (THF) stabilized with butylated hydroxytoluene (BHT) 0.02 - 0.03% w/w (according to the supplier), dichloromethane (DCM) and diethyl ether were acquired from Biosolve (Valkenswaard, the Netherlands). Alamar Blue® reagent was purchased from Bio-Rad.

2.2 Synthesis of poly(D,L-lactic-co-glycolic-co-benzyloxymethyl glycolic acid) (PLGBMGA) and methoxy-PEG-PLGBMGA (MePEG-PLGBMGA)

PLGBMGA was prepared by ring-opening polymerization of D,L-lactide and BMG[7,11] at a molar ratio of 65:35. The polymerization was carried out in the melt (130 °C, overnight) using benzyl alcohol as initiator (300:1 monomer

to initiator molar ratio) and tin(II) 2-ethylhexanoate as catalyst (2:1 initiator to catalyst molar ratio)[19] (Figure 1). After polymerization, the crude product was dissolved in chloroform, precipitated in cold methanol (200 mL per gram of polymer), and the precipitate was vacuum dried overnight. MePEG-PLGBMGA was synthesized in the same way as PLGBMGA, but, instead of benzyl alcohol, poly(ethylene glycol) monomethyl ether (M_n 2,000 g/mol) was used as initiator[12].

2.3 Synthesis of poly(D,L-lactic-co-glycolic-co-hydroxymethyl glycolic acid) (PLGHMGA) and methoxy-PEG-PLGHMGA (MePEG-PLGHMGA) (Deprotected polymers)

The benzyl groups of PLGBMGA and MePEG-PLGBMGA were removed by hydrogenation catalyzed by Pd/C as described elsewhere[7,11] (Figure 1), a process that will be referred to as deprotection. Briefly, the polymers were dissolved in THF (stabilized with BHT) to a concentration of 8 mg/mL and Pd/C was added to the polymer solution at a 2:1 Pd/C to BMG w/w ratio. The mixture was placed under hydrogen atmosphere and left to stir overnight at room temperature (20 °C). Subsequently, the Pd/C catalyst was removed by filtration with HyFlo and THF was removed by evaporation under reduced pressure. The resulting polymers, PLGHMGA or MePEG-PLGHMGA were either used as such (i.e. non-purified polymers), or they were dissolved in dichloromethane and purified by precipitation in cold diethyl ether (200 mL per gram of polymer). The precipitated polymers were recovered by filtration and dried under vacuum overnight and are referred to in this text as PLGHMGA$_{purif}$ and MePEG-PLGHMGA$_{purif}$.

2.4 Polymer characterization

The composition of the synthesized polymers was determined by ^{1}H NMR in deuterated DMSO, as follows[12]:

$$\begin{aligned} I_L &= [(I_{5.1-5.4}) - (I_{3.6-3.9}/2)] \\ I_G &= (I_{4.7-5.0})/2 \\ I_{BMG\,or\,HMG} &= [(I_{3.6-3.9})/2 + (I_{4.1-4.5})/3] \end{aligned}$$

$$\begin{aligned} \%_L &= I_L/(I_L + I_G + I_{BMG\,or\,HMG}) \times 100 \\ \%_G &= I_G/(I_L + I_G + I_{BMG\,or\,HMG}) \times 100 \\ \%_{BMG\,or\,HMG} &= I_{BMG\,or\,HMG}/(I_L + I_G + I_{BMG\,or\,HMG}) \times 100 \end{aligned}$$

Where I_{ppm} = peak integrals, L = lactic acid, G = glycolic acid, BMG = benzyloxymethyl glycolic acid (in the protected polymer) and HMG = hydroxymethyl glycolic acid (in the deprotected polymer).

The M_n and the % PEG in the PEGylated polymers was also determined using ^{1}H NMR analysis, as reported elsewhere[12]:

$$\begin{aligned} &Calculated\,polymer\,M_n = \\ &(I_L/I_{PEG}\times M_w Lunit)+(I_G/I_{PEG}\times M_w Gunit)+(I_{HMG}/I_{PEG}\times M_w HMGunit) \\ &\quad + PEG\,M_w \end{aligned}$$

$$\%_{PEG} = PEG\,M_w/calculated\,polymer\,M_n \times 100$$

The weight percent of BHT (w_{BHT}) contained in the polymers was calculated from the mole fractions *(m)* of the different components as follows:

$$\begin{aligned} m_L &= I_L/(I_L + I_G + I_{HMG} + I_{MePEG} + I_{BHT}) \\ m_G &= I_G/(I_L + I_G + I_{HMG} + I_{MePEG} + I_{BHT}) \\ m_{HMG} &= I_{HMG}/(I_L + I_G + I_{HMG} + I_{MePEG} + I_{BHT}) \\ m_{MePEG} &= I_{MePEG}/(I_L + I_G + I_{HMG} + I_{MePEG} + I_{BHT}) \\ m_{BHT} &= I_{BHT}/(I_L + I_G + I_{HMG} + I_{MePEG} + I_{BHT}) \end{aligned}$$

where peak integrals per proton were defined as above, and $I_{MePEG} = I_{3.5}/182$ and $I_{BHT} = I_{1.3}/18$

$$w_{BHT} = \frac{m_{BHT} \times Mw_{BHT}}{[(m_L \times Mw_L)+(m_G \times Mw_G)+(m_{HMG} \times Mw_{HMG})+(m_{MePEG} \times Mw_{MePEG})+(m_{BHT} \times Mw_{BHT})]} \times 100\%$$

The molecular weights of the polymers were determined by GPC equipped with a Waters 2695 separating module and a Waters 2414 refractive index detector. The samples were run through two PL-gel 5 μm Mixed-D columns at 60 °C, using THF (1 mL/min) as mobile phase. Calibration was done with polystyrene standards (EasiCal Agilent, California, USA) and PEG standards.

The thermal properties of the polymers were studied by differential scanning calorimetry (DSC) (Discovery DSC, TA instruments, Delaware, USA). In a typical experiment, ∼5 mg of polymer was transferred into an aluminum pan and the sample was heated from room temperature to 120 °C at a rate of 5 °C/min. The polymer was cooled down to -50 °C at 5 °C/min and subsequently heated to 120 °C at 2 °C/min with temperature modulation at ± 1 °C.

DSC analysis was also conducted on a sample of PLGHMGA$_{purif}$ spiked with 4% w/w BHT. The sample was prepared as follows: 6 mg of PLGHMGA$_{purif}$ was dissolved in 150 μL of a DCM also containing 1.6 mg/mL of BHT. The solution was transferred into a low weight aluminum DSC pan and DCM was evaporated at room temperature. Residual solvent was removed under vacuum for 16 hours.

The theoretical T_g of a mix of BHT and PLGHMGA was calculated using the Fox equation[29]:

$$\frac{1}{T_g mix} = \sum_x \frac{w_x}{T_{g,x}}$$

Where w_x is the mass fraction of each component and $T_{g,x}$ is the glass transition temperature of each component (in Kelvin). This equation assumes molecular dissolution of the components and a volume of mixing equal to zero[30].

2.5 Preparation and characterization of polymeric nanoparticles (NPs)

NPs were prepared from a blend of PLGHMGA and MePEG-PLGHMGA at a 4:1 w/w ratio using a double emulsion solvent evaporation method[12,31]. In short, the polymers were dissolved in DCM at 5% w/v. Next, 100 μL of water was added to 1 mL of the polymer solution and the mixture was emulsified in

an ice bath for 1 min at 20 W power using a probe sonicator (SONOPULS HD 2200 Bandelin, Berlin, Germany). The resulting W/O emulsion was added dropwise to 10 mL of an aqueous solution of PVA 5% w/v, in an ice bath, while sonicating for 2 min at 20 W power. The formed W/O/W emulsion was stirred at 600 rpm for 2 h at room temperature to remove the DCM. The NPs were recovered by centrifugation for 30 min, 20,000 g at 4 °C and washed twice with saline solution (0.9% NaCl in water). After the second washing, the NPs were resuspended in 3 mL of UltraPure™ distilled water and freeze dried at -40 °C and <1 mbar (Christ Alpha 1-2 freeze dryer, Osterode am Harz, Germany). The average diameter of the freeze dried NPs was determined by Dynamic Light Scattering (ALV CGS-3 Malvern) at 25 °C in MilliQ water.

The composition of the NPs (in terms of lactic acid, glycolic acid and hydroxymethyl glycolic acid) was determined by ^{1}H NMR in deuterated DMSO and the weight percent of BHT contained in the NPs was calculated as described in section 2.4.

2.6 Cell lines and culture conditions

The cell lines SkBr3 (human breast cancer, ATCC HTB-30) and MDA-MB-231 (human breast cancer, ATCC CRM-HTB-26) were purchased from American Type Culture Collection (ATCC, Wesel, Germany). The cells were cultured in Dulbecco's Modified Eagle's Medium (DMEM) supplemented with 10% fetal calf serum (FCS), 100 units/mL penicillin and 0.1 mg/mL streptomycin, at 37 °C in a humidified atmosphere containing 5% CO_2.

2.7 NPs cytocompatibility tests

SkBr3 and MDA-MB-231 were seeded in a 96-well plate at a density of 5,000 cells/well and incubated overnight at 37 °C and 5% CO_2. Next, the cell culture medium (100 μL) was replaced by NPs suspensions prepared in DMEM at concentrations ranging from 0.4 to 3.25 mg/mL, and the cells were incubated with the NPs for 72 hours. Cell viability was determined with the Alamar Blue assay as follows. The medium containing NPs was removed from the wells and the cells were washed twice with fresh DMEM. Next, 100 μL of DMEM containing Alamar Blue reagent (10:1 v/v) was added to the cells, followed by a 2 h incubation in the dark at 37 °C, 5% CO_2. The fluorescent signal was measured at 550 nm excitation / 590 nm emission using a FluoStar-Optima spectrofluorimeter (BMG Labtech). Cell viability was calculated relative to a non-treated control. The EC50 value of the NPs was calculated from the cell viability data with the software GraphPad Prism 7 (GraphPad, California,

USA) (analysis: nonlinear regression, log[inhibitor] vs. normalized response variable slope).

3 Results and Discussion

3.1 Polymer synthesis and characterization

PLGBMGA and MePEG-PLGBMGA were synthesized by ring-opening polymerization of D,L-lactide and BMG in the melt at 130 °C , catalyzed by tin(II) 2-ethylhexanoate. Benzyl alcohol was used as initiator for the synthesis of PLGBMGA and PEG monomethyl ether was the initiator for MePEG-PLGBMGA [12]. The removal of the benzyl groups in the polymers was achieved by hydrogenation in THF using Pd/C as catalyst [7,11] (Figure 1).

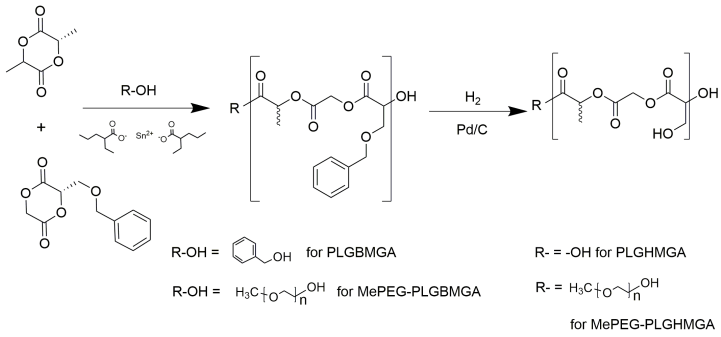

Figure 1: Synthesis of PLGBMGA and MePEG-PLGBMGA and removal of the benzyl groups by hydrogenation catalyzed by Pd/C to yield PLGHMGA and MePEG-PLGHMGA.

The ^{1}H NMR spectra of the PLGBMGA (Figure 2A) and MePEG-PLGBMGA (Figure 2B) confirmed that the polymers were composed of lactic acid, glycolic acid, and BMG (and PEG in the case of MePEG-PLGBMGA). The presence of a signal at 7.3 ppm in the ^{1}H NMR spectra of the synthesized polymers confirmed the presence of aromatic groups in the polymer chains.

Deprotection of PLGBMGA and MePEG-PLGBMGA using Pd/C in THF efficiently removed the aromatic groups in the polymers, as confirmed by the ^{1}H NMR spectra of PLGHMGA and MePEG-PLGHMGA (Figure 3). In addition to the polymer peaks, sharp singlet peaks at 1.3, 2.2, 6.6 and 6.9 ppm were observed in the spectra of the non-purified polymers (Figure 3A and 3D). These peak signals can be assigned to BHT [32] (Figure 4), the stabilizer of THF,

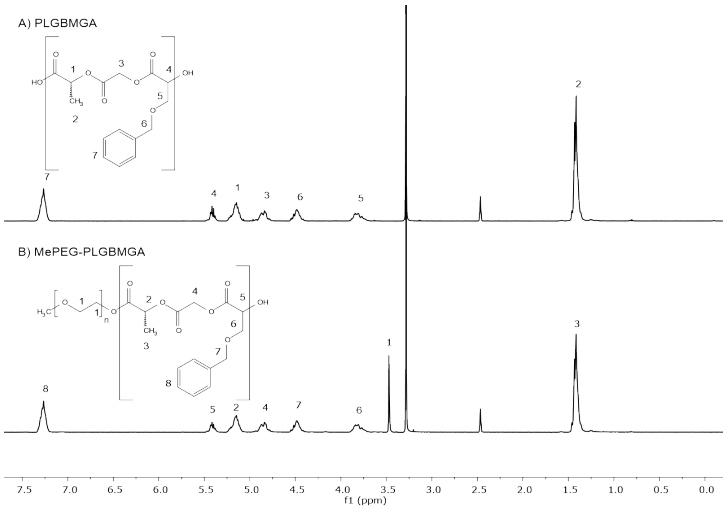

Figure 2: ^{1}H NMR spectra of the protected polymers used in this study. A) PLGBMGA and B) MePEG-PLGBMGA in DMSO-d6.
Polymer peaks: δ = 1.4 (3 H, CH_3); 3.5 (4 H, O-$\underline{CH_2}$-$\underline{CH_2}$ of PEG); 3.8 (2 H, CH-$\underline{CH_2}$-O-CH_2-C_6H_5); 4.5 (2 H, O-$\underline{CH_2}$-C_6H_5); 4.9 (2 H, O-$\underline{CH_2}$-C(O)O-); 5.2 (1 H, $\underline{CH}$-CH_3); 5.4 (1 H, $\underline{CH}$-CH_2-O-CH_2-C_6H_5); 7.3 (5 H, C_6H_5).
Solvent peaks: δ = 2.5 (6 H, CH_3-S-CH_3, DMSO); 3.3 (2 H, H_2O).

and were absent in the spectra of the purified polymers, PLGHMGA$_{purif}$ (Figure 3B) and MePEG-PLGHMGA$_{purif}$ (Figure 3E) demonstrating that this impurity was removed by precipitation in diethyl ether. When PLGHMGA$_{purif}$ was spiked with BHT, the peaks for BHT were observed in the ^{1}H NMR spectrum (Figure 3C). Based on ^{1}H NMR analysis, the weight percent of BHT in the non-purified polymers was 4% for PLGHMGA (thus 40 mg BHT per g of polymer), and 12% for MePEG-PLGHMGA (thus 120 mg BHT per g of polymer). These values are in line with the amount of BHT that could be entrapped in the polymers based on the volume of BHT-stabilized THF used for deprotection. For instance, for the synthesis of PLGHMGA (yield 3.7 g), ∼900 mL of THF (ρ = 0.89 g/mL) stabilized with 0.02 - 0.03% w/w BHT was used, implying that 43 - 65 mg of BHT per g of PLGHMGA can be expected. For the synthesis of MePEG-PLGHMGA (yield 1.0 g), ∼400 mL of THF was used, therefore around 71 - 107 mg of BHT per g of MePEG-PLGHMGA can be expected. The amount of BHT calculated in the polymers by ^{1}H NMR analysis corresponds to an entrapment of ∼60 - 100% for PLGHMGA and

∼100% for MePEG-PLGHMGA. After purification, ^{1}H NMR analysis showed that PLGHMGA and MePEG-PLGHMGA contained 0.2 and 0.4% BHT respectively.

The characteristics of PLGBMGA and PLGHMGA and their PEGylated derivatives are shown in Table 1. Polymer analysis by ^{1}H NMR indicated that the composition of the protected and deprotected polymers was close to the feed ratio. Additionally, similar molecular weights were obtained by GPC analysis for protected and deprotected polymers, indicating that no chain scission occurred during deprotection. The increase in molecular weight of MePEG-PLGHMGA calculated by ^{1}H NMR might be caused by hydrolysis of the ester bond connecting the PEG and the PLGHMGA blocks during deprotection.

Table 1: Characteristics of the polymers used in this study.

Polymer	Composition a:b[a] ^{1}H NMR	Yield (%)	Molecular weight (kg/mol)				MePEG (w%)	T_g (°C)
			GPC		^{1}H NMR	Expected		
			M_n	M_w	M_n	M_n		
PLGBMGA	40:60	94	59	89		53		32
PLGHMGA	38:62	79	ND[b]		NA[c]	43	NA[c]	32
PLGHMGA$_{purif}$	40:60	71	43	62		43		56
MePEG-PLGBMGA	41:59	98	28	43	60	55	3.3	26
MePEG-PLGHMGA	44:56	53	ND[b]		90	45	2.2	25
MePEG-PLGHMGA$_{purif}$	44:56	75	22	31	89	45	2.2	48

[a] a:b represents the molar ratio of BMG/D,L-lactide (protected polymer) or HMG/D,L-lactide (deprotected polymer). Monomer feed was 35(a):65(b); [b] not determined; [c] not applicable.

The T_g of the protected polymers was similar to the T_g of the deprotected non-purified polymers. In contrast, the T_g of the deprotected purified polymers was >20 °C higher, which was consistent with previous reports [12,19]. This suggests that BHT is molecularly dissolved in the PLGHMGA matrix and acts as a plasticizer. To further study this possibility, thermal analysis of PLGHMGA$_{purif}$ spiked with 4% w/w BHT was carried out. PLGHMGA$_{purif}$ + BHT displayed a T_g of 35 °C, which is similar to the T_g of non-purified PLGHMGA (32 °C). Changes in the thermal properties of polymers upon addition of BHT has previously been reported for polysulfone films (decrease in T_g by 30 - 70 °C upon addition of 5 - 20% w/w BHT) [33]. Fox equation was

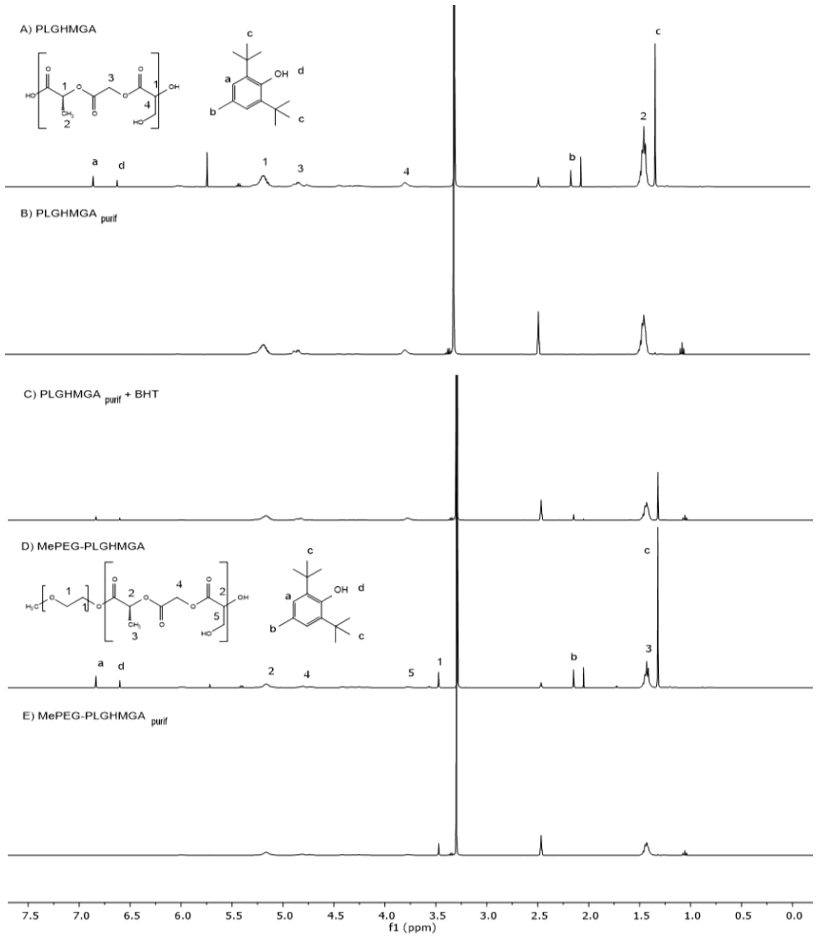

Figure 3: ^{1}H NMR spectra of the deprotected polymers used in this study. A) PLGHMGA, B) PLGHMGA$_{purif}$, C) PLGHMGA$_{purif}$ spiked with BHT, D) MePEG-PLGHMGA and E) MePEG-PLGHMGA$_{purif}$ in DMSO-d6.
Polymer peaks: δ = 1.4 (3 H, CH_3); 3.5 (4 H, O-$\underline{CH_2}$-$\underline{CH_2}$ of PEG); 3.8 (2 H, CH-$\underline{CH_2}$-OH); 4.8 (2 H, O-$\underline{CH_2}$-C(O)O-); 5.2 (1 H, $\underline{CH}$-CH_3).
BHT peaks: δ = 1.3 (18 H, 3($\underline{CH_3}$)-C-C_6H_5); 2.1 (3 H, $\underline{CH_3}$-C_6H_5); 6.6 (1 H $\underline{OH}$-C_6H_5); 6.8 (6 H, C_6H_5).
Solvent peaks: δ = 2.5 (6 H, CH_3-S-CH_3, DMSO); 3.3 (2 H, H_2O).

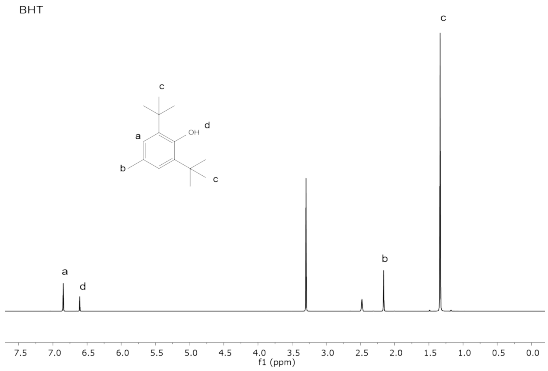

Figure 4: ^{1}H NMR spectra of BHT in DMSO-d6.
BHT peaks: δ = 1.3 (18 H, 3($\underline{CH_3}$)-C-C_6H_5); 2.1 (3 H, $\underline{CH_3}$-C_6H_5); 6.6 (1 H $\underline{OH}$-C_6H_5); 6.8 (6 H, C_6H_5).
Solvent peaks: δ = 2.5 (6 H, CH_3-S-CH_3, DMSO); 3.3 (2 H, H_2O).

used to calculate the T_g of mixtures consisting of 4% w/w BHT and 96% w/w PLGHMGA and 12% w/w BHT and 88% w/w MePEG-PLGHMGA (compositions of non-purified polymers according to the ^{1}H NMR analysis). The T_m of BHT is 344 K (72 °C)[34] and using the rule of thumb applicable for symmetric molecules where $T_g/T_m \leq 0.5$[35], its T_g can be calculated as 172 K (considering T_g/T_m as 0.5). According to Fox equation, the T_g for the BHT/PLGHMGA mix is 44 °C, and for the BHT/MePEG-PLGHMGA it is 18 °C. These T_g values calculated for the mixtures are similar to those found for the non-purified polymers (32 °C for PLGHMGA and 25 °C for MePEG-PLGHMGA) which is an indication that BHT is dissolved in the polymer matrix.

3.2 NPs characterization

NPs were prepared from a blend of PLGHMGA and MePEG-PLGHMGA (purified or not purified) and their characteristics are displayed in Table 2.

In agreement with the results of the ^{1}H NMR analysis of the polymers (Figure 3), ^{1}H NMR analysis of the NPs showed the presence of BHT in the formulations prepared from PLGHMGA and MePEG-PLGHMGA (Figure 5A) but not in those prepared from the purified polymers (Figure 5B).

The NPs were prepared from 80% PLGHMGA (containing 40 mg BHT per g of polymer, section 3.1) and 20% MePEG-PLGHMGA (containing 120 mg

Table 2: Characteristics of the polymeric NPs prepared in this study.

Formulation	Yield (%)	Diameter (nm)[a]	PDI
NPs PLGHMGA + MePEG-PLGHMGA	54	380	0.24
NPs PLGHMGA$_{purif}$ + MePEG-PLGHMGA$_{purif}$	45	330	0.21

[a] Diameter of freeze dried NPs after resuspension in water.

BHT per g polymer) implying that maximum 56 mg of BHT can be present per g of NPs. Based on ^{1}H NMR analysis, the weight percent of BHT in the NPs prepared from non-purified polymers was 2.3%, which corresponds to 23 mg BHT/g of polymer, indicating that ∼60% of BHT was not entrapped, most likely due to its dissolution in the aqueous PVA phase used during the preparation of the NPs.

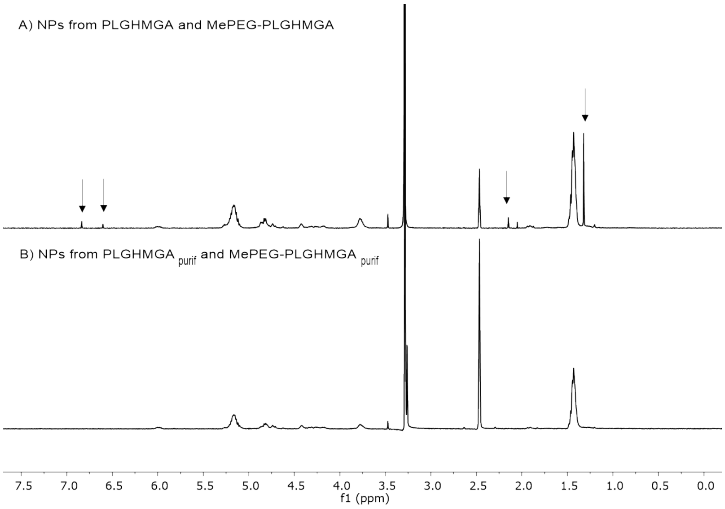

Figure 5: ^{1}H NMR spectra of the NPs used in this study. A) NPs from PLGHMGA and MePEG-PLGHMGA and B) NPs from PLGHMGA$_{purif}$ and MePEG-PLGHMGA$_{purif}$ in DMSO-d6. Peaks corresponding to BHT are shown with arrows.
Polymer peaks: δ = 1.4 (3 H, CH_3); 3.5 (4 H, O-$\underline{CH_2}$-$\underline{CH_2}$ of PEG); 3.8 (2 H, CH-$\underline{CH_2}$-OH); 4.8 (2 H, O-$\underline{CH_2}$-C(O)O-); 5.2 (1 H, $\underline{CH}$-CH_3).
BHT peaks: δ = 1.3 (18 H, 3($\underline{CH_3}$)-C-C_6H_5); 2.1 (3 H, $\underline{CH_3}$-C_6H_5); 6.6 (1 H $\underline{OH}$-C_6H_5); 6.8 (6 H, C_6H_5).
Solvent peaks: δ = 2.5 (6 H, CH_3-S-CH_3, DMSO); 3.3 (2 H, H_2O).

3.3 NPs cytocompatibility

The cytocompatibility of the NPs was evaluated in two breast cancer cell lines (Figure 6). The NPs prepared from the non-purified polymers showed high cytotoxicity with EC50 values around 1.2 and 1.6 mg/mL for SkBr3 and MDA-MB-231 cells, respectively. In contrast, NPs prepared from purified polymers were not cytotoxic and ∼100% cell viability was observed at concentrations as high as 3.25 mg/mL.

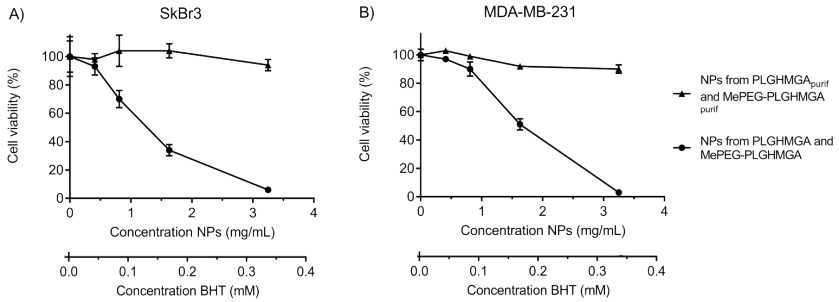

Figure 6: Cytocompatibility of NPs. The NPs were prepared from non-purified and purified PLGHMGA and MePEG-PLGHMGA and tested in in A) SkBr3 and B) MDA-MB-231 cells. Cell viability was calculated relative to a non-treated sample. For the non-purified polymers n=2 independent experiments conducted by triplicate. For the purified polymers n=1 experiment conducted by triplicate.

Based on the ^{1}H NMR data (section 3.2), 23 μg of BHT was present per mg of NPs. Assuming that BHT is fully released from the NPs during the cytocompatibility experiments (aqueous solubility of BHT is low, ∼1 mg/L[36] but the presence of lipids and proteins in the cell culture medium could have improved it), the concentration of BHT would be 0.04 - 1.36 mM. Several authors have also reported on cytotoxic effects of BHT in different cell types, including myocardial and endothelioid cells[37], hepatocytes[38], human cells of dermal[39] and oral origin (ED50 0.16 - 0.20 mM)[40], renal epithelial cells[41], and promyelocytic leukemia cells, as well as human squamous carcinoma cells (CC50 of 0.2 - 0.3 mM)[42]. Different mechanisms have been described for the cytotoxicity of BHT, including damage to biological membranes[38,43] and metabolism into highly reactive toxic compounds[44,45]. Thus, the observed cytotoxicity of the NPs prepared from non-purified polymers can indeed be ascribed to the presence of BHT in the particles.

4 Conclusions

The synthesis of PLGHMGA and MePEG-PLGHMGA using stabilized THF led to the accumulation of BHT (THF stabilizer) in these polymers. Although BHT can be removed from THF prior to polymer synthesis, working with unstabilized THF represents a safety hazard. Alternatively, as presented in this work, BHT can be easily and quantitatively removed after polymer synthesis by precipitation in a non-solvent such as diethyl ether. The data presented in this work shows that BHT, even if originally present in THF at very small quantities, can accumulate in PLGHMGA and MePEG-PLGHMGA to amounts that drastically decrease the cytocompatibility of these polymers, highlighting the importance of proper polymer purification and characterization.

Acknowledgements

Lucía Martínez-Jothar would like to thank the Consejo Nacional de Ciencia y Tecnología (CONACYT), México (grant no. 384743) for the funding provided in the framework of her PhD.

References

[1] Danhier, F., Ansorena, E., Silva, J. M., Coco, R., Le Breton, A., and Préat, V. PLGA-based nanoparticles: An overview of biomedical applications. *Journal of Controlled Release*, 161, 2012.

[2] Kamaly, N., Yameen, B., Wu, J., and Farokzhad, O. C. Degradable controlled-release polymers and polymeric nanoparticles: Mechanisms of controlling drug release. *Chemical Reviews*, 116, 2016.

[3] Nair, L. S. and Laurencin, C. T. Biodegradable polymers as biomaterials. *Progress in Polymer Science*, 32, 2007.

[4] Tong, R., Gabrielson, N. P., Fan, T. M., and Cheng, J. Polymeric nanomedicines based on poly (lactide) and poly (lactide-co-glycolide). *Current Opinion in Solid State & Materials Science*, 16, 2012.

[5] Kimura, Y., Shirotani, K., Yamane, H., and Kitao, T. Ring-opening polymerization of 3(S)-[(Benzyloxycarbonyl)methyl]-1,4-dioxane-2,5-dione: A new route to a poly(α-hydroxy acid) with pendant carboxyl groups. *Macromolecules*, 21, 1988.

[6] Vert, M. and Lenz, R. W. Preparation and properties of poly-beta-malic acid: A functional polyester of potential biomedical importance. *American Chemical Society Division of Polymer Chemistry*, 20, 1979.

[7] Leemhuis, M., Nostrum, C. F. V., Kruijtzer, J. A. W., Zhong, Z. Y., Breteler, M. R., Dijkstra, P. J., Feijen, J., and Hennink, W. E. Functionalized poly (alpha -hydroxy acid)s via ring-opening polymerization: Toward hydrophilic polyesters with pendant hydroxyl groups. *Macromolecules*, 39, 2006.

[8] Yang, J.-Y., Yu, J., Pan, H.-Z., Gu, Z.-W., Cao, W.-X., and Feng, X.-D. Synthesis of novel hydrophilic biodegradable polyester with functionalized side chain groups. *Chinese Journal of Polymer Science*, 19, 2001.

[9] Becker, G. and Wurm, F. R. Functional biodegradable polymers via ring-opening polymerization of monomers without protective groups. *Chemical Society Reviews*, 47, 2018.

[10] Seyednejad, H., Ghassemi, A. H., Nostrum, C. F. V., Vermonden, T., and Hennink, W. E. Functional aliphatic polyesters for biomedical and pharmaceutical applications. *Journal of Controlled Release*, 152, 2011.

[11] Leemhuis, M., Kruijtzer, J., van Nostrum, C., and Hennink, W. E. In vitro hydrolytic degradation of hydroxyl-functionalized poly (alpha-hydroxy acid)s. *Biomacromolecules*, 8, 2007.

[12] Samadi, N., van Steenbergen, M., van den Dikkenberg, J., Vermonden, T., van Nostrum, C., Amidi, M., and Hennink, W. Nanoparticles based on a hydrophilic polyester with a sheddable PEG coating for protein delivery. *Pharmaceutical Research*, 31, 2014.

[13] Ghassemi, A., Steenbergen, M., Talsma, H., van Nostrum, C. F., Jiskoot, W., Crommelin, D., and Hennink, W. Preparation and characterization of protein loaded microspheres based on a hydroxylated aliphatic polyester, poly(lactic-co-hydroxymethyl glycolic acid). *Journal of Controlled Release*, 138, 2009.

[14] Kazazi-Hyseni, F., van Vuuren, S., van der Giezen, D., Pieters, E., Ramazani, F., Rodriguez, S., Veldhius, G., Goldschmeding, R., van Nostrum, C., Hennink, W., and Kok, R. Release and pharmacokinetics of near-infrared labeled albumin from monodisperse poly(d,l-lactic-co-hydroxymethyl glycolic acid) microspheres after subcapsular renal injection. *Acta Biomaterialia*, 22, 2015.

[15] Rahimian, S., Fransen, M., Kleinovink, J., Christensen, J., Amidi, M., Hennink, W., and Ossendorp, F. Polymeric nanoparticles for co-delivery of synthetic long peptide antigen and poly IC as therapeutic cancer vaccine formulation. *Journal of Controlled Release*, 203, 2015.

[16] Ritsema, J., Herschberg, E., Borgos, S., Løvmo, C., Schmid, R., te Welscher, Y., Storm, G., and van Nostrum, C. Relationship between polarities of antibiotic and polymer matrix on nanoparticle formulations based on aliphatic polyesters. *International Journal of Pharmaceutics*, 548, 2018.

[17] Ghassemi, A., Steenbergen, M., Barendregt, A., Talsma, H., Kok, R., and van Nostrum, C. Controlled release of octreotide and assessment of peptide acylation from poly (D,L-lactide-co-hydroxymethyl glycolide) compared to PLGA microspheres. *Pharmaceutical Research*, 29, 2012.

[18] Shirangi, M., Hennink, W. E., Somsen, G. W., and van Nostrum, C. F. Identification and assessment of octreotide acylation in polyester microspheres by LC-MS/MS. *Pharmaceutical Research*, 32, 2015.

[19] Samadi, N., van Nostrum, C., Vermonden, T., Amidi, M., and Hennink, W. Mechanistic studies on the degradation and protein release characteristics of poly (lactic-co-glycolic-co-hydroxymethylglycolic acid) nanospheres. *Biomacromolecules*, 14, 2013.

[20] Samadi, N. *Biodegradable nanoparticles based on aliphatic polyesters and towards intracellular delivery of protein therapeutics*. Thesis, Utrecht University, 2014.

[21] Liu, G., Li, Y., Yang, L., Wei, Y., Wang, X., Wang, Z., and Tao, L. Cytotoxicity study of polyethylene glycol derivatives. *RSC Advances*, 7, 2017.

[22] Tanzi, M. C., Verderio, P., Lampugnani, M. G., Resnati, M., Dejana, E., and Sturani, E. Cytotoxicity of some catalysts commonly used in the synthesis of copolymers for biomedical use. *Journal of Materials Science: Materials in Medicine*, 5, 1994.

[23] Xia, Y., Shen, J., Alamri, H., Hadjichristidis, N., Zhao, J., Wang, Y., and Zhang, G. Revealing the cytotoxicity of residues of phosphazene catalysts used for the synthesis of poly(ethylene oxide). *Biomacromolecules*, 18, 2017.

[24] Humpolicek, P., Kasparkova, V., Saha, P., and Stejskal, J. Biocompatibility of polyaniline. *Synthetic Metals*, 162, 2012.

[25] Anderson, J. M. and Shive, M. S. Biodegradation and biocompatibility of PLA and PLGA microspheres. *Advanced Drug Delivery Reviews*, 64, 1997.

[26] Fatih Canbolat, M., Tang, C., Bernacki, S. H., Pourdeyhimi, B., and Khan, S. Mammalian cell viability in electrospun composite nanofiber structures. *Macromolecular Bioscience*, 11, 2011.

[27] Szekely, G., De Sousa, M. C. A., Gil, M., Ferreira, F. C., and Heggie, W. Genotoxic impurities in pharmaceutical manufacturing: Sources, regulations, and mitigation. *Chemical Reviews*, 115, 2015.

[28] Yehye, W., Rahman, N., Ariffin, A., Abd Hamid, S., Alhadi, A., Kadir, F., and Yaeghoobi, M. Understanding the chemistry behind the antioxidant activities of butylated hydroxytoluene (BHT): A review. *European Journal of Medicinal Chemistry*, 101, 2015.

[29] Fox, T. *Bulletin of the American Physical Society*, 1:123, 1956.

[30] Kalogeras, I. M. and Brostow, W. Glass transition temperatures in binary polymer blends. *Journal of Polymer Science: Part B: Polymer Physics*, 47, 2009.

[31] Zambaux, M. F., Bonneaux, F., Gref, R., Maincent, P., Dellacherie, E., Alonso, M. J., Labrude, P., and Vigneron, C. Influence of experimental parameters on the characteristics of poly (lactic acid) nanoparticles prepared by a double emulsion method. *Journal of Controlled Release*, 50, 1998.

[32] Fulmer, G., Miller, A., Sherden, N., Gottlieb, H., Nudelman, A., Stoltz, B., Bercaw, J., Goldberg, K., Gan, R., and Apiezon, H. NMR chemical shifts of trace impurities: Common laboratory solvents, organics, and gases in deuterated solvents relevant to the organometallic chemist. *Organometallics*, 29, 2010.

[33] Vidotti, S., Chinellato, A., Hu, G., and Pessan, L. Effects of low molar mass additives on the molecular mobility and transport properties of polysulfone. *Journal of Applied Polymer Science*, 101, 2006.

[34] Baluja, S., Bhesaniya, K., Bhalodia, R., and Chanda, S. Solubility of butylated hydroxytoluene (BHT) in aqueous and alcohol solutions from 293.15 to 313.15 K. *International Letters of Chemistry, Physics and Astronomy*, 9, 2014.

[35] van Krevelen, D. and te Nijenhuis, K. *Properties of Polymers*. Elsevier Science, 4th edition, 2009.

[36] Fries, E. and Wilhelm, P. Analysis of the antioxidant butylated hydroxytoluene (BHT) in water by means of solid phase extraction combined with GC / MS. *Water Research*, 36, 2002.

[37] Leslie, S., Gad, S., and Acosta, D. Cytotoxicity of butylated hydroxytoluene and butylated hydroxyanisol in cultured heart cells. *Toxicology*, 10, 1978.

[38] Thompson, D. and Moldéus, P. Cytotoxicity of butylated hydroxyanisole and butylated hydroxytoluene in isolated rat hepatocytes. *Biochemical Pharmacology*, 37, 1988.

[39] Babich, H. and Borenfreund, E. Cytotoxic effects of food additives and pharmaceuticals on cells in culture as determined with the neutral red assay. *Journal of Pharmaceutical Sciences*, 79, 1990.

[40] Geurtsen, W., Lehmann, F., Spahl, W., and Leyhausen, G. Cytotoxicity of 35 dental resin composite monomers / additives in permanent 3T3 and three human primary fibroblast cultures. *Journal of Biomedical Materials Research*, 41, 1998.

[41] Hallman, M. A., Tchao, R., and Tarloff, J. B. Effect of antioxidants on para-aminophenol-induced toxicity in LLC-PK1cells. *Toxicology*, 156, 2000.

[42] Saito, M., Sakagami, H., and Fujisawa, S. Cytotoxicity and apoptosis induction by butylated hydroxyanisole (BHA) and butylated hydroxytoluene (BHT). *Anticancer Research*, 23, 2003.

[43] Sgaragli, G., Della Corte, L., Rizzotti-Conti, M., and Giotti, A. Effects of monocyclic compounds on biomembranes. *Biochemical Pharmacology*, 26, 1977.

[44] Thompson, D., Thompson, J., Sugumaran, M., and Moldéus, P. Biological and toxicological consequences of quinone methide formation. *Chemico-Biological Interactions*, 86, 1992.

[45] Witschi, H., Malkinson, A., and Thompson, J. Metabolism and pulmonary toxicity of butylated hydroxytoluene (BHT). *Pharmacology and Therapeutics*, 42, 1989.

Chapter **5**

Selective cytotoxicity to HER2 positive breast cancer cells by saporin-loaded nanobody-targeted polymeric nanoparticles in combination with photochemical internalization

Lucía Martínez-Jothar[†], Nataliia Beztsinna[†], Cornelus F. van Nostrum[†], Wim E. Hennink[†] and Sabrina Oliveira[†,‡]

† Department of Pharmaceutics, Utrecht Institute for Pharmaceutical Sciences, Utrecht University, Utrecht, the Netherlands

‡ Division of Cell Biology, Department of Biology, Utrecht University, Utrecht, the Netherlands

Molecular Pharmaceutics 2019, 16(4), 1633 - 1647

Abstract

In cancer treatment, polymeric nanoparticles (NPs) can serve as a vehicle for the delivery of cytotoxic proteins that have intracellular targets but that lack well-defined mechanisms for cellular internalization, such as saporin. In this work we have prepared PEGylated poly(lactic acid-co-glycolic acid-co-hydroxymethyl glycolic acid) (PLGHMGA) NPs for the selective delivery of saporin in the cytosol of HER2 positive cancer cells. This selective uptake was achieved by decorating the surface of the NPs with the 11A4 nanobody that is specific for the HER2 receptor. Confocal microscopy observations showed rapid and extensive uptake of the targeted NPs (11A4-NPs) by HER2 positive cells (SkBr3), but not by HER2 negative cells (MDA-MB-231). This selective uptake was blocked upon pre-incubation of the cells with an excess of nanobody. Non-targeted NPs (Cys-NPs) were not taken up by either type of cells. Importantly, a dose-dependent cytotoxic effect was only observed on SkBr3 cells when these were treated with saporin-loaded 11A4-NPs in combination with photochemical internalization (PCI), a technique that uses a photosensitizer and local light exposure to facilitate endosomal escape of entrapped nanocarriers and biomolecules. The combined use of saporin-loaded 11A4-NPs and PCI strongly inhibited cell proliferation and decreased cell viability through induction of apoptosis. Also the cytotoxic effect could be reduced by an excess of nanobody, reinforcing the selectivity of this system. These results suggest that the combination of the targeting nanobody on the NPs with PCI are effective means to achieve selective uptake and cytotoxicity of saporin-loaded NPs.

1 Introduction

Proteins are widely recognized as valuable therapeutic agents because of their high potency and target specificity. A large number of the currently approved therapeutic proteins is indicated for cancer therapy, one of the leading causes of death worldwide, as classic low molecular weight chemotherapeutic drugs result in substantial off-target toxicity [1].

In the search for new antineoplastic drugs the ribosome-inactivating protein (RIP) saporin (from the plant *Saponaria officinalis*), has emerged as an agent of interest because of its potent cytotoxic effect, stability at high temperature, resistance to denaturation and ease of chemical modification [2,3]. Several cytotoxic mechanisms have been described for saporin, including inhibition of protein synthesis, DNA-fragmentation and induction of apoptosis via the intrinsic and extrinsic pathways [4–7]. Saporin is a type I RIP and, unlike type II RIPs, it lacks the galactose-specific lectin that mediates cell binding and entrance. It has been reported that saporin can enter some cells via endocytosis mediated by the α2-macroglobulin receptor [8] or by receptor-independent mechanisms [9]. However, the mechanism of internalization of saporin is not yet completely clear and alternatives have been developed in order to achieve enhanced, cell-specific uptake of this protein to increase its cytotoxicity. Particularly, saporin-antibody conjugates (immunotoxins) have been commonly used for this purpose [10–13]. While immunotoxins have shown promising efficacy *in vitro* and *in vivo*, their use in clinical settings has been mostly limited by their immunogenicity and induction of vascular leak syndrome [14,15]. Furthermore, the preparation of immunotoxins often requires conjugation strategies to chemically link the toxin to the antibody.

The use of nanocarriers is another approach for the efficient intracellular delivery of saporin [16–19] and other biotherapeutics with limited membrane permeability (proteins and nuclei acid based drugs) [20–22]. In particular, polymeric nanoparticles (NPs) have attracted increasing attention as nanocarriers over the past 20 years due to their ability to increase the physicochemical stability of their cargo and provide certain control over when, where and how it is released, thus improving its pharmacokinetic and pharmacodynamic profiles [23,24]. In the present study, NPs made from PEGylated poly(lactic acid-co-glycolic acid-co-hydroxymethyl glycolic acid) (PLGHMGA) were used for the encapsulation and delivery of saporin. PLGHMGA is structurally related to poly(lactic-co-glycolic acid) (PLGA), though it contains pending hydroxyl groups that increase its hydrophilicity and shorten its degradation time [25]. Encapsulation of a peptide in PLGHMGA microparticles resulted in less chemical modifications (acylation) than in PLGA microparticles [26,27], which points to

an improved compatibility of PLGHMGA with biomolecules and suggests that PLGHMGA NPs could be a suitable nanocarrier for saporin.

The efficiency and selectivity of polymeric NPs as nanocarriers can be further increased by functionalization of their surface with targeting ligands that bind to cell surface receptors overexpressed in tumors[28–31]. Nanobodies, also known as VHHs, are variable domains of the heavy chain of heavy chain antibodies present in camelids[32] and they are the smallest naturally occurring antigen binding fragments. The structure and small size of nanobodies (∼15 kDa) confers them advantages over conventional antibodies or fragments thereof, including an increased solubility and stability, less propensity for aggregation, easier production, and greater ability to reach and neutralize targets that are not easily accessible[33,34]. Furthermore, nanobodies display low immunogenicity because of their high sequence homology with the VH of human antibodies[35] and, if needed, additional homology can be easily obtained by humanization of specific residues without detrimental effects on their stability and affinity[36]. Importantly, nanobodies can selectively target a variety of receptors, including HER2 (Human Epidermal Growth Factor Receptor 2), which is overexpressed in several types of malignancies such as breast, gastric, lung and ovarian cancers, and is associated with poor prognosis[37,38]. The nanobody 11A4 binds specifically to the HER2 receptor with high affinity and has shown promise for optical imaging of breast cancer *in vivo*[39,40] and for immunolabeling of HER2 for electron microscopy[41]. Nanobodies targeting the HER2 receptor, as well as other receptors such as the epidermal growth factor receptor (EGFR) and the hepatocyte growth factor receptor (HGFR), have been used in the field of drug delivery for the functionalization of liposomes[42,43], polymeric micelles[44,45], albumin nanoparticles[46,47] and polymersomes[48], resulting in selective and efficient receptor-mediated uptake of these systems. In the present work, the targeting properties of the nanobody 11A4 were explored to achieve enhanced and selective uptake of polymeric NPs by HER2 overexpressing breast cancer cells.

Upon ligand-receptor interaction, polymeric NPs are internalized by endocytosis and can therefore act as intracellular delivery systems. However, those NPs are then inside endocytic vesicles, which later fuse with lysosomes[49]. Thus, to prevent that cargo molecules such as proteins are degraded, strategies have been developed for endosomal escape of nanocarriers and/or their cargo. Release of the NPs from the endosome can be accomplished either by nanoparticle design (incorporation of elements for proton sponge effect, membrane disruption or pore formation)[50–52] or by means of external stimuli, such as photochemical internalization (PCI). This technique makes use of an amphiphilic photosensitizer (PS) which localizes in the cell membrane and, upon

endocytosis of the NPs, becomes a part of the endosomal membrane where the NPs are entrapped. Upon excitation with light of the appropriate wavelength, the PS will produce reactive oxygen species that damage the endosomal membrane, which results in destabilization of this membrane and subsequently in release of its contents into the cytosol[53]. PCI has been successfully used both *in vitro* and *in vivo* for the delivery of proteins, immunotoxins, chemotherapeutics, genetic material and nanocarriers[54–56]. Importantly, phase I clinical trials have proven the safety and tolerability of the PS disulfonated tetraphenyl chlorin ($TPCS_{2a}$) used for PCI of bleomycin for the treatment of cutaneous and subcutaneous malignancies[57]. Additionally, a phase I/II clinical trial involving PCI of gemcitabine for the treatment of cholangiocarcinomas is currently underway[58].

In the present work, the potency and selectivity of a new formulation was investigated combined with PCI, to assess its capacity to locally deliver a cytotoxic molecule to target cells. For this purpose, PEG-PLGHMGA NPs loaded with saporin and functionalized with the 11A4 nanobody were prepared and characterized. The uptake of these NPs was investigated and their cytotoxicity was evaluated in combination with PCI in both HER2 positive and negative breast cancer cell lines. The contribution of each one of the elements under study to the cytotoxicity of the treatment was also evaluated.

2 Experimental section

2.1 Materials

D,L-lactide was obtained from Corbion (Gorinchem, the Netherlands). BMG, a dilactone containing a protected benzyl group, was synthesized as described previously[59]. Benzyl alcohol, tin(II) 2-ethylhexanoate, poly(vinyl alcohol) (PVA) M_w 30,000 - 70,000 Da (87 - 90% hydrolyzed) and L-cysteine hydrochloride monohydrate were purchased from Sigma-Aldrich (Steinheim, Germany). Poly(ethylene glycol) monomethyl ether (M_n ~2,000 Da) and palladium on carbon (10 wt% loading) were acquired from Aldrich (Steinheim, Germany). Poly(lactide-co-glycolide)-cysteine ethyl ester (PLGA-SH, M_w 30,000 Da) and poly(lactide-co-glycolide)-b-poly(ethylene glycol)-maleimide (maleimide-$PEG_{5,000}$-$PLGA_{20,000}$) were purchased from Polyscitech, Akina Inc (Indiana, USA). Micro BCA™ Protein Assay Kit and Pierce™ Silver Stain Kit were purchased from Thermo Scientific (Illinois, USA). Alexa-568 C5 maleimide was obtained from Thermo Fisher Scientific (Oregon, USA). Saporin from *Saponaria officinalis* seeds (as a lyophilized powder containing protein, glucose and sodium phosphate buffer salts), Dulbecco's phosphate

buffered saline (8.0 g NaCl, 1.15 g Na_2HPO_4, 0.2 g KCl and 0.2 g KH_2PO_4 in 1 L of water, pH 7.4), McCoy's 5A medium, Dulbecco's Modified Eagle's Medium (DMEM) - high glucose, fetal bovine serum, antibiotic antimycotic solution (10,000 units penicillin, 10 mg streptomycin, and 25 μg amphotericin B/mL), resazurin sodium salt, staurosporine from *Streptomyces sp.* and Triton X-100 were purchased from Sigma (Steinheim, Germany). The PS meso-tetraphenyl porphyrin disulphonate ($TPPS_{2a}$)[60] was kindly provided by Dr. Anders Høgset (PCI Biotech, Oslo, Norway). The BrdU assay kit was acquired from Roche (Manheim, Germany). Annexin V - FITC (90 μg/mL) was purchased from Biolegend (California, USA). Propidium iodide (1.0 mg/mL) was acquired from Invitrogen (Oregon, USA).

2.2 Synthesis of poly(D,L-lactic-co-glycolic-co-hydroxymethyl glycolic acid) (PLGHMGA) and methoxy-PEG-PLGHMGA (MePEG-PLGHMGA)

Poly(D,L-lactic-co-glycolic-co-benzyloxymethyl glycolic acid) (PLGBMGA) was synthesized by copolymerization of D,L-lactide and benzyloxymethyl glycolide (BMG) in the melt at a ratio of 65:35 mol/mol%. Benzyl alcohol was used as initiator at a 300:1 monomer to initiator molar ratio and the catalyst tin(II) 2-ethylhexanoate was employed at a 2:1 molar ratio of initiator to catalyst as reported elsewhere[61]. The protecting benzyl groups of the polymer were removed by hydrogenation catalyzed by palladium on carbon following a previously described protocol[59]. The resulting polymer, PLGHMGA, was purified by precipitation in cold diethyl ether, recovered by filtration and dried under vacuum. MePEG-PLGHMGA was prepared as described for PLGHMGA, but poly(ethylene glycol) monomethyl ether was used as an initiator instead of benzyl alcohol[61].

2.3 Polymer characterization

The composition of PLGHMGA was determined by ^{1}H NMR in deuterated DMSO. The molar % of lactic acid (L), glycolic acid (G) and hydroxymethyl glycolic acid (HMG) was calculated based on the peak integrals (I_{ppm}) of the monomers[61], as follows:

$$I_L = [(I_{5.1-5.4}) - (I_{3.6-3.9}/2)]$$
$$I_G = (I_{4.7-5.0})/2$$
$$I_{HMG} = [(I_{3.6-3.9})/2 + (I_{4.1-4.5})/3]$$

$$\%_L = I_L/(I_L + I_G + I_{HMG}) \times 100$$
$$\%_G = I_G/(I_L + I_G + I_{HMG}) \times 100$$
$$\%_{HMG} = I_{HMG}/(I_L + I_G + I_{HMG}) \times 100$$

The % PEG in MePEG-PLGHMGA was also determined based on ^{1}H NMR analysis[61] as follows:

$$Calculated\,polymer\,M_n = (I_L/I_{PEG}\times M_w Lunit)+(I_G/I_{PEG}\times M_w Gunit)+(I_{HMG}/I_{PEG}\times M_w HMGunit) + PEG\,M_w$$

$$\%_{PEG} = PEG\,M_w/calculated\,polymer\,M_n \times 100$$

The molecular weights of the polymers were determined by gel permeation chromatography (GPC) (Waters 2695 separating module and Waters 2414 refractive index detector) using two PL-gel 5 μm Mixed-D columns and tetrahydrofuran as the mobile phase (1 mL/min) at 60 °C. Polystyrene standards (EasiCal Agilent, California, USA) and PEG standards were used for calibration.

The thermal properties of the polymers were studied using differential scanning calorimetry (Discovery DSC, TA instruments, Delaware, USA). Briefly, a sample of ∼5 mg of polymer was transferred into an aluminum pan and heated from room temperature to 120 °C at a rate of 5 °C/min and subsequently cooled down to -50 °C at the same rate. The polymer was then heated to 120 °C at a rate of 2 °C/min with temperature modulation at ± 1 °C.

2.4 Synthesis of Alexa-568-PLGA

Fluorescently labeled PLGA was prepared by maleimide-thiol reaction of PLGA-SH (thiol endcap) and Alexa-568 C5 maleimide at an equimolar ratio[62]. Briefly, PLGA-SH was dissolved in acetonitrile (25 mg/mL) and Alexa-568 C5 maleimide was dissolved in PBS/EDTA 4 mM (10 mg/mL, pH 7.4).

The Alexa dye (0.1 mL) was added to PLGA-SH (1 mL) and the mixture was stirred in the dark at room temperature for 2 h. The polymer was recovered by precipitation in cold methanol followed by centrifugation (20 min, 20,000 g, 4 °C). The polymer pellet was recovered and dried under reduced pressure.

2.5 Polymeric nanoparticles (NPs) preparation and characterization

The NPs were prepared using a double emulsion solvent evaporation method[61,63,64], starting from a mixture of PLGHMGA, MePEG-PLGHMGA and maleimide-PEG-PLGA in a 8:1:1 w/w ratio. For the preparation of fluorescent particles, 2% w/w of Alexa-568-PLGA was added to the polymer mixture. The polymers were dissolved in dichloromethane at 5% w/v and 200 μL of an aqueous solution of saporin (5 mg protein/mL) or 200 μL of water (for preparation of placebo NPs) were added to 1 mL of this polymer solution. The mixture was subsequently emulsified for 1 min at 20 W power using a probe sonicator (SONOPULS HD 2200 Bandelin, Berlin, Germany) in an ice bath. Next, this W/O emulsion was added dropwise to 10 mL of an aqueous solution of PVA 5% w/v and NaCl 0.9% w/v. The addition was done while sonicating the sample in an ice bath for 2 min at 20 W power. The resulting W/O/W emulsion was stirred at 600 rpm for 2 h at room temperature to evaporate the dichloromethane. Subsequently, the NPs were collected by centrifugation for 20 min, 20,000 g at 4 °C, washed with PBS and finally with UltraPure™ distilled water (Invitrogen, Paisley, UK). After the second washing, the NPs were resuspended in 1 mL of UltraPure™ distilled water and divided into aliquots of equal volume (200 μL). One of the aliquots was freeze dried at -40 °C, <1 mbar (Christ Alpha 1-2 freeze dryer) and used to determine the yield of the NPs and their protein content (section 2.6). The other aliquots were supplemented with sucrose at a final concentration of 5% w/v and freeze dried at -40 °C, <1 mbar.

The diameter of the different NPs was determined by Dynamic Light Scattering (Zetasizer Nano S, Malvern, Worcestershire, UK) at 25 °C in MilliQ water (the concentration of the suspension was 100 μg NPs/mL) and their zeta potential (Zetasizer Nano Z, Malvern, Worcestershire, UK) was measured at 25 °C in HEPES 10 mM pH 7.0 (100 μg NPs/mL).

2.6 Determination of saporin loading of the NPs

The saporin encapsulation efficiency of the NPs was determined by a previously described method[65]. In short, 5 mg of freeze dried NPs was degraded in

3 mL of a solution of 0.05 M NaOH containing 0.5% w/v of sodium dodecyl sulfate at 37 °C for 2 h. The protein content in the resulting solution was determined by MicroBCA Assay (according to the specifications of the manufacturer). A sample of saporin was treated in the same way as the NPs and used for calibration in the range of 2 - 40 μg/mL. The encapsulation efficiency and loading capacity were calculated as follows:

$$Encapsulation\ efficiency\ \% = \frac{Amount\ of\ protein\ entrapped}{Amount\ of\ protein\ used\ in\ preparation} \times 100$$

$$Loading\ \% = \frac{Amount\ of\ protein\ entrapped}{Dry\ weight\ of\ NPs\ used\ in\ the\ test} \times 100$$

2.7 *In vitro* release of saporin from the NPs

Freeze dried saporin-loaded NPs were suspended at a concentration of 5 mg/mL in PBS. The NPs suspension was divided into aliquots of 300 μL which were incubated at 37 °C under mild agitation. At different time points, an aliquot was taken and centrifuged for 10 min, 20,000 g at 4 °C and the supernatant (containing the released saporin) was collected and stored at -20 °C until the end of the study. The supernatants were analyzed by SDS PAGE under reducing conditions: 30 μL of the supernatants was diluted with 10 μL of sample buffer (8% w/v SDS, 40% v/v glycerol, 0.008% w/v bromophenol blue, 20% v/v 2-mercaptoethanol in buffer Tris-HCl pH 6.8) and 20 μL of the diluted sample was loaded into a Bolt™ 4 - 12% Bis-Tris Plus gel (Invitrogen, California, USA). The same procedure was followed for standards containing known amounts of saporin (2 - 8 ng/ μL). The protein in the gel was visualized by silver staining (performed according to the instructions of the manufacturer). The gel was imaged using a ChemiDoc™ MP imager (Bio-Rad, California, USA) and analyzed with ImageJ software (NIH, USA). The gel analysis function on ImageJ was used to generate plots from the intensity of the pixels in a selected area (area of the protein band). The amount of saporin in the release samples was calculated by comparing the peak areas of the plots to the peak areas from the standards.

2.8 Conjugation of 11A4 nanobody to the NPs

The 11A4 nanobody containing a C-terminal cysteine (theoretical M_w 14,813 Da by ExPASy ProtParam) was produced and purified, as previously described[39,40]. The conjugation reaction was conducted according to our pre-

vious study[66]. In short, an amount of freeze dried NPs was resuspended in water and pelleted by centrifugation (10 min, 3,000 g at 4 °C). Subsequently, the NPs pellet was resuspended in PBS / EDTA 0.4 mM to a concentration of ∼3.5 mg NPs/mL and mixed with the nanobody at a molar ratio of 10:1 maleimide-PEG-PLGA to nanobody. The samples were incubated for 2 h at room temperature on a nutating mixer. Subsequently, the non-conjugated nanobody was separated from the 11A4 functionalized NPs (11A4-NPs) by centrifugation and quantified by UPLC[66]. The conjugation efficiency was determined as:

$$\text{Conjugation efficiency (\%)} = \left(1 - \frac{\text{[Ligand in the supernatant]}}{\text{[Ligand added in the conjugation reaction]}}\right) \times 100\%$$

The same protocol was used to prepare control NPs in which the maleimide groups were blocked with cysteine (Cys-NPs) with two differences: the molar ratio of the reactants was 1:2 maleimide-PEG-PLGA to cysteine and the non-conjugated cysteine was quantified by MicroBCA Assay, as described by the provider.

2.9 Cell lines and culture conditions

Human breast cancer cell lines SkBr3 (HER2 positive, ATCC HTB-30) and MDA-MB-231 (HER2 negative, ATCC CRM-HTB-26) were obtained from American Type Culture Collection (Virginia, USA). Mycoplasma tests were performed regularly on the cells in culture. SkBr3 cells were cultured in McCoy's 5A medium, supplemented with 10% fetal bovine serum, while MDA-MB-231 cells were maintained in DMEM - high glucose with 10% fetal bovine serum. The cells were incubated at 37 °C in a humidified atmosphere containing 5% CO_2. These conditions were also used in all cell incubation steps in the experiments described below.

2.10 Cellular uptake of NPs

SkBr3 or MDA-MB-231 cells were seeded at a density of 10,000 cells/well in 96 well μClear® black plates (Greiner Bio-One, Frickenhausen, Germany). The cell nuclei were stained with 10 nM Hoechst 33342 in PBS for 10 min at 37 °C and after washing off the excess of dye, fresh medium was added to the cells. The cells were incubated with placebo 11A4-NPs or with Cys-NPs, both labelled with Alexa-568 at 37 °C. The NPs concentration in the wells was 22

μg/mL. In order to study the uptake kinetics of NPs, confocal microscopy of living cells was conducted using a Yokogawa CV7000s high-content imager (Yokogawa Electric Corporation, Tokyo, Japan). Cells were kept at 37 °C, in a humidified atmosphere with 5% CO_2 during the imaging process, and confocal images through the middle plane of the cells were taken 15 min, 30 min, 1 h, 2 h, 4 h, 6 h and 8 h after the addition of the NPs to the cells. Images were captured in two channels: Hoechst 33342 for nuclei (λ_{ex} 405 nm, λ_{em} 445 nm) and Alexa-568 to visualize the NPs (λ_{ex} 561 nm, λ_{em} 600 nm). The image analysis was performed with the Columbus Image Data Storage and Analysis System (Perkin Elmer). The reported values are the mean and SD of the data obtained from 3 wells containing 5 imaging fields each.

To investigate whether the uptake occurred via the HER2 receptor, competition experiments were conducted with an excess of 11A4 present in the medium. To this end, cells were preincubated with free 11A4 nanobody at a concentration of 12 μg/mL for 30 min, followed by the addition of the Alexa-568 labelled placebo NPs functionalized with the 11A4 nanobody, at a final concentration of 80 μg/mL. Consequently, there was a 55 fold molar excess of free 11A4 nanobody compared to the 11A4 conjugated to the NPs. After 30 min of incubation, the medium (containing free 11A4 and the 11A4-NPs) was removed, the cells were washed with PBS and fresh medium was added. Confocal microscopy of living cells was conducted as described above, and including phase contrast imaging to better delineate the cell membrane.

2.11 Photochemical internalization (PCI)

PCI was conducted using the PS $TPPS_{2a}$, which was dissolved in dimethyl sulfoxide at a concentration of 1 mg/mL, aliquoted and stored at -20 °C. The samples containing PS were handled under dim light and incubated in the dark. The PCI experiments were conducted on cells seeded at a density of 5,000 cells/well on 96 well plates (100 μL of cell suspension per well), after overnight culture, as described previously[55,67]: $TPPS_{2a}$ was diluted in cell culture medium supplemented with antibiotics (1,200 units penicillin, 1.2 mg streptomycin, and 3 μg amphotericin B/mL) to a concentration of 6 μg/mL. Next, 10 μL of this solution was added per well and the cells were incubated for 14 h. Subsequently, 10 μL of a suspension of placebo NPs or saporin-loaded NPs in cell culture medium was added per well (NPs concentrations for each experiment are given in sections 2.13 and 2.14). The cells were incubated with the PS and the NPs for 4 h (total incubation time with the PS was therefore 18 h), followed by removal of the medium and addition of fresh medium containing antibiotics (100 units penicillin, 0.1 mg streptomycin, and

0.25 μg amphotericin B/mL). The cells were incubated with fresh medium for an additional 4 h (to favor removal of the PS from the cell membrane)[68], and subsequently the plate was illuminated for 40 s at 420 nm using a LumiSource blue light lamp (PCI Biotech, Oslo, Norway), with an irradiance of $\sim$13.5 mW/cm^2 (corresponding to a total light dose of $\sim$0.5 J/cm^2). After illumination, the cells were incubated for 40 h without medium refreshment and then subjected to viability or proliferation assays (sections 2.13).

2.12 Cytotoxic effect of PCI

The cytotoxic effect of PCI, also referred to as photochemical cytotoxicity, was evaluated as follows: SkBr3 and MDA-MB-231 cells were seeded at a density of 5,000 cells/well on 96 well plates. After overnight culture, 10 μL of a $TPPS_{2a}$ solution (6 μg/mL) were added per well, followed by incubation of the cells with the PS for 18 h. Next, the medium was removed and replaced with fresh medium containing antibiotics (100 units penicillin, 0.1 mg streptomycin, and 0.25 μg amphotericin B/mL, Sigma). The cells were incubated for an additional 4 h, and subsequently the plate was illuminated for 20, 40 and 60 seconds at 420 nm with an irradiance of $\sim$13.5 mW/cm^2, corresponding to a total light dose of $\sim$0.3, 0.5 and 0.8 J/cm^2. The cells were subjected to viability and proliferation assays (section 2.13) 40 h after illumination.

2.13 Cytotoxicity of the NPs

SkBr3 or MDA-MB-231 cells were seeded at a density of 5,000 cells/well on 96 well plates and incubated overnight, after which they were subjected to PCI as described in section 2.11 (briefly: 14 h incubation with $TPPS_{2a}$, 4 h incubation with PS and NPs, then 4 h incubation with fresh medium and subsequent illumination). Placebo or saporin-loaded NPs, functionalized with 11A4 or cysteine (11A4-NPs or Cys-NPs, section 2.8), were used. The final NPs concentration in the wells ranged from 0.3 to 180 μg/mL, and was slightly adjusted between NPs batches in order to have total saporin concentrations ranging from 0.1 to 32 nM based on the saporin loading studies in section 2.6. These concentration range corresponds to 0.01 to 4.2 nM of saporin based on the *in vitro* release (section 2.7) for the time frame of the study. The cell viability and cell proliferation were assessed 40 h after the cells were illuminated for PCI. Cell viability was determined using resazurin, a weakly fluorescent dye that can be reduced to a fluorescent product (resorufin) by metabolically active cells[69]. In short, 10 μL of a 500 mM solution of resazurin was added to each well and after 4 h of incubation the fluorescent signal was

measured at 530 nm excitation / 600 nm emission in a multimode microplate reader Mithras LB 940 (Berthold Technologies, Bad Wildbad, Germany). Cell proliferation was determined by BrdU assay (according to the instructions of the manufacturer). The EC50 value of the NPs was determined by analysis of the cell proliferation data (respective to a control exposed to PCI without protein and NPs) with the software GraphPad Prism 7 (GraphPad, California, USA) (nonlinear regression, log[inhibitor] vs. normalized response - variable slope).

To investigate that the HER2 mediated uptake is essencial for the cytotoxic effect, competition experiments were conducted on SkBr3 cells: after 14 h incubation with the PS, the cells were incubated with the PS and free 11A4 nanobody at a concentration of 12 μg/mL for 30 min. Subsequently, saporin-loaded NPs functionalized with the 11A4 nanobody were added to the cells at a final concentration of 80 μg/mL. The cells were incubated with the PS and the NPs for 4 h at 37 °C (total incubation time with the PS was therefore 18 h). Next, the cells were irradiated as described in section 2.11 and cell viability and cell proliferation were evaluated.

Dose-response assays were also conducted using free saporin. In short, the same protocol described for the dose-response assays of the NPs was followed but the cells were incubated with saporin instead of NPs. The final saporin concentration in the wells ranged from 0.002 to 200 nM (6 x 10^{-5} to 6 μg/mL).

2.14 Apoptosis assay

SkBr3 cells were seeded at a density of 5,000 cells/well in 96 well plates, incubated overnight and subjected to PCI as described in section 2.11. The cells were incubated with saporin-loaded NPs functionalized with 11A4 nanobody or with cysteine (control formulation) at a final concentration of 90 μg/mL. After illumination, the cells were incubated for 40 or 120 h without medium refreshment and then subjected to the apoptosis assay according to the instructions of the manufacturer. Briefly, the medium was replaced with a solution containing PI diluted 1:1000 and Annexin V - FITC diluted 1:80 in McCoy's 5A cell culture medium supplemented with 10% fetal bovine serum. Cells exposed to 10 μM staurosporine overnight were used as a positive control for apoptosis. Alternatively, cells incubated for 15 min with 1% Triton X-100 were used as positive controls for necrosis[70]. Thereafter and in both cases, the medium was replaced with the Annexin V / PI solution. After incubation for 10 min at 37 °C with the Annexin V and PI, the cells were imaged with an EVOS microscope (Thermo Fischer Scientific, Bleiswijk, the Nerherlands) using the bright field, GFP (for Annexin V) and Texas Red (for PI) channels.

The images were analyzed with the ImageJ software (NIH, USA) (mean gray value measurements).

2.15 Statistical Analysis

Statistical significance was evaluated using the unequal variance t-test for comparison of the cytotoxicity of Cys-NPs + PCI vs 11A4-NPs + PCI (at different concentrations of NPs), and for the comparison of the cytotoxicity of 11A4-NPs + PCI vs 11A4 + 11A4-NPs + PCI. A value of $p \leq 0.05$ was considered significant. Statistical significance was depicted as * $p \leq 0.05$ and ** $p \leq 0.01$.

3 Results and Discussion

The potent cytotoxic effect of saporin makes it a promising anti-cancer agent. Nevertheless, the mechanism of internalization of this protein varies amongst cell types and is not yet clearly understood[8,9,71]. In the present work, we encapsulated saporin in PEG-PLGHMGA NPs functionalized with the nanobody 11A4 to favor uptake and cell-specific toxicity in HER2 overexpressing cancer cells. As receptor-mediated uptake of NPs can lead to lysosomal degradation of their contents, PCI was employed to promote endosomal escape, and to guarantee the release of saporin into the cytosol, where it can ultimately exert its cytotoxic effect.

3.1 Characterization of the polymers PLGHMGA and MePEG-PLGHMGA

The polymers used in this study were synthesized by ring opening polymerization of D,L-lactide and BMG using benzyl alcohol as initiator for PLGHMGA and poly(ethylene glycol) monomethyl ether as initiator for MePEG-PLGHMGA, and tin(II) 2-ethylhexanoate as catalyst for both polymers[61] (Figure 1).

The synthesized polymers were analyzed by ^{1}H NMR, GPC and DSC (Table 1). The polymer composition as determined by ^{1}H NMR was, within the experimental error, close to the feed ratio. The molecular weight of the polymers determined by GPC only slightly decreased after deprotection indicating that no chain scission had occurred. The molecular weight of MePEG-PLGHMGA calculated by ^{1}H NMR increased after deprotection which might be ascribed to hydrolysis of the ester bond that connects the PEG and the PLGHMGA block during deprotection and/or subsequent purification. According to DSC

analysis the polymers were completely amorphous (Figure S1) and their T_g is consistent with previous reports[61].

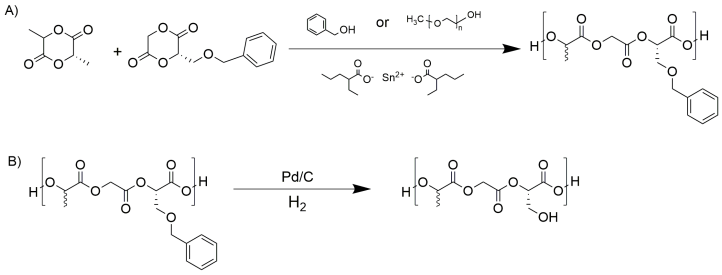

Figure 1: Synthesis of PLGHMGA. A) Copolymerization of D,L-lactide and BMG results in the formation of PLGBMGA. B) Removal of the protecting benzyl groups yields PLGHMGA.

Table 1: Characteristics of the polymers prepared for this study.

	PLGB-MGA	PLGH-MGA	MePEG-PLGBMGA	MePEG-PLGHMGA
Composition ratio a:b[a]				
^{1}H NMR	40:60	40:60	41:59	45:55
Yield (%)	94	71	98	53
Molecular weight (kDa)				
M_n (GPC)	59	43	28	22
M_w (GPC)	89	62	43	31
PDI (GPC)	1.50	1.47	1.52	1.42
M_n (^{1}H NMR)	NA[b]	NA[b]	55	83
M_n (expected)	53	43	55	45
MePEG (w%)	NA[b]	NA[b]	3.6	2.4
T_g (°C)	32	56	26	48

[a] a:b represents the molar ratio of BMG/D,L-lactide or HMG/D,L-lactide. Monomer feed was 35(a):65(b). Monomer to initiator ratios were 300:1. [b] Not applicable.

The structure and ^{1}H NMR spectra of PLGHMGA and MePEG-PLGHMGA are presented in Figure S2. The absence of a peak at 7.3 ppm confirmed that the benzyl groups were successfully removed from the polymers by hydrogenolysis (Figure S3), which resulted in pending hydroxyl groups on the polymer chain.

3.2 Preparation and characterization of the polymeric NPs

Placebo and saporin-loaded NPs were prepared using a blend of PLGHMGA, MePEG-PLGHMGA and maleimide-PEG-PLGA. To prepare fluorescent NPs, PLGA-Alexa-568 was also added to the aforementioned polymer mixture. HER2 targeted NPs were prepared by conjugating the nanobody 11A4 (containing a C-terminal cysteine) to the nanoparticle surface, i.e. 11A4-NPs, exploiting the maleimide-thiol reaction. In the non-targeted NPs, cysteine was used to block the maleimide groups, i.e. Cys-NPs, because free maleimide groups can interact with cellular thiols and lead to enhanced, non-specific cellular uptake[72,73]. The physicochemical properties of the NPs used in this study are displayed in Table 2.

Table 2: Size, zeta potential and conjugation efficiency of polymeric NPs.

Formulation	Yield (%)	Code	Ligand	Diameter (nm)[a]	PDI[b]	Zeta potential (mV)	Conjugation efficiency (%)[c]	11A4 molecules per NP[d]
Placebo NPs[e]	55±5	1	None	369±46	0.32	-7.1±0.9	NA[f]	
		2	Cys	374±34	0.22	-8.2±1.2	58±1	
		3	11A4	435±32	0.27	-11.7±0.8	55±7	∼7,100
Saporin-loaded NPs[e]	55±2	4	None	344±12	0.17	-3.3±0.6	NA[f]	
		5	Cys	375±11	0.12	-3.6±0.6	61±4	
		6	11A4	414±26	0.16	-4.0±0.8	31±4	∼3,400
Fluorescent placebo NPs[g]	49	7	None	ND[h]	ND[h]	-8.5	NA[f]	
		8	Cys	405	0.23	-7.4	58	
		9	11A4	445	0.31	-12.8	46	∼6,300

[a] Diameter of freeze dried NPs after resuspension in PBS/EDTA 0.4 mM and conjugation with different ligands. [b] SD ≤ 0.1. [c] Conjugation efficiency = (1 ([Ligand in the supernatant] / [Ligand added in the conjugation reaction])) x 100%. [d] Calculated as reported in[66]. [e] n=3. [f] Not applicable. [g] n=1. [h] Not determined

For all formulations tested (NPs, Cys-NPs and 11A4-NPs) the surface charge of saporin-loaded NPs (formulations 4 - 6) was closer to neutrality than the charge of placebo NPs (formulations 1 - 3 and 7 - 9). Since saporin has an isoelectric point of ∼9.4 (ExPASy ProtParam tool), the protein will carry a net positive charge at neutral pH. The less negative zeta potential of the saporin-loaded NPs can therefore be explained by the presence of surface associated saporin[74,75]. Since saporin lacks free thiol groups in its sequence (UniProtKB) its association to the NPs is not a result of conjugation to maleimide.

The Cys-NPs (formulations 2 and 5) had similar size and surface charge to the placebo NPs without surface decoration (formulations 1 and 4). On the

other hand, 11A4-NPs (formulations 3 and 6) were larger and displayed a more negative surface charge than the non-decorated NPs. Based on the isoelectric point of the nanobody 11A4 (∼7.9 according to ExPASy ProtParam tool), a slightly positive charge of 11A4-NPs would be expected at the pH conditions used for their preparation and analysis (pH 7.4). Nevertheless, the isoelectric point refers to the charge of the protein determined by its primary structure, while the folded protein can carry a different charge, depending on the amino acids located on its surface. In the case of 11A4-NPs, the zeta potential suggests that negative amino acid residues are exposed to the medium. In a previous study conducted by our research group, PLGA NPs conjugated to 11A4 also showed a more negative zeta potential than non-conjugated NPs[66].

In addition to the physicochemical characteristics of the NPs, the efficiency of the conjugation reaction was also determined. Cysteine was conjugated to the NPs with an efficiency of ∼60%. In a previous study, our group reported a similar conjugation efficiency for another small molecule, i.e. cRGDfK, to polymeric NPs via maleimide-thiol chemistry[66]. Theoretically, a 100% conjugation efficiency could have been achieved because a molar excess of cysteine to maleimide (2:1) was used. However, due to the miscibility of PEG and PLGA it is likely that not all maleimide groups are exposed on the surface of the NPs and available for reaction[76,77].

The conjugation efficiency of cysteine was similar for placebo and saporin-loaded NPs (formulations 2 and 5). In contrast, the conjugation efficiency of 11A4 was higher for placebo NPs (formulation 3) than for saporin-loaded NPs (formulation 6). As previously mentioned, some saporin molecules can be associated with the surface of the NPs resulting in partial obstruction of nearby maleimide groups and limiting the extent of functionalization of the surface with the nanobody. This steric hindrance may have been less relevant for conjugation to cysteine due to the smaller size of this ligand.

The encapsulation efficiency of saporin in the NPs was 26 ± 2% (n=2), which corresponded to 0.52 ± 0.03 loading weight % (or 5.2 ± 0.3 μg of saporin/mg NPs). After resuspension in PBS, the NPs showed a very small burst release (< 5% of the total saporin content), followed by a sustained release of the protein. An estimation from SDS-PAGE analysis indicates that around 13% of the saporin loading was released from the NPs during 2 days of incubation in PBS (Figure S4). Similar sustained release patterns (10 - 40% release of protein after 5 days of incubation) have been reported in literature for protein-loaded PLGA[78,79] and PLGHMGA NPs[61].

3.3 Cellular uptake of targeted and non-targeted NPs

The kinetics of cellular uptake of Cys-NPs and 11A4-NPs were studied by live confocal microscopy from 15 minutes to 8 hours in SkBr3 (HER2 positive) and MDA-MB-231 (HER2 negative) cells. The binding and uptake of Cys-NPs was poor at all the time points evaluated, as shown by the low fluorescent signal in the cytoplasm of the cells (Figures 2A and 2C). In contrast, the uptake of 11A4-NPs by SkBr3 cells was already detected at early time points of the study ($\leq$ 30 minutes), and it increased over time (Figure 2B and 2C). Throughout the study, the number of fluorescent spots per area of cytoplasm was between 8 and 18 times higher in the cells exposed to 11A4-NPs compared to those incubated with Cys-NPs (Figure S5), which indicates an enhanced internalization of 11A4-NPs, likely mediated by the interaction between the nanobody 11A4 and the HER2 receptor. This observation is further supported by the almost negligible uptake of both, 11A4-NPs and Cys-NPs, by the HER2 negative MDA-MB-231 cell line (Figure 2C and Figure S6).

To confirm that the specific uptake of 11A4-NPs was mediated by the interaction of the 11A4 nanobody with the HER2 receptor, competition studies were carried out by pre-incubating the cells with free 11A4 prior to exposure to 11A4-NPs. Microscopic observations showed that, in the presence of free nanobody, the internalization of 11A4-NPs was considerably inhibited (Figure 2D), as compared to cells incubated with 11A4-NPs in the absence of free nanobody (Figure 2E). Image analysis confirmed that the fluorescent signal of 11A4-NPs inside the cells was remarkably lower in the samples subjected to competition (Figure 2F), thus corroborating the results from the visual observations.

Altogether, the results from the confocal microscopy studies demonstrate that the endocytosis of 11A4-NPs is mediated by the specific interaction between the nanobody 11A4 and the HER2 receptor. Since the focus of the present work is to target HER2 for the treatment of breast cancer, the selective accumulation of the 11A4-NPs was evaluated in HER2 positive cancer cells (SkBr3), using HER2 negative cancer cells (MDA-MB-231) as a negative control. Alternatively, normal cells could also be used as a control since they express 100-fold less HER2 than HER2 positive cancer cells[80]. In that case, it would be expected that the 11A4-NPs would interact similarly with normal cells and with the HER2 negative breast cancer cells (i.e. poor internalization). In addition to our results, other studies from our research group have confirmed that the uptake of nanobody-targeted nanocarriers is truly mediated by specific ligand-receptor interactions. In that regard, the use of a non-tumor specific nanobody as ligand resulted in neither binding, nor uptake

of different types of nanocarriers [43,47].

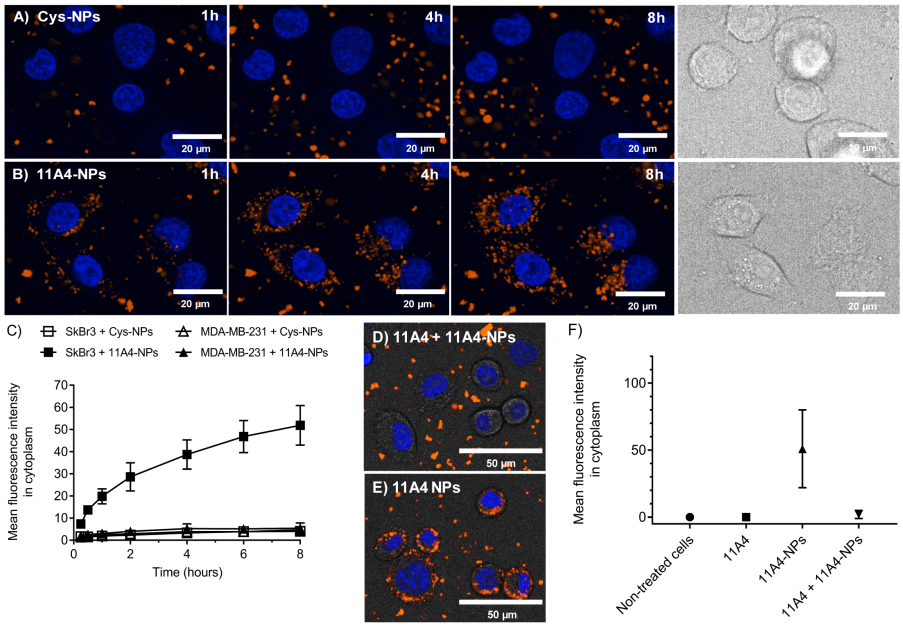

Figure 2: Cellular uptake of fluorescently labeled, targeted and non-targeted placebo NPs. Confocal images of SkBr3 cells incubated with (A) Cys-NPs (22 μg/mL) and (B) 11A4-NPs (22 μg/mL) at different time points (nuclei are stained in blue, NPs are observed in orange and the phase contrast image is in gray). The NPs remained in contact with the cells throughout the whole assay (no washing steps). (C) Mean fluorescence intensity in cytoplasm of SkBr3 and MDA-MB-231 cells after incubation with Cys-NPs and 11A4-NPs, data represent mean ± SD (n=15 imaging fields). Confocal images of SkBr3 cells (D) pre-incubated for 30 min with free 11A4 (12 μg/mL) followed by incubation for 30 min with 11A4-NPs (80 μg/mL) and (E) incubated for 30 min with 11A4-NPs alone (80 μg/mL). Nuclei are stained in blue and NPs are observed in orange, overlay of phase contrast image shows the cell borders. (F) Mean fluorescence intensity in cytoplasm of SkBr3 cells exposed to the competition conditions, data represent mean ± SD (n=15 imaging fields).

In general, the cargo internalized by receptor-mediated endocytosis is initially localized in early endosomes and then sorted to one of several pathways, including the recycling and degradative pathways [81–83]. The uptake images (Figure 2B, at 8h) suggest that the 11A4-NPs are entrapped in intracellular

vesicles, likely late endosomes and/or lysosomes, as proposed by the highly punctuated fluorescence pattern observed in the cytoplasm of SkBr3 cells[84,85]. To prevent that the 11A4-NPs and/or their released cargo (saporin) are degraded in the lysosomes, an external stimulus was applied to induce endosomal escape and to maximize the cytotoxicity of the formulation: i.e. photochemical internalization or PCI.

3.4 Optimization of photochemical internalization (PCI)

The outcome of PCI is influenced by the concentration of PS and the illumination time[55,86]. In general, high concentrations of PS and long illumination times can induce cell death, here described as photochemical cytotoxicity. In the present work, a concentration of 0.5 μg/mL of PS was chosen based on previous studies conducted in our research group[55,67]. Since the aim was to specifically evaluate the PCI-mediated cytotoxicity of saporin-loaded NPs, it was important to distinguish between the effects of PCI (PS + light + NPs) and the photochemical cytotoxicity (PS + light). The illumination time was optimized in a way that PCI was achieved without significantly compromising the viability of cells. To this end, the cytotoxicity of the PS $TPPS_{2a}$ combined with different illumination times was first evaluated on SkBr3 and MDA-MB-231 cells without NPs. For both cell lines, a decrease in cell viability was observed with increasing illumination time up to 60 seconds (Figure 3A and 3B). In that time frame, the cell viability decreased by 40% for both SkBr3 and MDA-MB-231, while cellular proliferation decreased by 40% for SkBr3 and by 20% for the MDA-MB-231 cells.

Subsequently, the influence of the different illumination times was studied in combination with the saporin-loaded NPs. At all the illumination times tested, higher cytotoxicity was observed on SkBr3 cells that were incubated with saporin-loaded 11A4-NPs, compared to cells incubated with placebo 11A4-NPs (Figure 3C and 3D), implying that PCI successfully mediates the endosomal escape of the NPs leading to saporin release in the cytosol. Since 40 seconds of illumination provided the best compromise between relatively low photochemical cytotoxicity (caused by PS + light), and high cytotoxicity caused by the presence of the saporin-loaded NPs, this setting was chosen for further in depth studies.

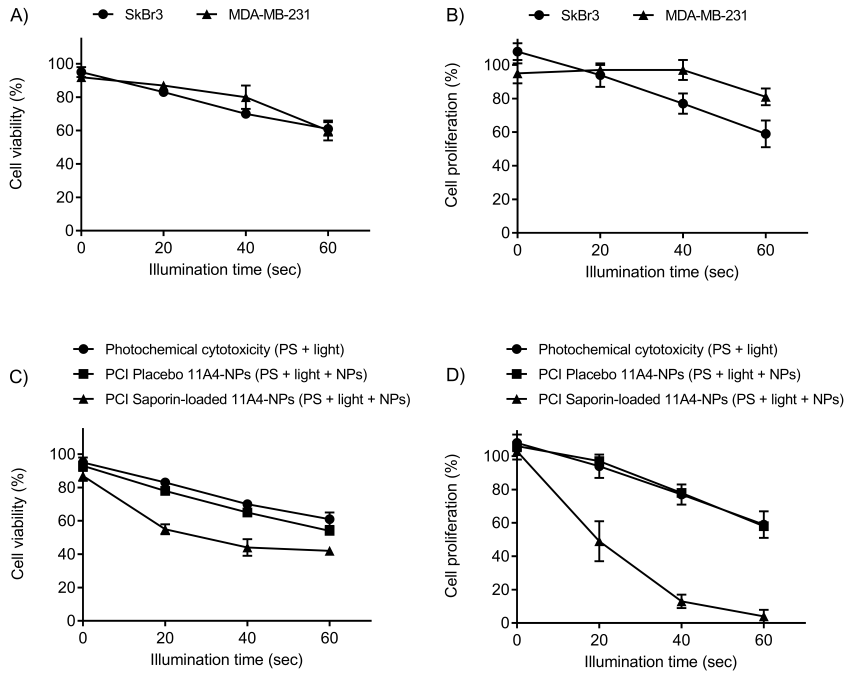

Figure 3: Cytotoxicity of $TPPS_{2a}$ (0.5 μg/mL) combined with different illumination times. (A) Cell viability and (B) cell proliferation of SkBr3 and MDA-MB-231 cells exposed to PS and illumination, without NPs, relative to the non-treated control (no PS, no light). Data represent mean ± SD (n=6). (C) Cell viability and (D) cell proliferation of SkBr3 cells in the absence and presence of placebo 11A4-NPs and saporin-loaded 11A4-NPs relative to the non-treated control (no PS, no light, no NPs). Final NPs concentration in the wells was 90 μg/mL. Data represent mean ± SD (n=6 for tests in the absence of NPs, n=3 tests in the presence of NPs). Illumination for 20, 40 and 60 seconds corresponds to light doses of ∼0.3, 0.5, and 0.8 J/cm^2.

3.5 Cytotoxicity of saporin-loaded targeted and untargeted NPs in combination with PCI

The cytotoxic effect of saporin-loaded Cys-NPs and 11A4-NPs was evaluated in SkBr3 and MDA-MB-231 cells with or without PCI. In parallel, placebo NPs were also investigated, as well as the effect of free saporin. As a control, cells incubated only with PS and with light exposure (no NPs) were compared to non-treated cells (no PS, no light, no NPs).

Placebo Cys-NPs and placebo 11A4-NPs used without PCI, did neither affect cell viability nor proliferation of SkBr3 (Figure S7A and S7B) as well as of MDA-MB-231 (Figure S7C and S7D) cells. Even though a decrease in cell viability and proliferation was observed for both cell lines treated with NPs and PCI, this effect was not dependent on the dose of NPs and can be explained as toxicity induced by the PS applied in combination with light, i.e. photochemical cytotoxicity: compared to a non-treated control, cell viability was 66 ± 3% for SkBr3 and 75 ± 3% for MDA-MB-231, and cell proliferation was 66 ± 3% for SkBr3 and 88 ± 5% for MDA-MB-231.

Saporin-loaded Cys- and 11A4- NPs without PCI did not affect the cell viability or proliferation of MDA-MB-231 cells, while incubation of NPs combined with PCI slightly decreased these parameters (Figure 4A and 4B), which corresponds to the photochemical cytotoxicity: compared to non-treated cells, cell viability was 77 ± 9% and cell proliferation was 91 ± 10%. In addition, the lack of toxicity of both Cys-NPs and 11A4-NPs in MDA-MB-231 cells is in line with the low uptake of these formulations (Figure 2C). Similarly to the results in MDA-MB-231, saporin-loaded Cys- or 11A4- NPs without PCI were not cytotoxic to SkBr3 cells. Incubation of SkBr3 cells with Cys-NPs and PCI slightly and stably decreased cell viability and proliferation, which is in the range of photochemical cytotoxicity reported above: compared to a non-treated control, cell viability was 69 ± 5% and cell proliferation was 67 ± 10%. In contrast, only the incubation of SkBr3 cells with saporin-loaded 11A4-NPs and PCI resulted in a dose-dependent decrease in cell viability and cell proliferation (Figure 4C and 4D), confirming that the NPs and their content were initially entrapped in the endosome and were subsequently released into the cytosol upon PCI.

At the highest concentrations tested, the saporin-loaded 11A4-NPs combined with PCI reduced the cell proliferation of SkBr3 cells by ∼95% and the cell viability by ∼60%. The residual metabolic acitivity of the cells detected in the viability studies could be explained by the ability of saporin to induce apoptosis which, being energy-dependent, requires the cells to remain active in order to provide energy until late stages of the process[87].

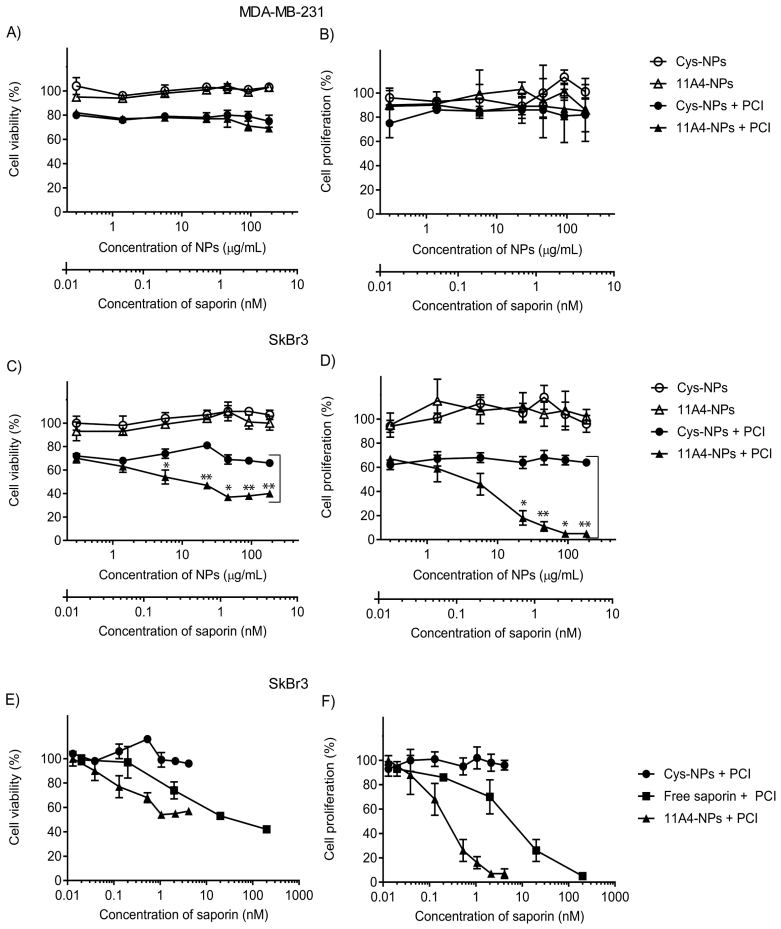

Figure 4: Cytotoxicity of saporin-loaded NPs with or without PCI. The concentration of saporin reported in the graphs is 13% of the dose loaded in the NPs. Cytotoxicity of saporin-loaded NPs on (A,B) MDA-MB-231 and (C,D) SkBr3 cells. Cell viability and cell proliferation were calculated respective to the non-treated control (no PCI, no NPs). (E) Cell viability and (F) cell proliferation of SkBr3 cells incubated with free saporin and saporin-loaded NPs calculated respective to a control exposed to PCI in absence of protein and NPs. This control had 73 ± 5% cell viability and 73 ± 8% cell proliferation relative to a non-treated sample (no PCI, no free protein, no NPs). Data represent mean ± SD (n=3). Data Cys-NPs + PCI vs 11A4-NPs + PCI analyzed by unequal variances t-test, * p-value < 0.05 and ** p-value < 0.001.

Taken together, the results of Figure 4C and 4D demonstrate that, when loaded in NPs, effective saporin delivery is fully dependent on HER2 targeting and PCI, which is favorable for enhancing the selectivity of the therapy. Other studies have shown that PCI enhances the efficacy of untargeted nanocarriers, loaded with or conjugated to cytotoxic agents[88–91], although in these cases the selectivity of these nanocarriers towards specific cells was not evaluated.

The dose-dependent cytotoxicity of free saporin (i.e. not encapsulated in the NPs) was compared to the cytotoxicity induced by saporin-loaded NPs on SkBr3 cells when used in combination with PCI (Figure 4E and 4F). In this particular study, the dose of free saporin added to the cells is compared to the concentration of saporin expected to be released from the NPs after 2 days of incubation with the cells based on the release studies conducted in PBS (13% release, Figure S4). Nevertheless, it is possible that more saporin was released from the NPs in cell culture medium/intracellularly, compared to PBS, as shown for other compounds[92]. Based on the cell proliferation assays (Figure 4F), the EC50 of saporin when delivered by 11A4-NPs and PCI, estimated at 0.3 nM (n=6, 95% CI = 0.25 - 0.34) was substantially lower (15-fold difference) than the EC50 for free saporin administered in combination with PCI, i.e. 4.5 nM (n=6, 95% CI = 3.5 - 5.7). In addition, the dose-response profiles of saporin-loaded Cys- and 11A4- NPs differ significantly, indicating that the cytotoxicity from saporin-loaded 11A4-NPs is most likely caused by the intracellular release of saporin after the internalization of these HER2 targeted NPs, and not by PCI of free saporin.

Interestingly, saporin in its free form was not toxic to the cells here investigated when administered without PCI (Figure S8A - 8D). In contrast, combination of free saporin with PCI exhibited cytotoxic effect on both cell lines, although the effect was lower in MDA-MB-231 (EC50 = 67 nM, n=6, 95% CI = 43 - 111) than in SkBr3 (EC50 = 4.5 nM, n=6, 95% CI = 3.5 - 5.7). Cell line-dependent differences of the effects of saporin have also been reported in other studies[9,93]. Remarkably, saporin-induced cytotoxicity has also been reported even when it is administered without PCI or any other endosomal escape technique[4,71,94]. Therefore, administration of free saporin *in vivo* could result in substantial toxicity in non-targeted cells and tissues. This problem can be overcome by encapsulating saporin in receptor-targeted nanoparticles, which combined with PCI, can lead to selective and local delivery to the cytosol of the targeted cells, as proposed by the *in vitro* data presented in this work. While the *in vivo* evaluation of the efficacy of saporin-loaded 11A4-NPs combined with PCI is beyond the scope of the present manuscript, some considerations for the *in vivo* translation of this treatment include (1) reducing the size of the NPs for more efficient extravasation and passive accumulation

in the tumor site (favorable for nanocarriers with sizes < 200 nm [95,96]), and (2) using photosensitizers such as $TPCS_{2a}$ [97] which are activated at wavelengths that are optimal for tissue penetration, i.e. 600 - 800 nm. Furthermore, the treatment proposed in this manuscript should be envisioned for use in combination with other cancer therapies in order to efficiently treat heterogeneous tumors in which only some cells express the HER2 receptor, and to decrease the chances for development of cancer drug resistance.

To further investigate the selectivity of the cytotoxicity of the 11A4-NPs, competition assays were performed. When the cells were pre-incubated with free 11A4, subsequent incubation with 11A4-NPs and PCI application did not substantially decrease cell proliferation or cell viability, in contrast with cells that were not pre-incubated with the free nanobody (Figure 5). These results are in agreement with confocal microscopy observations, where pre-incubation with free 11A4 inhibited the cellular uptake of 11A4-NPs (Figure 2D and 2F).

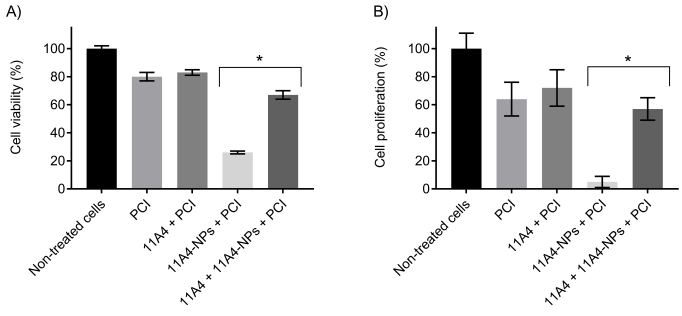

Figure 5: Cytotoxicity of saporin-loaded 11A4-NPs with PCI on SkBr3 cells with and without pre-incubation with free 11A4. (A) Cell viability and (B) cell proliferation were assessed in cells incubated with 11A4-NPs and subjected to PCI treatment or in cells pre-incubated with an excess of free 11A4 followed by the addition of 11A4-NPs and PCI treatment. Data represent mean ± SD (n=3). Data 11A4-NPs + PCI vs 11A4 + 11A4-NPs + PCI analyzed by unequal variances t-test, * p-value < 0.05.

Similar to our findings, a previous study on the effect of saporin-loaded EGFR-targeted liposomes on OVCAR-3 cells also highlighted the advantages of combining the use of targeted nanocarriers with PCI [55]. While high uptake and cytotoxicity were observed for the EGFR-targeted liposomes, the non-targeted liposomes were also internalized and cytotoxic, though to a lesser extent. In contrast, the non-targeted NPs used in our work did not show any

uptake or cytotoxicity, indicating that our system has improved selectivity over the aforementioned liposomes. Targeting, as achieved by the 11A4-NPs, can induce clustering of HER2 and promote its internalization[98–100], resulting in efficient receptor-mediated endocytosis of the NPs and subsequent intracellular delivery of its cytotoxic cargo (saporin).

Other types of nanocarriers, such as nanogels and lipopepsomes, have also been successfully used for the targeted intracellular delivery of saporin in cancer cells. These nanocarriers were not used in combination with PCI, instead they achieved endosomal escape by membrane destabilization[19] or by membrane fusion driven by coiled-coil motifs[16]. Although direct comparison between these studies is difficult due to the different nature of the nanocarriers and targeted cell lines, these studies suggest other approaches are also effective in ensuring endosomal escape of saporin.

3.6 Cell death mechanism induced by saporin-loaded 11A4-NPs and PCI

Microscopic observations of cells treated with saporin-loaded 11A4-NPs and PCI, 40 and 120 hours after illumination revealed significant morphological alterations suggesting apoptosis (Figure 6). In contrast, only a few cells with morphological alterations were observed in the cells subjected to PCI only or to Cys-NPs and PCI. A striking difference in the cell number was also observed, particularly at the 120 hours time point: while there are only a few cells left after treatment with 11A4-NPs and PCI, a large number of cells are present in the samples exposed to PCI only (i.e. photochemical cytotoxicity). These observations are in agreement with the results from the cytotoxicity assays (Figure 4), which indicated that the decrease in cell viability caused by saporin-loaded 11A4-NPs combined with PCI is accompanied by a strong anti-proliferative effect.

The visual analysis of cells exposed to PCI (with or without incubation with NPs) and stained with Annexin V / PI revealed a fluorescent pattern indicative of apoptosis both in its early and late stage, though the intensity of the fluorescent signal (and extent of apoptosis) differed between samples (Figure 6, non-cropped images Figure S9A). In contrast, a very low fluorescent signal was observed for cells non exposed to PCI (even when incubated with NPs). The highest Annexin V signal was observed for the cells incubated with saporin-loaded 11A4-NPs combined with PCI 40 hours after illumination (Figure S9B). While in this sample the signal is more intense for Annexin V than for PI at the 40 hours time point, both signals have similar intensities at the 120 hours time point (Figure 6), indicating an increase in the number of

cells undergoing late apoptosis / secondary necrosis at that time. This implies an efficient but relatively slow onset and progression of apoptosis. While apoptosis is often depicted as an event that lasts between 12 and 24 hours [101], longer times could be required for cell death due to the asynchronous nature of the process and to its susceptibility to factors such as cell type, as well as the nature and intensity of the apoptotic stimulus.

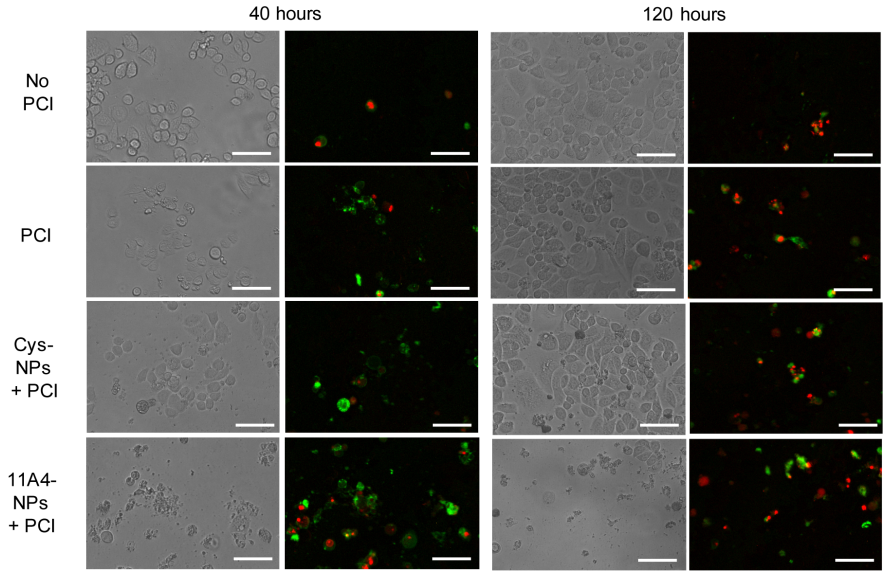

Figure 6: Microscopic observations of SkBr3 cells at 40 and 120 hours after treatment with saporin-loaded NPs and/or PCI. Representative images obtained by phase contrast and by overlay of the channels depicting the signals for Annexin V-FITC (apoptotic cells, in green) and PI (dead cells, in red). Scale bar = 100 μm.

4 Conclusions

The findings presented in this work show that saporin-loaded PEG-PLGHMGA NPs decorated with the 11A4 nanobody in combination with PCI can be used to selectively induce cell death of HER2 positive breast cancer cells. The selectivity of this system is a consequence of the specific interactions between the 11A4 nanobodies on the NPs and the HER2 receptors on the cell surface, which result in receptor mediated endocytosis of the NPs.

Precise light exposure during the subsequent PCI allows for the time- and space- controlled release of the NPs and/or their cargo from the endosome, thereby exposing the cells to the cytotoxic effects of saporin. The tailorability of PEG-PLGHMGA NPs is an added advantage to the system under study, for instance, the NPs could be loaded with proteins other than saporin. In conclusion, the tailorability, selectivity and efficiency of the 11A4-NPs used in combination with PCI makes them a promising modality for cancer treatment.

Acknowledgements

The authors would like to thank Dr. Anders Høgset for providing the photosensitizer $TPPS_{2a}$ used in this study and MSc Irati Beltrán Hernández for her guidance in the apoptosis assays. Lucía Martínez - Jothar would like to thank the Consejo Nacional de Ciencia y Tecnología (CONACYT), México (grant no. 384743) for the funding provided in the framework of her PhD.

References

[1] Nurgali, K., Jagoe, R. T., and Abalo, R. Editorial: Adverse effects of cancer chemotherapy: Anything new to improve tolerance and reduce sequelae? *Front. Pharmacol.*, 9, 2018.

[2] Polito, L., Bortolotti, M., Mercatelli, D., Battelli, M. G., and Bolognesi, A. Saporin-S6: A useful tool in cancer therapy. *Toxins*, 5, 2013.

[3] Santanché, S., Bellelli, A., and Brunori, M. The unusual stability of saporin, a candidate for the synthesis of immunotoxins. *Biochem. Biophys. Res. Commun.*, 234, 1997.

[4] Bagga, S., Seth, D., and Batra, J. K. The cytotoxic activity of ribosome-inactivating protein saporin-6 is attributed to its rRNA N-glycosidase and internucleosomal DNA fragmentation activities. *J. Biol. Chem.*, 278, 2003.

[5] Cimini, A., Mei, S., Benedetti, E., Laurenti, G., Koutris, I., Cinque, B., Cifone, M. G., Galzio, R., Pitari, G., Di Leandro, L., Giansanti, F., Lombardi, A., Fabbrini, M. S., and Ippoliti, R. Distinct cellular responses induced by saporin and a transferrin-saporin conjugate in two different human glioblastoma cell lines. *J. Cell. Physiol.*, 227, 2012.

[6] Polito, L., Bortolotti, M., Farini, V., Battelli, M. G., Barbieri, L., and Bolognesi, A. Saporin induces multiple death pathways in lymphoma cells with different intensity and timing as compared to ricin. *Int. J. Biochem. Cell Biol.*, 41, 2008.

[7] Sikriwal, D., Ghosh, P., and Batra, J. K. Ribosome inactivating protein saporin induces apoptosis through mitochondrial cascade, independent of translation inhibition. *Int. J. Biochem. Cell Biol.*, 40, 2008.

[8] Cavallaro, U., Nykjaer, A., Nielsen, M., and Soria, M. R. α2-macroglobulin receptor mediates binding and cytotoxicity of plant ribosome-inactivating proteins. *Eur. J. Biochem.*, 232, 1995.

[9] Ferreras, J., Barbieri, L., Girbés, T., Battelli, M. G., Rojo, M. A., Arias, F. J., Rocher, M. A., Soriano, F., Mendéz, E., and Stirpe, F. Distribution and properties of major ribosome-inactivating proteins (28 S rRNA N-glycosidases) of the plant Saponaria officinalis L. (Caryophyllaceae). *Biochim. Biophys. Acta, Gene Struct. Expression*, 1216, 1993.

[10] Giansanti, F., Flavell, D. J., Angelucci, F., Fabbrini, M. S., and Ippoliti, R. Strategies to improve the clinical utility of saporin-based targeted toxins. *Toxins*, 10, 2018.

[11] Gilabert-Oriol, R., Thakur, M., Von Mallinckrodt, B., Hug, T., Wiesner, B., Eichhorst, J., Melzig, M. F., Fuchs, H., and Weng, A. Modified trastuzumab and cetuximab mediate efficient toxin delivery while retaining antibody-dependent cell-mediated cytotoxicity in target cells. *Mol. Pharmaceutics*, 10, 2013.

[12] Gilabert-oriol, R., Weng, A., Mallinckrodt, B. V., Melzig, M. F., and Fuchs, H. Immunotoxins constructed with ribosome-inactivating proteins and their enhancers: A lethal cocktail with tumor specific efficacy proteins. *Curr. Pharm. Des.*, 20, 2014.

[13] Polito, L., Bortolotti, M., Pedrazzi, M., and Bolognesi, A. Immunotoxins and other conjugates containing saporin-s6 for cancer therapy. *Toxins*, 3, 2011.

[14] Alewine, C., Hassan, R., and Pastan, I. Advances in anticancer immunotoxin therapy. *The Oncologist*, 20, 2015.

[15] Li, M., Liu, Z. S., Liu, X. L., Hui, Q., Lu, S. Y., Qu, L. L., Li, Y. S., Zhou, Y., Ren, H. L., and Hu, P. Clinical targeting recombinant immunotoxins for cancer therapy. *OncoTargets Ther.*, 10, 2017.

[16] Ding, L., Jiang, Y., Zhang, J., Klok, H. A., and Zhong, Z. pH-Sensitive Coiled-Coil Peptide-Cross-Linked Hyaluronic Acid Nanogels: Synthesis and Targeted Intracellular Protein Delivery to CD44 Positive Cancer Cells. *Biomacromolecules*, 19, 2018.

[17] Jiang, Y., Yang, W., Zhang, J., Meng, F., and Zhong, Z. Protein Toxin Chaperoned by LRP-1-Targeted Virus-Mimicking Vesicles Induces High-Efficiency Glioblastoma Therapy In Vivo. *Adv. Mater.*, 30, 2018.

[18] Jiang, Y., Zhang, J., Meng, F., and Zhong, Z. Apolipoprotein e Peptide-Directed Chimeric Polymersomes Mediate an Ultrahigh-Efficiency Targeted Protein Therapy for Glioblastoma. *ACS Nano*, 12, 2018.

[19] Qiu, M., Zhang, Z., Wei, Y., Sun, H., Meng, F., Deng, C., and Zhong, Z. Small-Sized and Robust Chimaeric Lipopepsomes: A Simple and Functional Platform with High Protein Loading for Targeted Intracellular Delivery of Protein Toxin in Vivo. *Chem. Mater.*, 30, 2018.

[20] Cheng, L., Yang, L., Meng, F., and Zhong, Z. Protein Nanotherapeutics as an Emerging Modality for Cancer Therapy. *Adv. Healthcare Mater.*, 7, 2018.

[21] Lächelt, U. and Wagner, E. Nucleic acid therapeutics using polyplexes: A journey of 50 years (and beyond). *Chem. Rev.*, 115, 2015.

[22] Li, D., van Nostrum, C. F., Mastrobattista, E., Vermonden, T., and Hennink, W. E. Nanogels for intracellular delivery of biotherapeutics. *J. Controlled Release*, 259, 2017.

[23] Onoue, S., Yamada, S., and Chan, H. K. Nanodrugs: Pharmacokinetics and safety. *Int. J. Nanomed.*, 9, 2014.

[24] Pérez-Herrero, E. and Fernández-Medarde, A. Advanced targeted therapies in cancer: Drug nanocarriers, the future of chemotherapy. *Eur. J. Pharm. Biopharm.*, 93, 2015.

[25] Leemhuis, M., Kruijtzer, J. A. W., van Nostrum, C. F., and Hennick, W. E. In vitro hydrolytic degradation of hydroxyl-functionalized poly(α-hydroxy acid)s. *Biomacromolecules*, 8, 2007.

[26] Ghassemi, A. H., van Steenbergen, M. J., Barendregt, A., Talsma, H., Kok, R. J., van Nostrum, C. F., Crommelin, D. J. A., and Hennink, W. E. Controlled Release of Octreotide and Assessment of Peptide Acylation from Poly(D,L-lactide-co-hydroxymethyl glycolide) Compared to PLGA Microspheres. *Pharm. Res.*, 29, 2012.

[27] Shirangi, M., Hennink, W. E., Somsen, G. W., and Van Nostrum, C. F. Identification and assessment of octreotide acylation in polyester microspheres by LC-MS/MS. *Pharm. Res.*, 32, 2015.

[28] Prabhu, R. H., Patravale, V. B., and Joshi, M. D. Polymeric nanoparticles for targeted treatment in oncology: Current insights. *Int. J. Nanomed.*, 10, 2015.

[29] Serna, N., Sánchez-García, L., Unzueta, U., Díaz, R., Vázquez, E., Mangues, R., and Villaverde, A. Protein-based therapeutic killing for cancer therapies. *Trends Biotechnol.*, 36, 2017.

[30] van der Meel, R., Vehmeijer, L. J. C., Kok, R. J., Storm, G., and van Gaal, E. V. B. Ligand-targeted particulate nanomedicines undergoing clinical evaluation: Current status. *Adv. Drug Delivery Rev.*, 65, 2013.

[31] Zhong, Y., Meng, F., Deng, C., and Zhong, Z. Ligand-directed active tumor-targeting polymeric nanoparticles for cancer chemotherapy. *Biomacromolecules*, 15, 2014.

[32] Muyldermans, S. and Lauwereys, M. Unique single-domain antigen binding fragments derived from naturally occurring camel heavy-chain antibodies. *J. Mol. Recognit.*, 12, 1999.

[33] Kolkman, J. A. and Law, D. A. Nanobodies - from llamas to therapeutic proteins. *Drug Discovery Today: Technol.*, 7, 2010.

[34] Oliveira, S., Heukers, R., Sornkom, J., Kok, R. J., and Van Bergen En Henegouwen, P. M. P. Targeting tumors with nanobodies for cancer imaging and therapy. *J. Controlled Release*, 172, 2013.

[35] Arbabi-Ghahroudi, M. Camelid single-domain antibodies: Historical perspective and future outlook. *Front. Immunol.*, 8, 2017.

[36] Vincke, C., Loris, R., Saerens, D., Martinez-Rodriguez, S., Muyldermans, S., and Conrath, K. General strategy to humanize a camelid single-domain antibody and identification of a universal humanized nanobody scaffold. *J. Biol. Chem.*, 284, 2009.

[37] Omar, N., Yan, B., and Salto-Tellez, M. HER2: An emerging biomarker in non-breast and non-gastric cancers. *Pathogenesis*, 2, 2015.

[38] Tai, W., Mahato, R., and Cheng, K. The role of HER2 in cancer therapy and targeted drug delivery. *J. Controlled Release*, 146, 2010.

[39] Kijanka, M. M., van Brussel, A. S. A., van der Wall, E., Mali, W. P. T. M., van Diest, P. J., van Bergen en Henegouwen, P. M. P., and Oliveira, S. Optical imaging of pre-invasive breast cancer with a combination of VHHs targeting CAIX and HER2 increases contrast and facilitates tumour characterization. *EJNMMI Res.*, 6, 2016.

[40] Kijanka, M., Warnders, F.-J., El Khattabi, M., Lub-de Hooge, M., van Dam, G. M., Ntziachristos, V., de Vries, L., Oliveira, S., and van Bergen en Henegouwen, P. M. P. Rapid optical imaging of human breast tumour xenografts using anti-HER2 VHHs site-directly conjugated to IRDye 800CW for image-guided surgery. *Eur. J. Nucl. Med. Mol. Imaging*, 40, 2013.

[41] Kijanka, M., van Donselaar, E. G., Müller, W. H., Dorresteijn, B., Popov-Celeketic, D., el Khattabi, M., Verrips, C. T., van Bergen en Henegouwen, P. M. P., and Post, J. A. A novel immuno-gold labeling protocol for nanobody-based detection of HER2 in breast cancer cells using immuno-electron microscopy. *J. Struct. Biol.*, 199, 2017.

[42] Oliveira, S., Schiffelers, R. M., van der Veeken, J., van der Meel, R., Vongpromek, R., van Bergen en Henegouwen, P. M. P., Storm, G., and Roovers, R. C. Downregulation of EGFR by a novel multivalent nanobody-liposome platform. *J. Controlled Release*, 145, 2010.

[43] Van Der Meel, R., Oliveira, S., Altintas, I., Haselberg, R., Van Der Veeken, J., Roovers, R. C., Van Bergen En Henegouwen, P. M. P., Storm, G., Hennink, W. E., Schiffelers, R. M., and Kok, R. J. Tumor-targeted nanobullets: Anti-EGFR nanobody-liposomes loaded with anti-IGF-1R kinase inhibitor for cancer treatment. *J. Controlled Release*, 159, 2012.

[44] Talelli, M., Oliveira, S., Rijcken, C. J. F., Pieters, E. H. E., Etrych, T., Ulbrich, K., van Nostrum, R. C. F., Storm, G., Hennink, W. E., and Lammers, T. Intrinsically active nanobody-modified polymeric micelles for tumor-targeted combination therapy. *Biomaterials*, 34, 2013.

[45] Talelli, M., Rijcken, C. J. F., Oliveira, S., Van Der Meel, R., Van Bergen En Henegouwen, P. M. P., Lammers, T., Van Nostrum, C. F., Storm, G., and Hennink, W. E. Nanobody - Shell functionalized thermosensitive core-crosslinked polymeric micelles for active drug targeting. *J. Controlled Release*, 151, 2011.

[46] Altintas, I., Heukers, R., Van Der Meel, R., Lacombe, M., Amidi, M., Van Bergen En Henegouwen, P. M. P., Hennink, W. E., Schiffelers, R. M., and Kok, R. J. Nanobody-albumin nanoparticles (NANAPs) for the delivery of a multikinase inhibitor 17864 to EGFR overexpressing tumor cells. *J. Controlled Release*, 165, 2013.

[47] Heukers, R., Altintas, I., Raghoenath, S., De Zan, E., Pepermans, R., Roovers, R. C., Haselberg, R., Hennink, W. E., Schiffelers, R. M., Kok, R. J., and Van Bergen en Henegouwen, P. M. P. Targeting hepatocyte growth factor receptor (Met) positive tumor cells using internalizing nanobody-decorated albumin nanoparticles. *Biomaterials*, 35, 2014.

[48] Zou, T., Dembele, F., Beugnet, A., Sengmanivong, L., Trepout, S., Marco, S., Marco, A. d., and Li, M. H. Nanobody-functionalized PEG-b-PCL polymersomes and their targeting study. *J. Biotechnol.*, 214, 2015.

[49] Sahay, G., Alakhova, D. Y., and Kabanov, A. V. Endocytosis of nanomedicines. *J. Controlled Release*, 145, 2010.

[50] Canton, I. and Battaglia, G. Endocytosis at the nanoscale. *Chem. Soc. Rev.*, 41, 2012.

[51] Selby, L. I., Cortez-Jugo, C. M., Such, G. K., and Johnston, A. P. R. Nanoescapology: progress toward understanding the endosomal escape of polymeric nanoparticles. *Wiley Interdiscip. Rev.: Nanomed. Nanobiotechnol.*, 9, 2017.

[52] Varkouhi, A. K., Scholte, M., Storm, G., and Haisma, H. J. Endosomal escape pathways for delivery of biologicals. *J. Controlled Release*, 151, 2011.

[53] Selbo, P., Høgset, A., Prasmickaite, L., and Berg, K. Photochemical Internalisation: A novel drug delivery system. *Tumor Biol.*, 23, 2002.

[54] Bostad, M., Kausberg, M., Weyergang, A., Olsen, C. E., Berg, K., Høgset, A., and Selbo, P. K. Light-triggered, efficient cytosolic release of IM7-saporin targeting the putative cancer stem cell marker CD44 by photochemical internalization. *Mol. Pharmaceutics*, 11, 2014.

[55] Fretz, M. M., Hogset, A., Koning, G. A., Jiskoot, W., and Storm, G. Cytosolic delivery of liposomally targeted proteins induced by photochemical internalization. *Pharm. Res.*, 24, 2007.

[56] Selbo, P. K., Weyergang, A., Høgset, A., Norum, O. J., Berstad, M. B., Vikdal, M., and Berg, K. Photochemical internalization provides time- and space-controlled endolysosomal escape of therapeutic molecules. *J. Controlled Release*, 148, 2010.

[57] Sultan, A. A., Jerjes, W., Berg, K., Høgset, A., Mosse, C. A., Hamoudi, R., Hamdoon, Z., Simeon, C., Carnell, D., Forster, M., and Hopper, C. Disulfonated tetraphenyl chlorin ($TPCS_{2a}$)-induced photochemical internalisation of bleomycin in patients with solid malignancies: a phase 1, dose-escalation, first-in-man trial. *Lancet Oncol.*, 17, 2016.

[58] Selbo, P. K., Finnesand, L., Ekholt, K., Berg, K., Høgset, A., and Sturgess, R. Photochemical internalization (PCI) of gemcitabine and chemotherapy for the treatment of cholangiocarcinomas From lab bench to bedside. *Photodiagn. Photodyn. Ther.*, 17, 2017.

[59] Leemhuis, M., van Nostrum, C. F., Kruijtzer, J. A. W., Zhong, Z. Y., ten Breteler, M. R., Dijkstra, P. J., Feijen, J., and Hennink, W. E. Functionalized Poly(α-hydroxy acid)s via Ring-Opening Polymerization: Toward Hydrophilic Polyesters with Pendant Hydroxyl Groups. *Macromolecules*, 39, 2006.

[60] Berg, K., Western, A., Bommer, J. C., and Moan, J. Intracellular localization of sulfonated mesotetraphenylporphines in a human carcinoma cell line. *Photochem. Photobiol.*, 52, 1990.

[61] Samadi, N., van Steenbergen, M. J., van den Dikkenberg, J. B., Vermonden, T., van Nostrum, C. F., Amidi, M., and Hennink, W. E. Nanoparticles based on a hydrophilic polyester with a sheddable PEG coating for protein delivery. *Pharm. Res.*, 31, 2014.

[62] Samadi, N. *Biodegradable nanoparticles based on aliphatic polyesters and towards intracellular delivery of protein therapeutics*. Thesis, Utrecht University, 2014.

[63] Péan, J. M., Venier-Julienne, M. C., Filmon, R., Sergent, M., Phan-Tan-Luu, R., and Benoit, J. P. Optimization of HSA and NGF encapsulation yields in PLGA microparticles. *Int. J. Nanomed.*, 166, 1998.

[64] Zambaux, M. F., Bonneaux, F., Gref, R., Maincent, P., Dellacherie, E., and Alonso, M. J. Influence of experimental parameters on the characteristics of poly (lactic acid) nanoparticles prepared by a double emulsion method. *J. Controlled Release*, 50, 1998.

[65] Sah, H. A new strategy to determine the actual protein content of poly(lactide- co-glycolide) microspheres. *J. Pharm. Sci.*, 86, 1997.

[66] Martínez-Jothar, L., Doulkeridou, S., Schiffelers, R. M., Sastre Torano, J., Oliveira, S., van Nostrum, C. F., and Hennink, W. E. Insights into maleimide-thiol conjugation chemistry: Conditions for efficient surface functionalization of nanoparticles for receptor targeting. *J. Controlled Release*, 282, 2018.

[67] Oliveira, S., Fretz, M. M., Høgset, A., Storm, G., and Schiffelers, R. M. Photochemical internalization enhances silencing of epidermal growth factor receptor through improved endosomal escape of siRNA. *Biochim. Biophys. Acta, Biomembr*, 1768, 2007.

[68] Weyergang, A., Selbo, P. K., and Berg, K. Y1068 phosphorylation is the most sensitive target of disulfonated tetraphenylporphyrin-based photodynamic therapy on epidermal growth factor receptor. *Biochem. Pharmacol.*, 74, 2007.

[69] Rampersad, S. N. Multiple applications of alamar blue as an indicator of metabolic function and cellular health in cell viability bioassays. *Sensors*, 12, 2012.

[70] Gupta, S., Chan, D. W., Zaal, K. J., and Kaplan, M. J. A high-throughput real-time imaging technique to quantify netosis and distinguish mechanisms of cell death in human neutrophils. *J. Immunol.*, 200, 2017.

[71] Bagga, S., Hosur, M. V., and Batra, J. K. Cytotoxicity of ribosome-inactivating protein saporin is not mediated through α2-macroglobulin receptor. *FEBS Lett.*, 541, 2003.

[72] Kichler, A., Remy, J. S., Boussif, O., Frisch, B., Boeckler, C., Behr, J. P., and Schuber, F. Efficient gene delivery with neutral complexes of lipospermine and thiol reactive phospholipids. *Biochem. Biophys. Res. Commun.*, 209, 1995.

[73] Li, T. and Takeoka, S. Enhanced cellular uptake of maleimide-modified liposomes via thiol-mediated transport. *Int. J. Nanomed.*, 9, 2014.

[74] Jeong, J. H., Lim, D. W., Han, D. K., and Park, T. G. Synthesis, characterization and protein adsorption behaviors of PLGA/PEG di-block co-polymer blend films. *Colloids Surf. B*, 18, 2000.

[75] Rafati, A., Boussahel, A., Shakesheff, K. M., Shard, A. G., Roberts, C. J., Chen, X., Scurr, D. J., Rigby-Singleton, S., Whiteside, P., Alexander, M. R., and Davies, M. C. Chemical and spatial analysis of protein loaded PLGA microspheres for drug delivery applications. *J. Controlled Release*, 162, 2012.

[76] Javiya, C. and Jonnalagadda, S. Physicochemical characterization of spray-dried PLGA/PEG microspheres, and preliminary assessment of biological response. *Drug Dev. Ind. Pharm.*, 42, 2016.

[77] Malzert, A., Boury, F., Saulnier, P., Benoit, J. P., and Proust, J. E. Interfacial Properties of Mixed Polyethylene Glycol/Poly(d,l-lactide-co-glycolide) Films Spread at the Air/Water Interface. *Langmuir*, 16, 2000.

[78] Rietscher, R., Czaplewska, J. A., Majdanski, T. C., Gottschaldt, M., Schubert, U. S., Schneider, M., and Lehr, C. M. Impact of PEG and PEG-b-PAGE modified PLGA on nanoparticle formation, protein loading and release. *Int. J. Pharm.*, 500, 2016.

[79] Samadi, N., Abbadessa, A., Di Stefano, A., Van Nostrum, C. F., Vermonden, T., Rahimian, S., Teunissen, E. A., Van Steenbergen, M. J., Amidi, M., and Hennink, W. E. The effect of lauryl capping group on protein release and degradation of poly(d,l-lactic-co-glycolic acid) particles. *J. Controlled Release*, 172, 2013.

[80] Lee, H., Dam, D., Ha, J., Yue, J., and Odom, T. Enhanced HER2 Degradation in Breast Cancer Cells by Lysosome-Targeting Gold Nanoconstructs. *ACS Nano*, 9, 2015.

[81] Friedman, L. M., Rinon, A., Schechter, B., Lyass, L., Lavi, S., Bacus, S. S., Sela, M., and Yarden, Y. Synergistic down-regulation of receptor tyrosine kinases by combinations of mAbs: Implications for cancer immunotherapy. *Proc. Natl. Acad. Sci. U. S. A.*, 102, 2005.

[82] Li, J. Y., Perry, S. R., Muniz-Medina, V., Wang, X., Wetzel, L. K., Rebelatto, M. C., Hinrichs, M. J. M., Bezabeh, B. Z., Fleming, R. L., Dimasi, N., Feng, H., Toader, D., Yuan, A. Q., Xu, L., Lin, J., Gao, C., Wu, H., Dixit, R., Osbourn, J. K., and Coats, S. R. A biparatopic HER2-targeting antibody-drug conjugate induces tumor regression in primary models refractory to or ineligible for HER2-targeted therapy. *Cancer Cell*, 29, 2016.

[83] Xu, S., Olenyuk, B. Z., Okamoto, C. T., and Hamm-Alvarez, S. F. Targeting receptor-mediated endocytotic pathways with nanoparticles: Rationale and advances. *Adv. Drug Delivery Rev.*, 65, 2013.

[84] Boeneman, K., Delehanty, J. B., Blanco-canosa, J. B., Stewart, M. H., Oh, E., Huston, A. L., Dawson, G., Walters, R., Domowicz, M., Deschamps, J. R., Algar, W. R., Dimaggio, S., Manono, J., Spillmann, C. M., Thompson, D., Jennings, L., Dawson, P. E., and Medintz, I. L. Selecting improved peptidyl motifs for cytosolic delivery of disparate protein and nanoparticle materials. *ACS Nano*, 7, 2014.

[85] Salomone, F., Cardarelli, F., Di Luca, M., Boccardi, C., Nifosì, R., Bardi, G., Di Bari, L., Serresi, M., and Beltram, F. A novel chimeric cell-penetrating peptide with membrane-disruptive properties for efficient endosomal escape. *J. Controlled Release*, 163, 2012.

[86] O'Rourke, C., Hopper, C., MacRobert, A. J., Phillips, J. B., and Woodhams, J. H. Could clinical photochemical internalisation be optimised to avoid neuronal toxicity? *Int. J. Pharm.*, 528, 2017.

[87] Helm, K., Beyreis, M., Mayr, C., Ritter, M., Jakab, M., Kiesslich, T., and Plaetzer, K. In vitro cell death discrimination and screening method by simple and cost-effective viability analysis. *Cell. Physiol. Biochem.*, 41, 2017.

[88] Cabral, H., Nakanishi, M., Kumagai, M., Jang, W. D., Nishiyama, N., and Kataoka, K. A photo-activated targeting chemotherapy using glutathione sensitive camptothecin-loaded polymeric micelles. *Pharm. Res.*, 26, 2009.

[89] Lai, P. S., Lou, P. J., Peng, C. L., Pai, C. L., Yen, W. N., Huang, M. Y., Young, T. H., and Shieh, M. J. Doxorubicin delivery by polyamidoamine dendrimer conjugation and photochemical internalization for cancer therapy. *J. Controlled Release*, 122, 2007.

[90] Wang, S., Hüttmann, G., Zhang, Z., Vogel, A., Birngruber, R., Tangutoori, S., Hasan, T., and Rahmanzadeh, R. Light-controlled delivery of monoclonal antibodies for targeted photoinactivation of Ki-67. *Mol. Pharmaceutics*, 12, 2015.

[91] Zhu, K., Liu, G., Hu, J., and Liu, S. Near-infrared light-activated photochemical internalization of reduction-responsive polyprodrug vesicles for synergistic photodynamic therapy and chemotherapy. *Biomacromolecules*, 18, 2017.

[92] Xu, P., Gullotti, E., Tong, L., Highley, C. B., Errabelli, D. R., Hasan, T., Cheng, J.-x., Kohane, D. S., Yeo, Y., Martin, S., and Drive, J. Intracellular drug delivery by poly(lactic-co-glycolic acid) nanoparticles, revisited. *Mol. Pharmaceutics*, 6, 2010.

[93] Battelli, M. G., Montacuti, V., and Stirpe, F. High sensitivity of cultured human trophoblasts to ribosome-inactivating proteins. *Exp. Cell Res.*, 201, 1992.

[94] Bergamaschi, G., Perfetti, V., Tonon, L., Novella, A., Lucotti, C., Danova, M., Glennie, M. J., Merlini, G., and Cazzola, M. Saporin, a ribosome-inactivating protein used to prepare immunotoxins, induces cell death via apoptosis. *Br. J. Haematol.*, 93, 1996.

[95] Dai, L., Liu, J., Luo, Z., Li, M., and Cai, K. Tumor therapy: targeted drug delivery systems. *J. Mater. Chem. B*, 4, 2016.

[96] Danhier, F., Feron, O., and Préat, V. To exploit the tumor microenvironment: Passive and active tumor targeting of nanocarriers for anti-cancer drug delivery. *J. Controlled Release*, 148, 2010.

[97] Berg, K., Nordstrand, S., Selbo, P. K., Tran, D. T. T., Angell-Petersen, E., and Høgset, A. Disulfonated tetraphenyl chlorin ($TPCS_{2a}$), a novel photosensitizer developed for clinical utilization of photochemical internalization. *Photochem. Photobiol. Sci.*, 10, 2011.

[98] Hapuarachchige, S., Zhu, W., Kato, Y., and Artemov, D. Bioorthogonal , two-component delivery systems based on antibody and drug-loaded nanocarriers for enhanced internalization of nanotherapeutics. *Biomaterials*, 35, 2014.

[99] Moody, P. R., Sayers, E. J., Magnusson, J. P., Alexander, C., Borri, P., Watson, P., and Jones, A. T. Receptor crosslinking : A general method to trigger internalization and lysosomal targeting of therapeutic receptor:ligand complexes. *Mol. Ther.*, 23, 2015.

[100] Zhu, W., Okollie, B., and Artemov, D. Controlled internalization of Her-2/neu receptors by cross-linking for targeted delivery. *Cancer Biol. Ther.*, 6, 2007.

[101] Saraste, A. Morphologic Criteria and Detection of Apoptosis. *Herz*, 24, 1999.

Supporting Information

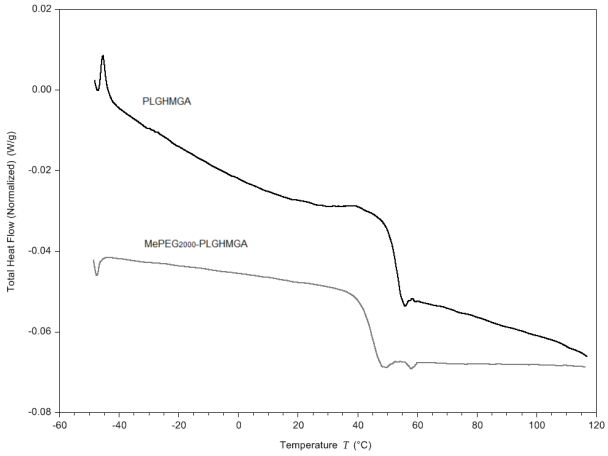

Figure S1: DSC termograms of PLGHMGA and MePEG$_{2,000}$-PLGHMGA.

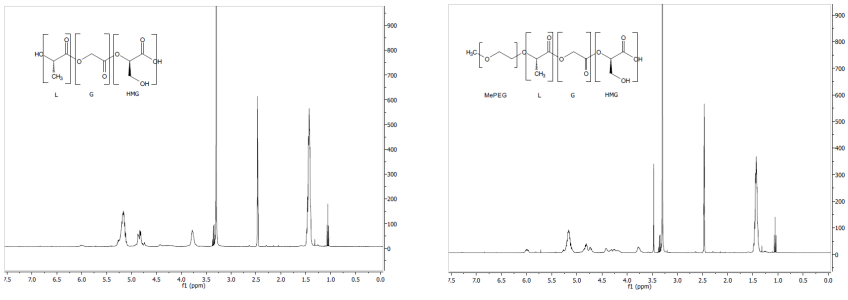

Figure S2: ^{1}H-NMR spectra of the synthesized polymers A) PLGHMGA and B) MePEG-PLGHMGA in DMSO-d6. δ = 1.3 - 1.5 (3 H, CH_3); 3.5 (4 H, O-$\underline{CH_2}$-$\underline{CH_2}$ of PEG); 3.6 - 3.9, (2 H, CH-$\underline{CH_2}$-OH), 4.7 - 5.0 (2 H, O-$\underline{CH_2}$-C(O)O); 5.1 - 5.3 (1 H, $\underline{CH}$-CH_3 and 1 H, $\underline{CH}$-CH_2-OH).
δ = 2.5 (6 H, CH_3-S-CH_3, DMSO); 3.3 (2 H, H_2O)

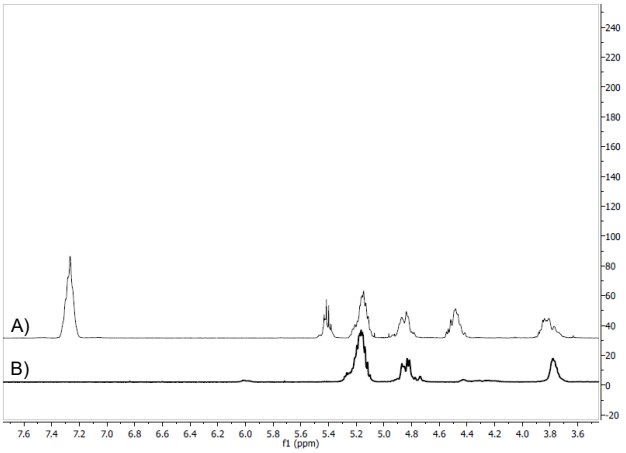

Figure S3: Superimposed ^{1}H NMR spectra of A) PLGBMGA and B) PLGHMGA in DMSO-d6.
A) δ = 3.6 - 3.9 (2 H, CH-$\underline{CH_2}$-O-CH_2-C_6H_5); 4.3 - 4.6 (2 H, CH-CH_2-O-$\underline{CH_2}$-C_6H_5); 4.7 - 5.0 (2 H, O-$\underline{CH_2}$-C(O)O); 5.1 - 5.3 (1 H, $\underline{CH}$-CH_3 and 1 H); 5.3 - 5.6 (1 H, $\underline{CH}$-CH_2-O-CH_2-C_6H_5); 7.2 -7.4 (5 H, -C_6H_5).
B) δ =3.6 - 3.9 (2 H, CH-$\underline{CH_2}$-OH); 4.7 - 5.0 (2 H, O-$\underline{CH_2}$-C(O)O); 5.1 - 5.3 (1 H, $\underline{CH}$-CH_3 and 1 H, $\underline{CH}$-CH_2-OH).

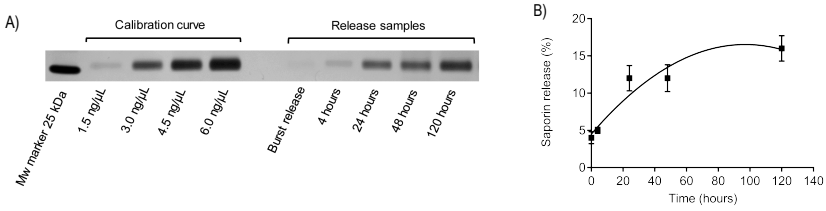

Figure S4: SDS-PAGE analysis of the saporin released from Mal-PEG-PLGHMGA NPs. A) SDS-PAGE gel image. The bands for the samples are detected at a height close to the mark of 25 kDa, which is consistent with the M_w for saporin: ∼28 kDa (ExPASy ProtParam tool). B) Release profile of saporin obtained from two independent analysis of samples through SDS-PAGE gel analysis.

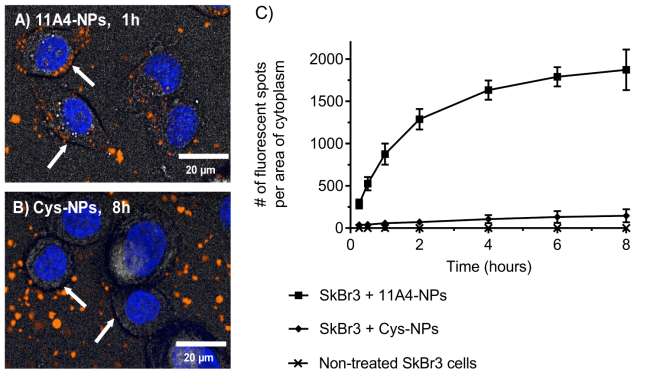

Figure S5: Uptake of targeted and non-targeted NPs by SkBr3 cells. Images showing the location of A) 11A4-NPs and B) Cys-NPs relative to the cell membrane. Nuclei are stained in blue and NPs are observed in orange. Overlay of the phase contrast image shows the cell borders, also signaled by arrows. C) Number of fluorescent spots present per area of cytoplasm over time. Data represent mean ± SD (n=15 imaging fields).

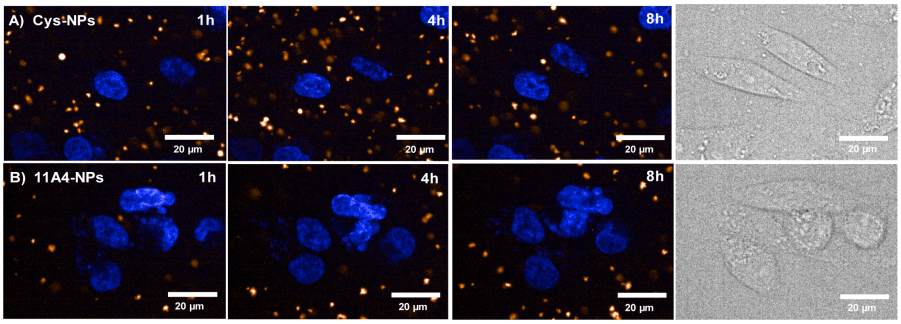

Figure S6: Cellular uptake of fluorescently labeled, targeted and non-targeted placebo NPs. Confocal images of MDA-MB-231 cells incubated with (A) Cys-NPs (22 μg/mL) and (B) 11A4-NPs (22 μg/mL) at different time points (nuclei are stained in blue, NPs are observed in orange, and the phase contrast image is in gray). The NPs remained in contact with the cells throughout the whole assay (no washing steps).

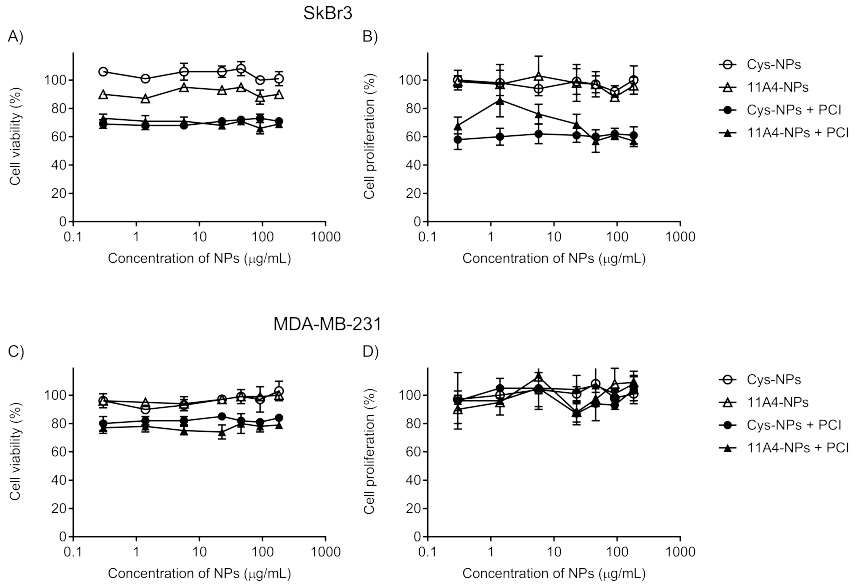

Figure S7: Cytotoxicity of placebo NPs with or without PCI in (A,B) SkBr3 and (C,D) MDA-MB-231 cells. Cell viability and cell proliferation were calculated relative to the non-treated control (no PCI, no NPs). Treatment by PCI in absence of NPs, resulted in 66 ± 3% cell viability and 66 ± 3% cell proliferation in SkBr3, and 75 ± 3% cell viability and 88 ± 5% cell proliferation in MDA-MB-231. Data represent mean ± SD (n=3).

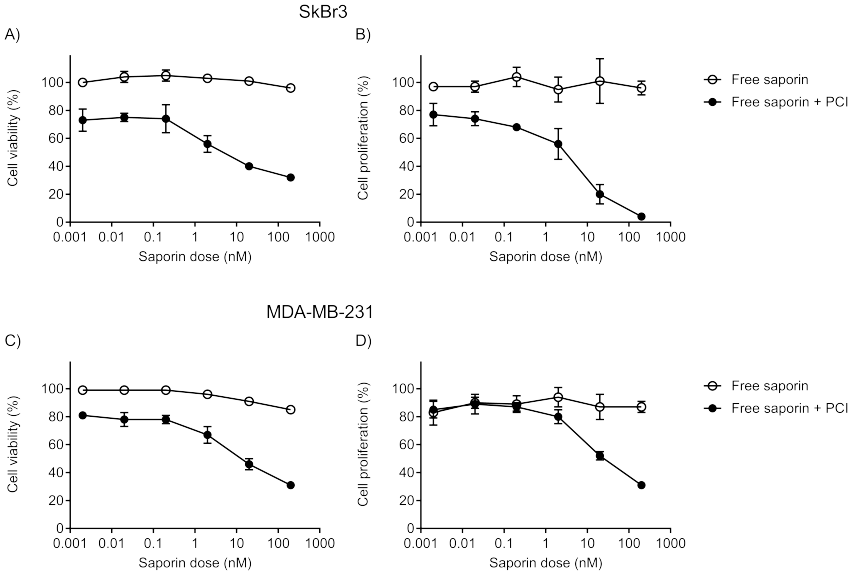

Figure S8: Cytotoxicity of free saporin with or without PCI in (A,B) SkBr3 and (C,D) MDA-MB-231 cells. Cell viability and cell proliferation were calculated respective to the non-treated control (no PCI, no NPs). Treatment by PCI in absence of NPs resulted in 76 ± 4% cell viability and 79 ± 13% cell proliferation in SkBr3, and 81 ± 3% cell viability and 90 ± 8% cell proliferation in MDA-MB-231. Data represent mean ± SD (n=3).

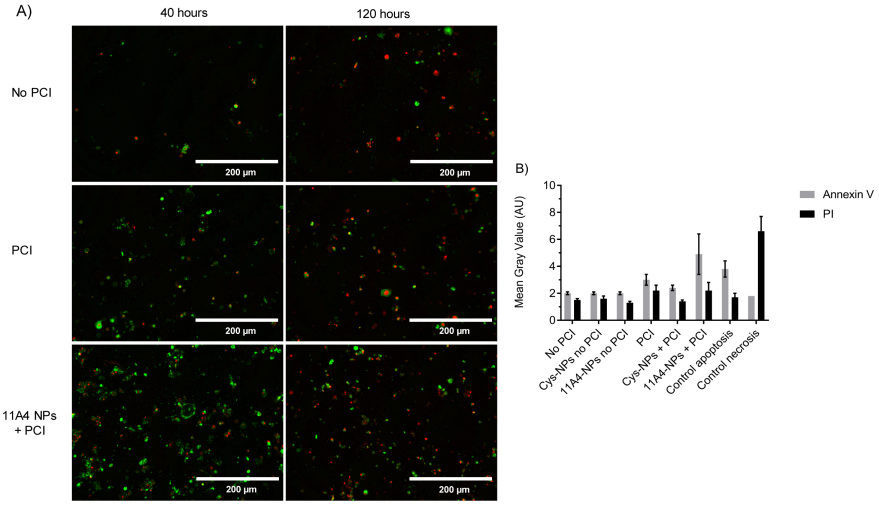

Figure S9: Microscopic observations of SkBr3 cells stained with Annexin V - FITC / PI, 40 and 120 hours after treatment with saporin loaded NPs with or without PCI. A) Microscopic observations of SkBr3 cells: apoptotic cells are stained with Annexin V - FITC (green), while dead cells are stained with PI (red). Representative images obtained by overlay of the channels depicting the signals for Annexin V - FITC and PI. B) Image analysis: fluorescent signal is reported as mean gray value (n=3). Staurosporine was used as a control to induce apoptosis and Triton X-100 was used to induce necrosis.

Chapter 6

PLGA microparticles for the sustained release of the neuroprotective peptide NDP-MSH

Lucía Martínez-Jothar[†,*], Nadine Mykicki[‡,*], Cornelus F. van Nostrum[†], Sabrina Oliveira[†,§], Karin Loser[‡,*] and Wim E. Hennink[†,*]

† Department of Pharmaceutics, Utrecht Institute for Pharmaceutical Sciences, Utrecht University, Utrecht, the Netherlands

‡ Department of Dermatology and Transregional Collaborative Research Center SFB TR-128, University of Münster, Münster, Germany.

§ Division of Cell Biology, Department of Biology, Utrecht University, Utrecht, the Netherlands

* Authors contributed equally

Manuscript in preparation

Abstract

Poly(lactic-co-glycolic acid) (PLGA) has proven to be a suitable polymer for the design of sustained release formulations for therapeutic agents that are highly susceptible to proteolytic inactivation and/or that have poor pharmacokinetics, such as the peptide Nle^4, D-Phe^7-α-melanocyte stimulating hormone (NDP-MSH). This tridecapeptide is an interesting drug candidate for the treatment of neuroinflammatory diseases due to its anti-inflammatory, immunomodulatory and neuroprotective properties, but its short half-life poses a challenge for its clinical use. In this work, NDP-MSH has been encapsulated in PLGA microparticles (μPs) that release this peptide for 50 - 70 days. NDP-MSH loaded μPs were prepared by a double emulsion solvent evaporation method and had a diameter of 17 $\pm$ 4 μm, an encapsulation efficiency of 20 $\pm$ 3% and a loading capacity of 0.14 $\pm$ 0.02%. *In vitro* release assays conducted in 10 mM phosphate buffer (pH 7.4) showed that NDP-MSH loaded μPs had a small burst release (<10%) and a lag phase of $\sim$20 days, followed by acidification of the medium and increased release of NDP-MSH which reached $\sim$90% after 50 days. In contrast, NDP-MSH loaded μPs incubated in 100 mM phosphate buffer displayed a much slower release of the peptide with 50% of the loading released after 70 days. Preliminary *in vivo* studies suggest that one subcutaneous administration of NDP-MSH loaded μPs (corresponding to an expected release of 2.8 μg of peptide during the study, based on *in vitro* data) had a similar therapeutic effect as four intravenous administrations of the free peptide (total dose of 20 μg) in a mouse model of experimental autoimmune encephalomyelitis (EAE). These findings position PLGA μPs as a suitable vehicle for the sustained release of NDP-MSH.

1 Introduction

Poly(lactic-co-glycolic acid) (PLGA) has been extensively evaluated for the design and development of pharmacologically active compounds including small drugs, therapeutic peptides and proteins, as well as antigens for vaccination purposes and nucleic acids for gene modulation[1–4]. This polymer, which is biodegradable and biocompatible, has been successfully used for the fabrication of drug delivery systems including microparticles (μPs), nanoparticles, implants and films[5]. In fact, several PLGA microparticle formulations loaded with small molecules (i.e. risperidone and buprenorphine) or therapeutic peptides (i.e. octreotide, exenatide and leuprolide) are FDA-approved and clinically used[6]. PLGA is particularly suitable for the delivery of therapeutic agents that have poor pharmacokinetic properties and that require repeated administration. The encapsulation of these agents in PLGA μPs allows for their sustained release over prolonged periods of time (1 - 6 months), which can be tailored by modulating the properties that determine the degradation rate of the polymer, such as comonomer ratio, molecular weight and end-capping group[7–10]. PLGA microparticle sustained release formulations decrease the number of administrations needed, and therefore potentially increase patient compliance and the efficacy of the treatment.

The α-melanocyte stimulating hormone (α-MSH) is an example of a peptide with interesting pharmacological properties and promising therapeutic applications which can benefit from its administration in PLGA systems. α-MSH is produced by post-translational processing of proopiomelanocortin and is quickly inactivated by a prolylcarboxypeptidase present in peripheral tissues, the central nervous system, white blood cells and endothelial cells[11,12]. α-MSH binds to the melanocortin receptors Mcr1-Mcr5 present in the central and peripheral nervous system, in melanocytes, in the adrenal cortex and in cells from the immune system (mainly myeloid cells), and mediates skin pigmentation, synthesis of steroid hormones and energy homeostasis through the regulation of glucose and lipid metabolism, and appetite/food intake[13,14]. Additionally, this peptide presents antibiotic[15], anti-inflammatory and immunomodulatory properties[16]. Analogues of α-MSH have been synthesized in an effort to prolong its activity and therefore its clinical application, with one of the most notable examples being (Nle^4, D-Phe^7)-α-MSH (NDP-MSH), also known as afamelanotide. NDP-MSH is characterized by an increased protease resistance[17,18], an increased affinity for the Mcr1 receptor (which mediates its immunomodulatory effects) and a decreased affinity to the Mcr4 receptor (which regulates food intake)[19]. In 2014, a PLGA implant loaded with NDP-MSH (Scenesse®) was approved by the EMA for use in the pre-

vention of phototoxicity in patients with erythropoietic porphyria[20]. In this system, the degradation and erosion of the polymer lead to a zero-order release of the peptide over a period of ∼1 month[21,22]. Even though NDP-MSH is currently mostly known for its photoprotecting properties, a recent study reported on its potential for the treatment of inflammatory neurological diseases due to its anti-inflammatory and immunomodulatory properties[23]. In that study, the neuroprotective effect of NDP-MSH was demonstrated in a mouse model of experimental autoimmune encephalomyelitis (EAE), a model that partly mimics the pathogenesis of multiple sclerosis (MS). Briefly, this transient inflammatory and neurodegenerative disease of the CNS is induced by immunization of the animals with myelin peptides in combination with adjuvants such as Pertussis toxin and *Mycobacterium tuberculosis*, which results in the activation of $CD4^+$ T cells that differentiate towards Th1 and Th17 cells. These cells express integrins that allow them to cross the blood-brain barrier, where the presence of myelin reactivates them, resulting in the secretion of cytokines and recruitment of other immune cells which provokes an inflammatory response and the destruction of myelin[24,25]. The severity of EAE (and of MS) can be exacerbated by an impaired suppressive capacity of regulatory T cells (Treg) which, in normal conditions, limit the differentiation, activation and proliferation of pathogenic effector T cells[26]. While intravenous administration of NDP-MSH ameliorated the progression of EAE and provided a long-lasting neuroprotective effect in a model of Devics disease[23], repeated administration of the peptide was necessary (5 μg NDP-MSH every 48 hours). In order to overcome the potential clinical limitations associated to this administration regime (i.e. reduced patient compliance), a sustained release formulation based on NDP-MSH loaded PLGA μPs was prepared and characterized for peptide-loading and *in vitro* release. Additionally, preliminary *in vivo* studies were conducted in mice with EAE to compare the efficacy and anti-inflammatory activity of free NDP-MSH and that of NDP-MSH loaded μPs.

2 Experimental section

2.1 Materials

PLGA (50:50 ratio DL-lactide/glycolide, IV 0.39 dl/g, M_w ∼44,000 Da) was purchased from Corbion (Gorinchem, the Netherlands). Poly(vinyl alcohol) (PVA) of M_w 30,000 - 70,000 Da, 87 - 90% hydrolyzed, sodium dihydrogen phosphate (NaH_2PO_4), disodium hydrogen phosphate (Na_2HPO_4),

sodium chloride, sodium azide (NaN_3), trifluoroacetic acid, complete Freund's adjuvant, hematoxylin, eosin and Luxol® fast blue (LFB) were obtained from Sigma-Aldrich (Steinheim, Germany). Peptide grade dichloromethane (DCM) and acetonitrile HPLC-S grade (ACN) were acquired from Biosolve (Valkenswaard, the Netherlands). (Nle^4, D-Phe^7)-α-MSH trifluoroacetate salt (NDP-MSH, M_w 1,647 Da) was purchased from Bachem (Bubendorf, Switzerland). MicroBCA™ Protein Assay Kit was purchased from Thermo Scientific (Illinois, USA). Dulbecco's phosphate buffered saline (8.0 g NaCl, 1.15 g Na_2HPO_4, 0.2 g KCl and 0.2 g KH_2PO_4 in 1 L of water, pH 7.4) was acquired from Sigma (Steinheim, Germany). Myelin oligodendrocyte glycoprotein (MOG) peptide was synthesized by Dr. Rudolf Volkmer, Institute for Medical Immunology, Charité (Berlin, Germany). *Mycobacterium tuberculosis* H37RA was obtained from Difco. Pertussis toxin was purchased from Enzo Life Sciences. APC/Fire750-labelled anti-mouse CD4 (clone RM4-5), PE/Cy7-labelled anti-mouse CD3ε (clone 145-2C11) and FITC-labelled anti-mouse CD25 (clone PC61) were purchased from Biolegend. eFluor 610-labelled anti-mouse Foxp3 (clone FJK-16s) and eFluor 450-labelled anti-human/mouse Helios (clone 22F6) were acquired from Thermo Fisher Scientific.

2.2 Preparation and characterization of polymeric microparticles (μPs)

Polymeric μPs were prepared by a double emulsion solvent evaporation method[10,27,28]. PLGA was dissolved in DCM at a concentration of 15% w/v and the NDP-MSH peptide was dissolved in UltraPure™ distilled water (Invitrogen, Paisley, UK) at a concentration of 3.5 mg/mL. For the preparation of NDP-MSH loaded μPs, 286 μL of the NDP-MSH solution (thus 1 mg peptide) was added to 1 mL of the PLGA solution. The mixture was subsequently emulsified in an ice bath for 1 min at 30,000 rpm using a T 10 basic ULTRA-TURRAX® homogenizer (IKA, Germany) and a W/O emulsion was formed. Next, this emulsion was added dropwise to 10 mL of a solution of PVA 2.5% w/v in NaCl 0.9% w/v; the addition was done while sonicating the PVA solution in an ice bath for 1 min at 30,000 rpm. The resulting W/O/W emulsion was poured in 20 mL of a solution of PVA 1.0% w/v in NaCl 0.9% w/v, and stirred at 600 rpm for 2 h at room temperature to evaporate DCM. Subsequently, the μPs were collected by centrifugation for 20 min, 5,000 g at 4 °C using a centrifuge with a swing-out rotor (Sigma 4-16 KS, Osetrode am Harz, Germany). One mL of the supernatant was recovered and used for the quantification of the non-encapsulated peptide (section 2.3). The rest of the supernatant was discarded and the pellet was washed with Dulbecco's PBS.

The washing step (washing + centrifugation) was repeated once more using distilled water, after which the pellet of μPs was resuspended in 1 mL of distilled water and freeze dried at -40 °C, <1 mbar (Christ Alpha 1-2 freeze dryer).

Placebo μPs were prepared using the method described for the NDP-MSH loaded μPs but using distilled water for the preparation of the first emulsion instead of the NDP-MSH solution. The diameter of the μPs was determined by light blocking technology using an AccuSizer 780 (PSS, Santa Barbara, California, USA).

2.3 Determination of peptide-loading in the μPs

The amount of peptide encapsulated in the μPs was determined by particle degradation using a protocol adapted from a previously described method [29]. Briefly, 5 mg of freeze dried μPs was incubated in 3 mL of a solution of NaOH 0.1 M at 37 °C on a nutating mixer for ∼16 h. The peptide concentration in the resulting solution was analyzed by MicroBCA™ Assay according to the specifications of the manufacturer. A solution of a known concentration of NDP-MSH was treated the same way as the μPs and was used to prepare standards of different concentrations for calibration in the determination of the peptide (detection limit 2 μg/mL). The encapsulation efficiency (EE) and the loading capacity (LC) were calculated as:

$$Encapsulation\ efficiency\ \% = \frac{Amount\ of\ peptide\ encapsulated}{Amount\ of\ peptide\ used\ in\ preparation} \times 100$$

$$Loading\ capacity = \frac{Amount\ of\ peptide\ encapsulated}{Dry\ weight\ of\ \mu Ps\ used\ in\ the\ test} \times 100$$

The amount of NDP-MSH not encapsulated in the μPs was quantified by UPLC analysis of the washings solutions collected during the preparation of the μPs (section 2.2), by injection of 7.5 μL of sample in a UPLC system (Acquity UPLC) equipped with a BEH C4 300Å column (1.7 μm, 50 mm x 2.1 mm, Waters). A gradient from 100% eluent A: 5.0% ACN, 94.9% water, 0.1% trifluoroacetic acid, to 100% eluent B: 99.9% ACN, 0.1% trifluoroacetic acid, was run over 5 minutes. The peptide was detected by fluorescence (excitation at 280 nm, emission at 340 nm). Standard solutions of NDP-MSH (concentrations ranging from 1 to 35 μg/mL) were used for calibration (detection limit 1 μg/mL).

2.4 *In vitro* release of NDP-MSH from μPs

Suspensions of freeze dried NDP-MSH loaded μPs (10 mg/mL) were prepared in isotonic PBS containing either 10 or 100 mM phosphate. In the first case (Dulbecco's PBS), the composition of the buffer was 137 mM NaCl, 8 mM Na_2HPO_4, 3 mM KCl and 2 mM KH_2PO_4, pH 7.4, while in the second case it was 56 mM NaCl, 66 mM Na_2HPO_4 and 33 mM NaH_2PO_4, pH 7.4. Both buffers were supplemented with 0.05% w/v NaN_3 to prevent bacterial growth. The μPs suspensions (500 μL) were incubated at 37 °C under mild agitation and at defined time intervals they were centrifuged for 10 min, 5,000 g at 4 °C. An aliquot of the supernatant was taken for peptide analysis and replaced by an equal volume of fresh PBS: 400 μL was collected/refreshed for the samples in 10 mM phosphate PBS and 200 μL for the samples in 100 mM phosphate PBS; these volumes were chosen based on preliminary data in order to obtain samples with peptide concentrations above the detection limit of the UPLC method, i.e. 1 μg/mL. After medium refreshment, the μPs were resuspended in the buffer and placed back in the incubator (37 °C). The peptide content in the release samples was determined by UPLC as described in section 2.3. The pH of the release medium was measured using pH indicator strips (MColorpHast®, Sigma-Aldrich).

2.5 Mice

Animal experiments were performed in C57BL/6 mice (male and female, purchased from Janvier Labs, Le Genest-Saint-Isle, France) at the age of 10 - 12 weeks. Mice were housed under specific pathogen-free conditions and were given chow and water *ad libitum*. Animal experiments were approved by the State Review Board of North Rhine-Westphalia, Germany (animal approval number 84-02.04.2013.A139).

2.6 Pre-incubation of μPs prior to injection in mice

Suspensions of freeze dried placebo μPs or NDP-MSH loaded μPs (10 mg/mL) were prepared in PBS containing 10 mM phosphate (Dulbecco's PBS, composition mentioned in section 2.1) and incubated for 7 days at 37 °C under mild agitation. The μPs suspensions were then centrifuged for 10 min, 5,000 g at 4 °C, and the supernatants of the NDP-MSH loaded μPs were recovered for peptide analysis. The μPs in the pellets were resuspended in PBS to a concentration of 200 mg/mL and administered to the mice as described in section 2.8.

2.7 Induction of Experimental Autoimmune Encephalomyelitis (EAE) in mice

EAE was induced by immunization of the animals with MOG peptide (MEVGWYRSPFSRVVHLYRNGK) following a previously described protocol[23]. Briefly, an emulsion of MOG peptide (200 μg) in complete Freund's adjuvant (containing 200 μg *Mycobacterium tuberculosis* H37RA) was administered subcutaneously into the right and left flanks of the mice. Pertussis toxin (400 ng in 200 μL PBS) was injected intraperitoneally at the day of immunization and 2 days later.

2.8 Treatment of mice with free NDP-MSH and NDP-MSH loaded μPs

At the day of immunization, the mice were randomly allocated to one of 3 treatment groups (7 mice each). For the group receiving free NDP-MSH, 5 μg of peptide (in 100 μL PBS) was administered intravenously every 2 days, starting when the mice showed the first clinical symptoms of the disease. The animals received a total of 4 intravenous injections of free NDP-MSH (thus a total dose of 20 μg of peptide). In the groups receiving treatment with the μPs, a single dose of 20 mg of either placebo or NDP-MSH loaded μPs (in 100 μL of PBS) was administered subcutaneously when the mice showed the first clinical symptoms of the disease (thus on the same day when the treatment started for the free NDP-MSH group).

2.9 Assessment of EAE clinical score

The severity of EAE was scored daily on a scale from 0 to 10 (experimental autoimmune neuritis score)[30] in a blinded manner by two independent researchers.

2.10 Histological studies

At day 13 after immunization the mice were sacrificed and CNS tissues were embedded in paraffin, cut into 3 μm sections, deparaffinized and stained with H&E using an autostainer (Tissue-Tek Prisma, Sakura Finetek), or with LFB by overnight incubation in 1% LFB dissolved in ethanol, followed by rinsing with distilled water, and differentiation with 0.05% lithium carbonate. The slides were analyzed using an Olympus BX63 microscope with the cellSens software (Olympus).

2.11 Flow cytometry analysis of mononuclear cells from the CNS

Cell preparation and flow cytometry were conducted as previously reported [23]. Briefly, single-cell suspensions of mononuclear cells from the brain and spinal cord were obtained by perfusion of the mice with Dulbecco's PBS through the left ventricle, homogenization of the tissues through cell strainers (100 μm pore size) and Percoll gradient centrifugation. Analysis of the expression of cell surface and intracellular markers was performed by multicolor flow cytometry on a Gallios flow cytometer (Beckman Coulter) with the Kaluza 2.1 software. Staining of surface markers was performed in PBS using antibodies against CD4, CD3 and CD25. For the staining of intracellular markers the cells were permeabilized using the Foxp3-Fix/Perm Buffer set (BioLegend) [23].

3 Results and Discussion

3.1 Preparation and characterization of polymeric μPs

Placebo and NDP-MSH loaded μPs were prepared from PLGA (50:50 ratio DL-lactide/glycolide) using a double emulsion solvent evaporation method. The peptide content in the loaded μPs was determined after forced degradation of the μPs. The properties of the prepared μPs are presented in Table 1.

Table 1: Characteristics of PLGA μPs.

Formulation	Yield (%)	Vol-WT diameter (μm)	Vol-WT cumulative distribution (μm)[a]	EE (%)[b]	LC (%)[c]
Placebo μPs	72 ± 2	16 ± 2	7 - 25	NA[d]	NA[d]
NDP-MSH loaded μPs	75 ± 2	17 ± 4	7 - 28	20 ± 3	0.14± 0.02

n = 3 independent batches of μPs. [a] Volume-WT cumulative distribution range 10% - 90% of total particle volume. [b] Encapsulation efficiency and [c] loading capacity determined after forced degradation of the μPs (section 2.3). [d] Not applicable.

Peptide encapsulation in polymeric particles was evaluated using either an indirect approach (quantification of non-encapsulated drug present in the washings collected during particle preparation) or a direct method consisting of quantification of the peptide released as a result of degradation of the particles. Forced particle degradation by alkaline hydrolysis was chosen for the determination of NDP-MSH loading since it has been reported to be more accurate than drug extraction using organic and aqueous solvents [31–33]. The

encapsulation of NDP-MSH in PLGA μPs was rather low ($\sim$20 $\pm$ 3%), probably due to the small size and hydrophilic nature of the peptide that could favor its partition into the outer water phase during particle preparation by the double emulsion method[34,35]. The analysis of the washings collected during the preparation of the μPs confirmed that $\sim$72% of the peptide used during the preparation of the μPs was recovered in the non-encapsulated fraction. Similar to this finding, relatively low encapsulation efficiencies have also been reported for other proteins and peptides in PLGA particles[36–39].

3.2 *In vitro* release of NDP-MSH from PLGA μPs

The release of NDP-MSH was studied in a buffer with a relatively low (10 mM phosphate) and high (100 mM phosphate) buffering capacity. These solutions were chosen in order to study the interplay between PLGA degradation and the pH of the surrounding environment and, in turn, how this affects the release kinetics of the peptide from the μPs. The release of NDP-MSH in both buffers was followed for 70 days and the results are shown in Figure 1.

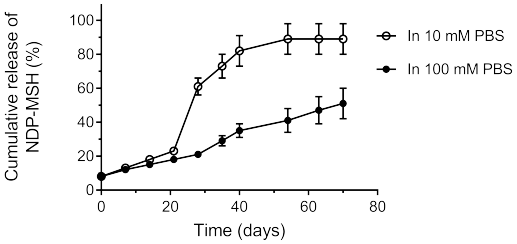

Figure 1: Cumulative release of NDP-MSH from PLGA μPs incubated in 10 or 100 mM phosphate PBS. n = 2 and n = 3 independent particle batches for 10 and 100 mM PBS respectively. Release at time 0 days corresponds to the peptide released within minutes after resuspension of the μPs in the buffer.

The NDP-MSH loaded μPs showed a low burst release ($<$ 10%) in both buffers, a property that is desirable for most drug delivery applications[40]. After this small burst, the formulation displayed a similar release profile during the first 21 days in both buffers. For the μPs dispersed in 10 mM phosphate PBS a sudden increase in the release was observed at around day 21, which reached a plateau at $\sim$50 days. The total amount of peptide released was $\sim$90% of the peptide loaded as determined with the direct determination (Table 1).

The release of NDP-MSH in 10 mM phosphate PBS coincides with the triphasic drug release profile often reported for PLGA particles[8,41,42]. In general, this profile can be described as follows: phase I consists of the burst release of cargo molecules present on the particle surface or in close proximity to it, which easily diffuse out upon contact with the aqueous medium[41,43]. Phase II (sometimes referred to as lag-phase) is characterized by slow release via pores and/or by diffusion of dissolved cargo molecules through the matrix. In this stage, degradation of the polymer occurs through ester bond hydrolysis, causing a decrease in the M_w of the polymer, but no substantial mass loss of the particles[9,44]. Acidic products resulting from the degradation of PLGA progressively accumulate in the core of the particles, causing a decrease in pH that further accelerates the degradation process (autocatalysis)[45,46]. Phase III consists of the fast release of the cargo driven by erosion of the particles. This process is associated with the extraction of degradation products (lactic and glycolic acid as well as their oligomers), resulting in mass loss of the particles and in the creation of pores or cracks through which the cargo diffuses out of the particles[9,10]. In contrast, the release of NDP-MSH from the μPs dispersed in 100 mM phosphate PBS showed, after a small burst ($\sim$10% of the loading), a zero-order release of 50% of the loading during 70 days, as shown in Figure 1.

The difference in release profiles of the μPs dispersed in 10 and 100 mM PBS can be ascribed to the buffer capacities of the release medium. Figure 2 shows that the acidic products released during PLGA degradation could not be neutralized by the 10 mM PBS, resulting in acidification which could have further accelerated the degradation of the μPs. No polymer residue was observed in the samples incubated in 10 mM PBS after 63 days, which also coincides with an increase in pH due to medium refreshment and because of the absence of formation of acid degradation products. Medium acidification did not occur in the μPs dispersed in 100 mM phosphate PBS, also shown in Figure 2, which most likely delayed the degradation of PLGA (polymer residue was still observed at day 70), leading to slower release of the peptide. It is also possible that buffer ions penetrated into the particles and neutralized the acid degradation products, slowing down the autocatalytic degradation process.

The UPLC chromatograms of NDP-MSH released from the μPs shortly after resuspension in 10 and 100 mM PBS (release time 0 days) showed a main peak at 2.10 min which corresponded to this peptide. The same peak was present in the release samples at day 70 of the assay, whereas a smaller peak with a longer retention time ($\sim$3.30 min) was also observed, as shown in Figure 3. The appearance of additional peaks in the chromatograms of *in vitro* release studies has been previously described in PLGA μPs loaded with oc-

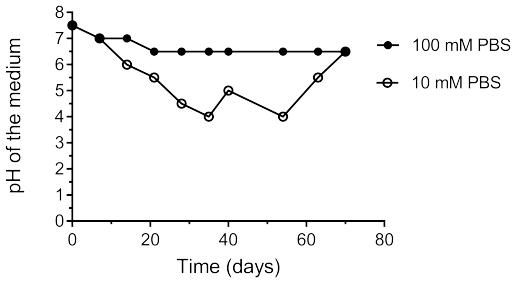

Figure 2: pH profile of the release medium at different incubation times of PLGA μPs dispersed in PBS of different buffer capacities.

treotide[47,48], atrial natriuretic peptide[49], goserelin[50] and leuprorelin[51]. Upon mass spectrometry analysis, the identity of those new peaks was attributed to acylated peptides, and the N-terminal group, as well as the primary amines of lysine, the NH of the guanidine group of arginine, and the hydroxyl group in serine, were identified as potential targets of acylation. It is therefore possible that NDP-MSH (which contains one lysine, one arginine and two serine residues) also undergoes acylation inside PLGA μPs, although the majority of the peptide is unaffected and retains its original elusion profile (Figure 3).

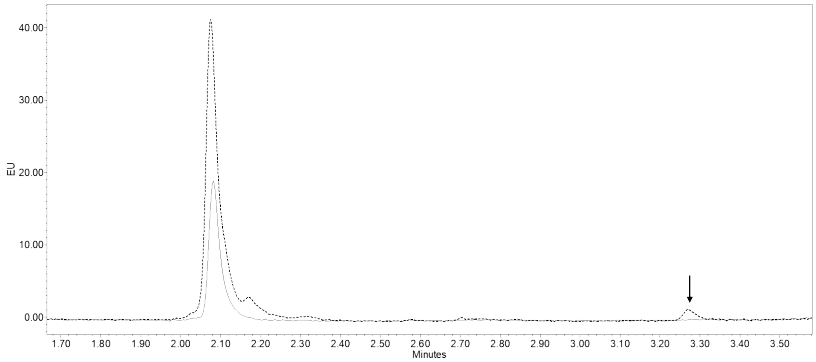

Figure 3: UPLC chromatograms of NDP-MSH released from PLGA μPs after 0 days (continuous line) and 70 days (dashed line) of incubation in 100 mM PBS. The additional peak appearing in the 70 days chromatogram is signaled with an arrow. Similar chromatograms were obtained for the release studies in 10 mM PBS.

The results from the release experiments obtained in the present work demonstrate that the nature of the release medium undoubtedly influences the degradation and release profiles of PLGA μPs. These findings highlight the importance of reporting the composition of the PBS used in release experiments, which is often lacking in many publications. In many cases the information provided is limited to the overall molarity and the starting pH of the buffer, but not on whether and how the pH changes during the release study.

3.3 Clinical scores and histological studies in mice with EAE treated with NDP-MSH

The pharmacological effect of NDP-MSH loaded μPs was compared to the effect of free NDP-MSH in a mouse model of EAE. EAE experiments were conducted over a time period of roughly 2 weeks, comprising the preclinical phase (days ∼2 - 6) and a symptomatic phase (days 6 - 13). MOG-induced EAE is a transient disease and animals almost completely recover 3 or 4 weeks after immunization. As a consequence of the restricted time frame for the study of NDP-MSH loaded μPs in this EAE model, and because the degradation of PLGA μPs takes several weeks, the μPs were pre-incubated in 10 mM phosphate buffer at 37 °C before subcutaneous injection in the animals. During this *in vitro* pre-incubation step, 0.16 μg of peptide was released per mg of μPs, which is equivalent to 11% of the loading and is in agreement with the release data presented in Figure 1. It is mentioned that a single dose of 20 mg of NDP-MSH loaded μPs was administered per mouse, and that the readout was done 7 days after administration. This means that based in the *in vitro* release experiment (Figure 1, peptide released between 7 - 14 days in both buffers tested), the amount of NDP-MSH released from the μPs during the animal studies was 2.8 μg. Nevertheless, it is possible that more peptide was released from the NDP-MSH loaded μPs during the *in vivo* tests, since faster degradation of different PLGA systems (and thus release of the loaded therapeutic agent) has been reported *in vivo* compared to *in vitro*[52–54]. Even if this is the case, a single injection of our formulation is as effective as a 4 fold administration of the free peptide. During the same animal experiment, mice of another group received 4 intravenous administrations of 5 μg of free NDP-MSH, thus a total of 20 μg of peptide (around 7 times more peptide than what is released from the μPs *in vitro* in the same time frame).

The preliminary results shown in Figure 4 indicate that mice treated with placebo μPs showed disease perpetuation from paralysis of the tip of the tail (EAN score 0.5 - 1, day 8) until the paralysis of one hind limb (EAN score 5

- 6, day 13). Mice that received free NDP-MSH and NDP-MSH loaded μPs showed comparable clinical scores, and in both groups the clinical symptoms were indicative of mild EAE (partial tail limpness, EAN score 1 from day 10 in mice treated with the free peptide and from day 13 in mice treated with NDP-MSH loaded μPs). The onset of the disease was delayed in the animals treated with NDP-MSH loaded μPs compared to those that received the free peptide.

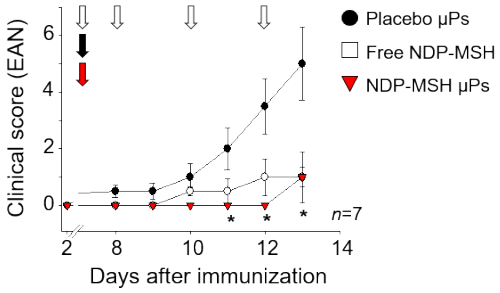

Figure 4: Clinical score of mice treated with placebo μPs, free NDP-MSH or NDP-MSH loaded μPs. The free peptide and the μPs were administered at the time points indicated with arrows (n = 7 mice per group, * = $p < 0.05$ versus placebo μPs).

Representative images of lumbar spinal cord sections stained with LFB (myelin stain) and H&E (nuclei and cytoplasm stain) are shown in Figure 5. LFB and H&E are commonly used for the visualization of demyelinated areas in the CNS (LFB) or the infiltration of mononuclear inflammatory cells (H&E)[24,55]. The spinal cord of mice that received placebo μPs presented more extensive signs of demyelination and infiltration of mononuclear cells (as indicated by the arrows) than the spinal cord of mice treated with either free NDP-MSH or NDP-MSH loaded μPs.

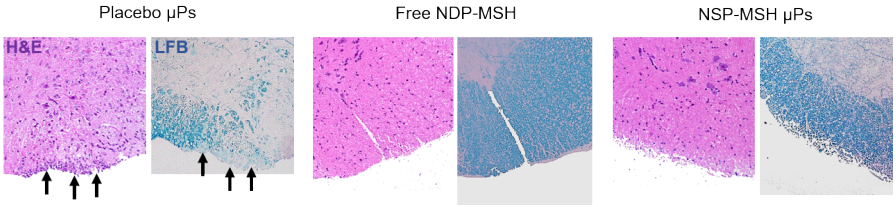

Figure 5: Histological analysis of the lumbar spinal cord from mice treated with placebo μPs, free NDP-MSH or NDP-MSH loaded μPs. Tissues were stained with H&E (nuclei stained in purple, cytoplasm in pink) and LFB (myelin stained in blue). Representative images for each group are depicted and the arrows show areas of cell infiltration or demyelination.

3.4 Immune effects of free and encapsulated NDP-MSH in EAE mice

Flow cytometry analysis was performed to identify the types of leukocytes isolated from the CNS of mice after treatment. Total CNS infiltrating leukocytes were gated on $CD3^+CD4^+$ T cells and, within this subset, all $CD25^+$ cells were analyzed in detail. Foxp3 staining was used to differentiate Treg ($Foxp3^+$) from effector T cells ($Foxp3^-$) within the $CD3^+CD4^+CD25^+$ population, since in mice the transcription factor Foxp3 is specifically expressed in Treg. Helios staining was used to differentiate resting Treg ($Foxp3^+Helios^-$) from activated ones ($Foxp3^+Helios^+$). Flow cytometry analysis presented in Figure 6 shows that, at day 13 after immunization, the presence of activated Treg was lower in the CNS of mice treated with placebo μPs compared to mice that received either free NDP-MSH or NDP-MSH loaded μPs. This finding suggests that NDP-MSH (administered free or in μPs) might have mediated the expansion of Treg. It has been previously reported that activated (functional) Treg induced or expanded by treatment with NDP-MSH suppress pathogenic Th1 and Th17 in mice with EAE, and ameliorate disease progression [23].

Overall, the results of the preliminary *in vivo* study suggest that, compared to placebo μPs, treatment with both free NDP-MSH or NDP-MSH loaded μPs is associated with a decreased clinical score, and less inflammatory foci as well as demyelinated areas in the CNS. Additional experiments, and in particular experiments in models of spontaneous EAE, are necessary to assess the efficacy of the free and encapsulated NDP-MSH, and the duration of the beneficial effect of the NDP-MSH loaded PLGA μPs.

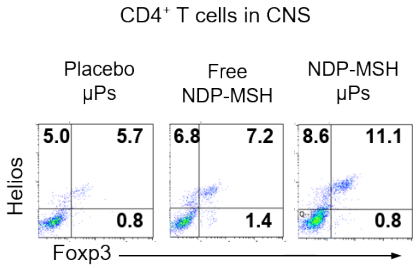

Figure 6: Representative flow cytometry dot-plots of Treg in the CNS of mice treated with placebo μPs, free NDP-MSH or NDP-MSH loaded μPs. Foxp3 and Helios expression was quantified in T-cells gated on $CD3^+CD4^+CD25^+$. Analysis was performed at day 13 after immunization and Foxp3 as well as Helios staining was performed after cell permeabilization.

4 Conclusions

NDP-MSH loaded PLGA μPs were prepared and evaluated *in vitro* and *in vivo* as a formulation for the sustained release of NDP-MSH. The EE of NDP-MSH in these μPs was 20 ± 3%, corresponding to a LC of 0.14%. The μPs were characterized for peptide release in two different buffers (10 and 100 mM phosphate PBS) and, after 3 weeks of incubation, a strong influence of the phosphate concentration was observed on the release profile of the peptide. The pharmacological effect of NDP-MSH loaded μPs was tested in mice with EAE, and preliminary results indicate that a single subcutaneous administration of these μPs was able to significantly reduce the disease severity as compared to mice that received placebo μPs. Furthermore, NDP-MSH loaded μPs injected once at the appearance of first clinical symptoms had similar effects as four intravenous administrations of the free peptide (7 times higher dose compared to the peptide released from the μPs according to the *in vitro* assays). While more extensive studies need to be performed in a larger number of animals to corroborate these findings, the preliminary data might suggest that PLGA μPs are a promising vehicle for the sustained release of NDP-MSH for the *in vivo* treatment of inflammatory neurological diseases.

Acknowledgements

Lucía Martínez - Jothar would like to thank the Consejo Nacional de Ciencia y Tecnología (CONACYT), México (grant no. 384743) for the funding provided

in the framework of her PhD.

References

[1] Kumar Malik, D., S, B., Ahuja, A., Hasan, S., and J, A. Recent advances in protein and peptide drug delivery systems. *Current Drug Delivery*, 4, 2007.

[2] Rezvantalab, S., Drude, N. I., Moraveji, M. K., and Gagliardi, P. A. PLGA-based nanoparticles in cancer treatment. *Frontiers in Pharmacology*, 9, 2018.

[3] Sun, Q., Barz, M., Geest, B. G. D., Hennink, W. E., Kiessling, F., and Lammers, T. Nanomedicine and macroscale materials in immuno-oncology. *Chemical Society Reviews*, 48, 2019.

[4] Tong, R., Gabrielson, N. P., Fan, T. M., and Cheng, J. Polymeric nanomedicines based on poly (lactide) and poly (lactide-co-glycolide). *Current Opinion in Solid State & Materials Science*, 16, 2013.

[5] Jain, R. A. The manufacturing techniques of various drug loaded biodegradable poly(lactide-co-glycolide) (PLGA) devices. *Biomaterials*, 21, 2000.

[6] Zhong, H., Chan, G., Hu, Y., Hu, H., and Ouyang, D. A comprehensive map of FDA-approved pharmaceutical products. *Pharmaceutics*, 10, 2018.

[7] Anderson, J. M. and Shive, M. S. Biodegradation and biocompatibility of PLA and PLGA microspheres. *Advanced Drug Delivery Reviews*, 64, 1997.

[8] Kamaly, N., Yameen, B., Wu, J., and Farokzhad, O. C. Degradable controlled-release polymers and polymeric nanoparticles: Mechanisms of controlling drug release. *Chemical Reviews*, 116, 2016.

[9] Makadia, K. H. and Siegel, S. J. Poly lactic-co-glycolic acid (PLGA) as biodegradable controlled drug delivery carrier. *Polymers*, 3, 2011.

[10] Samadi, N., Abbadessa, A., Di Stefano, A., Van Nostrum, C. F., Vermonden, T., Rahimian, S., Teunissen, E. A., Van Steenbergen, M. J., Amidi, M., and Hennink, W. E. The effect of lauryl capping group on protein release and degradation of poly(d,l-lactic-co-glycolic acid) particles. *Journal of Controlled Release*, 172, 2013.

[11] D'Agostino, G. and Diano, S. alpha-Melanocyte stimulating hormone: production and degradation. *Journal of Molecular Medicine*, 88, 2010.

[12] Diano, S. New Aspects Of Melanocortin Signaling: A role for PRCP in alpha-MSH degradation. *Frontiers in Neuroendocrinology*, 32, 2011.

[13] Brennan, M. B., Lynn, C. J., Forbes, S., Reed, P., Bui, S., and Hochgeschwender, U. alpha-melanocyte-stimulating hormone is a peripheral, integrative regulator of glucose and fat metabolism. *Annals of the New York Academy of Science*, 994, 2003.

[14] Ramachandrappa, S., Gorrigan, R. J., Clark, A. J. L., and Chan, L. F. Melanocortin receptors and their accessory proteins. *Frontiers in endocrinology*, 4, 2013.

[15] Cutuli, M., Cristiani, S., Lipton, J. M., and Catania, A. Antimicrobial effects of α-MSH peptides. *Journal of Leukocyte Biology*, 67, 2000.

[16] Luger, T. A. and Brzoska, T. α-MSH related peptides: A new class of anti-inflammatory and immunomodulating drugs. *Annals of the Rheumatic Diseases*, 66, 2007.

[17] Hadley, M. E., Hruby, V. J., Dorr, R. T., Levine, N., Dawson, B. V., Al-Obeidi, F., and Sawyer, T. K. *Discovery and Development of Novel Melanogenic Drugs*, pages 575–595. Plenum Press, New York, 1998.

[18] Sawyer, T. K., Sanfilippo, P. J., Hruby, V. J., Engel, M. H., Heward, C. B., Burnett, J. B., and Hadley, M. E. 4-Norleucine, 7-D-phenylalanine-alpha-melanocyte-stimulating hormone: a highly potent alpha-melanotropin with ultralong biological activity. *Proceedings of the National Academy of Sciences of the United States of America*, 77, 1980.

[19] Haskell-Luevano, C., Holder, J. R., Monck, E. K., and Bauzo, R. M. Characterization of melanocortin NDP-MSH agonist peptide fragments at the mouse central and peripheral melanocortin receptors. *Journal of Medicinal Chemistry*, 44, 2001.

[20] Scenesse® Assessment Report. Report, European Medicines Agency, 2014.

[21] Bhardwaj, R. and Blanchard, J. In vitro characterization and in vivo release profile of a poly (D,L-lactide-co-glycolide)-based implant delivery system for the α-MSH analog, melanotan-I. *International Journal of Pharmaceutics*, 170, 1998.

[22] Bhardwaj, R. and Blanchard, J. In vitro evaluation of Poly(D,L-lactide-co-glycolide) polymer-based implants containing the α-melanocyte stimulating hormone analog, Melanotan-I. *Journal of Controlled Release*, 45, 1997.

[23] Mykicki, N., Herrmann, A. M., Schwab, N., Deenen, R., Sparwasser, T., Limmer, A., Wachsmuth, L., Klotz, L., Köhrer, K., Faber, C., Wiendl, H., Luger, T. A., Meuth, S. G., and Loser, K. Melanocortin-1 receptor activation is neuroprotective in mouse models of neuroinflammatory disease. *Science Translational Medicine*, 8, 2016.

[24] Constantinescu, C. S., Farooqi, N., O'Brien, K., and Gran, B. Experimental autoimmune encephalomyelitis (EAE) as a model for multiple sclerosis (MS). *British Journal of Pharmacology*, 164, 2011.

[25] Miller, S., Karpu, W., and Davidson, T. Experimental autoimmune encephalomyelitis in the mouse. *Current Protocols in Immunology*, 2007.

[26] Kleinewietfeld, M. and Hafler, D. Regulatory T cells in autoimmune neuroinflammation. *Immunological Reviews*, 259, 2014.

[27] Alonso, M. J., Cohen, S., Park, T. G., Gupta, R. K., Siber, G. R., and Langer, R. Determinants of release rate of tetanus vaccine from polyester microspheres. *Pharmaceutical Research*, 10, 1993.

[28] Zambaux, M. F., Bonneaux, F., Gref, R., Maincent, P., Dellacherie, E., and Alonso, M. J. Influence of experimental parameters on the characteristics of poly (lactic acid) nanoparticles prepared by a double emulsion method. *Journal of Controlled Release*, 50, 1998.

[29] Sah, H. A new strategy to determine the actual protein content of poly(lactide- co-glycolide) microspheres. *Journal of Pharmaceutical Sciences*, 86, 1997.

[30] Bittner, S., Ruck, T., Schuhmann, M. K., Herrmann, A. M., Maati, H. M. O., Bobak, N., Göbel, K., Langhauser, F., Stegner, D., Ehling, P., Borsotto, M., Pape, H. C., Nieswandt, B., Kleinschnitz, C., Heurteaux, C., Galla, H. J., Budde, T., Wiendl, H., and Meuth, S. G. Endothelial TWIK-related potassium channel-1 (TREK1) regulates immune-cell trafficking into the CNS. *Nature Medicine*, 19, 2013.

[31] Blanco, M. and Alonso, M. Development and characterization of protein-loaded poly(lactide-co-glycolide) nanospheres. *European Journal of Pharmaceutics and Biopharmaceutics*, 43, 1997.

[32] Feng, L., Rong, X., Jun, X., Maitani, Y., and Cong, S. Pharmaceutical and immunological evaluation of a single-dose hepatitis B vaccine using PLGA microspheres. *Journal of Controlled Release*, 112, 2006.

[33] Sharif, S. and O'Hagan, D. T. A comparison of alternative methods for the determination of the levels of proteins entrapped in poly(lactide-co-glycolide) microparticles. *International Journal of Pharmaceutics*, 115, 1995.

[34] Ramazani, F., Chen, W., Van Nostrum, C. F., Storm, G., Kiessling, F., Lammers, T., Hennink, W. E., and Kok, R. J. Strategies for encapsulation of small hydrophilic and amphiphilic drugs in PLGA microspheres: State-of-the-art and challenges. *International Journal of Pharmaceutics*, 499, 2016.

[35] Ye, M., Kim, S., and Park, K. Issues in long-term protein delivery using biodegradable microparticles. *Journal of Controlled Release*, 146, 2010.

[36] Bouissou, C., Potter, U., Altroff, H., Mardon, H., and Walle, C. Controlled release of the fibronectin central cell binding domain from polymeric microspheres. *Journal of Controlled Release*, 95, 2004.

[37] Kostadinova, A. I., Middelburg, J., Ciulla, M., Garssen, J., Hennink, W. E., Knippels, L. M. J., van Nostrum, C., and Willemsen, L. PLGA nanoparticles loaded with beta-lactoglobulin-derived peptides modulate mucosal immunity and may facilitate cow's milk allergy prevention. *European Journal of Pharmacology*, 818, 2018.

[38] Li, Z., Li, L., Liu, Y., Zhang, H., Li, X., Luo, F., and Mei, X. Development of interferon alpha-2b microspheres with constant release. *International Journal of Pharmaceutics*, 410, 2011.

[39] Nicoli, S., Santi, P., Couvreur, P., Couarraze, G., and Colombo, P. Design of triptorelin loaded nanospheres for transdermal iontophoretic administration. *International Journal of Pharmaceutics*, 214, 2001.

[40] Allison, S. Analysis of initial burst in PLGA microparticles Analysis of initial burst in PLGA microparticles. *Expert Opinion on Drug Delivery*, 5, 2008.

[41] Fredenberg, S., Wahlgren, M., Reslow, M., and Axelsson, A. The mechanisms of drug release in poly (lactic-co-glycolic acid) - based drug delivery systems A review. *International Journal of Pharmaceutics*, 415, 2011.

[42] Wischke, C. and Schwendeman, S. P. Principles of encapsulating hydrophobic drugs in PLA/PLGA microparticles. *International Journal of Pharmaceutics*, 364, 2008.

[43] Wang, J., Wang, B. M., and Schwendeman, S. P. Characterization of the initial burst release of a model peptide from poly (D,L -lactide-co-glycolide) microspheres. *Journal of Controlled Release*, 82, 2002.

[44] Wu, X. and Wang, N. Synthesis, characterization, biodegradation, and drug delivery application of biodegradable lactic/glycolic acid polymers. Part II: Biodegradation. *Journal of Biomaterials Science, Polymer Edition*, 12, 2001.

[45] Spenlehauer, G., Vert, M., Benoit, J. P., and Boddaert, A. Poly (D,L lactide / glycolide) type microspheres made by solvent evaporation method. *Biomaterials*, 10, 1989.

[46] Vert, M., Schwach, G., Engel, R., and Coudane, J. Something new in the field of PLA / GA bioresorbable polymers? *Journal of Controlled Release*, 53, 1998.

[47] Ghassemi, A. H., Steenbergen, M. J. V., Barendregt, A., Talsma, H., Kok, R. J., and Nostrum, C. F. V. Controlled release of octreotide and assessment of peptide acylation from poly (d,l-lactide-co-hydroxymethyl glycolide) compared to PLGA microspheres. *Pharmaceutical Research*, 29, 2012.

[48] Shirangi, M., Hennink, W. E., Somsen, G. W., and Van Nostrum, C. F. Identification and assessment of octreotide acylation in polyester microspheres by LC-MS/MS. *Pharmaceutical Research*, 32, 2015.

[49] Lucke, A. and Kiermaier, J. Peptide acylation by poly (alpha-hydroxy esters). *Pharmaceutical Research*, 19, 2002.

[50] Shirangi, M., Hennink, W. E., Somsen, G. W., and van Nostrum, C. F. Acylation of arginine in goserelin-loaded PLGA microspheres. *European Journal of Pharmaceutics and Biopharmaceutics*, 99, 2016.

[51] Guo, N., Zhang, Q., Sun, Y., and Yang, H. Separation and identification of acylated leuprorelin inside PLGA microspheres. *International Journal of Pharmaceutics*, 560, 2019.

[52] Grayson, A. C. R., Voskerician, G., Lynn, A., Anderson, J. M., Cima, M. J., and Langer, R. Differential degradation rates in vivo and in vitro of biocompatible poly(lactic acid) and poly(glycolic acid) homo- and co-polymers for polymeric drug-delivery microchip. *Journal of Biomaterials Science, Polymer Edition*, 15, 2004.

[53] Lu, L., Peter, S. J., D. Lyman, M., Lai, H. L., Leite, S. M., Tamada, J. A., Uyama, S., Vacanti, J. P., Langer, R., and Mikos, A. G. In vitro and in vivo degradation of porous poly(DL-lactic-co-glycolic acid) foams. *Biomaterials*, 21, 2000.

[54] Zolnik, B. S. and Burgess, D. J. Evaluation of in vivo in vitro release of dexamethasone from PLGA microspheres. *Journal of Controlled Release*, 127, 2008.

[55] Steinbach, K. and Merkler, D. Neuropathological techniques to investigate CNS pathology in experimental autoimmune encephalomyelitis (EAE). *Methods in Molecular Biology*, 1304, 2014.

Chapter 7

Summary and perspectives

1 Summary

Proteins and peptides have long been regarded as valuable therapeutic agents because of their potency and specificity [1], and > 160 therapeutic proteins [2,3] and > 60 therapeutic peptides [4] have currently been approved for clinical use. While the market of biotherapeutics continues to expand, a substantial number of proteins and peptides with short half-lives would benefit from formulation technologies to facilitate their clinical application. In this regard, polymeric microparticles (μPs) and nanoparticles (NPs) are attractive delivery systems to improve the efficacy of these biomolecules by protecting them from inactivation and increasing their circulation time and accumulation at the target site [5,6].

A substantial number of FDA-approved biotherapeutics (i.e. monoclonal antibodies and coagulation factors) are directed at extracellular targets, which is not surprising since proteins and peptides have low cell membrane permeability that limits their access to the cytoplasm. This challenge can, however, be overcome by the use of NPs. The composition, size, charge and surface characteristics of these nanocarriers determine their cellular internalization and the intracellular release of their loaded cargo. For instance, the surface of NPs loaded with a therapeutic protein/peptide, can be decorated with ligands that will favor the binding of the NPs to, and uptake by, specific cells.

The research presented in this thesis is focused on the preparation, characterization and *in vitro* testing of polymeric particles for the administration of therapeutic proteins and peptides. Targeted and non-targeted nano- and microparticles were explored for the intra- and extra- cellular delivery of these biotherapeutics.

Chapter 1 of this thesis provides a general introduction on therapeutic proteins and peptides and the description of two interesting therapeutic candidates: saporin and (Nle^4, D-Phe^7)-α-melanocyte-stimulating hormone (NDP-MSH). Challenges in protein/peptide delivery are discussed, and polymeric particles (micro- and nano- metric sizes) are presented as carrier systems to improve the physicochemical stability, pharmacokinetics and pharmacodynamics of these biotherapeutics. Two biodegradable aliphatic polyesters, poly(lactic-co-glycolic) acid (PLGA) and poly(D,L-lactic-co-glycolic-co-hydroxymethyl glycolic acid) (PLGHMGA), are introduced as suitable polymers for the preparation of particles aimed for the extra- or intra- cellular delivery of biotherapeutics. Physicochemical characteristics of the particles, as well as the anatomy and physiology of tissues are discussed as important factors that determine the distribution and accumulation of particles in the disease site. In cases where intracellular delivery is needed, the decoration of NPs with targeting

ligands is proposed as a way to facilitate their uptake by target cells. Two targeting ligands are explored in this thesis, namely the 11A4 nanobody and the cyclic RGD peptide (cRGD), both of which have shown potential for cancer treatment. Cellular internalization and endosomal trafficking of the NPs are discussed, and photochemical internalization (PCI) is investigated as a strategy to induce endosomal escape of protein loaded NPs, thus assisting the cytosolic delivery of therapeutic proteins.

In **Chapter 2**, maleimide-thiol conjugation chemistry was used for the preparation of PLGA NPs decorated with cRGD or the 11A4 nanobody as targeting ligands on their surface. The influence of different conditions on the efficiency of the conjugation reaction of cRGD and the 11A4 nanobody to the NPs was systematically studied. Parameters such as the NPs preparation method (i.e. single or double emulsion), and the type and concentration of surfactant used during the procedure (poly(vinyl alcohol) and sodium cholate, 1 - 5% w/v), did not influence the efficiency of the reaction. In contrast, the storage conditions of the NPs affected the reactivity of maleimide and, while high conjugation efficiencies (∼90%) were obtained for NPs stored at 4 °C for up to 7 days, storage at 20 °C resulted in lower conjugation efficiencies (∼60%), probably due to maleimide hydrolysis.

The efficiency of the maleimide-thiol conjugation reaction was evaluated at different reactant ratios and reaction times, and the preparation of ligand-decorated NPs was optimized. NPs surface decoration with cRGD (M_w 678 Da) was optimal at a maleimide to thiol molar ratio of 2:1 and reached a conjugation efficiency of 84 ± 4% (corresponding to ∼50,000 cRGD molecules per NP) after only 30 minutes of incubation (room temperature, pH 7.0). Interestingly, conjugation at 1:1 ratios resulted in lower efficiencies (52 ± 7%), suggesting that not all maleimide groups on the surface of the particles are available for reaction. NPs decoration with 11A4 nanobody (M_w 14,813 Da) was optimal at a maleimide to thiol molar ratio of 5:1 and reached 58 ± 12% conjugation efficiency (corresponding to ∼5,500 11A4 molecules per NP) after 2 h (room temperature, pH 7.4). The difference in reaction efficiencies and kinetics for both ligands can be explained by the differences in their size and structure (higher diffusion coefficient for cRGD and better accessibility of its thiol group compared to that of the 11A4 nanobody).

The findings from this study provided valuable information on the optimal conditions for preparation of ligand-decorated NPs by maleimide-thiol chemistry, particularly in terms of reaction times and reactant ratios. These insights were applied in the preparation of the targeted NPs presented in other chapters.

In **Chapter 3**, PLGA NPs decorated with cRGD were prepared, and their targeting properties were investigated on human umbilical vein endothelial cells (HUVECs) under static and flow conditions. PLGA NPs were decorated with cRGD in different densities (i.e. "low" ∼11,000, "medium" ∼31,700 and "high" ∼117,600 cRGD/μm2; corresponding to ∼3,400, ∼9,700 and ∼40,700 cRGD molecules per NP) in order to study the impact of ligand density on cell-targeting.

Association and uptake of cRGD-NPs incubated with HUVECs under static conditions was assessed by flow cytometry and confocal microscopy. Interaction of NPs with HUVECs was not observed for NPs that were not decorated with cRGD. In contrast, cell-association was observed for cRGD-NPs, and it was positively correlated to the incubation time (1 and 3 h), NPs concentration (0.016 - 0.4 mg/mL) and cRGD surface density (∼11,000 - ∼117,600 cRGD/μm2 or ∼3,400 - ∼40,700 cRGD/NP). In this regard, the association of high cRGD-NPs to HUVECs was ∼4 fold higher than for low cRGD-NPs (at the highest concentrations tested). Given that in physiological settings the targeting of vascular endothelial cells occurs under dynamic conditions (rather than static ones), experiments under flow were conducted using a pump-controlled perfusion system and cell association was visualized using an epifluorescence microscope. Similar to the findings under static conditions, cell-association of NPs with HUVECs under flow was observed for cRGD-NPs but not for non-decorated NPs. Interactions with HUVECs were also dependent on the surface density of cRGD, and after 1 and 16 h of incubation, the cell-association of high cRGD-NPs was ∼9 and 6 fold higher than the association of low cRGD-NPs, suggesting that ligand density is more relevant for cell-particle interactions under flow than under static conditions. Flow experiments were also conducted in medium containing washed red blood cells (RBCs) and, under this condition, the association of cRGD-NPs to HUVECs was also ligand-density dependent. Comparison of the flow experiments conducted in medium with and without RBCs, shows that association of NPs to the cells is substantially higher in presence of RBCs (∼6 and 3 fold difference for low and high cRGD-NPs, respectively). This observation is very likely caused by RBCs pushing the NPs towards the HUVECs and promoting their contact with them. The work reported in this chapter is a step towards evaluating vascular targeting in settings that more closely resemble physiological conditions. This approach would be of great value for the development of new endothelium-targeted nanocarriers using a reduced number of laboratory animals.

In **Chapter 4**, poly(D,L-lactic-co-glycolic-co-hydroxymethyl glycolic acid) (PLGHMGA) and PEGylated PLGHMGA (MePEG-PLGHMGA) were syn-

thesized, characterized, and used for NPs preparation as an alternative for PLGA. The cytocompatibility of MePEG-PLGHMGA NPs was tested in two cell lines which were of interest for future experiments, SkBr3 and MDA-MB-231. Unexpected cytotoxicity of these NPs was observed at concentrations > 0.4 mg/mL in SkBr3 and > 0.8 mg/mL in MDA-MB-231. This toxicity was attributed to the presence of butylated hydroxytoluene (BHT) as an impurity in the NPs. The synthesis of (MePEG-) PLGHMGA involves a hydrogenation step performed in tetrahydrofuran (THF), a solvent stabilized with BHT. Although the amount of BHT present in THF is small (0.02 - 0.03% w/w), the use of large volumes of THF during hydrogenation led to the accumulation of BHT in the polymers to an extent that significantly affected the cytocompatibility of the NPs (2.3% w/w BHT in NPs). BHT was removed from the polymers by precipitation in diethyl ether, and this purification step resulted in a striking increase in the cytocompatibility of the NPs, with no toxicity being observed at concentrations up to 3.2 mg/mL. The purified polymers were employed for the preparation of the NPs used in the work presented in Chapter 5.

In **Chapter 5**, PEGylated PLGHMGA NPs loaded with a cytotoxic protein (saporin) and decorated with the 11A4 nanobody (11A4-NPs) were prepared and their selective cytotoxicity towards HER2 overexpressing breast cancer cells was tested. Confocal microscopy studies demonstrated that the 11A4-NPs were rapidly and extensively taken up by HER2 positive cells (SkBr3) but not by HER2 negative cells (MDA-MB-231). Competition studies with free 11A4 nanobody blocked the uptake of 11A4-NPs in HER2 positive cells, confirming that the internalization of the NPs was mediated by the specific interaction between the 11A4 nanobody and the HER2 receptor. Saporin loaded 11A4-NPs used in combination with an endosomal escape strategy (PCI), strongly and selectively inhibited cell proliferation and decreased the cell viability of HER2 positive cells by induction of apoptosis. In contrast, no cytotoxic effect was observed in these cells when they were treated with saporin loaded 11A4-NPs without PCI. By combining the use of 11A4 nanobody as a targeting ligand and light exposure during the PCI treatment, 11A4-NPs allowed for the specific delivery of saporin into the cytoplasm of HER2 positive breast cancer cells.

In **Chapter 6**, PLGA microparticles (μPs) were evaluated for the encapsulation and sustained release of NDP-MSH, a peptide with short half-life that limits its clinical applicability. The NDP-MSH loaded PLGA μPs had an encapsulation efficiency of 20 $\pm$ 3% and a loading capacity of 0.14 $\pm$ 0.02%. *In vitro* release assays conducted in 10 mM phosphate buffer (pH 7.4) showed that these μPs had a small burst release (<10%) and a lag phase of ~20 days,

followed by a sharp increase in the release of the peptide reaching a plateau at ∼50 days. Approximately ∼90% of the peptide was released during this time. In contrast, NDP-MSH loaded μPs incubated in 100 mM phosphate buffer showed a slower zero-order release, with 50% of the peptide released after 70 days. Preliminary *in vivo* studies in a mouse model of experimental autoimmune encephalomyelitis (EAE) showed promising results for the NDP-MSH loaded μPs. A single subcutaneous administration of these μPs had a similar therapeutic effect as four intravenous administrations of the free peptide (7 times higher dose compared to the peptide released from the μPs according to the *in vitro* assays).

2 Summarizing discussion and perspectives

Apart from a few examples of clinical success[7], the widespread application of polymeric particles for peptide/protein delivery is still limited. In this regard, current challenges and areas of improvement will be discussed in this section.

2.1 Considerations for formulation and manufacturing of polymeric particles

Difficulties associated with the manufacturing of polymeric formulations can pose a threat for their large scale production and commercial success, as exemplified by the case of Nutropin Depot®, a PLGA-based formulation for the sustained release of human growth hormone. Nutropin Depot® was approved by the FDA in 1999 but discontinued 5 years later as a result of the significant resources required for its production[8]. In this regard, recent technological advances have the potential to facilitate the (large scale) production of protein/peptide loaded particles. For instance, microfluidics technology has gained increased attention since it allows for the controlled, reproducible production of micro- and nano- particles with uniform size and improved drug loading[9–11], as well as smaller diameters compared to bulk nanoprecipitation[12]. The membrane emulsification method is also an alternative for the preparation of uniform-sized particles with high drug loading efficiencies[13,14]. As small sizes facilitate the accumulation of NPs in target tissues, these techniques could be explored for the preparation of a smaller version of the NPs presented in **Chapters 2 and 5** of this thesis.

Efficient encapsulation of proteins/peptides also represents a challenge, with low drug loadings often reported[15,16]. Different approaches have been proposed to solve this challenge, such as the use of electrostatic interac-

tions or protecting agents to increase protein/peptide loading[15,17]. Different preparation methods have also been explored for this purpose, including microfluidics[11], membrane emulsification[13], and post-loading of proteins in porous PLGA particles, followed by pore closure at near physiological temperatures[18,19]. Different properties, such as structure, charge and molecular weight, make it impossible to develop standardized procedures that would be suitable for the successful encapsulation of every existing pharmaceutical protein/peptide, and optimization is thus required. In this regard, further studies could be conducted to improve the loading efficiency of the formulations presented in **Chapters 5 and 6**. These formulations showed promising effects, most likely due to the potency of their cargo, but improved drug loading could be regarded as an economic and pharmaceutical advantage in future applications.

An additional challenge in the formulation of polymeric micro- and nanoparticles loaded with peptides/proteins is guaranteeing the structural and functional integrity of the cargo[20]. PLGA particles are often studied as delivery vehicles for biotherapeutics. Unfortunately, the structure of peptides/proteins encapsulated in these formulations may be modified due to the acidification resulting from polymer degradation[21–24]. These modifications can lead to incomplete release of the cargo and/or loss of functionality[25]. In this regard, in **Chapters 4 and 5** of this thesis we propose the use of PLGHMGA as an alternative polymer for the preparation of protein loaded nanoparticles. PLGHMGA, which contains pendant hydroxyl groups in its structure, is more hydrophilic than PLGA, which contributes to a faster release of degradation products, less acidification of the microenvironment[26] and improved compatibility with peptides, as previously reported by our research group[27].

2.2 Intracellular delivery of proteins by ligand decorated nanoparticles

Polymeric NPs decorated with surface ligands are a valuable tool for the delivery of therapeutic proteins with intracellular targets but poor cell membrane permeability[28]. One of the most widely used techniques for the covalent attachment of ligands to the surface of NPs is the maleimide-thiol conjugation reaction. Many publications using this technique for the preparation of targeted nanocarriers fail to report on the rationale for choosing certain reaction conditions, prompting us to perform an in-depth study on this matter, which is presented in **Chapter 2**. The evaluation of different reaction conditions and their impact on the conjugation efficiency, allows for a better understanding of the functionalization process and a better use of resources. Importantly,

the information obtained from this study can be applied in the preparation and evaluation of NPs with tailored surface ligand densities, as done in **Chapter 3** of this thesis. Control of the surface ligand density can be used to influence particle-cell interactions in terms of binding and uptake[29–31], and to improve the efficiency of intracellular protein delivery. Efforts should also be made on evaluating the impact of ligand density on the stealth properties of the NPs, their opsonization, and their interaction with non-target cells, since these influence the pharmacokinetics of the formulation[32].

2.3 Particle internalization and endosomal escape

Endosomal entrapment is probably the most important obstacle for the cytosolic delivery of nanoparticulate formulations internalized by receptor-mediated endocytosis[33,34]. The relevance of endosomal escape in therapies based on ligand targeted polymeric NPs is indeed highlighted in **Chapter 5** of this thesis. HER2 targeted PLGHMGA NPs loaded with the cytotoxic protein saporin, were only toxic to cancer cells when administered in combination with PCI, a technique requiring a photosensitizer (PS) and light. While PCI efficiently triggered the endosomal escape of these NPs *in vitro*, future studies should focus on how to efficiently achieve the cellular co-localization of the NPs and the PS in animal models. The pharmacokinetics of the formulation and the PS must be elucidated in order to determine the correct administration regime for clinical applications. Alternatively, incorporation of the PS in the NPs could be explored as an attempt to ensure the colocalization of both elements in the target cells[35,36].

Other techniques can also be explored to induce the endosomal escape of polymeric NPs. For instance, elements that destabilize or rupture the endosome, such as polymers with high buffering capacities, pore-forming peptides, or polymers and peptides with membrane disruptive properties[33,37,38], could be incorporated in the NPs.

2.4 Suitability of *in vitro* models commonly used for the evaluation of NPs

An important hurdle for the *in vivo* translation of the *in vitro* data obtained during the development of drug delivery systems, is the over-simplification of reality by some of the currently used *in vitro* tests[39]. In this regard, information obtained by experiments traditionally performed in monolayer cell culture could be complemented by using 3-D culture systems, such as multicellular spheroids. Multicellular spheroids (i.e. stroma-containing) are a valuable *in*

vitro tool towards a better understanding of the *in vivo* conditions for the interaction between NPs and tissues, and to evaluate the effect of extracellular matrix and non-target tissue components on tissue penetration of NPs and drug delivery to target cells[40,41]. Experiments conducted in 3-D cell culture models could indeed provide interesting information on the properties of the formulation presented in **Chapter 5**.

Additionally, some authors have highlighted the importance of conducting *in vitro* experiments under dynamic conditions, as most cell-particle interactions *in vivo* would occur under blood flow[42]. In line with this reasoning, **Chapter 3** presents a dynamic approach for the evaluation of the interactions between targeted NPs and endothelial cells in the presence of washed red blood cells. As flowing blood is the first tissue that the NPs would encounter after intravenous administration, experiments that at least partially mimic this conditions would provide valuable information for the evaluation of *in vitro* - *in vivo* correlations[43].

2.5 Clinical translation of polymeric NPs

Despite the extensive research conducted for the design, preparation and testing of ligand targeted polymeric NPs, clinical approval of such systems has remained elusive. The heterogeneity of the enhanced permeability and retention effect (EPR) has been identified as a reason for the limited clinical applicability of ligand targeted NPs in cancer treatment[44]. The EPR effect is based on the consideration that the permeability of tumor vasculature is increased due to anatomical alterations and augmented expression of permeability mediators, which promotes the accumulation of macromolecules in the tumor[45]. Nevertheless, it is now known that the EPR effect varies between and within patients and tumors, and new approaches have been studied to improve the EPR effect for the delivery of nanomedicines. In general, these approaches involve the use of pharmacological agents or physical stimuli (i.e. hyperthermia, sonoporation and phototerapy) to permeabilize, normalize, disrupt or promote the formation of blood vessels[46,47]. Non-invasive imaging techniques can be used to monitor the EPR in patients and aid in the selection of an adequate pharmacological treatment[48]. Proper characterization and modulation of EPR is key for the successful delivery of targeted and non-targeted NPs to the tumor site. It is only after the NPs have reached the tumor site that the presence of targeting ligands becomes a valuable asset, contributing to the tissue retention and cellular internalization of the NPs[32].

Concerns about the suitability of certain animal models for the evaluation of anti-cancer treatments have also been raised[49,50]. For instance, commonly

used subcutaneous iso/allograft or xenograft tumor models overlook the role of the components of tumor stroma (i.e. basement membrane, fibroblasts, extracellular matrix, etc) on tumor support. Additionally, the vasculature of these tumor models does not accurately represent the vasculature on human tumors[51]. These shortcomings should be carefully considered in the interpretation of data obtained from animal experiments.

Undesired immune responses after (repeated) administration of therapeutic proteins/peptides is a possibility that must be meticulously evaluated. The effects of the activation of the immune system can range from the production of neutralizing anti-drug antibodies that render the treatment ineffective, to life-threatening hypersensitivity reactions[52]. In this regard, the development of advanced *in silico*, *in vitro* and *ex vivo* tools could be valuable assets in the pre-clinical assessment of the immunogenicity of peptides and proteins[53]. Humanization has been classically used as an approach to reduce the immunogenicity of proteins, and this approach has found extensive applications to improve the compatibility of murine monoclonal antibodies and human-murine chimeric antibodies[54]. The discovery and development of nanobodies, a new class of antigen binding-fragments with low immunogenicity[55,56], could present an alternative for the use of antibodies. In **Chapter 5** of this thesis, such possibility is explored by using the 11A4 nanobody as a targeting ligand for the selective delivery of NPs to breast cancer cells.

When dealing with targeted nanocarriers, it is particularly important to evaluate the changes in the immune interaction and response that may arise from the conjugation of weakly or non-immunogenic proteins or peptides to a larger scaffold[57,58]. The importance of this issue was recently emphasized in a study showing that repeated administration of liposomes decorated with cRGD induced hypersensitivity-like reactions in mice that were, at times, lethal[59]. In that work, the immunotoxicity of this peptide was found to be related to the RGD sequence and to the cyclic structure. Immunotoxicity was not observed when the cRGD-liposomes were loaded with a cytotoxic agent with immunosuppressive effect. This information must be considered for future work conducted with the formulation presented in **Chapter 3**.

While many challenges must be overcome in order to achieve the clinical translation of targeted-NPs, it has been advocated that a better understanding of the fundamental principles underlying the *in vivo* behavior of nanocarriers, and the use of integrative approaches to enhance the effect of nanomedicines, could bring us closer to this goal[60].

3 Conclusion

The research presented in this thesis shows the applicability of PLGA and PLGHMGA vehicles for the delivery of therapeutic proteins and peptides. In particular, in-depth studies were conducted on different aspects of targeted nanocarriers, including the optimal conditions for their preparation, their suitability for the cell-specific intracellular delivery of proteins, and the influence of ligand-surface density on particle-cell interactions. Additional studies in more complex *in vitro* settings or in *in vivo* models are expected to elucidate the clinical potential of these systems.

References

[1] Leader, B., Baca, Q., and Golan, D. Protein Therapeutics: A Summary And Pharmacological Classification. *Nature Reviews Drug Discovery*, 7, 2008.

[2] Dimitrov, D. S. Therapeutic Proteins. In Voynov, V. and Caravella, J., editors, *Therapeutic Proteins. Methods in Molecular Biology (Methods and Protocols)*, volume 899. Humana Press, Totowa, NJ, 2012.

[3] Lagassé, H. A. D., Alexaki, A., Simhadri, V. L., Katagiri, N. H., Jankowski, W., Sauna, Z. E., and Kimchi-Sarfaty, C. Recent Advances In (Therapeutic Protein) Drug Development. *F1000Research*, 6, 2017.

[4] Lau, J. L. and Dunn, M. K. Therapeutic Peptides: Historical Perspectives, Current Development Trends, And Future Directions. *Bioorganic and Medicinal Chemistry*, 26, 2018.

[5] Kamaly, N., Xiao, Z., Valencia, M. P., Radovic-Moreno, A. F., and C, F. O. Targeted Polymeric Therapeutic Nanoparticles: Design, Development And Clinical Translation. *Chemical Society Reviews*, 41, 2012.

[6] Pinto Reis, C., Neufeld, R. J., Ribeiro, A. J., and Veiga, F. Nanoencapsulation II. Biomedical Applications And Current Status Of Peptide And Protein Nanoparticulate Delivery Systems. *Nanomedicine: Nanotechnology, Biology, and Medicine*, 2, 2006.

[7] Mitragotri, S., Burk, P. A., and Langer, R. Overcoming The Challenges In Administering Biopharmaceuticals: Formulation And Delivery Strategies. *Nature Reviews Drug Discovery*, 13, 2014.

[8] Brown, L. R. Commercial Challenges Of Protein Drug Delivery. *Expert Opinion on Drug Delivery*, 2, 2005.

[9] Dendukuri, B. D. and Doyle, P. S. The Synthesis and Assembly of Polymeric Microparticles Using Microfluidics. *Advanced Materials*, 21, 2009.

[10] Lakkireddy, H. R. and Bazile, D. Building The Design, Translation And Development Principles Of Polymeric Nanomedicines Using The Case Of Clinically Advanced Poly(Lactide(Glycolide))Poly(Ethylene Glycol) Nanotechnology As A Model: An Industrial Viewpoint. *Advanced Drug Delivery Reviews*, 107, 2016.

[11] Valencia, P. M., Farokhzad, O. C., Karnik, R., and Langer, R. Microfluidic Technologies For Accelerating The Clinical Translation Of Nanoparticles. *Nature Nanotechnology*, 7, 2012.

[12] Karnik, R., Gu, F., Basto, P., Cannizzaro, C., Dean, L., Kyei-Manu, W., Langer, R., and Farokhzad, O. C. Microfluidic Platform for Controlled Synthesis of Polymeric Nanoparticles. *Nano Letters*, 8, 2008.

[13] Ma, G. Microencapsulation Of Protein Drugs For Drug Delivery: Strategy, Preparation, And Applications. *Journal of Controlled Release*, 193, 2014.

[14] Nakashima, T., Shimizu, M., and Kukizaki, M. Particle Control Of Emulsion By Membrane Emulsification And Its Applications. *Advanced Drug Delivery Reviews*, 45, 2000.

[15] Ye, M., Kim, S., and Park, K. Issues In Long-Term Protein Delivery Using Biodegradable Microparticles. *Journal of Controlled Release*, 146, 2010.

[16] Yu, M., Wu, J., Shi, J., and Farokhzad, O. C. Nanotechnology for Protein Delivery: Overview and Perspectives. *Journal of Controlled Release*, 240, 2016.

[17] McClements, D. J. Encapsulation, Protection, And Delivery Of Bioactive Proteins And Peptides Using Nanoparticle And Microparticle Systems: A Review. *Advances in Colloid and Interface Science*, 253, 2018.

[18] Desai, K.-G. H. and Schwendeman, S. P. Active Self-Healing Encapsulation Of Vaccine Antigens In PLGA Microspheres. *Journal of Controlled Release*, 165, 2013.

[19] Shah, R. B. and Schwendeman, S. P. A Biomimetic Approach to Active Self-Microencapsulation of Proteins in PLGA. *Journal of Controlled Release*, 196, 2014.

[20] Jiskoot, W., Randolph, T. W., Volkin, D. B., Middaugh, C. R., Schoneich, C., Winter, G., Friess, W., Crommelin, D. J. A., and Carpenter, J. F. Protein Instability and Immunogenicity: Roadblocks to Clinical Application of Injectable. *Journal of Pharmaceutical Sciences*, 101, 2012.

[21] Fu, K., Klibanov, A. M., and Langer, R. Protein Stability In Controlled-Release Systems. *Nature Biotechnology*, 18, 2000.

[22] Schwendeman, S. P. Recent Advances in the Stabilization of Proteins Encapsulated in Injectable PLGA Delivery Systems. *Critical Reviews in Therapeutic Drug Carrier Systems*, 19, 2002.

[23] Spenlehauer, G., Vert, M., Benoit, J. P., and Boddaert, A. Poly (D,L lactide/glycolide) Type Microspheres Made by Solvent Evaporation Method. *Biomaterials*, 10, 1989.

[24] Weert, M. V. D., Hennink, W. E., and Jiskoot, W. Protein Instability in Poly (Lactic-co-Glycolic Acid) Microparticles. *Pharmaceutical research*, 2000.

[25] Giteau, A., Venier-Julienne, M. C., Aubert-Pouëssel, A., and Benoit, J. P. How To Achieve Sustained And Complete Protein Release From PLGA-Based Microparticles? *International Journal of Pharmaceutics 2008, 350, 14-26.*, 350, 2008.

[26] Liu, Y., Ghassemi, A., Hennink, W. E., and Schwendeman, S. P. The Microclimate pH In Poly(D,L-Lactide-co-Hydroxymethyl Glycolide) Microspheres During Biodegradation. *Biomaterials*, 33, 2012.

[27] Shirangi, M., Hennink, W. E., Somsen, G. W., and Van Nostrum, C. F. Identification and Assessment of Octreotide Acylation in Polyester Microspheres by LC-MS/MS. *Pharmaceutical Research*, 32, 2015.

[28] Yameen, B., Choi, W. I., Vilos, C., Swami, A., Shi, J., and Farokhzad, O. C. Insight Into Nanoparticle Cellular Uptake And Intracellular Targeting. *Journal of Controlled Release*, 190, 2014.

[29] Elias, D. R., Poloukhtine, A., Popik, V., and Tsourkas, A. Effect Of Ligand Density, Receptor Density, And Nanoparticle Size On Cell Targeting. *Nanomedicine: Nanotechn*, Biology, logy.

[30] Gu, F., Zhang, L., Teply, B. A., Mann, N., Wang, A., Radovic-Moreno, A. F., Langer, R., and Farokhzad, O. C. Precise Engineering Of Targeted Nanoparticles By Using Self-Assembled Biointegrated Block Copolymers. *Proceedings of the National Academy of Sciences*, 105, 2008.

[31] Shen, Y., Chen, J., Liu, Q., Feng, C., Gao, X., Wang, L., Zhang, Q., and Jiang, X. Effect Of Wheat Germ Agglutinin Density On Cellular Uptake And Toxicity Of Wheat Germ Agglutinin Conjugated PEG-PLA Nanoparticles In Calu-3 Cells. *International Journal of Pharmaceutics*, 413, 2011.

[32] van der Meel, R., Vehmeijer, L. J. C., Kok, R. J., Storm, G., and van Gaal, E. V. B. Ligand-Targeted Particulate Nanomedicines Undergoing Clinical Evaluation: Current Status. *Advanced Drug Delivery Reviews*, 65, 2013.

[33] Selby, L. I., Cortez-Jugo, C. M., Such, G. K., and Johnston, A. P. R. Nanoescapology: Progress Toward Understanding The Endosomal Escape Of Polymeric Nanoparticles. *Wiley Interdisciplinary Reviews: Nanomedicine and Nanobiotechnology*, 9, 2017.

[34] Shete, H. K., Prabhu, R. H., and Patravale, V. B. Endosomal Escape: A Bottleneck in Intracellular Delivery. *Journal of Nanoscience and Nanotechnology*, 14, 2014.

[35] Hong, E. J., Choi, D. G., and Suk, M. Targeted And Effective Photodynamic Therapy For Cancer Using Functionalized Nanomaterials. *Acta Pharmaceutica Sinica B*, 6, 2016.

[36] Konan, Y. N., Gurny, R., and Allemann, E. State Of The Art In The Delivery Of Photosensitizers For Photodynamic Therapy. *Journal of Photochemistry and Photobiology B: Biology*, 66, 2002.

[37] Martens, T. F., Remaut, K., Demeester, J., De Smedt, S. C., and Braeckmans, K. Intracellular Delivery Of Nanomaterials: How To Catch Endosomal Escape In The Act. *Nano Today*, 9, 2014.

[38] Varkouhi, A. K., Scholte, M., Storm, G., and Haisma, H. J. Endosomal Escape Pathways For Delivery Of Biologicals. *Journal of Controlled Release*, 151, 2011.

[39] Grainger, D. W. Cell-Based Drug Testing and This World Is Not Flat. *Advanced Drug Delivery Reviews*, 69-70, 2014.

[40] Goodman, T., Ng, P., and Pun, H. 3-D Tissue Culture Systems For The Evaluation And Optimization Of Nanoparticle-Based Drug Carriers. *Bioconjugate Chemistry*, 19, 2008.

[41] Priwitaningrum, D. L., Blondé, J.-b. G., Sridhar, A., Baarlen, J. V., Hennink, W. E., Storm, G., Le, S., and Prakash, J. Tumor Stroma-Containing 3D Spheroid Arrays : A Tool To Study Nanoparticle Penetration. *Journal of Controlled Release*, 244, 2016.

[42] Ruenraroengsak, P., Cook, J. M., and Florence, A. T. Nanosystem Drug Targeting: Facing Up To Complex Realities. *Journal of Controlled Release*, 141, 2010.

[43] Charoenphol, P., Mocherla, S., Bouis, D., Namdee, K., Pinsky, D. J., and Eniola-Adefeso, O. Targeting Therapeutics To The Vascular Wall In Atherosclerosis - Carrier Size Matters. *Atherosclerosis*, 217, 2011.

[44] Lammers, T. Macro-Nanomedicine: Targeting The Big Picture. *Journal of Controlled Release*, 294, 2019.

[45] Maeda, H., Wu, J., Sawa, T., Matsumura, Y., and Hori, K. Tumor Vascular Permeability And The EPR Effect In Macromolecular Therapeutics: A Review. *Journal of Controlled Release*, 65, 2000.

[46] Brambilla, D., Luciani, P., and Leroux, J.-C. Breakthrough Discoveries In Drug Delivery Technologies: The Next 30 Years. *Journal of Controlled Release*, 190, 2014.

[47] Ojha, T., Pathak, V., Shi, Y., Hennink, W., Moonen, C., Storm, G., Kiessling, F., and Lammers, T. Pharmacological and Physical Vessel Modulation Strategies to Improve EPR-Mediated Drug Targeting to Tumors. *Advanced Drug Delivery Reviews*, 119, 2017.

[48] Lammers, T. SMART Drug Delivery Systems: Back to the Future vs. Clinical Reality. *International Journal of Pharmaceutics*, 454, 2013.

[49] Begley, C. G. and Ellis, L. M. Raise Standards For Preclinical Cancer Research. *Nature*, 483, 2012.

[50] Park, K. The Drug Delivery Field At The Inflection Point: Time To Fight Its Way Out Of The Egg. *Journal of Controlled Release*, 267, 2017.

[51] Crommelin, D. J. A. and Florence, A. T. Towards More Effective Advanced Drug Delivery Systems. *International Journal of Pharmaceutics*, 454, 2013.

[52] Baker, M. P., Reynolds, H. M., Lumicisi, B., and Bryson, C. J. Immunogenicity Of Protein Therapeutics The Key Causes, Consequences And Challenges. *Self/Nonself*, 1, 2010.

[53] Rosenberg, A. S. and Sauna, Z. E. Immunogenicity Assessment During The Development Of Protein Therapeutics. *Journal of Pharmacy and Pharmacology*, 70, 2018.

[54] De Groot, A. S. and Scott, D. W. Immunogenicity of Protein Therapeutics. *Trends in Immunology*, 28, 2007.

[55] Arbabi-Ghahroudi, M. Camelid Single-Domain Antibodies: Historical Perspective And Future Outlook. *Frontiers in Immunology*, 8, 2017.

[56] Oliveira, S., Heukers, R., Sornkom, J., Kok, R. J., and Van Bergen En Henegouwen, P. M. P. Targeting Tumors With Nanobodies For Cancer Imaging And Therapy. *Journal of Controlled Release*, 172, 2013.

[57] Jiskoot, W., Schie, R. M. F. V., Carstens, M. G., and Schellekens, H. Immunological Risk of Injectable Drug Delivery Systems. *Pharmaceutical Research*, 26, 2009.

[58] Sofias, A. M., Andreassen, T., and Hak, S. Nanoparticle Ligand-Decoration Procedures Affect in Vivo Interactions with Immune Cells. *Molecular Pharmaceutics*, 15, 2018.

[59] Wang, X., Wang, H., Jiang, K., Zhang, Y., Zhan, C., Ying, M., Zhang, M., Lu, L., Wang, R., Wang, S., Burgess, D. J., and Wang, H. Liposomes With Cyclic RGD Peptide Motif Triggers Acute Immune Response In Mice. *Journal of Controlled Release*, 293, 2019.

[60] Witzigmann, D., Hak, S., and van der Meel, R. Translating Nanomedicines: Thinking Beyond Materials? A Young Investigator's Reply To The Novelty Bubble. *Journal of Controlled Release*, 290, 2018.

Appendices

Nederlandse samenvatting

Eiwitten en peptiden worden al lange tijd beschouwd als waardevolle therapeutische middelen vanwege hun potentie en specificiteit, en > 160 therapeutische eiwitten en > 60 therapeutische peptiden zijn momenteel goedgekeurd voor klinisch gebruik. Terwijl de markt voor biotherapeutica blijft groeien, zou een substantieel aantal eiwitten en peptiden met korte halfwaardetijden baat hebben bij formuleringstechnieken om hun klinische toepassing te faciliteren. In dit opzicht zijn polymere microdeeltjes (μPs) en nanodeeltjes (NPs) aantrekkelijke afgiftesystemen om de werkzaamheid van deze biomoleculen te verbeteren door ze te beschermen tegen inactivatie en hun circulatietijd en accumulatie op de doelplaats te verhogen. Een aanzienlijk aantal door de FDA goedgekeurde biotherapeutica (dat wil zeggen monoklonale antilichamen en coagulatiefactoren) is gericht op extracellulaire doelwitten, hetgeen niet verrassend is omdat eiwitten en peptiden een lage celmembraanpermeabiliteit hebben die hun toegang tot het cytoplasma beperkt. Deze uitdaging kan echter worden overwonnen door het gebruik van NPs. De samenstelling, grootte, lading en oppervlakte-eigenschappen van deze nanodragers bepalen hun cellulaire internalisatie en de intracellulaire afgifte van hun lading. Het oppervlak van NPs beladen met een therapeutisch eiwit/peptide kan bijvoorbeeld worden gedecoreerd met liganden die de binding van de NPs aan en opname door specifieke cellen begunstigen.

Het onderzoek gepresenteerd in dit proefschrift is gericht op de bereiding, karakterisering en in vitro testen van polymeerdeeltjes voor de toediening van therapeutische eiwitten en peptiden. Gerichte en niet-gerichte nano- en microdeeltjes werden onderzocht voor de intra- en extracellulaire afgifte van deze biotherapeutica.

Hoofdstuk 1 van dit proefschrift geeft een algemene inleiding over therapeutische eiwitten en peptiden, alsmede de beschrijving van twee interessante therapeutische kandidaten: saporine en (Nle^4, D-Phe^7)-α-melanocyten-stimulerend hormoon (NDP-MSH). Uitdagingen in eiwit/peptide-afgifte worden besproken en polymere deeltjes (micro- en nanometrische maten) worden gepresenteerd als dragersystemen om de fysisch-chemische stabiliteit, farmacokinetiek en farmacodynamiek van deze biotherapeutica te verbeteren. Twee biologisch afbreekbare alifatische polyesters, poly(melk-co-glycolzuur) (PLGA) en poly(D, L-melkzuur-co-glycol-co-hydroxymethylglycolzuur) (PLGHMGA), worden geïntroduceerd als geschikte polymeren voor de bereiding van deeltjes gericht op de extra- of intracellulaire levering van biotherapeutica. Fysisch-chemische kenmerken van de deeltjes, evenals de anatomie en fysiologie van weefsels worden besproken

als belangrijke factoren die de verdeling en ophoping van deeltjes in het ziek weefsel bepalen. In gevallen waar intracellulaire aflevering nodig is, wordt de decoratie van NPs met doelzoekende liganden voorgesteld als een manier om hun opname door doelwitcellen te vergemakkelijken. Twee doelzoekende liganden worden onderzocht in dit proefschrift, namelijk het 11A4-nanobody en het cyclische RGD-peptide (cRGD), die beide hun potentieel voor kankerbehandeling hebben aangetoond. Cellulaire internalisatie en endosomale transport van de NPs worden besproken en fotochemische internalisatie (PCI) wordt onderzocht als een strategie om endosomale ontsnapping van met eiwit geladen NPs te induceren en aldus de afgifte van therapeutische eiwitten in het cytosol te bewerkstelligen.

In **Hoofdstuk 2** werd de maleïmide-thiol conjugatiechemie gebruikt voor de bereiding van PLGA NPs gedecoreerd met cRGD of het 11A4 nanobody als doelzoekende liganden op hun oppervlak. De invloed van verschillende omstandigheden op de efficiëntie van de conjugatiereactie van cRGD en het 11A4-nanobody met de NPs werd systematisch bestudeerd. Parameters zoals de NPs-bereidingsmethode (dwz enkele of dubbele emulsie) en het type en de concentratie van de oppervlakteactieve stof die tijdens de procedure werd gebruikt (poly(vinylalcohol) en natriumcholaat) hadden geen invloed op de efficiëntie van de reactie. Daarentegen beïnvloedden de bewaarcondities van de NPs de reactiviteit van maleïmide en terwijl hoge conjugatie-efficiënties ($\sim$ 90%) werden verkregen voor NPs die tot 7 dagen bij 4 °C waren bewaard, resulteerde opslag bij 20 °C in lagere conjugatie-efficiënties ($\sim$ 60%), waarschijnlijk vanwege hydrolyse van maleïmide. De efficiëntie van de maleïmide-thiol-conjugatiereactie werd geëvalueerd bij verschillende reactantverhoudingen en reactietijden en de bereiding van met ligand gedecoreerde NPs werd geoptimaliseerd. Oppervlaktedecoratie van NPs met cRGD (M_w 678 Da) was optimaal bij een maleïmide tot thiol-molaire molaire verhouding van 2:1 en bereikte een conjugatie-efficiëntie van 84 $\pm$ 4% (overeenkomend met $\sim$ 50.000 cRGD-moleculen per NP) na slechts 30 minuten incubatie (kamertemperatuur, pH 7,0). Interessant genoeg resulteerde conjugatie bij 1:1 ratio's in lagere efficiënties (52 $\pm$ 7%), hetgeen suggereert dat niet alle maleïmide-groepen op het oppervlak van de deeltjes beschikbaar zijn voor reactie. NP-decoratie met 11A4-nanobody (M_w 14.813 Da) was optimaal bij een maleïmide tot thiol-molverhouding van 5: 1 en bereikte een conjugatie-efficiëntie van 58 $\pm$ 12% conjugatie-efficiëntie (corresponderend met $\sim$ 5.500 11A4 moleculen per NP) na 2 uur (kamertemperatuur, pH 7,4)). Het verschil in reactie-efficiëntie en kinetiek voor beide liganden kan worden verklaard door de verschillen in grootte en structuur (hogere diffusiecoëfficiënt voor cRGD en betere toegankelijkheid van de thiolgroep in vergelijking met die van het 11A4-nanobody).

De bevindingen van deze studie leverden waardevolle informatie op over de optimale omstandigheden voor de bereiding van ligand-gedecoreerde NPs door maleïmide-thiolchemie, in het bijzonder in termen van reactietijden en reactantverhoudingen. Deze inzichten werden toegepast bij de vervaardiging van de beoogde NPs die in andere hoofdstukken worden gepresenteerd.

In **Hoofdstuk 3** werden PLGA NPs gedecoreerd met cRGD bereid en hun targeting karakteristieken werden onderzocht op menselijke navelstrengendotheelcellen (HUVECs) onder statische en flowomstandigheden. PLGA NPs waren gedecoreerd met cRGD in verschillende dichtheden (dwz "laag" $\sim$ 11.000, "gemiddeld" $\sim$ 31.700 en "hoog" $\sim$ 117.600 cRGD/μm2; corresponderend met $\sim$ 3.400, $\sim$ 9.700 en $\sim$ 40.700 cRGD-moleculen per NP) om de impact van liganddichtheid op celtargeting te onderzoeken. Associatie en opname van cRGD-NPs geïncubeerd met HUVECs onder statische omstandigheden werd bestudeerd door flowcytometrie en confocale microscopie. Interactie van NPs met HUVECs werd niet waargenomen voor NPs die niet waren gedecoreerd met cRGD. Daarentegen werd celassociatie waargenomen voor cRGD-NPs en deze was positief gecorreleerd met de incubatietijd (1 en 3 uur), NPsconcentratie (0,016 - 0,4 mg/ml) en cRGD-oppervlaktedichtheid ($\sim$ 11.000 - $\sim$ 117.600 cRGD/μm2 of ($\sim$ 3.400 - $\sim$ 40.700 cRGD/NP) . In dit verband was de associatie van hoge cRGD-NPs met HUVECs $\sim$ 4 maal hoger dan bij lage cRGD-NPs (bij de hoogste geteste concentraties). Aangezien de targeting van vasculaire endotheelcellen gebeurt onder dynamische omstandigheden (in plaats van statische), werden experimenten onder flow uitgevoerd met behulp van een pompgecontroleerd perfusiesysteem en celassociatie werd gevisualiseerd met behulp van een epifluorescentie microscoop. In overeenstemming met de bevindingen onder statische omstandigheden, werd cellulaire associatie van NPs met HUVECs onder flow waargenomen voor cRGD-NPs maar niet voor niet-gedecoreerde NPs. Interacties met HUVECs waren ook afhankelijk van de oppervlaktedichtheid van cRGD. Gevonden werd dat na 1 en 16 uur incubatie, de celassociatie van hoge cRGD -NPs $\sim$ 9 en 6 maal hoger was dan de associatie van lage cRGD-NPs, wat suggereert dat liganddichtheid relevanter is voor interacties van celdeeltjes onder flow dan onder statische omstandigheden. Flow-experimenten werden ook uitgevoerd in medium dat gewassen rode bloedcellen (RBCs) bevat en, onder deze omstandigheden, was de associatie van cRGD-NPs met HUVECs ook afhankelijk van de ligand-dichtheid. Vergelijking van de flowexperimenten uitgevoerd in medium met en zonder RBCs, toont aan dat de associatie van NPs met de cellen aanzienlijk hoger is in aanwezigheid van RBCs ($\sim$ 6 en 3-voudig verschil voor respectievelijk lage en hoge cRGD-NPs). Deze observatie wordt zeer waarschijnlijk veroorzaakt doordat RBCs de NPs naar de HUVECs hebben geduwd en daardoor hun contact

met hen hebben bevorderd. Het werk dat in dit hoofdstuk wordt beschreven, is een stap in de richting van het evalueren van vasculaire targeting onder condities die meer lijken op fysiologische omstandigheden. Deze aanpak kan van grote waarde zijn voor de ontwikkeling van nieuwe op endotheel gerichte nanodragers met een beperkt aantal proefdieren.

In **Hoofdstuk 4** werden poly(D, L-melkzuur-co-glycol-co-hydroxymethylglycolzuur) (PLGHMGA) en gePEGyleerde PLGHMGA (MePEG-PLGHMGA) gesynthetiseerd, gekarakteriseerd en gebruikt voor de bereiding van NPs als een alternatief voor PLGA. De cytocompatibiliteit van MePEG-PLGHMGA NPs werd getest in twee cellijnen die van belang waren voor toekomstige experimenten, SkBr3 en MDA-MB-231. Onverwachte cytotoxiciteit van deze NPs werd waargenomen bij concentraties $>$ 0,4 mg/ml in SkBr3 en $>$ 0,8 mg/ml in MDA-MB-231. Deze toxiciteit werd toegeschreven aan de aanwezigheid van gebutyleerd hydroxytolueen (BHT) als een onzuiverheid in de NPs. De synthese van (MePEG-) PLGHMGA vereist een hydrogeneringsstap uitgevoerd in tetrahydrofuraan (THF), een oplosmiddel gestabiliseerd met BHT. Hoewel de hoeveelheid aanwezig BHT in THF klein is (0,02 - 0,03% w/w), leidde het gebruik van grote hoeveelheden THF tijdens hydrogenering tot de accumulatie van BHT in de polymeren tot een mate die de cytocompatibiliteit van de NPs significant beïnvloedde (2,3% w/w BHT in NPs). BHT werd uit de polymeren verwijderd door precipitatie in diethylether en deze zuiveringsstap resulteerde in een opvallende toename in de cytocompatibiliteit van de NPs, waarbij geen toxiciteit werd waargenomen bij concentraties tot 3,2 mg/ml. De gezuiverde polymeren werden gebruikt voor de bereiding van de NPs die werden gebruikt in het werk gepresenteerd in Hoofdstuk 5.

In **Hoofdstuk 5** werden gepegyleerde PLGHMGA NPs beladen met een cytotoxisch eiwit (saporine) en gedecoreerd met het 11A4-nanobody (11A4-NPs) getest en hun selectieve cytotoxiciteit ten aanzien van HER2 overexpresserende borstkankercellen werd getest. Confocale microscopieonderzoeken toonden aan dat de 11A4-NPs snel en in sterke mate werden opgenomen door HER2-positieve cellen (SkBr3) maar niet door HER2-negatieve cellen (MDA-MB-231). Competitiestudies met vrij 11A4-nanobody blokkeerden de opname van 11A4-NPs in HER2-positieve cellen, wat bevestigt dat de internalisatie van de NPs werd gemedieerd door de specifieke interactie tussen het 11A4-nanobody en de HER2-receptor. Met saporine beladen 11A4-NPs, gebruikt in combinatie met een endosomale ontsnappingsstrategie (PCI), remden de celproliferatie sterk en selectief en verminderden de cellevensvatbaarheid van HER2-positieve cellen door inductie van apoptose. Daarentegen werd geen cytotoxisch effect waargenomen in deze cellen wanneer ze werden behandeld

met met saporine beladen 11A4-NPs zonder PCI. Door het gebruik van 11A4-nanobody als doelzoekend ligand en blootstelling aan licht tijdens de PCI-behandeling te combineren, zorgden 11A4-NPs voor de specifieke afgifte van saporine in het cytoplasma van HER2-positieve borstkankercellen.

In **Hoofdstuk 6** werden PLGA-microdeeltjes (μPs) geëvalueerd voor de inkapseling en aanhoudende afgifte van NDP-MSH, een peptide met een korte halfwaardetijd die de klinische toepasbaarheid beperkt. De NDP-MSH beladen PLGA μPs hadden een inkapselingsefficiëntie van 20 $\pm$ 3% en een beladingscapaciteit van 0,14 $\pm$ 0,02%. *In vitro* afgiftetests uitgevoerd in 10 mM fosfaatbuffer (pH 7,4) toonden aan dat deze μPs een kleine burst-afgifte (<10%) en een lag-fase van $\sim$ 20 dagen hadden, gevolgd door een sterke toename in de afgifte van het peptide met een plateau op $\sim$ 50 dagen. Ongeveer $\sim$ 90% van het peptide werd gedurende deze tijd afgegeven. Daarentegen vertoonden NDP-MSH beladen μPs geïncubeerd in 100 mM fosfaatbuffer een langzamere nulde-orde afgifte, waarbij 50% van het peptide na 70 dagen werd afgegeven. Inleidende *in vivo* studies in een muismodel van experimentele auto-immuun encefalomyelitis (EAE) toonden veelbelovende resultaten voor de met NDP-MSH beladen μPs. Een enkele subcutane toediening van deze μPs had een soortgelijk therapeutisch effect als vier intraveneuze toedieningen van het vrije peptide (7 maal hogere dosis vergeleken met het peptide afgegeven uit de μPs volgens de *in vitro* assays).

Curriculum vitae

Lucía Amine Martínez Jothar was born in 1987 in San Luis Potosí, Mexico. After obtaining her high school diploma, she enrolled in the Biological and Pharmaceutical Chemist bachelors program at the Autonomous University of San Luis Potosí. During this time she worked in projects related to biological applications of polymers, including the assessment of glucose oxidase activity in polyelectrolyte complexes, osteoblast culture in polyelectrolyte layers and the evaluation of the antibacterial activity of polymeric surfaces. After obtaining her bachelors degree, she pursued the masters program in Biomedical Sciences at the University of Liège, in Belgium. Her thesis concerned the evaluation of the *in vitro* hemocompatibility of polycations. After completing her masters, she started her PhD in the Drug Innovation program at Utrecht University, in the Netherlands. The results of her work are presented in this PhD thesis entitled "Polyester micro- and nanoparticles for the delivery of therapeutic peptides or proteins".

List of publications

L. Martínez-Jothar, N. Beztsinna, C.F. van Nostrum, W.E. Hennink, S. Oliveira, Selective Cytotoxicity to HER2 Positive Breast Cancer Cells by Saporin-Loaded Nanobody-Targeted Polymeric Nanoparticles in Combination With Photochemical Internalization. *Molecular Pharmaceutics* 2019, 16, 1633 - 1647.

L. Martínez-Jothar, S. Doulkeridou, R.M. Schiffelers, J. Sastre Torano, S. Oliveira, C.F. van Nostrum, W.E. Hennink, Insights into maleimide-thiol conjugation chemistry: Conditions for efficient surface functionalization of nanoparticles for receptor targeting. *Journal of Controlled Release* 2018, 282, 101 - 109.

L. Martínez-Jothar, A.D. Barendrecht, S. Oliveira, C. F. van Nostrum, R. M. Schiffelers, W. E. Hennink, Marcel H.A.M. Fens, Endothelial cell targeting by cRGD-functionalized polymeric nanoparticles under static and flow conditions. Manuscript in preparation.

*L. Martínez-Jothar**, N. Mykicki*, C. F. van Nostrum, S. Oliveira, K. Loser*, W.E. Hennink*. PLGA microparticles for the sustained release of the neuroprotective peptide NDP-MSH. Manuscript in preparation.

L. Flebus, F. Lombart, *L. Martinez-Jothar*, C. Sevrin, C. Delierneux, C. Oury, C. Grandfils, *In vitro* study of the specific interaction between poly(2-dimethylamino ethylmethacrylate) based polymers with platelets and red blood cells, *International Journal of Pharmaceutics* 2015, 492, 55 - 64.

S.G. Padilla-Martínez, *L. Martínez-Jothar*, J.G. Sampedro, F. Tristán, E. Pérez, Enhanced thermal stability and pH behavior of glucose oxidase on electrostatic interaction with polyethylenimine, *International Journal of Biological Macromolecules* 2015, 75, 453 - 459.

A.L. Galván Valdez, *L. Martínez-Jothar*, C.C. López Álvarez, M.R. Villasuso Palomares, M.A. Saldaña Flores A.Y. Martínez Castellanos, L.E. Fragoso Morales. Permanencia de la sonda de Foley asociada a infección urinaria y farmacorresistencia. *Enfermedades Infecciosas y Microbiología* 2011, 31.

Acknowledgements

When I started this PhD I didn't imagine that I would learn as much outside the lab as I did inside of it. It is difficult to summarize what the past 4 years have meant to me and how grateful I am to the people I have met in this journey, but I will give it a try.

This PhD wouldn't have been possible without the financial support of the Mexican National Council for Science and Technology (Consejo Nacional de Ciencia y Tecnología - CONACYT, México) obtained through the Council for Science and Technology of San Luis Potosí (COPOCYT). I am grateful for the opportunity they gave me to continue my education abroad.

I would like to thank my supervisors for their guidance throughout my PhD:

Wim, your commitment to your work is impressive. Thank you for your teachings and feedback, which have made me a better scientist.

Rene, thank you for your advice during my PhD and for helping me understand the world of polymers and chemistry.

Sabrina, your scientific guidance and your support have been invaluable to me. You have taught me a lot through the way you approach research and the way you engage with fellow scientists.

I would also like to thank our collaborators for sharing their knowledge, time and ideas with me:

Marcel, I learned a lot about your practical approach to experimental work. Your excitement over research is contagious and makes it a pleasure to work with you.

Karin, I am grateful for our enriching scientific discussions and your feedback on our work. I was proud to be involved in the NDP-MSH microparticles project and I am excited to see where it will lead.

Niels, even though the granzyme B project could not move forward during my PhD, I am happy to know that we have set down some foundations for the project to continue and I am looking forward to its results.

Sofia, Irati, Nataliia, Nadine and Arjan thank you very much for sharing your laboratory experience with me and for the fruitful scientific discussions we had.

Keeping the lab running is a challenging task that could not be accomplished without the commitment and hard work of our technicians. Joep, I was inspired by your excitement for science and your thoroughness in teaching. It was great to learn the art of cell work from you. Mies, I was always amazed at your laboratory knowledge and skills, thank you for all your help. Roel, even though you were often busy you always took the time to help me out if I needed it, and I am grateful for that. Louis, thank you for your work in keeping the biochemistry lab organized and working well. Barbara, thank you for your help with all the administrative work required before and during my PhD.

I also want to thank my students:

Joyce, it was great working with you, your laughter and positive attitude always lifted my spirits.

Wouter, I really enjoyed guiding you during your internship, your determination in the face of challenges is admirable. Thank you for your hard work, but mostly thank you for your friendship.

During my PhD I have had the fortune of working alongside great colleagues. Even if I don't mention you by name, I trust you know who you are. Please know that I greatly appreciated our conversations, your scientific advice, your encouragement during long working days, and your heartfelt support. Thank you for sharing a part of your work, culture, dreams and worries with me.

To our ever-changing lunch group in the past 4 years: thank you for your continuous friendship and for the fun we had during our often hectic working days. I truly enjoyed laughing with you, learning about your cultures and sharing all that delicious food!

To my close friends:

Dandan and Yinan, thank you for teaching me the art of hot pot and mahjong! I had a lot of fun during our dinners and our gym time.

Marzieh, Neda and Negar, I am constantly amazed by your kindness and hospitality. It was a wonderful surprise to find such great friends coming from a very distant land. Thank you for the wonderful times we have spent together, I am looking forward to many more!

Genoveva, your kindness and help meant more to me than I can say. Thank you for your friendship and for teaching me more about Dutch culture.

Armina, your support over the last months of my PhD was invaluable. I really enjoyed our conversations on different topics and I am grateful for all the times you cheered me up.

Maripaz, your vibrant, joyful personality made me feel like I was back in Mexico every time we met! Gracias por todo amiga!

Charo, Celia, Citla and Ugne: I am truly blessed to have friendships like ours that pass the test of distance and time. I have learned so much from you throughout the years and you have helped me become a better person. Thank you for your support and encouragement in difficult times. Las quiero mucho!

Bonus thanks to Neda and Armina for being such awesome paranymphs, and to my talented friend Alex Lee for designing the beautiful cover of this thesis!

To my family:

I was truly fortunate to grow up in a loving, supporting environment. Thank you for encouraging me to follow my dreams even if they meant me moving so far away from you. Your love, teachings and memories are with me no matter where I go.

Mom and dad, my love, gratitude and admiration for you is infinite. Papá, llevo conmigo tu honestidad y ética de trabajo a donde quiera que voy. Mamá, llevo conmigo tu amabilidad y fuerza día con día. Estoy convencida que si todos tuvieran la fortuna de tener unos padres tan maravillosos como ustedes, el mundo sería un lugar mejor.

Gaby, my little sister, you are a true inspiration to me. Keep on dreaming and fighting for the causes that you believe in. I will always be on your side.

Zoltán, Gabriella and Katinka, I couldnt have asked for a better second family. I will be forever thankful for your hospitality and kindness. Megtiszteltetés számomra, hogy részese lehetek szerető családotoknak, és várom, hogy elősegíthessem annak gyarapodását.

Dániel, I couldnt have completed this PhD without your love, patience and support. You have filled my life with happiness, laughter and adventure. Nem tudom, hová sodor minket az élet, de abban biztos vagyok, hogy amíg veled lehetek, bárhol otthon érzem majd magam. Szeretlek.